

UvA-DARE (Digital Academic Repository)

Biocatalytic synthesis of α -chiral amines

Selective immobilization of enzymes and their application in batch and continuous flow

Böhmer, W.

Publication date

2019

Document Version

Final published version

License

Other

[Link to publication](#)

Citation for published version (APA):

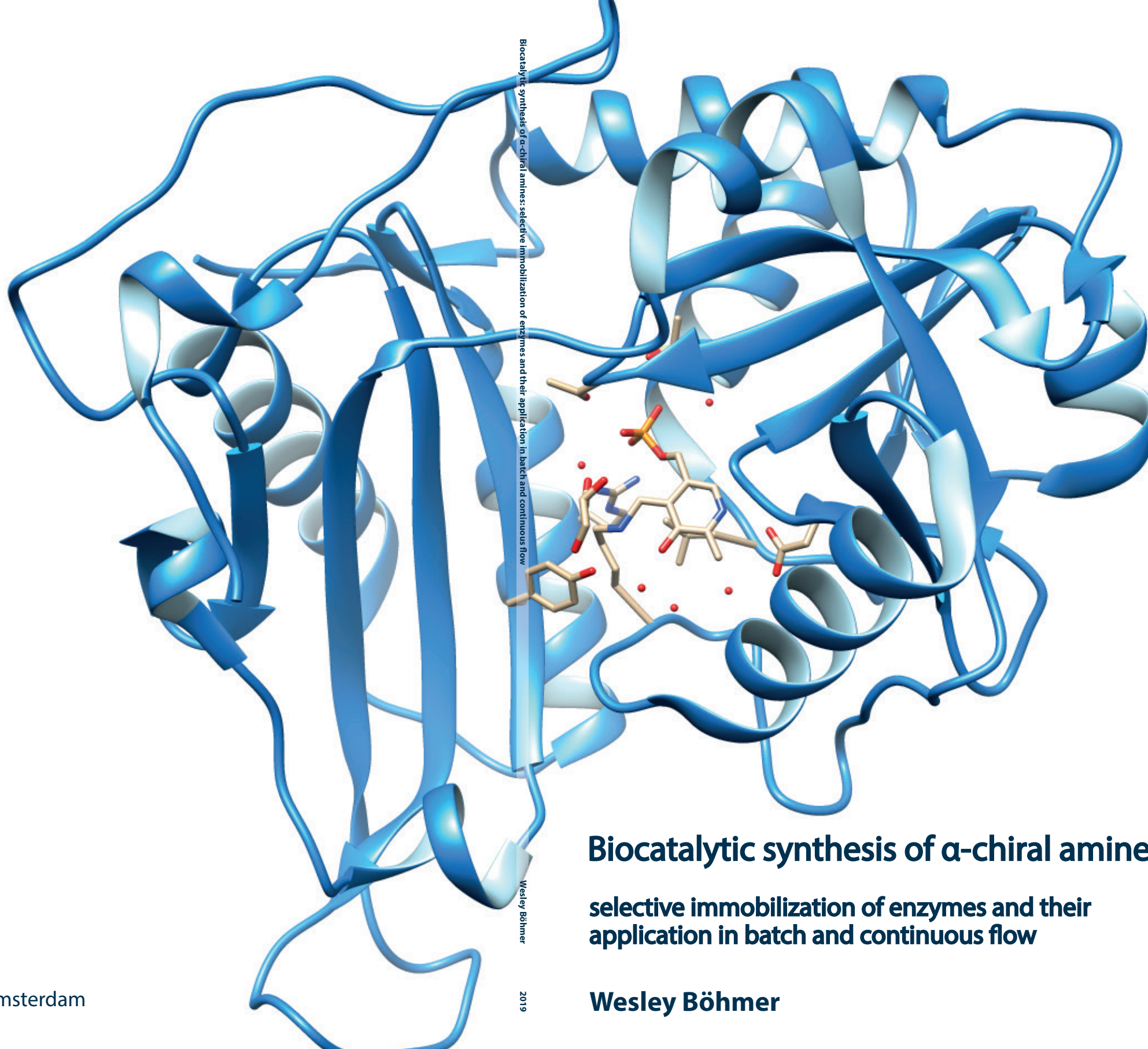
Böhmer, W. (2019). *Biocatalytic synthesis of α -chiral amines: Selective immobilization of enzymes and their application in batch and continuous flow*.

General rights

It is not permitted to download or to forward/distribute the text or part of it without the consent of the author(s) and/or copyright holder(s), other than for strictly personal, individual use, unless the work is under an open content license (like Creative Commons).

Disclaimer/Complaints regulations

If you believe that digital publication of certain material infringes any of your rights or (privacy) interests, please let the Library know, stating your reasons. In case of a legitimate complaint, the Library will make the material inaccessible and/or remove it from the website. Please Ask the Library: <https://uba.uva.nl/en/contact>, or a letter to: Library of the University of Amsterdam, Secretariat, Singel 425, 1012 WP Amsterdam, The Netherlands. You will be contacted as soon as possible.



Biocatalytic synthesis of α -chiral amines: selective immobilization of enzymes and their application in batch and continuous flow

Wesley Böhmer

2019

Biocatalytic synthesis of α -chiral amines:

selective immobilization of enzymes and their application in batch and continuous flow

Wesley Böhmer

*Biocatalytic synthesis of α -chiral amines:
selective immobilization of enzymes and their
application in batch and continuous flow*

Wesley Böhmer

2019

© 2019, W. Böhmer, Amsterdam

This project has received funding from the European Research Council (ERC) under the European Union's Horizon 2020 research and innovation programme (grant agreement No 638271, BioSusAmin)

Printed by Amsterdam University Press

*Biocatalytic synthesis of α -chiral amines:
selective immobilization of enzymes and their
application in batch and continuous flow*

ACADEMISCH PROEFSCHRIFT

ter verkrijging van de graad van doctor

aan de Universiteit van Amsterdam

op gezag van de Rector Magnificus

prof. dr. ir. K.I.J. Maex

ten overstaan van een door het College voor Promoties ingestelde
commissie, in het openbaar te verdedigen in de Aula der Universiteit

op donderdag 19 december 2019, te 15.00 uur

door

Wesley Böhmer

geboren te Alkmaar

Table of contents

Summary	8
List of abbreviations	9
Chapter 1 <i>Enzyme immobilization facilitating biocatalytic routes for the synthesis of enantiomerically pure α-chiral amines</i>	10
1.1 Chemical and biocatalytic syntheses of chiral α -amines.....	11
1.2 Enzyme immobilization.....	15
1.2.1 Advantages of using enzyme immobilization.....	15
1.2.2 Immobilization techniques.....	16
1.2.3 Support materials.....	18
1.2.4 Partition and diffusion phenomena.....	21
1.3 Immobilization of enzymes for the production of α -chiral amines in batch and flow reactors.....	24
1.4 Thesis outline.....	25
1.5 References.....	26
Chapter 2 <i>Reductive amination of carbonyl compounds by amine dehydrogenases</i>	31
2.1 Introduction.....	32
2.2 Optimization of the reaction conditions.....	34
2.3 Influence of the temperature and time studies.....	36
2.4 Substrate scope of the reductive amination using AmDHs.....	37
2.5 Representative biocatalytic reductive amination in preparative scale.....	46
2.6 Conclusion.....	47
2.7 Experimental section.....	49
2.7.1 General information.....	49
2.7.2 Optimized procedure for the biocatalytic reductive amination on analytical scale.....	49
2.7.3 Preparative biocatalytic reductive amination for the synthesis of (<i>R</i>)- 4b	49
2.7.4 Procedure for enzymatic synthesis of chiral reference amines using ω TAs.....	49
2.7.5 Chemical synthesis of substrates.....	50
2.7.6 Analytics.....	52
2.8 References.....	53
Chapter 3 <i>Co-immobilized dehydrogenases applied for the asymmetric hydrogen-borrowing bio-amination of alcohols</i>	57
3.1 Introduction.....	58
3.2 Results & discussion.....	62
3.2.1 Expression and purification of dehydrogenases.....	62
3.2.2 Catalytic activity of purified alcohol dehydrogenases.....	62
3.2.3 Co-immobilization of dehydrogenases.....	64
3.2.4 Optimizations for the bio-amination with co-immobilized dehydrogenases.....	64
3.2.5 Application of co-immobilized dehydrogenases in the amination of alcohols.....	70

3.2.6	Elaboration on limitations in recycling of the co-immobilized ADH-AmdDH cascade.....	70
3.2.7	Extending the reactivity of the ADH-AmdDH cascade.....	72
3.3	Conclusion.....	74
3.4	Experimental section.....	76
3.4.1	General information.....	76
3.4.2	Expression and purification of dehydrogenases.....	76
3.4.3	Activity testing of ADHs.....	76
3.4.4	General procedure for EziG metal-ion affinity co-immobilization of dehydrogenase.....	77
3.4.5	General procedure for analytical scale reactions with co-immobilized dehydrogenases.....	77
3.4.6	Preparative scale amination reaction with co-immobilized dehydrogenases.....	78
3.4.7	Analytics.....	78
3.5	Experimental data.....	79
3.5.1	SDS-PAGE.....	79
3.5.2	NMR.....	81
3.6	References.....	81
Chapter 4	<i>Immobilization of ω-transaminases for the kinetic resolution of amines in a continuous flow reactor.....</i>	<i>84</i>
4.1	Introduction.....	85
4.2	Result section.....	92
4.2.1	Expression and purification of ω -transaminases.....	92
4.2.2	EziG TM support materials.....	93
4.2.3	Immobilization of ω -transaminases.....	94
4.2.4	Influence of buffer (i.e. ionic strength) and PLP concentration on the immobilization process.....	94
4.2.5	Influence of type of buffer and pH on the immobilization process.....	96
4.2.6	Studies on single batch kinetic resolution of <i>rac</i> - α -MBA catalyzed by ω TAs immobilized on EziG ³	97
4.2.7	High substrate loading performance of EziG ³ -AsR.....	98
4.2.8	Biocatalyst recycling.....	99
4.2.9	In-flow immobilization and continuous flow kinetic resolution.....	101
4.3	Conclusion.....	101
4.4	Experimental section.....	102
4.4.1	General information.....	102
4.4.2	Expression and purification of ω -transaminases.....	102
4.4.3	Bradford assay.....	103
4.4.4	Optimized conditions for immobilization on EziG carrier materials.....	103
4.4.5	Optimized conditions for kinetic resolution with immobilized ω -transaminases.....	103
4.4.6	In-flow immobilization from purified enzyme solution.....	104
4.4.7	In-flow immobilization from crude cell extract (i.e., cell lysate).....	104
4.4.8	Continuous flow kinetic resolution with EziG TM -immobilized	

	ω -transaminases.....	105
4.4.9	Scanning electron microscopy (SEM) analysis.....	105
4.4.10	Analytics.....	105
4.5	Calculations and terminology.....	106
4.5.1	Yield of immobilization.....	106
4.5.2	Turnover number (TON).....	106
4.5.3	Immobilized enzyme activity or turnover frequency (TOF).....	107
4.5.4	Reaction rate in flow reactors.....	107
4.6	References.....	108
Chapter 5	<i>Application of Immobilized ω-transaminases on metal-ion affinity support material in neat organic solvents.....</i>	111
5.1	Introduction.....	112
5.2	Results & discussion.....	117
5.2.1	Immobilization and pre-treatment of ω TAs for application in organic solvents.....	117
5.2.2	Influence of support material, reaction solvent and conditions.....	120
5.2.3	Advantages and limitations in performance of the immobilized ω TAs in organic solvents.....	123
5.2.4	Immobilized ω TAs in organic solvents under continuous flow operation.....	124
5.3	Conclusion.....	127
5.4	Experimental Section.....	129
5.4.1	General information.....	129
5.4.2	Expression and purification of ω TAs.....	129
5.4.3	Bradford assay.....	130
5.4.4	Immobilization of ω TAs on EziG support materials.....	131
5.4.5	Analytical scale reactions in organic solvents with immobilized ω TAs.....	131
5.4.6	Flow reactions in organic solvents with immobilized ω TA.....	131
5.4.7	Analytics.....	132
5.4.8	Calculations and terminology.....	132
5.5	Appendix.....	135
5.6	References.....	141
Samenvatting		145
Acknowledgements		146
List of publications		147

Summary

Asymmetric synthesis of chiral α -amines with elevated catalytic efficiency and atom economy is a significant challenge in chemistry. Amines are important intermediates in the production of active pharmaceutical ingredients, fine chemicals and agrochemicals. Current chemical methods for obtaining them are often not selective enough and they use fossil-based feedstock. Although less applied in chemical industry, enzymatic processes possess exquisite chemo-, regio-, and stereoselectivities. Furthermore, they originate entirely from biological resources. Unfortunately, many biocatalytic processes are not yet suitable for operation under industrial conditions and therefore rendered undesirable. This thesis attempts to provide a different perspective in this regard. Enzymes for the synthesis of chiral α -amines (i.e., amine dehydrogenases and transaminases) are shown to be highly active biocatalysts with excellent catalytic efficiency. Applicability of these enzymes is significantly improved by selective immobilization creating easy-to-handle heterogeneous biocatalysts. Particularly, the ability to recycle the biocatalysts tremendously improves their catalytic turnover numbers and enables gram-scale production of chiral α -amines in batch as well as continuous flow. The application of immobilized transaminases is further extended to their use in neat organic solvents. Problems often encountered with enzymatic processes in industry were avoided, such as low solubility of hydrophobic substrates, less favorable thermodynamic equilibria, hydrolytic side reactions and difficult product recovery. This thesis highlights the potential of using enzymes in bio-organic synthesis of valuable chemical compounds and it provides a critical overview of currently applied methods for enzyme immobilization and flow biocatalysis.

List of abbreviations

AA-ADH	alcohol dehydrogenase originated from <i>Aromatoleum aromaticum</i>
AsR- ω TA	(<i>R</i>)-selective ω -transaminase from <i>Arthrobacter</i> species
Bb-PhAmDH	amine dehydrogenase variant originated from the phenylalanine dehydrogenase from <i>Bacillus badius</i>
Cb-FDH	formate dehydrogenase (variant) from <i>Candida boidinii</i>
Ch1-AmDH	chimeric amine dehydrogenase generated through domain shuffling of Bb-PhAmDH variant and L-AmDH variant
CPG	controlled porosity glass
Cv- ω TA	(<i>S</i>)-selective ω -transaminase from <i>Chromobacterium violaceum</i>
DCM	dichloromethane
DMAP	dimethylaminopyridine
DMSO	dimethylsulfoxide
<i>ee</i>	enantiomeric excess
EtOAc	ethyl acetate
EziG ³ -AsR	AsR- ω TA immobilized on EziG ³ Fe Amber
EziG ³ -Cv	Cv- ω TA immobilized on EziG ³ Fe Amber
GDH	glucose dehydrogenase from <i>Bacillus subtilis</i>
HEPES	4-(2-hydroxyethyl)-1-piperazineethanesulfonic acid
KOH	potassium hydroxide
MgSO ₄	magnesium sulfate
MOPS	3-(<i>N</i> -morpholino)propanesulfonic acid
PLP	pyridoxal 5'-phosphate
n.a.	not applicable
n.d.	not determined
NOx	recombinant nicotinamide oxidase
<i>rac</i> - α -MBA	<i>rac</i> - α -methylbenzylamine
Rs-PhAmDH	amine dehydrogenase variant originated from the phenylalanine dehydrogenase from <i>Rhodococcus</i> species
RT	room temperature
SEM	scanning electron microscopy
TOF	turnover frequency
TON	turnover number

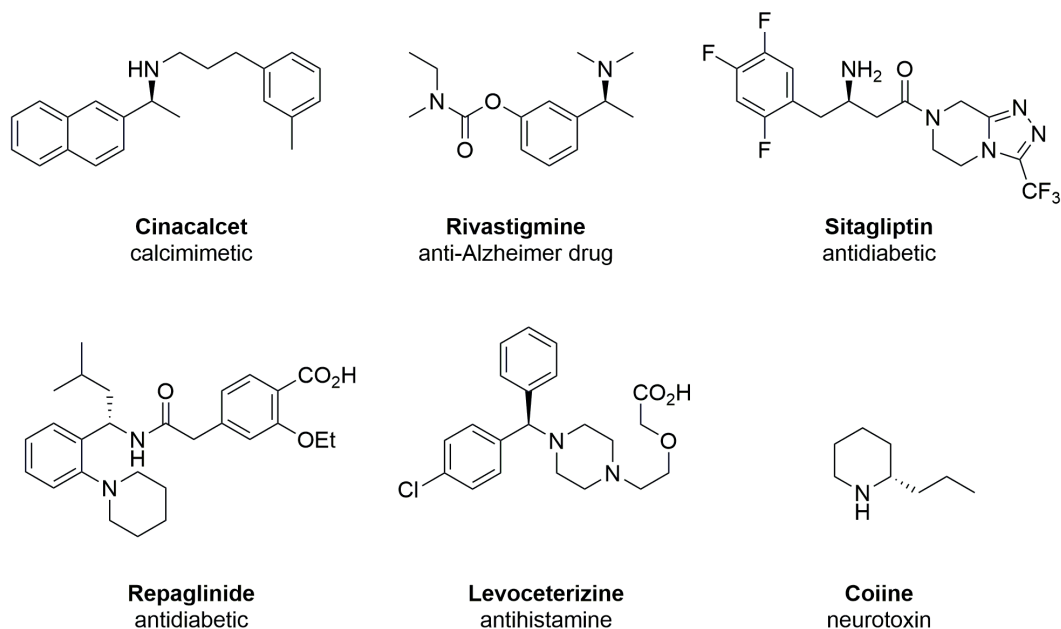
Chapter 1

Enzyme immobilization facilitating biocatalytic routes for the synthesis of enantiomerically pure α -chiral amines

1.1 Chemical and biocatalytic syntheses of chiral α -amines

Amines constitute major synthetic targets as chemically active and abundant moieties in pharmaceuticals, fine chemicals, agrochemicals and a significant number of bulk materials. Current estimates state that amine functionalities are present in over 40% of pharmaceutical compounds and approximately 20% of agrochemicals ^[1]. Especially, α -chiral primary amine building blocks are desired for the synthetic design of active pharmaceutical ingredients (APIs) and a broad class of natural products. A small selection of pharmaceutical target molecules bearing a chiral amine functionality is depicted in Scheme 1.1. Furthermore, chiral amines are often employed as chiral auxiliaries or resolving agents. Particularly, in α -chiral amines the stereogenic carbon center is located adjacent to the nitrogen atom. Both α - and β -amino acids, which contain an additional carboxylic moiety, are excluded in this respect. Synthetic strategies include those leading to the formation of α -chiral primary, secondary, tertiary or even quaternary amines (i.e. ammonium salt).

A plethora of synthetic routes for obtaining α -chiral amines have been developed over the past few decades, although development of operationally simple and preferably one-step procedures with high chemo-, regio-, and stereoselectivity has remained challenging ^[2]. Examples of well-established synthetic methods include Hofmann alkylation ^[3], Buchwald–



Scheme 1.1. A selection of important natural products and pharmaceutical compounds bearing an α -chiral amine functionality ^[11].

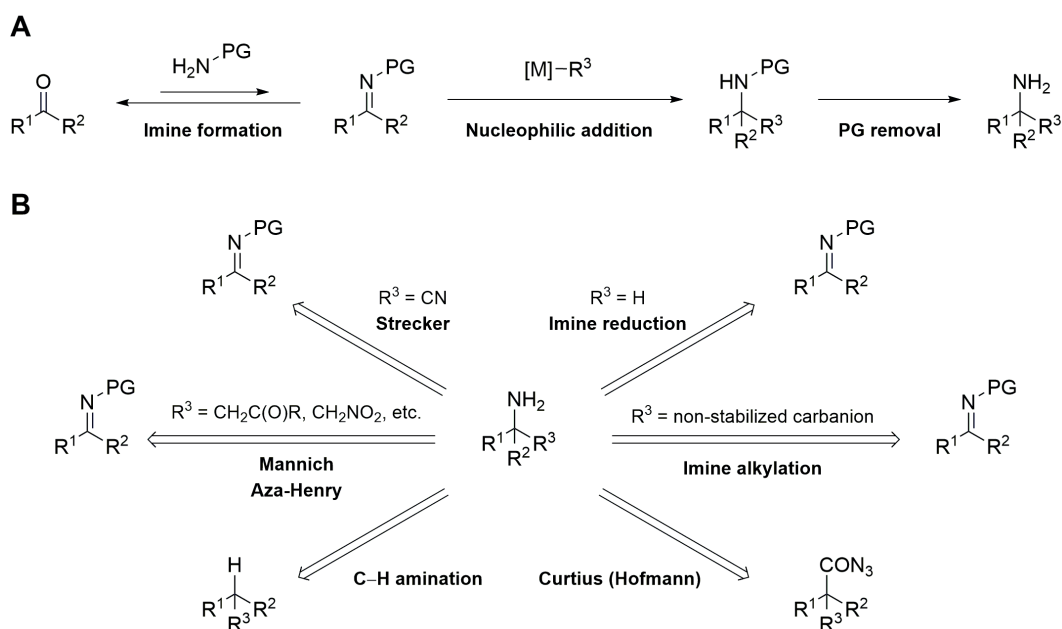
Hartwig ^[4] and Ullmann reactions ^[5], hydroamination ^[6], hydroaminomethylation ^[7], reduction of nitriles ^[8], and nitro compounds ^[9], or reductive amination ^[2a, 10]. The vast majority of synthetic routes relies on activation of prochiral precursors using an external amine source and typically requires three steps: 1) reversible imine formation; 2) nucleophilic addition; and 3) removal of protecting or activating groups (Scheme 1.2A). Asymmetric synthesis of chiral amines as building blocks for pharmaceutical products poses additional challenges since enantiomeric excess as high as 99.7% is desirable ^[12]. The most common synthetic methods for obtaining chiral amines include the stereoselective addition of nucleophiles to imines (i.e., Mannich and Strecker syntheses), the asymmetric C-H amination and C-C double bond hydroamination, and the asymmetric reduction of imines and enamines (Scheme 1.2B). The latter has been applied in industry utilizing predominantly metallocatalysts (Ru, Rh, Ir) for selective hydrogenation under high pressures of dihydrogen ^[2, 13]. Organocatalytic approaches have been developed as well involving the use of hydrosilanes or Hantzsch esters as the hydrogen donor and utilizing Brønsted acid species, such as Akiyama-Terada catalysts, to induce chirality ^[14]. Synthetic strategies for obtaining chiral amines, however, are limited in terms of moderate selectivities, necessity of introducing (de)protection steps, multi-step synthetic routes, formation of a large number of byproducts, and often the use of toxic reagents and metals.

Biocatalytic strategies for the synthesis of chiral amines are an attractive option as they possess considerable advantages over many synthetic methods ^[15]. Biocatalysts have been known for their exquisite chemo-, regio-, and stereoselectivities at near ambient conditions. Generally, functional group activation is not required and high catalytic activities can be obtained in a single-step process. Although highly selective, biocatalysts can be tailored and optimized for the reaction of interest through protein engineering ^[16], stabilization of biocatalysts can also be achieved by immobilization or cross-linking techniques ^[17]. Furthermore, application of biocatalysts has been established in batch as well as flow reactors ^[18].

General biocatalytic methods for obtaining chiral amines are: 1) kinetic resolution of racemic amines via enantioselective *N*-acylation using hydrolases, 2) deracemization using a combination of monoamine oxidases and reducing agents such as borane and 3) asymmetric reduction of imines which are either pre-formed or generated through condensation of amines and carbonyl compounds (Scheme 1.3). Kinetic resolution of racemic amines using hydrolases has been well-established in industry, but allows only

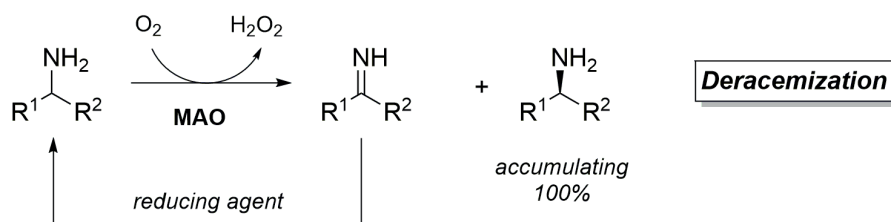
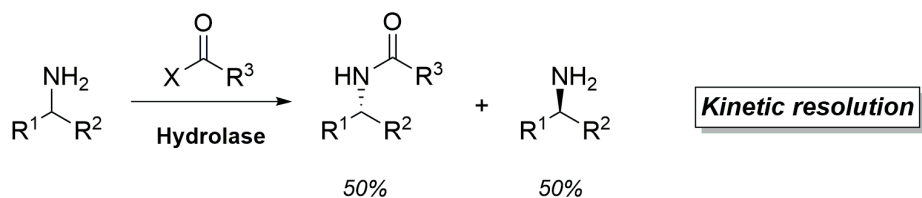
for a maximum conversion of 50% [19]. Monoamine oxidases (MAO) catalyze the oxidative deamination of aliphatic monoamines and aromatic amines to imines. Molecular oxygen is reduced to hydrogen peroxide in the process. The equilibrium for this reaction lies strongly on the side of the imine product, thus amine substrates are converted quantitatively. The synthesis of primary as well as secondary amines is feasible; however, racemic amines are required as substrates [1a, 20]. Several enzyme classes catalyze the asymmetric synthesis of amines. Transaminases (TA) catalyze the amino transfer from a simple amine donor molecule to the prochiral ketone substrate which is enabled by pyridoxal phosphate cofactor (PLP). This mechanism involves a formal reductive amination, since there is no actual hydrogenation step involved. Although transaminases are highly applicable in industry, the amino transfer mechanism allows only for the synthesis of primary amines rendering secondary and tertiary amines inaccessible through this route. Furthermore, most commonly at least a stoichiometric amount of amine donor is required to drive the unfavorable reaction equilibrium to the product side. Removal of keto-acceptor product is commonly required to prevent product inhibition phenomena [21].

Asymmetric reduction of imines is predominantly performed by NAD(P)H-dependent

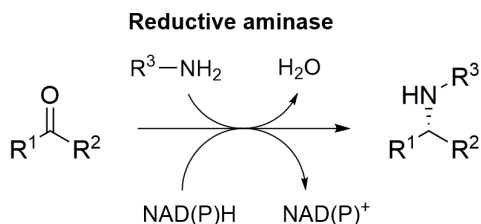
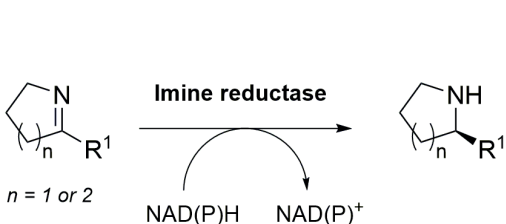
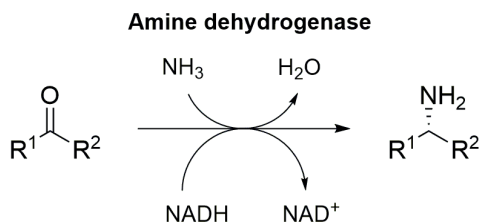
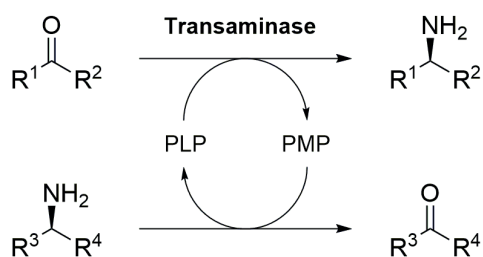


Scheme 1.2. Asymmetric synthesis of amines often relies on the activation of prochiral precursors with an external amine source, A) reversible imine formation, nucleophilic addition and removal of the activating or protecting group (PG). B) General methods in organic chemistry for the synthesis of amines [12].

enzymes. The required cofactors have become economically feasible as they are obtained in large quantities from industrial fermenting processes. Moreover, NAD(P)H cofactors are often recycled in the biocatalytic reaction by the use of coenzymes (for example glucose dehydrogenase (GDH) or formate dehydrogenase (FDH)) or (photo)chemical methods [22]. Imine substrates are generated mostly from prochiral carbonyl compounds by condensation



Asymmetric synthesis*



* Other enzymes: ammonia lyase, P450, berberine bridge, Pictet-Spenglerase

Scheme 1.3. Biocatalytic methods for obtaining chiral amines can be categorized in three groups: 1) kinetic resolution and 2) deracemization of racemic amines, and 3) asymmetric synthesis from prochiral precursors [11, 19b, 20-21, 23].

with small amine molecules such as ammonia or methyl amine. Imine reductases (IRED) catalyze mainly the reduction of pre-formed imines from solution (Scheme 1.3) [11, 20, 23]. The C=N bond is highly susceptible to attack by a wide range of nucleophiles due to its electronic character. However, imines are also hydrolytically labile posing severe limitations on the applied substrate scope for the reductive amination with IREDs. Cyclic (five- or six-membered) imines are most commonly accepted substrates or those bearing a carboxylic acid substituent on the imine carbon atom. This structural feature enables stabilization of the imine through internal hydrogen bonding and it was observed for aromatic iminium ions in *ortho*-position of the phenolate oxygen [24]. Amine dehydrogenases (AmDH) facilitate the formation of the imine intermediate in the active site of the enzyme enabling the conversion of a more structurally diverse panel of prochiral ketones and aldehydes to chiral α -amines. Additionally, AmDHs possess high atom-efficiency since they require ammonia as a nitrogen source and generate water as the sole byproduct. Furthermore, AmDHs display exquisite enantioselectivity (>99% *ee*, (*R*)). A more detailed discussion on AmDHs is provided in Chapter 2. Reductive aminases (RedAm) have recently been designed specifically for the generation of secondary and tertiary amines from carbonyl compounds. Although still rather underdeveloped and limited to a small substrate scope, several RedAms have been engineered; 1) from an opine dehydrogenase (OpDH) from *Arthrobacter* sp 1C [25], 2) AspRedAm from *Aspergillus oryzae* [26] and 3) a selection of IREDs showing similar reactivities [27]. Other enzymes that catalyze the asymmetric formation of amines are ammonia lyases, P450 monooxygenases, berberine bridge enzymes and Pictet-Spenglerases [20, 28].

1.2 Enzyme immobilization

1.2.1 Advantages of using enzyme immobilization

Immobilization of enzymes has been developed over the past decades as a general method for enabling the reuse of enzymes in biocatalytic applications. Industrial application of enzymes is often limited by a lack of long-term operational stability, complex down-stream processing, low productivity, difficult recovery of the enzyme and risk of product contamination by the other proteins if crude biocatalysts are utilized [17, 29]. Additionally, most enzyme scaffolds are hydrophilic and would aggregate when suspended in hydrophobic environments that are often applied in industrial reactions, such as transformations by lipases [30]. Immobilization provides easier handling of enzymes as a solid material and their facile separation from the product at the end

of the reaction. Immobilization enables applications in fixed-bed operations, thus increasing productivity and lowering cost of material ^[18]. In terms of catalytic efficiency, immobilization increases the volumetric biocatalyst loading in the reaction which allows for application of higher substrate concentrations and produces higher production rates ^[31]. Furthermore, immobilized enzymes have shown enhanced stability under storage and operational conditions towards denaturation by heat, contact with organic solvents or by autolysis (digestion of enzymes by other enzymes such as proteases) ^[32].

Immobilization is the physical confinement of an enzyme as a crosslinked unit or as a heterogeneous catalyst onto or inside a solid support. Re-use of the biocatalyst is enabled with significant retention of catalytic activity. There are three general methods for immobilization: 1) cross-linking of enzymes, 2) encapsulation in polymeric structures and 3) immobilization onto a solid support via physical adsorption or covalent attachment (Figure 1.1). Each immobilization method possess advantages and disadvantages in terms of ease-of-use, cost of carrier and fixing agents, physically imposed constraints (mass-transfer, diffusion limitations), extent of retained catalytic activity and enzyme stability. Choosing the optimal method for immobilization of an enzyme depends on the physiochemical properties of the enzyme itself, the support material and the reaction of interest. Furthermore, for an industrial set-up it is important that biotechnological applications are not only environmentally sustainable and elegant, but also competitive from an economic point of view ^[29a]. The next few paragraphs summarize each of the enzyme immobilization methods, a selection of support materials and the frequently observed physical characteristics of immobilized enzymes.

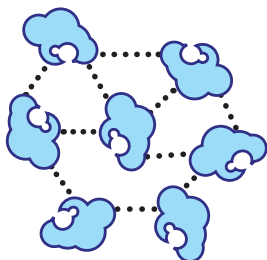
1.2.2 Immobilization techniques

Cross-linking involves aggregation of enzymes upon precipitation using inorganic salts, water-miscible organic solvents, or non-ionic polymers. The enzyme aggregates are subsequently linked together by cross-linking agents (often bifunctional such as glutaraldehyde) to obtain the active enzyme as a heterogeneous biocatalyst. This relatively simple and carrier-free immobilization procedure results in more stable biocatalysts with highly concentrated enzyme activity and a low production cost. Productivity of cross-linked enzymes is often high since addition of inactive bulk material is unnecessary. However, optimization of enzyme aggregate formation and successful cross-linking can be tedious and often poor recovery of enzyme activity is observed. In addition, cross-linked enzymes

possess poor mechanical stability which can make them less suitable for industrial application.

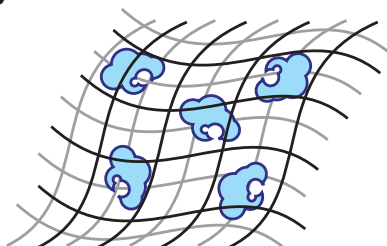
Encapsulation confines soluble or aggregated enzymes inside a bulk matrix or membrane device. It requires the synthesis of the polymeric matrix in the presence of the enzyme. The polymeric network significantly improves the mechanical stability of enzymes by shielding them from the bulk reaction medium. However, diffusion of reactants and products through the matrix should be feasible while avoiding enzyme leaching. Physical

A

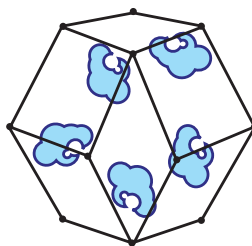


Carrier-free crosslinking

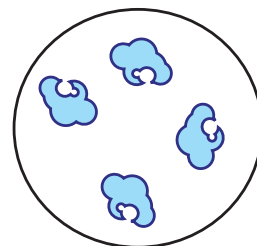
B



**Entrapment
polymer**



**Entrapment
inorganic material**



Encapsulation

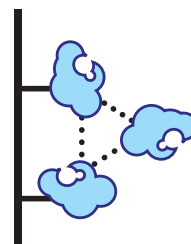
C



Physical adsorption



Covalent attachment



Cross-linking to support

Figure 1.1. Enzyme immobilization techniques were categorized in A) cross-linking of enzymes, B) encapsulation or entrapment and C) immobilization onto a solid support ^[17, 35].

entrapment is therefore more suitable for whole cell systems whereas free enzymes usually require some additional cross-linking to prevent enzyme leaching entirely. Encapsulated enzymes have gained considerable application in biosensing devices [33].

Enzymes can be immobilized on solid supports either through physical absorption or by covalent attachment. Reversible absorption of enzymes can occur through electrostatic interactions (van der Waals or hydrophobic interactions), ionic interactions and affinity binding. The latter is based on binding of a genetically fused poly-His tag of the enzyme to metal ions such as nickel, cobalt, copper and iron. These metal ions are embedded in the support material and bound to it through chelating functional groups (often nitrilotriacetic acid or iminodiacetic acid). Elution of the bound enzyme can easily be achieved using strongly binding competing ligands or by decreasing the pH. The support can also be regenerated by using a strong chelator such as ethylene diamine tetraacetic acid (EDTA) to remove the metal ions. The first example of such a system involved a His₆-tagged alanine racemase from *Geobacillus stearothermophilus* immobilized on a cobalt-functionalized silica support via metal-ion affinity binding [34]. Non-covalent immobilization allows for mild confinement of the enzyme that often minimizes enzyme conformational changes, but enzyme leaching can occur upon changes in the microenvironment of the enzyme (i.e., pH or ionic strength). Covalent immobilization is more robust and provides strong linkages that prevent enzyme leaching and can lead to higher operational stability, especially through multi-point attachment. It requires pre-activation of either the enzyme or the support by utilizing functional groups, such as aldehydes, amino groups or epoxides. Interactions are often established through Schiff's base formation followed by a chemical reduction to make it irreversible. Alternatively glutaraldehyde can be used for cross-linking the support and the enzyme. Although most frequently applied in industrial processes, covalently immobilized enzyme often show significant loss in catalytic activity. Figure 1.1 depicts an overview of enzyme immobilization techniques.

1.2.3 Support materials

Materials used for enzyme immobilization are not merely a means for making the enzyme reusable. They should also assist the enzyme in performing the reaction of interest. First of all, the support material should be stable under operational conditions (solvents, pH, temperature, mechanical forces) and provide sufficient stabilization of the enzyme through its properties. Physical characteristics of the support (particle diameter, swelling behavior,

mechanical stability and compression behavior) significantly influence the performance of the immobilized enzyme^[29a, 36]. An important parameter is the surface area which determines the loading capacity of the support. It is determined by the pore volume, pore diameter and particle size. A large surface area ($>100 \text{ m}^2 \text{ g}^{-1}$) is desirable and can generally be obtained by using smaller particles with higher pore volumes. However, the support should enable not only adsorption of the enzyme on the outer surface but also in the interior of the support^[37]. The pore size should be larger than the size of the enzyme to prevent limitations in enzyme conformational mobility. Furthermore, diffusion of the substrate to the active site of the enzyme should be unhindered. In certain cases, it can be more convenient to maintain the enzyme on the outer surface of the support if the substrate has a low solubility and tends to precipitation inside the pores or when the enzyme is poorly accessible. Finally, porous materials possess higher loading capacities and protect the enzyme from aggregation, autolysis, or inactivation by organic solvents and it stabilizes the enzyme microenvironment. Generally observed problems are related to mass-transfer and low diffusion rates which are also influenced by pore size, protein loading, substrate solubility and the nature of support.

Changes in enzyme conformation often occur upon immobilization because of the composition of the support and changes in the enzyme microenvironment. Hydrophilic support interactions such as hydrogen bonding, for example, influence water retention capacity, whereas hydrophobic interactions with non-polar enzyme residues can significantly improve catalytic activity in non-aqueous environments (i.e., hyper-activation – increased catalytic activity of an enzyme above that of the native enzyme^[38]). Additionally, the chemical structure of the support strongly affects its ability to be solvated by hydrophobic solvents and substrates. Chemical modifications of the support surface with introduced acidic (carboxylic acid) or basic (amine) functionalities can promote enzyme orientation and result in better process control. Ionic interactions generally promote the partition of enzyme onto the solid support. Ionic adsorption and charge interactions, however, can also hamper the diffusion of charged substrates and reaction intermediates. The choice of support and immobilization medium are of importance for obtaining an efficient biocatalyst. Displacement of water molecules on the enzyme surface with polar groups on the support can occur easily at low ionic strength whereas at high ionic strength it is recommended to promote the initial adsorption of the protein on polymeric organic resins (such as methacrylic or styrenic polymers^[29a, 37]); positively charged (tetra alkyl ammonium) or negatively charged (carboxy) resins can be used^[37, 39]. Polyethyleneimine

has also been used (epoxy-amino groups, ^[40]). However, highly charged supports can hamper the kinetics when substrates are charged and the pH optimum and pH stability of the enzyme may also change. Regarding the stability of the immobilized enzyme, introducing long spacer molecules on the support surface can widen the conformational flexibility of the enzyme whereas shorter spacer molecules ensure higher thermal stability by restricting enzyme mobility and preventing the unfolding process. Notably, in smart (or stimulus-responsive) polymers, conformational changes of the polymer structure occur upon small changes in the environment (temperature, pH, ionic strength). PolyNIPAM, for example, is a water-soluble enzyme polymer below the temperature limit which is minimizing mass-transfer and activity losses. Above a certain temperature the polymer precipitates out of the water and prevents the reaction from proceeding ^[41].

Cross-linking of enzymes has been performed through cross-linked enzyme crystals (CLECs ^[42]) and cross-linked enzyme aggregates (CLEAs ^[17, 43]). CLECs possess high operational stability, high catalyst productivity and high volumetric productivity. However, enzyme crystallization can be a challenging and laborious operation which requires enzyme of very high purity. CLEAs are formed through precipitation of an enzyme by the addition of salts (ammonium sulfate), water miscible organic solvents (acetone, ethanol, or 1,2-dimethoxyethane), or non-ionic polymers. The aggregates are then cross-linked using cross-linking agents, such as glutaraldehyde or dextran polyaldehyde, to form di-imine bonds utilizing lysine residues on the enzyme surface. CLEAs facilitate subsequent purification and immobilization of enzymes in one step from crude cell extracts. They possess high productivity (per mass unit of biocatalyst), facile recovery, improved storage and operational stability with regard to temperature, pH, and organic solvents; they are also stable towards enzyme leaching in aqueous media. Although the production protocols are fairly simple, they require optimization for each enzyme. Furthermore, a low number of lysine residues on enzyme surface can hinder the cross-linking process and cause enzyme leaching. Furthermore, substrate accessibility to the interior of the aggregate can be limited depending on the pore size and enzyme microenvironment. This can be prevented by co-precipitation of the enzyme with polymers, albumine, organic acids or solvents ^[44]. Low retained catalytic activity and low mechanical stability has been observed and difficulties in handling of the CLEA material makes recovery of biocatalyst problematic on an industrial scale. More sophisticated CLEAs have been developed over the years, such as layered CLEAs, combi-CLEAs ^[45] and magnetic CLEAs ^[46].

Over the past few decades a wide variety of support materials with distinct functional properties have been developed for entrapment and support immobilization of enzymes [47]. Organic materials (agarose, alginate, chitosan, gelatin) are abundant and biocompatible materials, but they possess low mechanical stability. Inorganic materials (metals, silica, zeolites) generally possess excellent mechanical properties and they improve the chemical and thermal stability of enzymes. The sol-gel process is particularly effective for the entrapment of enzymes and it involves hydrolytic polymerization of tetraoxysilane. Morphologies of the material have been reported and depend on the method of drying [48]. Other methods include the use of hydrogels such as polyvinylalcohol (PVA) cryogels [49] or Lentikats [50].

Support materials for the binding enzymes can be derived from natural, synthetic and inorganic polymers. Natural polymers include cellulose, starch, agarose, chitosan, gelatin and protein based supports [47a, 51]. They are relatively inexpensive and easy to obtain, but low particle sizes and pre-activation requirements make these support materials often less suitable for application. Several synthetic and commercial support materials have been developed possessing different chemical functionalities for enzyme binding (Eupergit [52], Sepabeads, AmberLite XAD-7 [53] and Accurel). Inorganic materials are mostly silica-based (meso-porous silica, celite, porous glass, MOFs) and possess very high surface areas ($300\text{-}1500\text{ m}^2\text{ g}^{-1}$), uniform pore diameters (2-40 nm), high pore volumes (ca. 1 mL g^{-1}) and they are easily functionalized. Well-known examples include MCM-41, SBA-15, and protein-coated microcrystals [54]. Furthermore, the use of functionalized nanoparticles (MNPs) has become more popular over the past few years. Their high surface-to-volume ratio enables minimal diffusional limitations, less mass-transfer problems and high protein loadings and surface reactivity. They are available in various shapes (spherical, fibers, tubes, or single metals such as gold) and possess high mechanical strength. Recovery of immobilized enzyme-MNPs has been improved by the use of magnetic materials (iron oxide, Fe_3O_4) coated with amino- or carboxyl-functionalized silica [55]. However, MNPs still suffer from high production costs and the possibility of agglomeration, the latter of which can be solved by encapsulation of the immobilized enzyme-MNPs. A general overview of immobilization support materials is given in Figure 1.2.

1.2.4 Partition and diffusion phenomena

Both the enzyme and the support contribute in establishing an active immobilized biocatalyst. Enzymatic properties (biochemical, reaction type and kinetics) and support

properties (chemical characteristics and mechanical properties) define mass transfer effects (efficiency), the optimal immobilization method (highest active loading) and the optimal operational stability (maximum number of cycles) that describe the overall performance of the system (enzyme consumption per amount of produced product and productivity per unit of biocatalyst) ^[29a]. For the adsorption and binding of the enzyme on the support, both the pore size of the support materials and the microenvironment inside the pores are important. Binding of the enzyme to the support should ideally be performed without restricting access to the enzyme active site. A correct orientation of the enzyme upon binding to the support can be crucial for obtaining high efficiency of the immobilized biocatalyst. Enzyme molecules are mainly immobilized on the outer layers of the support. Strong affinity of the enzyme for the support matrix and low affinity (or even repulsion) between immobilized enzyme molecules at the surface and dissolved enzyme molecules in solution, limits the extent to which the dissolved enzyme can reach and adsorb at the internal pores of the support ^[56]. This means that there is a certain penetration depth of the enzyme. However, enzyme penetration is only interesting when catalysis can take place throughout the whole support matrix (external and internal surface). Furthermore, protein loading should not exceed maximum capacity of functional groups on the support ^[57]. It can be challenging to determine the amount of enzyme to be loaded onto a certain support because enzymes differ in the amount of active amino groups on their surface and in molecular size. Subsequent washing steps after the immobilization are advisable, but will not assure complete removal on non-covalently adsorbed enzyme molecules. Moreover, loading an excess of enzyme onto the support is both a waste of biocatalyst and it can decrease the specific activity due to crowding of enzyme molecules on the support and subsequent diffusional limitations ^[29a, 57]. For the diffusion of substrate and product molecules throughout the support matrix, agitation largely affects mass transfer rates.

Although enzyme immobilization enables recycling of the biocatalyst and often improves enzyme stability, it can have a negative effect on the diffusion of solutes and pose mass-transfer limitations ^[58]. Measuring the activity of an immobilized enzyme can become challenging when diffusional limitations are playing a role. The intrinsic activity of the immobilized enzyme can decrease significantly with little changes in the measured activity when this is largely limited by the mass transfer rate ^[59]. Since physical adsorption interactions are often not sufficiently strong to prevent enzyme leaching in aqueous environment, it renders determination of the activity of an immobilized enzyme in aqueous

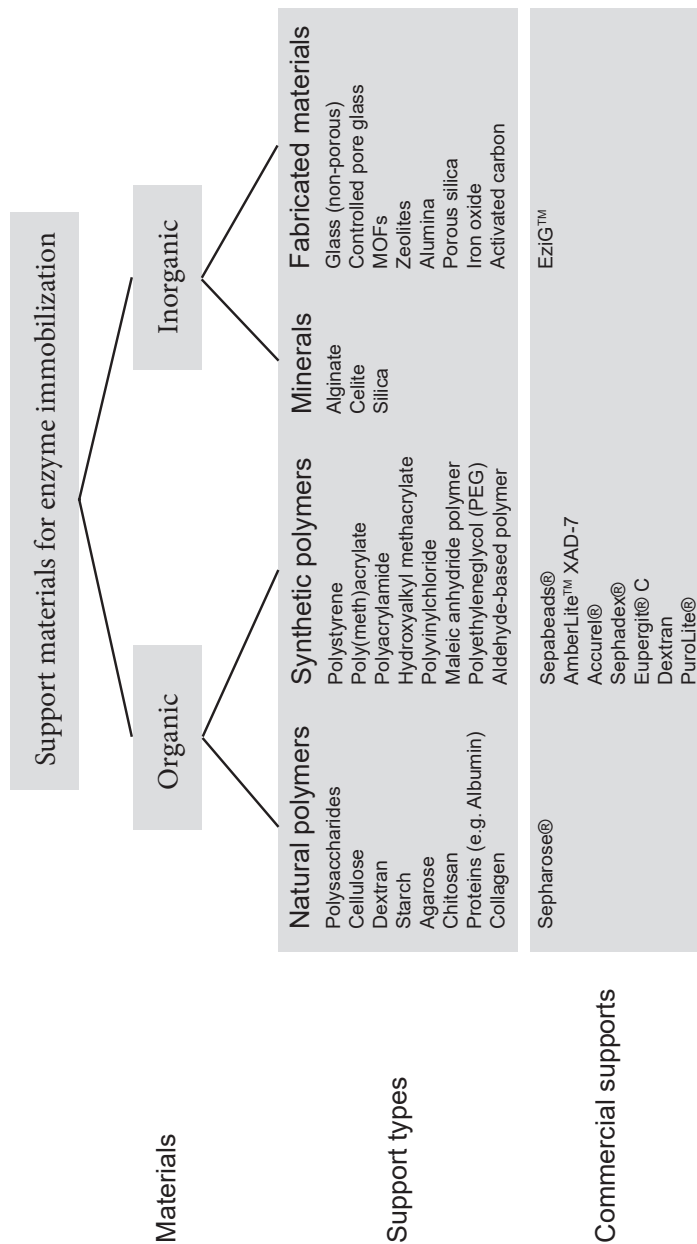


Figure 1.2. Support materials for enzyme immobilization are numerous and can generally be categorized in inorganic, organic and hybrid support materials [47b, 51].

media impossible. Particularly detached enzyme molecules can contribute significantly to the observed kinetics of the reaction [57]. In order to overcome the problem of enzyme leaching, crosslinking methods have been developed between enzyme molecules adsorbed on the support or by applying a silicon coating [60]. Enzyme purity has to be considered as well since interference of extra components in the enzyme preparation might complicate drawing conclusions on structural and functional properties of the system. Furthermore, there is a clear distinction between intrinsic and apparent loss of activity due to immobilization. Intrinsic loss of activity can occur in the process of immobilization due to, for example, mechanical stress or thermal inactivation of the enzyme. Apparent loss of activity can result from, for example, inaccessibility of a fraction of the enzyme molecules which are bound in the inner pores of the support material (e.g., diffusional limitations).

1.3 Immobilization of enzymes for the production of α -chiral amines in batch and flow reactors

Current application of enzymes for the asymmetric synthesis of α -chiral amines mostly involves the use of whole cell and cell-free biocatalysts in batch operations. Although high selectivity is often obtained and only mild reaction conditions are required, the employed biocatalysts lack reusability. Immobilization of enzymes has been used to enable recycling, but low retained catalytic activity and poor mechanical stability limits implementation of many biocatalysts in batch processes. For the asymmetric synthesis of α -chiral amines, transaminases have been effectively employed as immobilized biocatalysts in batch as well flow systems. Limitations, however, involve the unfavorable thermodynamic equilibrium of the transamination reaction if run in the amination direction with classical amine donors such as alanine. In aqueous systems supra-stoichiometric amounts of sacrificial amine donors are required. Moreover, keto coproducts formed in the process inhibit the enzyme and strategies for removing them from the reaction mixture are necessary. Other enzymes catalyzing amine synthesis, such as IREDs and AmDHs, have limited applications as immobilized enzymes until to date due to their NAD(P)H cofactor dependency. Especially in flow reactions, the cofactor content has to be supplied in a continuous manner since binding of the cofactor in the active site of the enzymes is reversible. Furthermore, IREDs have a very limited substrate scope in aqueous environment due to the hydrolytic instability of imine intermediates. AmDHs and RedAms, in this respect, appear more suitable for application as immobilized enzymes in batch as

well as in flow. In particular, reductive amination with ammonia starting from prochiral carbonyl compounds is a relatively low rate process and flow reactors can offer significant advantages over batch reactors. For example, inhibition phenomena can be prevented as products of the reaction are removed continuously. The higher surface to volume ratio in flow reactors can significantly speed up the reaction. Finally, issues in scaling up the process are minimized as excellent mixing and heat transfer are maintained ^[61].

In order to obtain a highly-active immobilized biocatalyst, the enzymes employed should be immobilized in a mild fashion and with minimal perturbation of their active folding state. Specific binding motives, such as genetically-fused enzyme linkers (i.e., His-tag), can facilitate selective binding of the enzyme on an inert support material, which provides stabilization effects in the enzyme microenvironment. Active and immobilized enzymes might enable (semi-)preparative scale production of valuable compounds thereby providing the means for applying biocatalysts in industry. Moreover, the reactivity of the immobilized biocatalysts might even be extended to different reaction conditions or alternative reaction media. Finally, it allows for facile application of biocatalysts in continuous processes and flow operations.

In this thesis, enzyme immobilization through metal-ion affinity binding is shown to facilitate the production of α -chiral amines in batch and flow operations. Enzyme selection, optimization, immobilization and application in the synthesis of α -chiral amines was performed using enzymes from the well-established family of ω -transaminases and the more recently developed group of AmDHs. Enzyme immobilization on a highly porous support material through metal-ion affinity binding proved suitable for improving amination reactions in aqueous reaction media. Compatibility of this immobilization strategy was proven by co-immobilization of dehydrogenase enzymes for the amination of alcohols. When utilizing transaminases, high catalytic activities and productivities were observed. The applicability of these immobilized enzymes was further extended to organic reaction media. Finally, reactions could be performed both in batch and in flow reactors leading to gram-scale synthesis of α -chiral amines in high optically pure form.

1.4 Thesis outline

Chapter 2 describes studies on identifying the optimal reaction conditions for the amination of prochiral ketones and aldehydes with AmDHs. The substrate scope of AmDHs was elucidated and the applicability of these enzymes was shown on semi-preparative

scale in a batch reaction.

Chapter 3 shows the improvement in applicability of AmDHs and ADHs as co-immobilized enzymes in the hydrogen-borrowing amination of alcohols. The enzymes were efficiently immobilized through metal-ion affinity binding on highly porous glass beads. The system showed high catalytic activity in batch reactions under the optimal reaction conditions. Recyclability proved limited, however, and the applied substrate concentrations have not yet met industrial requirements.

Chapter 4 demonstrates the use of metal-ion affinity immobilization as a versatile immobilization technique utilizing ω -transaminases. Highly active and stereo-complementary TAs were immobilized using an optimized procedure and parameters influencing the recovered enzyme activity were identified. Under the optimal reaction conditions the system showed excellent performance and recyclability both in batch as well as in flow reactors. Production rates of several grams per day were obtained through kinetic resolution of a racemic amine.

Chapter 5 extends the applicability of immobilized TAs to organic reaction media. In contrast to whole cell ω -TAs, which have been applied in organic solvent before, the use immobilized free ω -TAs on metal-ion affinity beads in organic solvents can be considered a novelty. An elegant reaction set-up was developed based on the use of hydrate salts, which precisely buffer the water content in the biocatalyst. High catalytic activity was observed in the reductive amination of phenoxyacetone utilizing isopropylamine as the amine donor. Further studies have indicated that higher reactivity can be obtained in non-polar and hydrophobic solvents. Substrate concentrations as high as 600 mM could be applied showing high productivities. Finally, immobilized ω -TA operated with good retention of activity in a continuous flow reactor.

1.5 References

- [1] a) Ghislieri, D.; Turner, N. J. *Topics in Catalysis*. **2013**, *57*, 284–300; b) Lawrence, S. A. *Amines: Synthesis, Properties and Applications*; Cambridge University Press; Cambridge, 2004.
- [2] a) Nugent, T. C.; El-Shazly, M. *Advanced Synthesis & Catalysis*. **2010**, *352*, 753–819; b) Nugent, T. C. *Chiral Amine Synthesis: Methods, Developments and Applications*; Wiley–VCH; Weinheim, Germany, 2010.
- [3] Hofmann, A. W. V. *Annalen der Chemie und Pharmacie*. **1851**, *78*, 253–286.

- [4] a) Kienle, M.; Dubbaka, S. R.; Brade, K.; Knochel, P. *European Journal of Organic Chemistry*. **2007**, 4166–4176; b) Buchwald, S. L.; Mauger, C.; Mignani, G.; Scholz, U. *Advanced Synthesis & Catalysis*. **2006**, *348*, 23–39; c) Navarro, O.; Marion, N.; Mei, J.; Nolan, S. P. *Chemistry*. **2006**, *12*, 5142–5148; d) Magano, J.; Dunetz, J. R. *Chemical Reviews*. **2011**, *111*, 2177–2250.
- [5] a) Sperotto, E.; Klink, G. P. V.; Koten, G. V.; Vries, J. G. D. *Dalton Trans.* **2010**, *39*, 10338–10351; b) Monnier, F.; Taillefer, M. *Angewandte Chemie International Edition*. **2008**, *47*, 3096–3099; c) Jiang, D.; Fu, H.; Jiang, Y.; Zhao, Y. *Journal of Organic Chemistry*. **2007**, *72*, 672–674.
- [6] a) Yadav, J. S.; Antony, A.; Rao, T. S.; Reddy, B. V. S. *Journal of Organometallic Chemistry*. **2011**, *696*, 16–36; b) Hesp, K. D.; Stradiotto, M. *ChemCatChem*. **2010**, *2*, 1192–1207; c) Alex, K.; Tillack, A.; Schwarz, N.; Beller, M. *ChemSusChem*. **2008**, *1*, 333–338.
- [7] Crozet, D.; Urrutigoity, M.; Kalck, P. *ChemCatChem*. **2011**, *3*, 1102–1118.
- [8] a) Das, S.; Zhou, S.; Addis, D.; Enthaler, S.; Junge, K.; Beller, M. *Topics in Catalysis*. **2010**, *53*, 979–984; b) Reguillo, R.; Grellier, M.; Vautravers, N.; Vendier, L.; Sabo-Etienne, S. *Journal of the American Chemical Society*. **2010**, *132*, 7854–7855.
- [9] a) Lou, X. B.; He, L.; Qian, Y.; Liu, Y. M.; Cao, Y.; Fan, K. N. *Advanced Synthesis & Catalysis*. **2011**, *353*, 281–286; b) Sharma, U.; Kumar, P.; Kumar, N.; Kumar, V.; Singh, B. *Advanced Synthesis & Catalysis*. **2010**, *352*, 1834–1840; c) Junge, K.; Wendt, B.; Shaikh, N.; Beller, M. *Chemical Communications*. **2010**, *46*, 1769–1771.
- [10] a) Wan, W.; Hou, J.; Jiang, H.; Yuan, Z.; Ma, G.; Zhao, G.; Hao, J. *European Journal of Organic Chemistry*. **2010**, *2010*, 1778–1786; b) Dangerfield, E. M.; Plunkett, C. H.; Win-Mason, A. L.; Stocker, B. L.; Timmer, M. S. *Journal of Organic Chemistry*. **2010**, *75*, 5470–5477; c) Steinhuebel, D.; Sun, Y.; Matsumura, K.; Sayo, N.; Saito, T. *Journal of the American Chemical Society*. **2009**, *131*, 11316–11317.
- [11] Schrittwieser, J. H.; Velikogne, S.; Kroutil, W. *Advanced Synthesis & Catalysis*. **2015**, *357*, 1655–1685.
- [12] Li, W.; Zhang, X. *Stereoselective Formation of Amines; Vol. 343*; Springer: Berlin, Heidelberg, 2014.
- [13] Breuer, M.; Ditrich, K.; Habicher, T.; Hauer, B.; Kessler, M.; Stürmer, R.; Zelinski, T. *Angewandte Chemie International Edition*. **2004**, *43*, 788–824.
- [14] a) Ogiwara, Y.; Uchiyama, T.; Sakai, N. *Angewandte Chemie International Edition*. **2016**, *55*, 1864–1867; b) Hoffmann, S.; Seayad, A. M.; List, B. *Angewandte Chemie International Edition*. **2005**, *44*, 7424–7427.
- [15] a) Adams, J. P.; Brown, M. J. B.; Diaz-Rodriguez, A.; Lloyd, R. C.; Roiban, G. D. *Advanced Synthesis & Catalysis*. **2019**, *361*, 2421–2432; b) Faber, K. *Biotransformations in Organic Chemistry*; 7 ed.; Springer International Publishing: Mannheim, Germany, 2018; c) Sheldon, R. A.; Brady, D. *ChemSusChem*. **2019**, *12*, 2859–2881; d) Narancic, T.; Davis, R.; Nikodinovic-Runic, J.; O' Connor, K. E. *Biotechnology Letters*. **2015**, *37*, 943–954.
- [16] a) Lutz, S.; Iamurri, S. M. *Protein Engineering. Methods in Molecular Biology; Vol. 1685*; Bormscheuer U. M., H. (Eds.); Humana Press: New York, 2018, p. 1–12; b) Cheng, F.; Zhu, L.; Schwaneberg, U.

Chemical Communications. **2015**, *51*, 9760–9772.

- [17] Sheldon, R. A.; Van Pelt, S.; Kanbak-Aksu, S.; Rasmussen, J. A.; Janssen, M. H. A. *Aldrichimica Acta*. **2013**, *46*, 81–93.
- [18] Britton, J.; Majumdar, S.; Weiss, G. A. *Chemical Society Reviews*. **2018**, *47*, 5891–5918.
- [19] a) Busto, E.; Gotor-Fernández, V.; Gotor, V. *Chemical Reviews*. **2011**, *111*, 3998–4035; b) Mata-Rodríguez, M.; Gotor-Fernández, V. *Science of Synthesis, 1: Biocatalysis in Organic Synthesis 1*; Faber, K. (Eds.); Thieme Verlagsgruppe; Stuttgart, 2015; c) Rantwijk, F. V.; Sheldon, R. A. *Tetrahedron*. **2004**, *60*, 501–519; d) Balkenhohl, F.; Hauer, B.; Ladner, W.; Pressler, U.; Nübling, C. *Racemate Cleavage of Primary and Secondary Amines by Enzyme-Catalysed Acylation*. EP0720655, July, 1999.
- [20] Patil, M. D.; Grogan, G.; Bommarium, A.; Yun, H. *ACS Catalysis*. **2018**, *8*, 10985–11015.
- [21] a) Guo, F.; Berglund, P. *Green Chemistry*. **2017**, *19*, 333–360; b) Slabu, I.; Galman, J. L.; Lloyd, R. C.; Turner, N. J. *ACS Catalysis*. **2017**, *7*, 8263–8284.
- [22] Groger, H. *Applied Microbiology and Biotechnology*. **2019**, *103*, 83–95.
- [23] Sharma, M.; Mangas-Sanchez, J.; Turner, N. J.; Grogan, G. *Advanced Synthesis & Catalysis*. **2017**, *359*, 2011–2025.
- [24] Crugeiras, J.; Rios, A.; Riveiros, E.; Richard, J. P. *Journal of the American Chemical Society*. **2009**, *131*, 15815–15824.
- [25] Haibin, C.; Collier, S. J.; Nazor, J.; Sukumaran, J.; Smith, D.; Moore, J. C.; Hughes, G. J.; Janey, J. M.; Huisman, G. W.; Novick, S. *Engineered Imine Reductases and Methods for the Reductive Amination of Ketone and Amine Compounds* US patent 2013/0302859, November, 2013.
- [26] Aleku, G. A.; France, S. P.; Man, H.; Mangas-Sanchez, J.; Montgomery, S. L.; Sharma, M.; Leipold, F.; Hussain, S.; Grogan, G.; Turner, N. J. *Nature Chemistry*. **2017**, *9*, 961–969.
- [27] Roiban, G.; Kern, M.; Liu, Z.; Hyslop, J.; Tey, P. L.; Levine, M. S.; Jordan, L. S.; Brown, K. K.; Hadi, T.; Ihnken, L. a. F.; Brown, M. J. B. *ChemCatChem*. **2017**, *9*, 4475–4479.
- [28] a) Cook, D. J.; Finnigan, J. D.; Cook, K.; Black, G. W.; Charnock, S. J. *Advances in Protein Chemistry and Structural Biology*. **2016**, *105*, 105–126; b) Busto, E.; Simon, R. C.; Richter, N.; Kroutil, W. *Green Biocatalysis*; Patel, R. N. (Eds.); Wiley-VCH; Weinheim, Germany, 2016, p. 17–57; c) Bartsch, S.; Vogel, A. *Science of Synthesis: Biocatalysis in Organic Synthesis*; Faber, K.; Fessner, W. D. Turner, N. J. (Eds.); George Thieme Verlag; Stuttgart, Germany, 2015; d) Zhang, R. K.; Huang, X.; Arnold, F. H. *Current Opinion in Chemical Biology*. **2019**, *49*, 67–75.
- [29] a) Cantone, S.; Ferrario, V.; Corici, L.; Ebert, C.; Fattor, D.; Spizzo, P.; Gardossi, L. *Chemical Society Reviews*. **2013**, *42*, 6262–6276; b) Gutarra, M. L. E.; Miranda, L. S. M.; De Souza, R. O. M. A. *Organic Synthesis Using Biocatalysis*; Goswami, A. Stewart, J. D. (Eds.); Elsevier; New York, US, 2016, p. 99–126.
- [30] Christensen, M. W.; Andersen, L.; Husum, T. L.; Kirk, O. *European Journal of Lipid Science and*

Technology. **2003**, *105*, 318–321.

- [31] Liese, A.; Hilterhaus, L. *Chemical Society Reviews*. **2013**, *42*, 6236–6249.
- [32] a) Dave, R.; Madamwar, D. *Process Biochemistry*. **2006**, *41*, 951–955; b) Hermanová, S.; Zarevúcká, M.; Bouša, D.; Pumera, M.; Sofer, Z. *Nanoscale*. **2015**, *7*, 5852–5858; c) Hosseini, S. H.; Hosseini, S. A.; Zohreh, N.; Yaghoubi, M.; Pourjavadi, A. *Journal of Agricultural Food Chemistry*. **2018**, *66*, 789–798.
- [33] Livage, J.; Coradin, T. *Handbook of Sol-Gel Science and Technology*; Klein L.; Aparicio M. A., J. (Eds.); Springer, Cham, 2018, p. 2909–2931.
- [34] Cassimjee, K. E.; Trummer, M.; Branneby, C.; Berglund, P. *Biotechnology and Bioengineering*. **2008**, *99*, 712–716.
- [35] Thompson, M. P.; Peñafiel, I.; Cosgrove, S. C.; Turner, N. J. *Organic Process Research & Development*. **2019**, *23*, 9–18.
- [36] Santos, J. C. S. D.; Barbosa, O.; Ortiz, C.; Berenguer-Murcia, A.; Rodrigues, R. C.; Fernández-Lafuente, R. *ChemCatChem*. **2015**, *7*, 2413–2432.
- [37] Hanefeld, U.; Gardossi, L.; Magner, E. *Chemical Society Reviews*. **2009**, *38*, 453–468.
- [38] a) Sintra, T. E.; Ventura, S. P. M.; Coutinho, J. a. P. *Journal of Molecular Catalysis B*. **2014**, *107*, 140–151; b) Schoffelen, S.; Hest, J. C. M. V. *Soft Matter*. **2012**, *8*, 1736–1746.
- [39] Cao, L. *Carrier–Bound Immobilized Enzymes: Principles, Application and Design*; Wiley–VCH; Weinheim, Germany, 2005.
- [40] Mateo, C.; Torres, R.; Fernández-Lorente, G.; Ortiz, C.; Fuentes, M.; Hidalgo, A.; Lopez-Gallego, F.; Abian, O.; Palomo, J. M.; Betancor, L.; Pessela, B. C.; Guisan, J. M.; Fernández-Lafuente, R. *Biomacromolecules*. **2003**, *4*, 772–777.
- [41] Galaev, I.; Mattiasson, B. *Smart Polymers for Bioseparation and Bioprocessing*; Taylor & Francis, CRC Press; London, 2001.
- [42] Margolin, A. L.; Navia, M. A. *Angewandte Chemie International Edition*. **2001**, *40*, 2204–2222.
- [43] Sheldon, R. A. *Catalysts*. **2019**, *9*, 261.
- [44] Sheldon, R. A. *Applied Microbiology and Biotechnology*. **2011**, *92*, 467–477.
- [45] Xu, M. Q.; Wang, S. S.; Li, L. N.; Gao, J.; Zhang, Y. W. *Catalysts*. **2018**, *8*, 460.
- [46] a) Talekar, S.; Ghodake, V.; Ghotage, T.; Rathod, P.; Deshmukh, P.; Nadar, S.; Mulla, M.; Ladole, M. *Bioresource Technology*. **2012**, *123*, 542–547; b) Tudorache, M.; Nae, A.; Coman, S.; Parvulescu, V. I. *RSC Advances*. **2013**, *3*, 4052–4058; c) Lee, J.; Na, H. B.; Kim, B. C.; Lee, J. H.; Lee, B.; Kwak, J. H.; Hwang, Y.; Park, J.; Gu, M. B.; Kim, J.; Joo, J.; Shin, C.; Grate, J. W.; Hyeon, T.; Kim, J. *Journal of Materials Chemistry*. **2009**, *19*, 7864–7870
- [47] a) Datta, S.; Christena, L. R.; Rajaram, Y. R. S. *3 Biotech*. **2013**, *3*, 1–9; b) Zdarta, J.; Meyer, A. S.;

- Jesionowski, T.; Pinelo, M. *Catalysts*. **2018**, *8*, 92.
- [48] Pierre, A. C.; Pajonk, G. M. *Chemical Reviews*. **2002**, *102*, 4243–4266.
- [49] Lozinsky, V. I.; Plieva, F. M. *Enzyme and Microbial Technology*. **1998**, *23*, 227–242.
- [50] Krasňan, V.; Stloukal, R.; Rosenberg, M.; Rebroš, M. *Applied Microbiology and Biotechnology*. **2016**, *100*, 2535–2553.
- [51] Elnashar, M. M. M. *The Art of Immobilization Using Biopolymers, Biomaterials and Nanobiotechnology*; IntechOpen, 2011, Available from: <https://www.intechopen.com/books/biotechnology-of-biopolymers/the-art-of-immobilization-using-biopolymers-biomaterials-and-nanobiotechnology>.
- [52] Katchalski-Katzir, E.; Kraemer, D. M. *Journal of Molecular Catalysis B*. **2000**, *10*, 157–176.
- [53] Kirk, O.; Christensen, M. W. *Organic Process Research & Development*. **2002**, *6*, 446–451.
- [54] a) Kreiner, M.; Parker, M. C. *Biotechnology Letters*. **2005**, *27*, 1571–1577; b) Hartmann, M.; Kostrov, X. *Chemical Society Reviews*. **2013**, *42*, 6277–6289; c) Zhou, Z.; Hartmann, M. *Topics in Catalysis*. **2012**, *55*, 1081–1100.
- [55] Bilal, M.; Zhao, Y.; Rasheed, T.; Iqbal, H. M. N. *International Journal of Biological Macromolecules*. **2018**, *120*, 2530–2544.
- [56] Mei, Y.; Miller, L.; Gao, W.; Gross, R. A. *Biomacromolecules*. **2003**, *4*, 70–74.
- [57] Hilterhaus, L.; Minow, B.; Müller, J.; Berheide, M.; Quitmann, H.; Katzer, M.; Thum, O.; Antranikian, G.; Zeng, A. P.; Liese, A. *Bioprocess and Biosystems Engineering*. **2008**, *31*, 163–171.
- [58] a) Buchholz, K.; Kasche, V.; Bornscheuer, U. T. *Biocatalysts and Enzyme Technology*; 2nd ed.; Wiley-VCH; Weinheim, Germany, 2012; b) Bommarius, A. S.; Riebel, B. R. *Biocatalysis: Fundamentals and Applications*; Wiley-VCH; Weinheim, Germany, 2004; c) Bailey, J.; Bailey, J. E.; Ollis, D. F.; Simpson, R. J. *Biochemical Engineering Fundamentals*; 2nd ed.; McGraw-Hill; New York, 1986.
- [59] Roon, J. L. V.; Arntz, M. M.; Kallenberg, A. I.; Paasman, M. A.; Tramper, J.; Schroën, C. G.; Beeftink, H. H. *Applied Microbiology and Biotechnology*. **2006**, *72*, 263–278.
- [60] Wiemann, L. O.; Weisshaupt, P.; Nieguth, R.; Thum, O.; Ansorge-Schumacher, M. B. *Organic Process Research & Development*. **2009**, *13*, 617–620.
- [61] Plutschack, M. B.; Pieber, B.; Gilmore, K.; Seeberger, P. H. *Chemical Reviews*. **2017**, *117*, 11796–11893.

Chapter 2

Reductive amination of carbonyl compounds by amine dehydrogenases

This chapter is based on the following publication:

Knaus, T.†; Böhmer, W.†; Mutti, F. G., *Green Chemistry*. **2017**, *19*, 453–463.

† Both authors contributed equally to this work

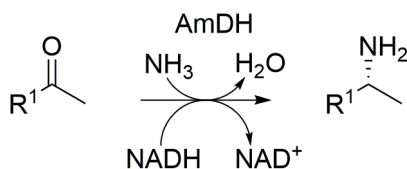
Supporting information is available under; doi: [10.1039/C6GC01987K](https://doi.org/10.1039/C6GC01987K)

2.1 Introduction

Amine dehydrogenases (AmDHs) are nicotinamide adenine dinucleotide (NAD)-dependent enzymes that catalyze the reductive amination of aldehydes and ketones at the expense of ammonia as the nitrogen source (Scheme 2.1). The cofactor is usually recycled in situ by coupling with an enzyme-catalyzed oxidation of a co-substrate, such as the transformation of glucose to gluconolactone catalyzed by a glucose dehydrogenase or the transformation of formate to carbon dioxide catalyzed by a formate dehydrogenase^[1]. Both methodologies are shifting the equilibrium to the formation of the desired products^[2]. AmDHs possess tremendous potential for the development of the next generation of processes for the synthesis of α -chiral amines^[3]. The applicability of this class of enzymes in organic synthesis has been demonstrated in notable studies through the use of isolated enzymes^[4], immobilized enzymes^[5] or whole-cell biocatalysts^[6]. In addition, AmDHs have been shown to possess the capability of synthesizing primary as well as secondary amines^[7].

Although AmDHs are rarely found in nature, a natural occurring amine dehydrogenase was isolated and purified from *Streptomyces virginiae* IFO 12827 strain^[8]. This AmDH was able to accept a broad range of substrates including various aldehydes, ketones, keto acids, and keto alcohols. However, no further studies were conducted due to poor reproducibility. It was several decades later that a panel of engineered AmDHs was created starting from wild-type amino acid dehydrogenases as scaffolds, such as leucine dehydrogenases^[9] or phenyl alanine dehydrogenases^[10]. One other natural AmDH was discovered from *Petrotoga mobiliz* sp. DSM 10674 and it catalyzes the reductive amination of ketones without the carboxylic group in α or β position^[11]. Additionally, a panel of native AmDHs was discovered that are evolutionarily unrelated to the engineered AmDHs^[12].

Engineered AmDHs were generated from wild-type amino acid dehydrogenase scaffolds using protein engineering strategies. As an initial protein scaffold leucine dehydrogenase from *Bacillus stearothermophilus* was used for altering the substrate specificity through



Scheme 2.1. Amine dehydrogenases catalyze the reductive amination of ketones and aldehydes to chiral amines utilizing a catalytic amount of nicotinamide coenzyme, which is recycled in situ.

saturation mutagenesis ^[9a]. The most active variant (L-AmDH; K68S/E114V/N261L/V291C) was able to produce (*R*)-1,3-dimethylbutylamine with 93% conversion and >99% *ee* from prochiral methyl isobutyl ketone. In addition, it showed complete loss of activity for the natural substrate leucine. Subsequently, another AmDH was developed using a phenylalanine dehydrogenase from *Bacillus badius* ^[10a] by introducing a double mutation (K77M/N276V) which enabled not only the amination of methyl isobutyl ketone, but also that of *p*-fluorophenyl-2-propanone. Further improvements by using focused mutagenesis generated Bb-PhAmDH (K77S/N276L) which showed an improved activity towards the reductive amination of phenoxy-2-propanone, 2-hexanone, and 3-methyl-2-butanone ^[10a, 13]. Nevertheless, both AmDHs (L-AmDH and Bb-PhAmDH) were poorly catalytically active towards benzylic ketones. Therefore, a chimeric AmDH was generated by domain shuffling of the substrate binding pocket from Bb-PhAmDH and the cofactor binding domain from L-AmDH ^[9b]. The chimeric AmDH (Ch1-AmDH) was catalytically active towards *p*-fluorophenyl-2-propanone, but also accepted acetophenone and adamantylmethylketone. The k_{cat} of Ch1-AmDH was further improved towards *p*-fluorophenyl-2-propanone by mutation of two adjacent asparagine residues (N270L/N271L). In later studies, other AmDHs were engineered from phenylalanine dehydrogenase scaffolds. AmDH from *Rhodococcus* species (Rs-PhAmDH) was generated by the mutation of K66 and N262 residues ^[9c]. One triple variant (K66Q/S149G/N262C) showed catalytic activity towards phenyl-2-propanone and 1-phenyl-3-methylpropan-2-one obtaining the corresponding chiral α -amines with elevated enantioselectivities (>98% *ee*). Another AmDH was generated from a phenylalanine dehydrogenase from *Caldalkalibacillus thermarum* showing significantly increased thermostability compared to Bb-PhAmDH ^[10b]. This AmDH was subsequently employed in the large-scale synthesis of (*R*)-phenoxy-2-propylamine (400 mM) utilizing a biphasic system (>99% *ee*). Finally, it is notable that only (*R*)-selective engineered AmDHs have been developed so far.

Initial reaction rates for engineered AmDHs were determined for the amination of a limited number of ketones, but a systematic investigation on the substrate acceptance, optimal reaction conditions as well as chemo- and stereoselectivity of the known AmDHs had not been undertaken. This chapter aims at providing this knowledge and at showing the potential of AmDHs for the efficient asymmetric synthesis of α -chiral amines. Biocatalytic reductive amination of carbonyl compounds was performed employing three distinct AmDHs operating in tandem with a formate dehydrogenase from *Candida boidinii* (Cb-

FDH) for recycling of the nicotinamide coenzyme (Table 2.1): 1) AmDH variant originated from the wild-type L-phenylalanine dehydrogenase from *Bacillus badius* (Bb-PhAmDH)^[9a], 2) the variant originated from the L-phenylalanine dehydrogenase from *Rhodococcus* sp. M4^[9c] (Rs-PhAmDH) and 3) the chimeric AmDH (Ch1-AmDH) obtained by domain shuffling of Bb-PhAmDH with a variant from the leucine dehydrogenase from *Bacillus stearothermophilus*^[9b]. This dual-enzyme system (AmDH – Cb-FDH) possesses elevated atom efficiency as it utilizes ammonium formate buffer as the source of both nitrogen and reducing equivalents and inorganic carbonate as the sole by-product. Efficient amination of a range of diverse aliphatic, aromatic and bicyclic ketones and a small panel of aldehydes was achieved with up to quantitative conversion and elevated turnover numbers (TONs). The reductive amination of prochiral ketones proceeded with perfect stereoselectivity, always affording the (*R*)-configured amines with more than 99% enantiomeric excess with the exception of a select number of cases that showed formation of the (*S*)-configured amine.

2.2 Optimization of the reaction conditions

The most elevated reaction rates for the reductive amination of (*p*-fluorophenyl)acetone (**1a**) catalyzed by Bb-PhAmDH, were observed in ammonium chloride and ammonium formate at pH between 8.2 and 8.8. Ca. 700 mM of ammonium cation/ammonia was required to achieve >99% conversion at 30 °C^[4a]. In that case, NAD⁺ was applied in catalytic amount (1 mM) and recycled using glucose (60 mM) and a commercial engineered glucose dehydrogenase (GDH). Nevertheless, the reaction with glucose as cosubstrate generates a stoichiometric amount of gluconic acid, hence reducing the atom economy of the reaction^[14]. Furthermore, a large amount of GDH (300 U mL⁻¹) had to be employed for sustaining the amination in ammonium buffer (pH 8.7, >700 mM) due to mediocre stability of the GDH enzyme under the reaction conditions. Consequently, a recycling system based on formate and formate dehydrogenase (FDH, recombinant enzyme from *Candida boidinii*^[15]) was envisioned to be the preferable alternative, because formate can be used in the reaction buffer as counteranion of the ammonium species. Moreover, these new experiments showed that an extremely low amount of FDH (2.0 – 3.0 U mL⁻¹) was sufficient to obtain a quantitative amination. Therefore, the performance of the reductive amination in the following cases was determined: 1) glucose/GDH (150 U) as system for the recycling of NADH in ammonium chloride buffer (pH 8.7, 1 M); 2) glucose/GDH (150 U) in ammonium formate buffer (pH 8.5, 1 M) and 3) formate/FDH (purified, 14 μM equal to 1.5 U) in ammonium formate buffer (pH

8.5, 1 M), (for details, Supporting Information section S5.2 and S5.3). This investigation was extended to all of the three AmDHs: 1) Bb-PhAmDH, 2) Rs-PhAmDH^[9c] and 3) Ch1-AmDH^[9b]. The reductive aminations were carried out with a representatively active substrate for each AmDH, *p*-fluorophenyl-2-propane (**1a**) for Bb-PhAmDH, 4-phenylbutan-2-one (**24a**) for Rs-PhAmDH and 2-heptanone (**11a**) for Ch1-AmDH. The initially tested reaction conditions were: substrate concentration (20 mM), NAD⁺ concentration (1 mM), AmDH concentration (80 - 130 μM) and ammonium buffer (1 M), at 30 °C, for 24 h. Under these reaction conditions it was not possible to reach quantitative conversion (within 21 h) using the glucose/GDH recycling system in ammonium chloride buffer with any of the three AmDHs, despite the use of 3 equivalents of glucose (Table 2.1, entries 1, 5 and 9). Interestingly, switching from ammonium chloride to ammonium formate and maintaining the same composition of the reaction mixture resulted in quantitative conversion for the amination of substrates **24a** and **11a** with Rs-PhAmDH and Ch1-AmDH respectively (Table 2.1, entries 6 and 10). However, no improvement was observed in the case of Bb-PhAmDH (Table 2.1, entry 2). When the third, preferred, option with formate as cosubstrate was tested, all the amination reactions afforded the related product with >99% conversion (Table 2.1, entries 3, 7 and 11). Probably due to its higher stability in ammonium/ammonia buffer at pH 8.5, the employed Cb-FDH^[15] was able to recycle NADH more efficiently than GDH. Notably,

Table 2.1. Optimization of the AmDH – FDH dual-enzyme system. The influence of the composition of the buffer solution, the enzyme loading and the substrate concentration was investigated.

Entry	Enzyme	Substrate	Substr. conc. [mM]	Enzyme conc. [μM]	Coenzyme/buffer system	Conv. [%]	ee% (R)
1	Bb	1a	20	115	GDH/NH ₄ Cl	79	>99
2	Bb	1a	20	115	GDH/HCOONH ₄	76	>99
3	Bb	1a	20	115	FDH/HCOONH ₄	>99	>99
4	Bb	1a	50	115	FDH/HCOONH ₄	88	>99
5	Rs	24a	20	130	GDH/NH ₄ Cl	72	>99
6	Rs	24a	20	130	GDH/HCOONH ₄	>99	>99
7	Rs	24a	20	130	FDH/HCOONH ₄	>99	>99
8	Rs	24a	50	50	FDH/HCOONH ₄	>99	>99
9	Ch1	11a	20	80	GDH/NH ₄ Cl	61	>99
10	Ch1	11a	20	80	GDH/HCOONH ₄	99	>99
11	Ch1	11a	20	80	FDH/HCOONH ₄	>99	>99
12	Ch1	24a	50	32	FDH/HCOONH ₄	98	>99

Reaction conditions: NAD⁺ (1 mM); recycling enzyme (GDH or FDH) in ammonium chloride buffer (1 M, pH 8.7) or ammonium formate buffer (1 M, pH 8.5); reaction volume 0.5 mL, T 30 °C, reaction time 24 h; agitation on an orbital shaker (180 rpm).

the stereoselective outcome of the reaction was perfect in all cases (Table 2.1, >99% (*R*)).

Aiming at increasing the overall catalytic efficiency of the reductive amination under the optimized reaction conditions, the concentration of the substrate was gradually increased up to 50 mM and the same concentration of AmDH (80 - 130 μ M) was maintained. Rs-PhAmDH and Ch1-AmDH converted the substrates **24a** and **11a** (50 mM), respectively, with >99% conversion and perfect stereoselectivity (>99% (*R*)) within 21 h (Supporting Information section S5.4). In contrast, Bb-PhAmDH was less efficient as the conversion of **1a** at 50 mM concentration slightly dropped to 88% within 21 h reaction time (Table 2.1, entry 4 and full data set in Supporting Information section S5.4). Finally, the catalyst loading was reduced for the reductive amination employing Rs-PhAmDH and Ch1-AmDH. The amination of **24a** and **11a** (50 mM) proceeded quantitatively within 21 h using 50 μ M of Rs-PhAmDH and 32 μ M of Ch1-AmDH, respectively. Additionally, the concentration of Cb-FDH could be lowered to only 9.5 μ M, still providing the same conversion.

2.3 Influence of the temperature and time studies

Under the selected reaction conditions (ammonium formate buffer pH 8.5, 1 M; substrate concentration 50 mM; NAD⁺ 1 mM; Cb-FDH 14 μ M; varied concentration of AmDHs), the influence of the temperature on the progress of the reductive amination was studied. It is probable that an increase in the temperature might accelerate the kinetics of the reaction, whereas an excessive temperature may be detrimental for the stability of the enzymes. The progress for the reductive amination of **1a** (50 mM) using Bb-PhAmDH (46 μ M) showed a consistent increase in the reaction rate when the temperature was raised from 20 °C, to 30 °C and finally 40 °C (Figure 2.1A). The conversion increased almost linearly over time for every temperature tested. Furthermore, the final conversion (taken after 24 h) at 40 °C doubled the value observed at 20 °C (83% vs. 37%). Nonetheless, the progress of the reaction at 50 °C was worse than at 20 °C, leading to a mediocre conversion of 21 % after 24 h. A further increase of the temperature up to 60 °C provoked a complete loss of the enzymatic activity (Supporting Information section S5.6). This lack of conversion at 60 °C cannot be attributed to the deactivation of Cb-FDH or the decomposition of the coenzyme NAD, because the reductive amination performed well up to 60 °C using Ch1-AmDH (Figure 2.1C). Furthermore, the data are in agreement with the previously reported profile of activity vs. stability of Bb-PhAmDH that shows a rapid denaturation of the enzyme above 50 °C [10a].

The reaction profiles for the reductive amination of substrates **24a** and **11a** (50 mM) with Rs-PhAmDH (48 μ M) and Ch1-AmDH (33 μ M), respectively, were significantly different. For both Rs-PhAmDH and Ch1-AmDH, the conversions increased hyperbolically over time (Figure 2.1B and 2.1C). In particular, Rs-PhAmDH is an extremely active enzyme on substrate **24a**. Considering the first hour of the reaction, wherein the conversion correlated linearly with time, the maximum turnover frequency (TOF) was reached already at 20 °C. In particular the increase of the temperature in the range 20 °C, 30 °C, 40 °C and 50 °C always led to the same conversion after 1 h (varying from 80% - 83%). Quantitative conversion (>98%) of **24a** was obtained at 20 °C and 30 °C within 3 h (Figure 2.1B and Supporting Information section S5.7). The efficiency at 40 °C was slightly lower as the reaction required 5 h to reach 99% conversion. In contrast, the kinetics of the reaction was negatively influenced at 50 °C with a drop in catalytic activity after 1 h. An additional 29 h were required to increase the conversion from 83% (after 1h) to 98% (after 30 h) at this temperature. The activity of Rs-PhAmDH was affected at 60 °C as the conversion raised smoothly, reaching a maximum of 93% only after 30 h. Conversely, the chimeric enzyme Ch1-AmDH performed the amination of **11a** almost equally well in the range of temperatures investigated that spans from 30 °C to 60 °C. After 5 h the conversion was above 90% for the aminations at 30 °C, 40 °C and 50 °C and reached 82% at 60 °C. The rate of the reductive amination, instead, was lower at 20 °C. Nevertheless, only with Ch1-AmDH, quantitative conversion (>98%) was obtained at every temperature from 20 °C to 60 °C at the end of the reaction (30 h, Supporting Information section S5.8). Only at 70 °C a mediocre conversion of 8% was observed after 18 h. These observations are in agreement with the previously determined half-life of 40 min for Ch1-AmDH at 70 °C [9b]. Regardless to the degree of conversion, the type of AmDH enzyme and substrate employed, the enantiomeric excess was not affected by the reaction time or the temperature and was always more than >99% for the *R*-configured amine product.

2.4 Substrate scope of the reductive amination using AmDHs

The initial reaction rates for the reductive amination of a limited number of carbonyl compounds and the oxidative deamination of a few amines catalyzed by AmDHs have been previously measured [9a, 10a]. However, a study describing the substrate scope of these enzymes for the organic synthesis of amines from prochiral ketones and aldehydes were not published. Moreover, the information regarding the stereoselectivity for the amination with AmDHs was limited to a very few compounds. Therefore, in this research, an extensive

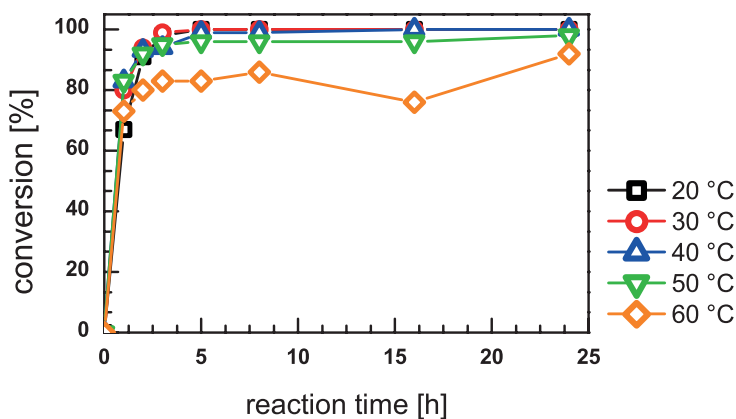
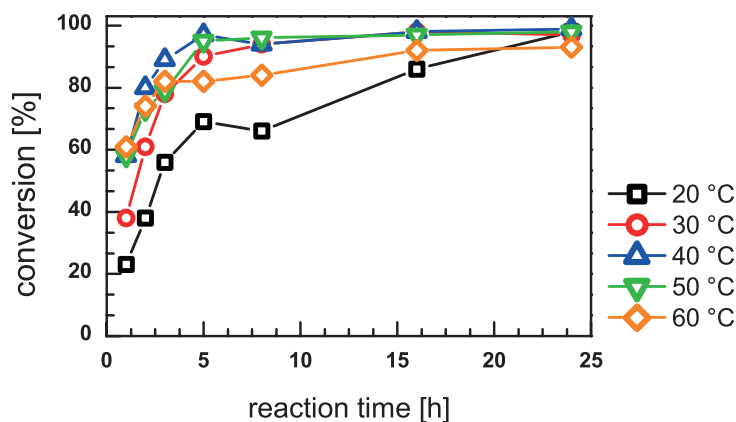
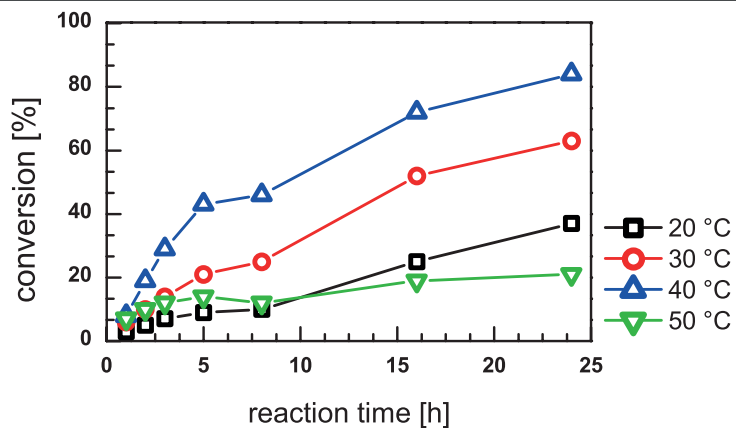


Figure 2.1. Progress of the reaction versus the time for the reductive amination of: A) **1a** using Bb-PhAmDH (46 μM), B) **24a** using by Rs-PhAmDH (48 μM), and C) **11a** using Ch1-AmDH (33 μM). The study was carried out at different temperatures: 20 °C (**black**), 30 °C (**red**), 40 °C (**blue**), 50 °C (**green**), and 60 °C (**orange**). Reaction conditions: substrate (50 mM), ammonium formate buffer (reaction volume; 0.5 mL, 1 M, pH 8.5), Cb-FDH (14 μM), NAD⁺ (1 mM), T 30 °C, agitation on an orbital shaker (180 rpm).

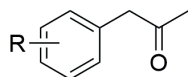
library of structurally diverse prochiral ketones was tested, such as phenylacetone derivatives (**1a–6a**, Table 2.2), aliphatic methyl ketones (**7a–13a**, Table 2.3), acetophenone derivatives (**14a–21a**, Table 2.4), a selection of more sterically demanding and bicyclic ketones (**22a–32a**, Table 2.5), and a few aldehydes (**33a–37a**, Table 2.6). The substrate concentration was kept at 50 mM, whereas the amount of enzyme and the reaction time was varied in order to achieve maximum efficiency (i.e., highest ratio [S]/[E] with highest conversion).

First, the family of phenylacetone derivatives was examined (Table 2.2). It was previously shown that Bb-PhAmDH accepts **1a** as the best substrate^[10a]. In an independent experiment (Table 2.2, entry 3), Bb-PhAmDH (50 μ M) converted **1a** (50 mM) to 93% of the amine product **1b** within 48 h (>99% (*R*)). Hence, other substituted phenylacetone derivatives could most likely be converted by Bb-PhAmDH as well. Indeed, Bb-PhAmDH converted *ortho*-, *meta*- and *para*-methoxy substituted phenylacetone derivatives (**2a–4a**), but the conversion within 48 h was mediocre (from 3% to 21%; Table 2.2, entries 6, 9, and 12). Bb-PhAmDH also accepted **5a** (7% conversion), whilst **6a** was not converted at all (Table 2.2, entries 15 and 18). Surprisingly the chimeric enzyme Ch1-AmDH, known to be active on aliphatic ketones^[4a] and acetophenone derivatives^[9b], was a superior catalyst for the amination of **1a**. Compared to the amination with Bb-PhAmDH, Ch1-AmDH afforded the product (*R*)-**1b** with the same conversion but in half of the reaction time (24 h) and at a significantly lower enzyme loading (30 μ M, Table 2.2, entry 1). Ch1-AmDH was also the best catalyst for the amination of **2a** that reached quantitative conversion in 48 h (Table 2.2, entry 4). Substrates **3a–5a** were moderately converted and Ch1-AmDH showed no activity towards **6a** (Table 2.2, entries 7, 10, 13, and 16). The third AmDH from this study, Rs-PhAmDH, was developed and tested previously only for the reductive amination of **24a** (Table 2.5, entry 6)^[9c]. In this study, we show that Rs-PhAmDH possesses a much wider substrate scope than reported before and it proved to be superior compared with Bb-PhAmDH in terms of substrate acceptance. Substrates **3a**, **4a**, **5a** and **6a** were converted with elevated conversions (\geq 98%) and excellent stereoselectivity (>99% (*R*); Table 2.2, entries 8, 11, 14, and 17). Interestingly, Rs-PhAmDH showed no activity towards **2a** (Table 2.2, entry 5), but the lower acceptance of **1a** is in accordance with previously reported data (Table 2.2, entry 2)^[9c].

Conversion of aliphatic methyl ketones by AmDHs revealed a similar trend (Table 2.3). Ch1-AmDH and Rs-PhAmDH were most active on the less sterically demanding aliphatic ketones. Substrates bearing a medium length linear chain such as **10a** and **11a** were

efficiently converted by Ch1-AmDH (30 μM) within 24 h (Table 2.3, entries 7 and 9). Rs-PhAmDH only showed lower conversion for **10a** (Table 2.3, entry 8). Ketones bearing a shorter linear chain (**7a** and **8a**) were accepted better by Ch1-AmDH than by RsPhAmDH; however, elevated concentration of enzyme was required (130 μM , Table 2.3, entries 1-4). The branched aliphatic ketone **9a** was accepted equally well by both enzymes (Table 2.3 entries 5 and 6). Conversely, longer chain ketones, such as **13a**, proved to be more challenging (Table 2.3, entry 13), albeit Rs-PhAmDH (50 μM) aminated **13a** with elevated conversion (93%, Table 2.3, entry 14). As an example of an aliphatic and more sterically demanding ketone, **12a** was tested. In this case, Ch1-AmDH was the most active enzyme (Table 2.3, entry 11) in agreement with the general trend of substrate acceptance observed for this

Table 2.2. Reductive amination of phenyl 2-propanone derivatives (**1a–6a**) employing AmDHs.



1a: R = *p*-F; **2a:** R = *o*-OCH₃;

3a: R = *m*-OCH₃; **4a:** R = *p*-OCH₃;

5a: R = *p*-CH₃; **6a:** R = *m*-CF₃.

Entry	Substrate	Enzyme	Enzyme conc. [μM]	Reaction time [h]	Conversion [%]	ee% (R)
1	1a	Ch1	32	24	93	>99
2		Rs	51	24	79	>99
3		Bb	50	48	93	>99
4	2a	Ch1	129	48	>99	>99
5		Rs	51	24	0	n.m.
6		Bb	50	48	10	>99
7	3a	Ch1	32	24	47	88
8		Rs	51	24	98	>99
9		Bb	50	48	21	>99
10	4a	Ch1	32	24	50	>99
11		Rs	51	24	>99	>99
12		Bb	50	48	3	n.d.
13	5a	Ch1	32	24	37	>99
14		Rs	129	48	98	>99
15		Bb	50	48	7	98
16	6a	Ch1	32	24	1	n.m.
17		Rs	129	48	98	>99
18		Bb	50	48	0	n.m.

Reaction conditions: substrate (50 mM), AmDH (30-130 μM), Cb-FDH (14 μM), ammonium formate buffer (1 M, pH 8.5), T 30°C, agitation on an orbital shaker (180 rpm).

enzyme. Notably, an AmDH from *Lysinibacillus fusiformis* (Lf-AmDH) was generated in a later study that showed good acceptance of longer linear chain aliphatic methyl ketones ^[9d].

For acetophenone derivatives (Table 2.4), the type and position of the substituents on the phenyl ring was particularly important for the amination catalyzed by AmDHs, possibly due to the existence of resonance and field effects ^[16]. This phenomenon is often not considered for enzymatic reactions and low catalytic rates are sometimes attributed solely to intrinsic low enzymatic turnovers (k_{cat}) or poor binding affinity of the substrate to the active site of the enzyme. In contrast, a number of publications on the reactivity of acetophenone derivatives with other oxidoreductases such as alcohol dehydrogenases showed that resonance and field effects can play a major role ^[17]. Ch1-AmDH and Rs-PhAmDH turned out to be the most efficient enzymes for the amination of acetophenone derivatives (Table 2.4), albeit requiring a higher amount of enzyme (up to 130 μ M) for obtaining moderate

Table 2.3. Reductive amination of aliphatic methyl ketones (**7a–13a**) employing AmDHs.



$\text{R}^2 = \text{CH}_3$;

8a: $\text{R}^1 = n$ -propyl; **9a**: $\text{R}^1 = iso$ -propyl;

10a: $\text{R}^1 = n$ -butyl; **11a**: $\text{R}^1 = n$ -pentyl;

12a: $\text{R}^1 = n$ -butyl; $\text{R}^2 = \text{CH}_2\text{CH}_3$; **13a**: $\text{R}^1 = n$ -hexyl.

Entry	Substrate	Enzyme	Enzyme conc. [μ M]	Reaction time [h]	Conv. [%]	ee% (<i>R</i>)
1	7a	Ch1	32	24	8	n.d.
2		Rs	51	24	4	n.d.
3	8a	Ch1	129	48	75	>99
4		Rs	51	24	15	98
5	9a	Ch1	129	48	96	>99
6		Rs	129	48	90	>99
7	10a	Ch1	32	24	92	>99
8		Rs	51	24	67	>99
9	11a	Ch1	32	24	98	>99
10		Rs	51	24	99	>99
11	12a	Ch1	92	48	57	>99
12		Rs	103	48	32	>99
13	13a	Ch1	32	48	50	>99
14		Rs	51	48	93	>99

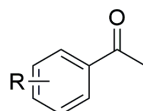
Reaction conditions: substrate (50 mM), AmDH (30-130 μ M), Cb-FDH (14 μ M), ammonium formate buffer (1 M, pH 8.5), T 30°C, agitation orbital shaker (180 rpm).

conversions. Substrate **17a**, possessing electron donating character, was converted at lower extent by Ch1-AmDH (9%, Table 2.4, entry 8) compared with **18a** (43%, Table 2.4, entry 10) which bears an electron withdrawing substituent. Furthermore, **21a** bearing an even higher electron donating substituent than **17a**^[16-17], was not converted at all (Table 2.4, entries 16). This electronic influence of aryl substituents on the outcome of the reaction has strong correlation with the expected trend from Hammett substituent constants. When excluding steric effects, *m*-CH₃ ($\sigma_m = -0.07$) and *p*-CH₃ ($\sigma_p = -0.17$) substituents have a negative effect on the formation of the imine intermediate in reductive amination where *m*-F ($\sigma_m = 0.34$) and *p*-F ($\sigma_p = 0.06$) substituents should have a more positive effect compared to the non-substituted aryl ring (R = H, $\sigma_m = \sigma_p = 0$)^[18]. Moreover, the higher conversions obtained with **16a** (as compared to **17a**) and with **18a** (as compared to **19a**) are supported by the Hammett values. Notably, Hammett substituent constants were determined for substituents on the aryl ring of benzoic acid, but apply also for substituted benzene derivatives. Although not based on a more rigorous determination of the initial reaction rates, this study suggests that enzymatic reductive amination with AmDHs is favored by delocalization of a higher partial positive charge on the reactive carbonyl carbon. This assumption is further supported by the fact that the same electronic influence of substituents was found for the reduction of acetophenone to alcohols catalyzed by alcohol dehydrogenases (ADH)^[17, 19]. Moreover, both ADHs and AmDHs belong to the class of the oxidoreductases (EC1) and share the same cofactor (NAD) and a similar reaction mechanism. None of the AmDHs from this study accepted **15a** as a substrate, indicating that steric effects caused by substituents in the *ortho*-position might play a significant role as well (Table 2.4, entries 3 and 4). Finally, Rs-PhAmDH showed no activity towards acetophenone derivatives as was expected from initial activity tests on its substrate acceptance (Table 2.4)^[9c].

The reactivity of the AmDHs was investigated on more sterically demanding and bicyclic substrates. Bulky-bulky ketones (**12a**, **23a**, **27a** and **28a**) (Table 2.5) were reported as challenging substrates for other aminating enzymes, such as ω -transaminases (ω -TAs). Natural occurring ω -TAs seem to accept mainly ketones possessing a bulky group on one side and a small methyl group on the other side^[20]. Alternatively, wild-type ω -TAs are active on bicyclic ketones^[21]. Several engineered ω -TAs have been generated recently by changing amino acid residues in the small^[22] and large^[23] substrate binding pockets of the active site. Notably, wild-type ω -TAs were engineered for accepting bulky-bulky substrates as well^[20f, 24]. Our study showed that AmDHs share a limitation in relation to converting bulky-

bulky ketones. All tested bulky-bulky ketones bearing the carbonyl moiety in conjugation with the phenyl ring, such as **22a**, **25a** and **26a**, were either not accepted or afforded mediocre conversions (Table 2.5, entries 1, 2, 7-10). Conversely, when the carbonyl moiety was positioned further away from the aromatic ring, amination was efficiently performed by Rs-PhAmDH (90-130 μ M). For example, **23a**, **27a** and **28a** afforded the amine product up to >99% conversion and perfect stereoselectivity (>99% (*R*)), (Table 2.5, entries 4, 12 and 14). In contrast, Bb-PhAmDH and Ch1-AmDH were poorly active on these substrates or not active at all (Table 2.5, entries 5, 11, and 13). Despite slight specific activity of Ch1-AmDH for **29a** was reported previously^[9b], bicyclic ketones **29a–32a** were not accepted by the AmDHs from this study (Table 2.5, entries 15-22). In a later study, another AmDH

Table 2.4. Reductive amination of acetophenone derivatives (**14a–21a**) employing AmDHs.



14a: R = H; **15a:** R = *o*-CH₃; **16a:** R = *m*-CH₃;
17a: R = *p*-CH₃; **18a:** R = *m*-F; **19a:** R = *p*-F;
20a: R = *p*-Cl; **21a:** R = OH.

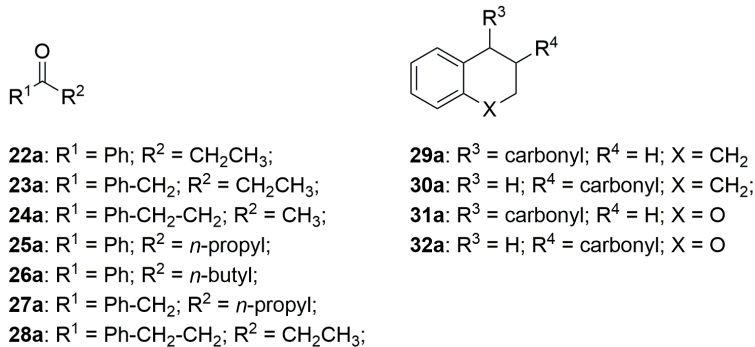
Entry	Substrate	Enzyme	Enzyme conc. [μ M]	Reaction time [h]	Conv. [%]	ee% (<i>R</i>)
1	14a	Ch	129	48	34	>99
2		Rs	51	48	0	n.m.
3	15a	Ch1	32	48	0	n.m.
4		Rs	51	48	0	n.m.
5	16a	Ch1	32	48	39	>99
6		Rs	51	24	0	n.m.
7		Bb	50	48	0	n.m.
8	17a	Ch1	129	48	9	>99
9		Rs	51	48	1	n.m.
10	18a	Ch1	129	48	43	>99
11		Rs	51	48	0	n.m.
12	19a	Ch1	129	48	22	>99
13		Rs	51	48	0	n.m.
14	20a	Ch1	32	48	36	>99
15		Rs	51	48	44	>99
16	21a	Ch1	32	48	0	n.m.
17		Rs	51	48	0	n.m.

Reaction conditions: substrate (50 mM), AmDH (30-130 μ M), Cb-FDH (14 μ M), ammonium formate buffer (1 M, pH 8.5), T 30°C, agitation orbital shaker (180 rpm).

(EsLeuDH-DM) as a mutant of the leucine dehydrogenase from *Exigobacterium sibiricum* was found to be more active towards **22a**, **25a**, **29a** and some acetophenone derivatives^[4e].

A small panel of aldehydes was tested in this study. Ch1-AmDH and Rs-PhAmDH rapidly

Table 2.5. Reductive amination of bulky-bulky and cyclic ketones (**22a–32a**) employing AmDHs.



Entry	Substrate	Enzyme	Enzyme conc. [μM]	Reaction time [h]	Conv. [%]	ee% (R)
1	22a	Ch1	92	48	8	n.d.
2		Rs	103	48	0	n.m.
3	23a	Ch1	32	24	14	>99
4		Rs	129	48	>99	>99
5		Bb	50	48	8	>99
6	24a	Rs	50	24	>99	>99
7	25a	Ch1	92	48	0	n.m.
8		Rs	103	48	1	n.m.
9	26a	Ch1	92	48	2	n.d.
10		Rs	103	48	2	n.d.
11	27a	Ch1	92	48	4	>99 ^[a]
12		Rs	103	48	71	>99 ^[a]
13	28a	Ch1	92	48	1	n.m.
14		Rs	103	48	87	>99
15	29a	Ch1	92	48	0	n.m.
16		Rs	103	48	0	n.m.
17	30a	Ch1	92	48	0	n.m.
18		Rs	103	48	0	n.m.
19	31a	Ch1	92	48	0	n.m.
20		Rs	103	48	0	n.m.
21	32a	Ch1	92	48	2	n.m.
22		Rs	103	48	0	n.m.

^[a] only (*S*)-configured amine observed. Reaction conditions: substrate (50 mM), AmDH (30–130 μM), Cb-FDH (14 μM), ammonium formate buffer (1 M, pH 8.5), T 30°C, agitation orbital shaker (180 rpm).

converted **34a** (Table 2.6, entry 3 and 4) even though both enzymes were inactive on **33a** and **35a** (Table 2.6, entries 1, 2, 5 and 6). Bb-PhAmDH proved to be a useful catalyst for the amination of **36a** whereas both Rs-PhAmDH and Ch1-AmDH were inactive on this substrate. (Table 2.6, entries 7-9). Rs-PhAmDH proved to be the optimal biocatalyst for the reduction of **37a** (96%, Table 2.6, entry 11). Interestingly, Ch1-AmDH quantitatively converted **37a**, but apart from the desired product 3-phenylpropan-1-amine **37b** (70%), hydrocinnamic alcohol **37c** was obtained as side-product (30%; Table 2.6 entry 10). So far, this is the only documented case wherein an amine dehydrogenase reduced a carbonyl compound into a significant amount of alcohol.

The conversion of **24a** catalyzed by Rs-PhAmDH sparked our interest whether derivatives bearing substituents on the aryl ring are accepted as well. A small panel of 4-phenyl-2-butanone derivatives (**38a–46a**) was chemically synthesized and tested in asymmetric reductive amination using Rs-PhAmDH under standard reaction conditions (Table 2.7). Interestingly, fluorophenyl derivatives (**44a–46a**) were fully converted (>99% ee

Table 2.6. Reductive amination of aldehydes (**33a–37a**) employing AmDHs.



33a: R¹ = H; R² = *n*-propyl;

34a: R¹ = H; R² = *n*-isopropyl;

35a: R¹ = Ph; R² = H;

36a: R¹ = Ph-CH₂; R² = H;

37a: R¹ = Ph-CH₂CH₂; R² = H;

Entry	Substrate	Enzyme	Enzyme conc. [μM]	Reaction time [h]	Conversion [%]	ee% (R)
1	33a	Ch1	32	24	0	n.m.
2		Rs	51	24	0	n.m.
3	34a	Ch1	32	24	0	n.a.
4		Rs	129	48	>99	n.a.
5	35a	Ch1	32	24	0	n.a.
6		Rs	51	24	0	n.a.
7	36a	Ch1	32	24	0	n.a.
8		Rs	51	24	0	n.a.
9		Bb	50	48	34	n.a.
10	37a	Ch1	92	48	70 ^[a]	n.a.
11		Rs	103	48	96	n.a.

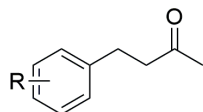
^[a] 30% alcohol **37c** was observed. Reaction conditions: substrate (50 mM), AmDH (30-130 μM), Cb-FDH (14 μM), ammonium formate buffer (1 M, pH 8.5), T 30°C, agitation orbital shaker (180 rpm).

(*R*) whereas more sterically demanding methoxyphenyl derivatives (**41a–43a**) were poorly accepted. Although this observation indicates that steric effects play a role in substrate acceptance, slightly more sterically demanding tolyl derivatives (**38a–40a**) showed better conversions (**40a**, 88% conversion; Table 2.7, entry 4). Since the ketone moiety in these substrates is not part of the aryl π -system through conjugation, electronic effects were logically ruled out as an explanation for our observations.

2.5 Representative biocatalytic reductive amination in preparative scale

In order to ensure that the optimized reaction conditions at analytical scale were applicable in preparative scale biocatalytic reactions, the asymmetric amination of **4a** was performed using Rs-PhAmDH (Scheme 2.2). The reaction with ca. 50 mM **4a** (208 mg), 43 μ M of Rs-AmDH, 15 μ M FDH, and 1 mM of NAD⁺ in ammonium formate buffer (1 M, pH 8.5) was performed at 30 °C. The substrate **4a** was converted into the optically

Table 2.7. Reductive amination of phenyl-3-methyl-2-propanone derivatives (**24a, 38a–46a**) employing Rs-PhAmDH.



24a: R = H; **38a:** R = *o*-CH₃; **39a:** R = *m*-CH₃;
40a: R = *p*-CH₃; **41a:** R = *o*-OCH₃; **42a:** *m*-OCH₃;
43a: R = *p*-OCH₃; **44a:** R = *o*-F; **45a:** R = *m*-F;
46a: R = *p*-F

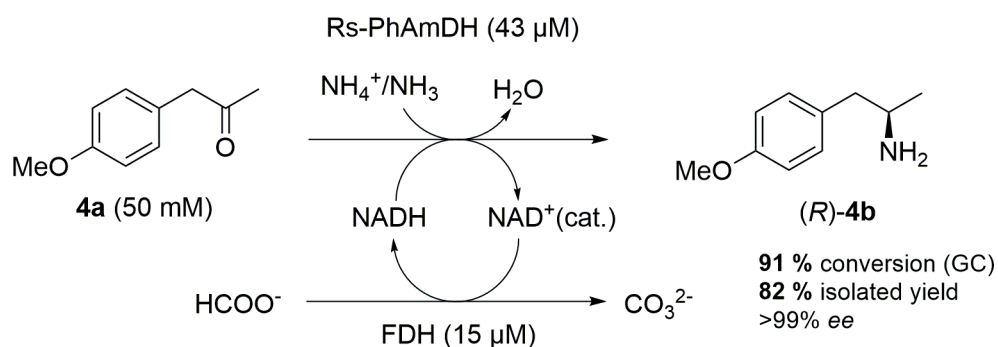
Entry	Substrate	Enzyme	Enzyme conc. [μ M]	Reaction time [h]	Conversion [%]	ee% (<i>R</i>)
1	24a	Rs	52	24	>99	>99
2	38a	Rs	26	24	27	90
3	39a	Rs	52	24	18	89
4	40a	Rs	52	24	87	92
5	41a	Rs	52	24	4	n.d.
6	42a	Rs	52	24	13	n.d.
7	43a	Rs	26	24	7	22 ^[a]
8	44a	Rs	52	24	>99	98
9	45a	Rs	52	24	>99	98
10	46a	Rs	52	24	>99	95

^[a] (*S*)-configured amine observed. Reaction conditions: substrate (50 mM), AmDH (26–52 μ M), Cb-FDH (14 μ M), ammonium formate buffer (1 M, pH 8.5), T 30°C, agitation orbital shaker (180 rpm).

pure amine (*R*)-**4b** with 91% conversion and >99% *ee* within 24 h reaction time. After work-up, (*R*)-**4b** was isolated with 82% yield and the purity and authenticity of the product were confirmed by ¹H-NMR and GC (Experimental section and Supporting Information section S6). (*R*)-**4b** was reported as an important building block for the synthesis of tacrine–selegiline hybrids that possess cholinesterase and monoamine oxidase inhibition activities for the treatment of Alzheimer’s disease [25]. Additionally, amine (*R*)-**4b** is the optically active intermediate for the synthesis of the blockbuster pharmaceutical formoterol sold under various trade names including Foradile and Oxeze [26].

2.6 Conclusion

In this work [27], the potential of AmDHs in the development of the next generation of chemical processes for the synthesis of α -chiral amines was demonstrated [28] by testing a set of available enzymes for the asymmetric amination of a range of structurally diverse prochiral ketones and aldehydes. The reductive amination catalyzed by AmDHs operating in tandem with Cb-FDH possesses an elevated atom efficiency as the ammonium formate buffer is simultaneously the source nitrogen and reducing equivalents. Stoichiometric inorganic bicarbonate (or carbon dioxide) is the sole by-product. Additionally, the reductive amination catalyzed by AmDH/Cb-FDH is performed under atmospheric pressure, which is more convenient and environmentally friendly over current industrial processes where amines are often obtained by hydrogenation of enamides utilizing dihydrogen under high pressure and temperature [29]. The most suitable enzyme, the optimal catalyst loading and the reaction times were determined for each substrate from this study. The influence of the temperature on the biocatalytic reductive amination with the three AmDHs variants



Scheme 2.2. Preparative reductive amination of **4a** using Rs-PhAmDH. Reaction conditions: **4a** (208 mg, 50 mM), ammonium formate buffer (1 M, pH 8.5), Cb-FDH (15 μ M), NAD^+ (1 mM), T 30 $^\circ\text{C}$, agitation on an orbital shaker (180 rpm), reaction volume 30 mL, reaction time 24 h.

was determined as well. The enzymes (AmDHs and FDH) and coenzyme (NAD) exhibited improved stability at a pH in the range of 8.2 – 8.8. The majority of the substrates tested were aminated with elevated conversion and nearly all α -chiral amine products were obtained with perfect optical purity (>99% (*R*)). This fact is of particular interest as ω -transaminases capable of giving access to (*R*)-configured amines are rare in nature and only very few (*R*)-selective ω -transaminases have been discovered [30]. Additionally, the calculated turnover number (TON, defined as the number of molecules of substrate converted per molecule of enzyme in the given reaction time) was equal or more than 1000 for the AmDHs and therefore comparable to the values previously obtained for the amination of ketones in aqueous buffers with ω -TAs [24a, 31]. Compared to the bio-amination with ω -TAs, AmDHs do not require sacrificial organic amine donors (e.g., L- or D-alanine [32], isopropylamine [33], or other small amines [34]) and inhibition phenomena are not so stringent (i.e., inhibition due to cosubstrate alanine and/or coproduct pyruvate [35]). It is, however, important to note that the amination reaction catalyzed by AmDHs is a reversible process and high concentrations of ammonia species (≥ 1 M) are required to drive the reaction towards the formation of amines. From this study, it became also evident that a single amine dehydrogenase capable of accepting a large variety of substrates is not available. For instance, the chimeric Ch1-AmDH is very active on aliphatic ketones and acetophenone derivatives, whereas Rs-PhAmDH is an excellent biocatalyst for the amination of phenylacetone derivatives and more sterically demanding ketones. The applicability of AmDHs was demonstrated as well for the synthesis of an important drug precursor on a preparative scale. It is expected that the herein described asymmetric reductive amination will be applied increasingly in the future. Since already new engineered AmDHs possessing expanded substrate scope have been developed [4e, 9d, 9e, 10b], further studies towards expanding catalytic reactivity, practical applicability and complementary stereoselectivity of AmDHs is likely to follow.

2.7 Experimental section

2.7.1 General information

The AmDH variants and the Cb-FDH were expressed as recombinant enzymes in *E. coli* BL21 (DE3). Details on materials, equipment and protocols are reported in the Supporting Information paragraph S3 and S4.

2.7.2 Optimized procedure for the biocatalytic reductive amination on analytical scale

The reactions were conducted in ammonium formate buffer (1 M, pH 8.5, final volume 0.5 mL) containing NAD⁺ (final concentration 1 mM). AmDH (30–130 μ M) and Cb-FDH (14.1 μ M) and the substrate (50 mM) were added. The reactions were run at 30 °C in an incubator for 21 hours (180 rpm) or longer if required in selected cases. Work-up was performed by the addition of KOH (100 μ L, 10 M) followed by the extraction with DCM (600 μ L). The water layer was removed after centrifugation and the organic layer was dried over MgSO₄. Conversion was determined by GC with an Agilent DB-1701 column. The enantiomeric excess of the amine product was determined after derivatization. Derivatization of the samples was performed by adding 4-dimethylaminopyridine in acetic anhydride (40 μ L stock solution of 50 mg mL⁻¹). The samples were shaken in an incubator at RT for 30 minutes. Afterwards water (300 μ L) was added and the samples were shaken for additional 30 minutes. After centrifugation, the organic layer was dried over MgSO₄. Enantiomeric excess was determined by GC with a Variant Chiracel DEX-CB column. Details on the GC analysis and methods are reported in the Supporting Information paragraph S7.

2.7.3 Preparative biocatalytic reductive amination for the synthesis of (R)-**4b**

NAD⁺ (final concentration 1 mM) was dissolved in ammonium formate buffer (30 mL, 1 M, pH 8.5) in a 50 mL round bottom flask. Ketone **4a** (195 μ L, 1.27 mmol), FDH (233 μ L from stock solution 80.7 mg mL⁻¹, final concentration 15 μ M), and Rs-PhAmDH (1.02 mL from stock solution 48.8 mg mL⁻¹, final concentration 43 μ M) were added and the reaction mixture was shaken in an incubator at 30 °C for 24 hours. The reaction mixture was acidified to pH 2–4 via addition of HCl (1 M). The water layer was washed with MTBE (20 mL) to remove any possible remaining ketone starting material. The pH of the water phase was increased to basic pH via KOH (10 M) while cooling in an ice bath. The water layer was extracted with MTBE (3 x 20 mL). The organic fractions containing the amine product were combined and dried over MgSO₄. After filtration and evaporation of the solvent, the desired product was obtained without the requirement for further purification steps. ¹H NMR (400 MHz, CDCl₃): δ 7.12 (d, J = 8.6 Hz, 2H), 6.86 (d, J = 8.7 Hz, 2H), 3.81 (s, 3H), 3.13 (m, 1H), 2.67 (dd, J = 13.4, 5.3 Hz, 1H), 2.47 (dd, J = 13.4, 8.1 Hz, 1H), 1.12 (d, J = 6.3 Hz, 3H).

2.7.4 Procedure for enzymatic synthesis of chiral reference amines using ω TAs

A stock solution of PLP (13 mg, 0.05 mmol, 1 mM) in KPi buffer (45 mL, 100 mM, pH 8.0) was prepared and two enzyme stocks were prepared from this: A) containing NAD⁺ (15 mg, 0.02 mmol, 1 mM), D-glucose (542 mg, 3.0 mmol, 150 mM), GDH (42 mg, 30 U), LDH (102 mg, 90 U), L-alanine (504 mg, 5.7 mmol, 250 mM) and ω TA-113 (210 mg, 10 mg mL⁻¹); B) containing NAD⁺ (15 mg, 0.02 mmol, 1 mM), D-glucose (542 mg, 3.0 mmol, 150 mM), GDH (44 mg, 30 U), LDH (102 mg, 90 U), D-alanine (501

mg, 5.6 mmol, 250 mM) and ωTA-117 (210 mg, 10 mg mL⁻¹). Biotransformations (reaction volume: 1 mL) were performed with 50 mM of ketone substrate in an incubator for 48 hours (30 °C, 190 rpm). Work-up was performed by addition of KOH (200 μL, 10 M) and extraction with EtOAc (2 x 500 μL). The organic layer was dried over MgSO₄. Conversion was determined by GC with an Agilent DB-1701 column. Derivatization of the samples was performed as described for biocatalytic reductive amination on analytical scale. Enantiomeric excess was determined by GC with a Variant Chiralcel DEX-CB column. Details on the GC analysis and methods are reported in the Supporting Information paragraph S7.

2.7.5 Chemical synthesis of substrates

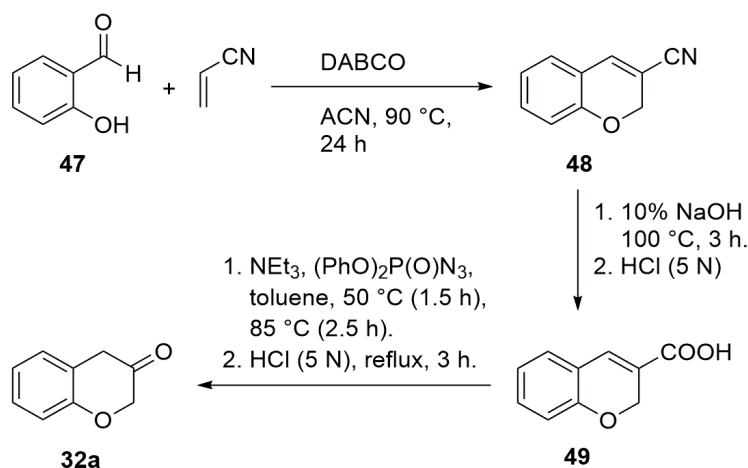
3-chromanone (**32a**) was synthesized in three steps from commercially available salicylaldehyde (**47**, Scheme 2.3) [36].

2H-Chromene-3-carbonitrile (**48**)

A 100 mL two-neck round bottom flask was equipped with condenser and charged with acrylonitrile (11.8 g, 0.2 mol), DABCO (1.0 g, 9.3 mmol), and **47** (4.4 mL, 41 mmol). The yellow mixture was stirred and heated up to 130 °C (reflux) upon which it turned slightly orange. The reaction progress was tracked by TLC in 7:3 PE:EtOAc; Rf 0.75 (**47**), Rf 0.68 (**48**). After 30 hours the work-up was performed by washing the mixture with NaHCO₃ (saturated) and brine followed by column chromatography purification (7:3 PE:EtOAc). The isolated product was recrystallized from the eluent as a yellow crystalline solid (5 g, 32 mmol, 78% isolated yield). ¹H-NMR (400 MHz, CDCl₃) δ 7.30 (dt, J = 8.1, 1.7 Hz, 1H), 7.20 (s, 1H), 7.13 (dd, J = 7.6, 1.6 Hz, 1H), 7.00 (td, J = 7.5, 1.1 Hz, 1H), 6.90 (d, J = 8.2 Hz, 1H), 4.85 (d, J = 1.4 Hz, 2H).

2H-Chromene-3-carboxylic acid (**49**)

A 100 mL two-neck round bottom flask was equipped with condenser and charged with **48** (1.0 g, 6.4 mmol) and 20 mL 10% NaOH. The yellow mixture was stirred and heated up to 130 °C (reflux).



Scheme 2.3. Chemical synthetic pathway towards **32a**.

The reaction progress was tracked by TLC (7:3 PE:EtOAc) and indicated full conversion after 3 h. 5N HCl was added dropwise to the solution until pH 3–4 was reached to provoke precipitation of **49**. Vacuum filtration and recrystallization from PE:Et₂O yielded the desired product as a white solid (880 mg, 5.7 mmol, 88% isolated yield). ¹H NMR (400 MHz, CDCl₃) δ 7.30 (dt, J = 8.1, 1.7 Hz, 1H), 7.20 (s, 1H), 7.13 (dd, J = 7.6, 1.6 Hz, 1H), 7.00 (td, J = 7.5, 1.1 Hz, 1H), 6.90 (d, J = 8.2 Hz, 1H), 4.85 (d, J = 1.4 Hz, 2H).

3-Chromanone (**32a**)

A 100 mL three-neck round bottom flask was equipped with condenser and charged with **49** (500 mg, 2.8 mmol) in DCM (6.5 mL, dried over 3Å mol. sieves) under dinitrogen atmosphere. NEt₃ (750 μL, 3.6 mmol) was added dropwise to the reaction mixture at RT. The initial suspension became a colorless clear solution. The reaction mixture was stirred at RT and diphenylphosphoryl azide (0.8 mL, 3.8 mmol) in toluene (3 mL, dried by distillation over CaCl₂) was added dropwise over a period of 40 minutes. The colorless mixture turned slightly yellow and the reaction mixture was heated to 50 °C for 1.5 hours. Another aliquot of toluene (6.5 mL) was added and the mixture was heated to 85 °C for 2.5 hours. After cooling of the mixture to RT, HCl (5 mL, 6 N) was added and the reaction mixture was heated to 87 °C (reflux, 18 h). The work up was performed by separation of the layers and washing the organic layer with saturated NaHCO₃ and brine. Column chromatography was performed in 5:1 PE:EtOAc to yield the desired product (175 mg, 1.18 mmol, 42% isolated yield). ¹H NMR (400 MHz, Chloroform-d) δ 7.30 – 7.23 (m, 1H), 7.17 – 7.11 (m, 1H), 7.11 – 7.04 (m, 1H), 4.44 (s, 2H), 3.65 (s, 2H).

General procedure for the synthesis of 4-phenyl-2-butanone derivatives (**38a–42a**,

44a–46a Scheme 2.4) ^[37]

A 25 mL Schlenk tube was charged with Pd(OAc)₂ (ca. 4.0 mg), substituted iodobenzene (4.25 mmol), 3-buten-2-ol (456 μL, 5.32 mmol), NEt₃ (742 μL, 5.32 mmol), ACN (dried over 3Å Mol. Sieves, 1.4 mL) under dinitrogen atmosphere. The reaction mixture was heated to 88 °C and stirred overnight. The crude reaction mixture was taken up in Et₂O/water (10 mL, 1:1) and the organic layer was washed with water (5 x 8 mL). Column chromatography was performed with 9:1 PE:EtOAc (2.5 mm, 12 cm, silica 60) to give the desired product:

38a: 15 mg, 0.1 mmol, 6% isolated yield. ¹H NMR (400 MHz, Chloroform-d) δ 7.16 (d, J = 3.5 Hz, 4H), 2.98 – 2.82 (m, 2H), 2.80 – 2.65 (m, 2H), 2.34 (s, 3H), 2.19 (s, 3H).

39a: 259 mg, 1.6 mmol, 41% isolated yield. ¹H NMR (400 MHz, Chloroform-d) δ 7.21 (t, J = 7.8 Hz, 1H), 7.03 (t, J = 9.1 Hz, 3H), 2.96 – 2.83 (m, 2H), 2.83 – 2.67 (m, 2H), 2.37 (s, 3H), 2.17 (s, 3H).

40a: 84 mg, 0.5 mmol, 45% isolated yield. ¹H NMR (400 MHz, Chloroform-d) δ 7.12 (s, 4H), 2.90 (t, J = 7.4 Hz, 2H), 2.83 – 2.68 (m, 2H), 2.36 (s, 3H), 2.17 (s, 3H).

41a: 218 mg, 1.2 mmol, 54% isolated yield. ¹H NMR (400 MHz, Chloroform-d) δ 7.21 (m, 1H), 7.16 (m, 1H), 6.95 – 6.81 (m, 2H), 3.84 (s, 3H), 2.94 – 2.87 (m, 2H), 2.75 (t, J = 7.6 Hz, 2H), 2.16 (s, 3H).

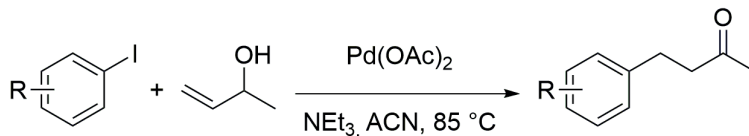
42a: 475 mg, 2.7 mmol, 63% isolated yield. ¹H NMR (400 MHz, Chloroform-d) δ 7.26 – 7.14 (m, 1H), 6.92 – 6.63 (m, 3H), 3.81 (s, 3H), 3.03 – 2.83 (m, 2H), 2.83 – 2.69 (m, 2H), 2.17 (s, 3H).

44a: 301 mg, 1.8 mmol, 42% isolated yield. ¹H NMR (400 MHz, Chloroform-d) δ 7.21 (m, 2H), 7.11 –

6.96 (m, 2H), 2.94 (t, $J = 7.6$ Hz, 2H), 2.78 (t, $J = 7.6$ Hz, 2H).

45a: 150 mg, 0.9 mmol, 21% isolated yield. ^1H NMR (400 MHz, Chloroform- d) δ 7.25 (m, 1H), 6.98 (d, $J = 7.9$ Hz, 1H), 6.90 (m, 2H), 2.91 (t, $J = 7.5$ Hz, 2H), 2.78 (t, $J = 7.4$ Hz, 2H).

46a: 493 mg, 3.0 mmol, 66% isolated yield. ^1H NMR (400 MHz, Chloroform- d) δ 7.19 – 7.11 (m, 2H), 7.02 – 6.93 (m, 2H), 2.89 (t, $J = 7.5$ Hz, 2H), 2.76 (t, $J = 7.3$ Hz, 2H).



Scheme 2.4. Chemical synthetic pathway towards 4-phenyl-2-butanone derivatives (**38a–42a** and **44a–46a**).

2.7.6 Analytics

Conversion for the reductive amination of the ketones was measured by GC using an Agilent 7890 A GC system, equipped with an FID detector and using an Agilent J&W DB-1701 column (60 m, 250 μm , 0.25 μm) or an Agilent J&W DB-1701 column (30 m, 250 μm , 0.25 μm). H₂ was used as carrier gas and DCM or EtOAc was used as solvent. The enantiomeric excess of the amines was measured (after derivatization with DMAP in acetic anhydride) by GC using an Agilent 7890 A GC system, equipped with a FID detector and using a Varian Chrompack Chiracel Dex-CB column (25 m, 320 μm , 0.25 μm). Additional information can be found in Supporting Information paragraph S7. GC retention times of compounds **1–28** and **33–37** are reported in Supporting Information Table S9 and S10.

DB1701_30m_A; constant pressure 13.5 psi, T injector 300 °C, split ratio 40:1, initial 80 °C 6.5 min; 10 °C/min 160 °C 5 min; 20 °C/min 200 °C 2 min; 20 °C/min 280 °C 1 min.

Table 2.8. GC retention times for measuring the conversion of substrates **29a–32a** and **38a–46a**.

Entry	Substrate	Ret. time [min]	Product	Ret. time [min]	Alcohol byproduct	Ret. time [min]	GC method
1	29a	17.5	29b	16.0	29c	n.d.	DB1701_30m_A
2	30a	17.3	30b	16.4	30c	n.d.	DB1701_30m_A
3	31a	16.5	31b	16.9	31c	n.d.	DB1701_30m_A
4	32a	15.2	32b	17.1	32c	n.d.	DB1701_30m_A
5	38a	27.5	38b	26.7	38c	n.d.	DB1701_60m
6	39a	27.1	39b	26.2	39c	n.d.	DB1701_60m
7	40a	27.3	40b	26.7	40c	n.d.	DB1701_60m
8	41a	29.5	41b	28.7	41c	n.d.	DB1701_60m
9	42a	30.3	42b	29.7	42c	n.d.	DB1701_60m
10	43a	30.5	43b	29.9	43c	n.d.	DB1701_60m
11	44a	24.4	44b	23.3	44c	n.d.	DB1701_60m
12	45a	25.4	45b	24.0	45c	n.d.	DB1701_60m
13	46a	25.4	46b	25.0	46c	n.d.	DB1701_60m

DB1701_60m: constant pressure 13.5 psi, T injector 300 °C, total flow 48.129 ml/min, split ratio 40:1, split flow 44.029 ml/min, initial 80 °C 6.5 min; 5 °C/min 160 °C 2 min; 20 °C/min 280 °C 1 min.

CP7503-DEX-CB_method_A: constant flow 1.4 mL/min, T injector 200 °C, split ratio 40:1, T initial 100 °C, hold 2 min; gradient 1 °C/min up to 130 °C, hold 5 min; gradient 10 °C/min up to 170 °C, hold 10 min.; gradient 10 °C/min up to 180 °C, hold 1 min.

Table 2.9. GC retention times for measuring the enantiomeric excess of amines **29b–32b** and **38b–46b**.

Entry	(S)-amine	Ret. time [min]	(R)-amine	Ret. time [min]	GC method
1	(S)- 29b	46.0	(R)- 29b	47.1	CP7503-DEX-CB_method_A
2	(S)- 30b	48.2	(R)- 30b	48.6	CP7503-DEX-CB_method_A
3	(S)- 31b	46.1	(R)- 31b	46.5	CP7503-DEX-CB_method_A
4	(S)- 32b	46.0	(R)- 32b	46.4	CP7503-DEX-CB_method_A
5	(S)- 38b	35.9	(R)- 38b	36.1	CP7503-DEX-CB_method_A
6	(S)- 39b	35.5	(R)- 39b	35.7	CP7503-DEX-CB_method_A
7	(S)- 40b	36.1	(R)- 40b	36.4	CP7503-DEX-CB_method_A
8	(S)- 41b	38.9	(R)- 41b	39.2	CP7503-DEX-CB_method_A
9	(S)- 42b	41.7	(R)- 42b	42.0	CP7503-DEX-CB_method_A
10	(S)- 43b	31.4	(R)- 43b	31.8	CP7503-DEX-CB_method_A
11	(S)- 44b	32.9	(R)- 44b	33.1	CP7503-DEX-CB_method_A
12	(S)- 45b	33.8	(R)- 45b	34.0	CP7503-DEX-CB_method_A
13	(S)- 46b	33.9	(R)- 46b	34.2	CP7503-DEX-CB_method_A

2.8 References

- [1] Drauz, K.; Gröger, H.; May, O. *Enzyme Catalysis in Organic Synthesis*; 3 ed.; Wiley-VCH: Weinheim, Germany, 2012.
- [2] Gröger, H. *Applied Microbiology and Biotechnology*. **2019**, *103*, 83–95.
- [3] a) Grogan, G. *Current Opinion in Chemical Biology*. **2018**, *43*, 15–22; b) Patil, M. D.; Grogan, G.; Bommarius, A.; Yun, H. *ACS Catalysis*. **2018**, *8*, 10985–11015.
- [4] a) Mutti, F. G.; Knaus, T.; Scrutton, N. S.; Breuer, M.; Turner, N. J. *Science*. **2015**, *349*, 1525–1529; b) Knaus, T.; Cariati, L.; Masman, M. F.; Mutti, F. G. *Organic & Biomolecular Chemistry*. **2017**, *15*, 8313–8325; c) Au, S. K.; Bommarius, B. R.; Bommarius, A. S. *ACS Catalysis*. **2014**, *4*, 4021–4026; d) Chen, F. F.; Liu, Y. Y.; Zheng, G. W.; Xu, J. H. *ChemCatChem*. **2015**, *7*, 3838–3841; e) Lowe, J.; Ingram, A. A.; Gröger, H. *Bioorganic & Medicinal Chemistry*. **2018**, *26*, 1387–1392; f) Thompson, M. P.; Turner, N. J. *ChemCatChem*. **2017**, *9*, 3833–3836; g) Uthoff, F.; Gröger, H. *Journal of Organic Chemistry*. **2018**, *83*, 9517–9521; h) Yu, H. L.; Li, T.; Chen, F. F.; Luo, X. J.; Li, A.; Yang, C.; Zheng, G. W.; Xu, J. H. *Metabolic Engineering*. **2018**, *47*, 184–189; i) Liu, J.; Li, Z. *Biotechnology and Bioengineering*. **2019**, *116*, 536–542.
- [5] a) Bohmer, W.; Knaus, T.; Mutti, F. G. *ChemCatChem*. **2018**, *10*, 731–735; b) Ahmad, A. L.; Low, E.

- M.; Abd Shukor, S. R. *Journal of Molecular Catalysis B*. **2013**, *88*, 26–31; c) Liu, J.; Pang, B. Q. W.; Adams, J. P.; Snajdrova, R.; Li, Z. *ChemCatChem*. **2017**, *9*, 425–431; d) Ren, H.; Zhang, Y.; Su, J.; Lin, P.; Wang, B.; Fang, B.; Wang, S. *Journal of Biotechnology*. **2017**, *241*, 33–41.
- [6] a) Jeon, H.; Yoon, S.; Ahsan, M. M.; Sung, S.; Kim, G. H.; Sundaramoorthy, U.; Rhee, S. K.; Yun, H. *Catalysts*. **2017**, *7*, 251–264; b) Yoon, S.; Patil, M. D.; Sarak, S.; Jeon, H.; Kim, G. H.; Khobragade, T. P.; Sung, S.; Yun, H. *ChemCatChem*. **2019**, *11*, 1898–1902.
- [7] Tseliou, V.; Masman, M. F.; Böhmer, W.; Knaus, T.; Mutti, F. G. *ChemBioChem*. **2019**, *20*, 800–812.
- [8] Itoh, N.; Yachi, C.; Kudome, T. *Journal of Molecular Catalysis B*. **2000**, *10*, 281–290.
- [9] a) Abrahamson, M. J.; Vázquez-Figueroa, E.; Woodall, N. B.; Moore, J. C.; Bommarius, A. S. *Angewandte Chemie International Edition*. **2012**, *51*, 3969–3972; b) Bommarius, B. R.; Schürmann, M.; Bommarius, A. S. *Chemical Communications*. **2014**, *50*, 14953–14955; c) Ye, L. J.; Toh, H. H.; Yang, Y.; Adams, J. P.; Snajdrova, R.; Li, Z. *ACS Catalysis*. **2015**, *5*, 1119–1122; d) Chen, F. F.; Zheng, G. W.; Liu, L.; Li, H.; Chen, Q.; Li, F. L.; Li, C. X.; Xu, J. H. *ACS Catalysis*. **2018**, *8*, 2622–2628; e) Franklin, R. D.; Whitley, J. A.; Robbins, J. M.; Bommarius, A. S. *Chemical Engineering Journal*. **2019**, *369*, 634–640.
- [10] a) Abrahamson, M. J.; Wong, J. W.; Bommarius, A. S. *Advanced Synthesis & Catalysis*. **2013**, *355*, 1780–1786; b) Pushpanath, A.; Siirola, E.; Bornadel, A.; Woodlock, D.; Schell, U. *ACS Catalysis*. **2017**, *7*, 3204–3209.
- [11] Mayol, O.; David, S.; Darii, E.; Debard, A.; Mariage, A.; Pellouin, V.; Petit, J. L.; Salanoubat, M.; De Berardinis, V.; Zaparucha, A.; Vergne-Vaxelaire, C. *Catalysis Science & Technology*. **2016**, *6*, 7421–7428.
- [12] Mayol, O.; Bastard, K.; Beloti, L.; Frese, A.; Turkenburg, J. P.; Petit, J. L.; Mariage, A.; Debard, A.; Pellouin, V.; Perret, A.; De Berardinis, V.; Zaparucha, A.; Grogan, G.; Vergne-Vaxelaire, C. *Nature Catalysis*. **2019**, *2*, 324–333.
- [13] Sharma, M.; Mangas-Sanchez, J.; Turner, N. J.; Grogan, G. *Advanced Synthesis & Catalysis*. **2017**, *359*, 2011–2025.
- [14] Sheldon, R. A.; Arends, I.; Hanefeld, U. *Green Chemistry and Catalysis*; 1 ed.; Wiley-VCH: Weinheim, Germany, 2007.
- [15] Schutte, H.; Flossdorf, J.; Sahm, H.; Kula, M. R. *European Journal of Biochemistry*. **1976**, *62*, 151–160.
- [16] Smith, M. B.; March, J. *March's Advanced Organic Chemistry: Reactions, Mechanisms, and Structure*; 6 ed. (Eds.); John Wiley & Sons, Inc.: New York, 2007, pp. 395–416.
- [17] a) Vogl, M.; Kratzer, R.; Nidetzky, B.; Brecker, L. *Organic & Biomolecular Chemistry*. **2011**, *9*, 5863–5870; b) Contente, M. L.; Serra, I.; Palazzolo, L.; Parravicini, C.; Gianazza, E.; Eberini, I.; Pinto, A.; Guidi, B.; Molinari, F.; Romano, D. *Organic & Biomolecular Chemistry*. **2016**, *14*, 3404–3408; c) Zhu, D. M.; Rios, B. E.; Rozzell, J. D.; Hua, L. *Tetrahedron: Asymmetry*. **2005**, *16*, 1541–1546.
- [18] Hansch, C.; Leo, A.; Taft, R. W. *Chemical Reviews*. **1991**, *91*, 165–195.

- [19] Rodriguez, C.; Borzecka, W.; Sattler, J. H.; Kroutil, W.; Lavandera, I.; Gotor, V. *Organic & Biomolecular Chemistry*. **2014**, *12*, 673–681.
- [20] a) Koszelewski, D.; Tauber, K.; Faber, K.; Kroutil, W. *Trends in Biotechnology*. **2010**, *28*, 324–332; b) Koszelewski, D.; Lavandera, I.; Clay, D.; Guebitz, G. M.; Rozzell, D.; Kroutil, W. *Angewandte Chemie International Edition*. **2008**, *47*, 9337–9340; c) Simon, R. C.; Grischek, B.; Zepeck, F.; Steinreiber, A.; Belaj, F.; Kroutil, W. *Angewandte Chemie International Edition*. **2012**, *51*, 6713–6716; d) O'reilly, E.; Iglesias, C.; Ghislieri, D.; Hopwood, J.; Galman, J. L.; Lloyd, R. C.; Turner, N. J. *Angewandte Chemie International Edition*. **2014**, *53*, 2447–2450; e) Koszelewski, D.; Göritzer, M.; Clay, D.; Seisser, B.; Kroutil, W. *ChemCatChem*. **2010**, *2*, 73–77; f) Mutti, F. G.; Fuchs, C. S.; Pressnitz, D.; Sattler, J. H.; Kroutil, W. *Advanced Synthesis & Catalysis*. **2011**, *353*, 3227–3233; g) Mutti, F. G.; Fuchs, C. S.; Pressnitz, D.; Turrini, N. G.; Sattler, J. H.; Lerchner, A.; Skerra, A.; Kroutil, W. *European Journal of Organic Chemistry*. **2012**, *2012*, 1003–1007; h) Schätzle, S.; Steffen-Munsberg, F.; Thontowi, A.; Höhne, M.; Robins, K.; Bornscheuer, U. T. *Advanced Synthesis & Catalysis*. **2011**, *353*, 2439–2445.
- [21] Pressnitz, D.; Fuchs, C. S.; Sattler, J. H.; Knaus, T.; Macheroux, P.; Mutti, F. G.; Kroutil, W. *ACS Catalysis*. **2013**, *3*, 555–559.
- [22] a) Hwang, B. Y.; Ko, S. H.; Park, H. Y.; Seo, J. H.; Lee, B. S.; Kim, B. G. *Journal of Microbiology and Biotechnology*. **2008**, *18*, 48–54; b) Park, E. S.; Park, S. R.; Han, S. W.; Dong, J. Y.; Shin, J. S. *Advanced Synthesis & Catalysis*. **2014**, *356*, 212–220; c) Nobili, A.; Steffen-Munsberg, F.; Kohls, H.; Trentin, I.; Schulzke, C.; Höhne, M.; Bornscheuer, U. T. *ChemCatChem*. **2015**, *7*, 757–760; d) Genz, M.; Melse, O.; Schmidt, S.; Vickers, C.; Dörr, M.; Van Den Bergh, T.; Joosten, H.-J.; Bornscheuer, U. T. *ChemCatChem*. **2016**, *8*, 3199–3202.
- [23] a) Cho, B. K.; Park, H. Y.; Seo, J. H.; Kim, J.; Kang, T. J.; Lee, B. S.; Kim, B. G. *Biotechnology and Bioengineering*. **2008**, *99*, 275–284; b) Han, S. W.; Park, E. S.; Dong, J. Y.; Shin, J. S. *Applied and Environmental Microbiology*. **2015**, *81*, 6994–7002; c) Han, S.-W.; Park, E.-S.; Dong, J.-Y.; Shin, J.-S. *Advanced Synthesis & Catalysis*. **2015**, *357*, 1732–1740; d) Han, S.-W.; Park, E.-S.; Dong, J.-Y.; Shin, J.-S. *Advanced Synthesis & Catalysis*. **2015**, *357*, 2712–2720.
- [24] a) Savile, C. K.; Janey, J. M.; Mundorff, E. C.; Moore, J. C.; Tam, S.; Jarvis, W. R.; Colbeck, J. C.; Krebber, A.; Fleitz, F. J.; Brands, J.; Devine, P. N.; Huisman, G. W.; Hughes, G. J. *Science*. **2010**, *329*, 305–309; b) Pavlidis, I. V.; Weiss, M. S.; Genz, M.; Spurr, P.; Hanlon, S. P.; Wirz, B.; Iding, H.; Bornscheuer, U. T. *Nature Chemistry*. **2016**, *8*, 1076–1082.
- [25] Lu, C.; Zhou, Q.; Yan, J.; Du, Z.; Huang, L.; Li, X. *European Journal of Medicinal Chemistry*. **2013**, *62*, 745–753.
- [26] a) Campos, F.; Bosch, M. P.; Guerrero, A. *Tetrahedron: Asymmetry*. **2000**, *11*, 2705–2717; b) Anderson, G. P. *Life Sciences*. **1993**, *52*, 2145–2160.
- [27] Knaus, T.; Böhmer, W.; Mutti, F. G. *Green Chemistry*. **2017**, *19*, 453–463.
- [28] Nestl, B. M.; Hammer, S. C.; Nebel, B. A.; Hauer, B. *Angew Chem Int Ed Engl*. **2014**, *53*, 3070–3095.
- [29] a) Nugent, T. C.; El-Shazly, M. *Advanced Synthesis & Catalysis*. **2010**, *352*, 753–819; b) Nugent, T. C. *Chiral Amine Synthesis: Methods, Developments and Applications*; Nugent, T. C. (Eds.); Wiley-VCH; Weinheim, Germany, 2010, pp. 225–245.

- [30] a) Iwasaki, A.; Yamada, Y.; Kizaki, N.; Ikenaka, Y.; Hasegawa, J. *Applied Microbiology and Biotechnology*. **2006**, *69*, 499–505; b) Höhne, M.; Schätzle, S.; Jochens, H.; Robins, K.; Bornscheuer, U. T. *Nature Chemical Biology*. **2010**, *6*, 807–813.
- [31] Mutti, F. G.; Sattler, J.; Tauber, K.; Kroutil, W. *ChemCatChem*. **2011**, *3*, 109–111.
- [32] Richter, N.; Farnberger, J. E.; Pressnitz, D.; Lechner, H.; Zepeck, F.; Kroutil, W. *Green Chemistry*. **2015**, *17*, 2952–2958.
- [33] Dawood, A. W. H.; Weiss, M. S.; Schulz, C.; Pavlidis, I. V.; Iding, H.; De Souza, R. O. M. A.; Bornscheuer, U. T. *ChemCatChem*. **2018**, *10*, 3943–3949.
- [34] a) Gomm, A.; Lewis, W.; Green, A. P.; O'reilly, E. *Chemistry*. **2016**, *22*, 12692–12695; b) Payer, S. E.; Schrittwieser, J. H.; Kroutil, W. *European Journal of Organic Chemistry*. **2017**, *2017*, 2553–2559.
- [35] a) Shin, J. S.; Kim, B. G. *Biotechnology and Bioengineering*. **1999**, *65*, 206–211; b) Shin, J.-S.; Kim, B.-G. *Bioscience, Biotechnology, and Biochemistry*. **2014**, *65*, 1782–1788; c) Shin, J. S.; Kim, B. G. *Biotechnology and Bioengineering*. **2002**, *77*, 832–837.
- [36] Alami, M.; Peyrat, J. F.; Belachmi, L.; Brion, J. D. *European Journal of Organic Chemistry*. **2001**, *2001*, 4207–4212.
- [37] Krubsack, A. J.; Sehgal, R.; Loong, W. A.; Slack, W. E. *Journal of Organic Chemistry*. **1975**, *40*, 3179–3182.

Chapter 3

Co-immobilized dehydrogenases applied for the asymmetric hydrogen-borrowing bio-amination of alcohols

This chapter is based on the following publication:

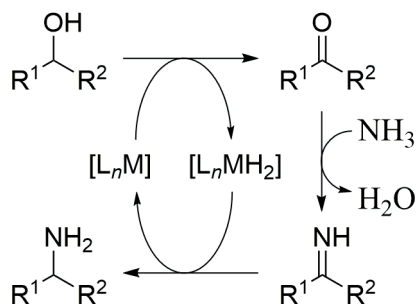
Böhmer, W.; Knaus, T.; Mutti, F.G., *ChemCatChem*. **2018**, *10*, 731–735.

Supporting information is available under; doi: [10.1002/cctc.201701366](https://doi.org/10.1002/cctc.201701366)

3.1 Introduction

Owing to an increased interest in the use of biomass as a feedstock for the synthesis of important chemical building blocks, efficient catalytic strategies for the direct and stereoselective amination of alcohols are in demand. Most biomass-derived compounds possess plenty of hydroxy groups whereas amine functionalities are often desired, for example, as building blocks for the synthesis of active pharmaceutical ingredients (APIs). For the amination reactions the use of ammonia as a readily-available, cheap and abundant resource, is preferable. In this context, hydrogen-borrowing (or hydrogen-shuttling) processes are of high interest since the amination is conducted with elevated atom efficiency forming water as the sole byproduct (Scheme 3.1) ^[1]. The first direct homogeneous catalytic amination of primary alcohols with ammonia was developed using a Ru/PNP pincer complex showing high selectivities (up to 87%) ^[2]. This method, however, was restricted to the conversion of water-insoluble primary alcohols. Several studies have been developed since utilizing mostly Ru or Ir-based metal catalysts ^[1-3]. Conversely, the reaction conditions applied in these processes complicate their use on a larger scale such as moderate chemoselectivity, moderate to low stereoselectivity, high catalyst loadings and substrate feed limitations. In addition, expensive chiral auxiliaries or chemically synthesized metal ligands are required that lower the applicability of the process.

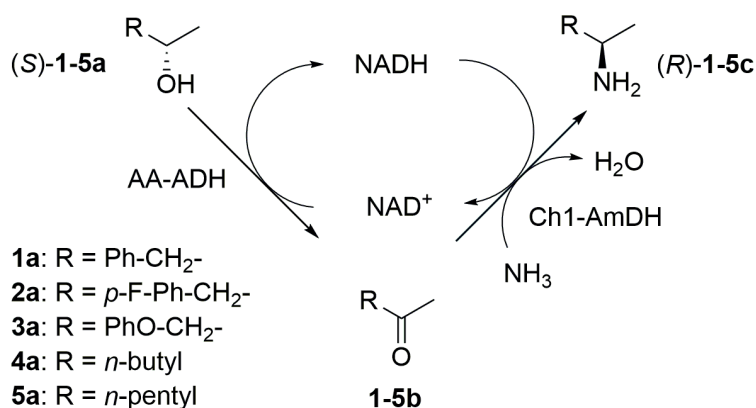
Although they are biological entities with high chemo-, regio-, and enantioselectivity, enzymes specifically for the amination of alcohols remain scarce. Our group developed the notable dual-enzyme and asymmetric hydrogen-borrowing amination cascade utilizing the tandem-operation of an alcohol dehydrogenase (ADH) with an amine dehydrogenase (AmDH) (Scheme 3.2) ^[4]. A catalytic quantity of the nicotinamide coenzyme (NADH/NAD⁺)



Scheme 3.1. Organometallic-catalyzed hydrogen-borrowing (or hydrogen-shuttling) processes for the amination of alcohols utilize ammonia as the nitrogen source, thereby releasing water as the sole byproduct ^[1].

shuttles the hydride in the oxidative and subsequent reductive step from the alcohol substrate to the amine product. Amination of enantiomeric secondary alcohols was achieved with inversion or retention of configuration as well as the asymmetric amination of several racemic secondary alcohols. Conversions up to 96% were achieved and the amine products were always obtained in enantiopure form (>99% *ee*). A previously reported biocatalytic cascade involving an ω -transaminase (ω -TA), an ADH, and an alanine dehydrogenase (AlaDH) exhibits lower atom-efficiency since it required ca. five equivalents of alanine as the sacrificial amine donor. Moreover, the amination of secondary alcohols was more problematic because of moderate conversion and chemoselectivity [5]. The significance of asymmetric hydrogen-borrowing amination cascades was further illustrated by application of the analogous dual-enzyme system in another independent study. The amination of a small panel of short aliphatic and cyclic alcohols was performed with moderate to high conversions and mostly excellent enantioselectivities [4a]. In later studies the hydrogen-borrowing bio-amination strategy was developed further to increase its applicability and give access to the synthesis of a wider range of primary as well as secondary amines [4b, 6].

Compared to other existing hydrogen-borrowing cascades, the ADH–AmDH cascade has several advantages in terms of reaction system simplicity and in-situ cofactor regeneration [4a, 4c]. However, NADH recycling in the ADH–AmDH cascade is limited by the slower amination step (ADH, k_{cat}/K_m : 10^4 – 10^5 s⁻¹ M⁻¹ and AmDH, k_{cat}/K_m : 10^2 – 10^3 s⁻¹ M⁻¹) [7]. Furthermore, catalytic turnover rates for this system were not determined at the time



Scheme 3.2. Hydrogen-borrowing amination of alcohols by using co-immobilized AA-ADH and Ch1-AmDH on EziG³ Fe-Amber metal ion affinity beads. Reaction conditions: EziG³ Fe Amber (10 mg, enzyme loading: 5% w w⁻¹), Ch1-AmDH (23 nmol, 11 μ M), AA-ADH (9 nmol, 4 μ M), ammonium chloride (2 M, pH 8.7, 0.5 mL), NAD⁺ (1 mM), substrate (20 mM), 30 °C, 170 rpm (orbital incubator), 48 h.

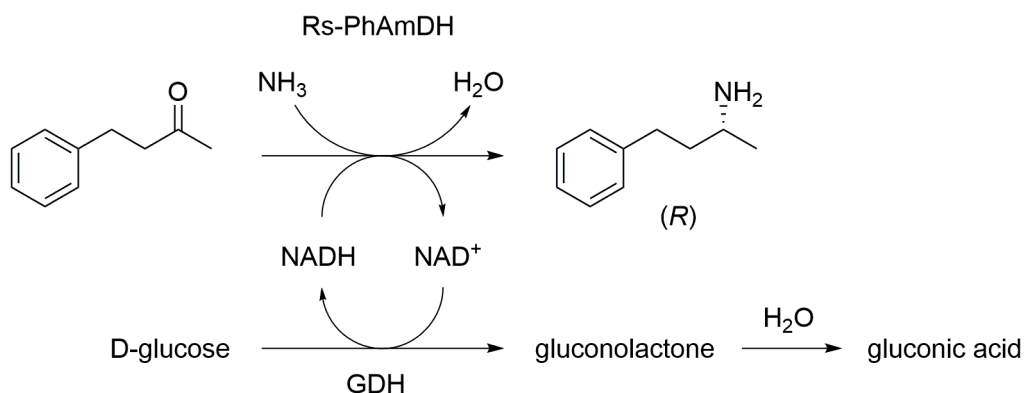
and the application of the ADH-AmDH system was limited to single batch experiments on analytical scale (i.e. 0.5–1 mL). Both recycling of the biocatalyst and the ability to apply high substrate concentrations are desirable elements in developing a possibly industrially relevant process. Additionally, the biocatalyst should possess high catalytic activity, robustness, and good thermal and mechanical stability. In order to achieve this, we envisioned the immobilization of the ADH-AmDH cascade on a support material followed by subsequent application as a heterogeneous dual-enzyme biocatalyst.

Immobilization of enzymes can confer advantageous properties such as enhanced thermal and mechanical stability, the possibility to recover and recycle the biocatalyst, and tolerance for wider reaction conditions [8]. Enzyme immobilization techniques include encapsulation in (in)organic microporous structures, attachment on functionalized supports, cross-linking, and coordination through ionic interactions [8–9]. A more elaborate discussion was provided in Chapter 1. Immobilization through ionic interactions can, for example, be performed by affinity binding between enzymes and metal ions such as Fe^{3+} , Cu^{2+} , Zn^{2+} , Ni^{2+} , and Co^{2+} . The process is based on the concept of immobilized metal ion affinity chromatography (IMAC), or metal chelate affinity chromatography, which enables facile purification of enzymes from crude cell lysate. Selective binding occurs through a genetically fused polyhistidine chain (His-tag, with 6 up to 12 histidine residues) at the C-terminus or N-terminus of the enzyme [10]. The first application of such a system for enzyme immobilization involved a His_6 -tagged alanine racemase from *Geobacillus stearothermophilus* immobilized on a cobalt(II)-functionalized silica surface [11]. Various His-tagged enzymes have been employed since that time on modified support materials in batch and flow synthesis [9b, 12]. For example, the AmDH engineered from phenylalanine dehydrogenase of *Rhodococcus* sp. M4 was co-immobilized with glucose dehydrogenase (GDH) on magnetic nanoparticles (MNP) through metal-ion affinity immobilization. The co-immobilized system was applied in the asymmetric reductive amination of 4-phenyl-2-butanone to give (*R*)-4-phenyl-2-aminobutane (74%, >99% ee) with a total turnover number (TTN) of 2940 for the NADH recycling (Scheme 3.3). The use of magnetic nanoparticles for the immobilization enabled facile recovery of the biocatalyst after the reaction. Recycling of the biocatalyst was performed showing 63% of its original activity after five reaction cycles [9b].

A method based on metal-ion affinity binding of His-tagged enzymes on controlled porosity glass (CPG) has recently been developed and commercialized (EziG™). This method

has been shown to minimize enzyme leaching and loss of activity with enzymes from several classes, including lipases, transaminases, Baeyer–Villiger monooxygenases, flavine reductases, and alanine dehydrogenases [12a, 13]. Further studies supported the versatility of EziG™ as a support material for transaminases [14], an arylmalonate decarboxylase [15], *Candida antarctica* lipase [16] and a norcoclaurine synthase [17]. Enzyme immobilization on CPG-derivatized metal-ion affinity particles offers several advantages over other methods. The support material is chemically and physically stable in aqueous media (pH<10) as well as in organic solvents under the applied reaction conditions. Furthermore, it possesses low solution flow resistance due to its interconnecting pore structure, which facilitates mass transfer of substrate and product. The process of immobilization is highly selective and allows for binding of the target enzyme from the crude cell lysate thereby avoiding pre-purification steps. General applicability to several families of enzymes stems from the selective His-tag interaction with the support material, making this immobilization method highly versatile. In addition, shorter times for immobilization are required and retained enzymatic activity is often significantly higher compared to other commercial supports. Finally, recovery of the support material can be achieved by using strong chelator agents, such as EDTA, and subsequent regeneration by loading fresh metal ions [18]. Some of these advantages may compensate the fact that the manufacturing costs of CPG carriers are higher than those of polymeric materials depending on the application.

In this study, an alcohol dehydrogenase from *Aromatoleum aromaticum* (AA-ADH) [7b] and a chimeric amine dehydrogenase (Ch1-AmDH) [19] were co-immobilized on CPG



Scheme 3.3. Asymmetric reductive amination of 4-phenyl-2-butanone to give (*R*)-4-phenyl-2-aminobutane by an AmDH. Phenylalanine dehydrogenase from *Rhodococcus* sp. M4 (Rs-PhAmDH) utilizes ammonia and generates water as a byproduct. Glucose dehydrogenase (GDH) regenerates the oxidized nicotinamide cofactor (NAD⁺) to its reduced form (NADH) thereby converting glucose to gluconolactone, which is hydrolyzed to gluconic acid in aqueous environment.

metal-ion affinity beads (EziG³ Fe-amber) to perform the hydrogen-borrowing amination of a panel of (*S*)-configured alcohols (i.e., (*S*)-**1a–5a**) with ammonia (Scheme 3.2). The selected reaction proceeds with perfect inversion of configuration ^[4c]. Thus, it exemplifies a highly atom-efficient alternative to amination by the Mitsunobu reaction ^[20]. The performance of the heterogeneous co-immobilized ADH-AmDH system was optimized in terms of loadings of the catalysts, molar ratio between ADH and AmDH, total amount of enzymes per mass of affinity beads, and substrate concentration. Application of the co-immobilized ADH-AmDH system, however, showed limited recyclability owing to poor resistance to mechanical forces under the applied reaction conditions. Furthermore, substrate concentrations did not meet industrial requirements and no improvements were obtained when applying other combinations of ADHs with Ch1-AmDH. Notably, compared with the free enzymes in solution, the co-immobilized ADH-AmDH system represents a significant improvement in terms of catalytic turnovers and high retention of activity.

3.2 Results & discussion

3.2.1 Expression and purification of dehydrogenases

ADHs were expressed as recombinant proteins with an N-terminal (or C-terminal) His₆-tag and purified by Ni²⁺ affinity chromatography. The concentrations of both enzymes were determined spectrophotometrically at $\lambda = 280$ nm (Experimental section and Supporting Information section S3). Unless stated otherwise, AA-ADH from *Aromatoleum aromaticum* ^[7b] was employed for the oxidative step in the ADH-AmDH cascade. Ch1-AmDH was expressed and purified as previously described ^[21]. Other alcohol dehydrogenases were expressed and purified accordingly: engineered ADHs from *Lactobacillus brevis* (LBv-ADH) ^[7c, 22], *Candida maris* (Cm-ADH) ^[23] or *Thermoanaerobacter ethanolicus* (Te-ADH-v3) ^[24] and cofactor dependency altered variants of *Thermoanaerobacter brockii* (Tb-ADH-v2-NAD) ^[6a] and *Thermoanaerobacter ethanolicus* (Te-ADH-v3-NAD). Although EziG Fe³⁺ ion affinity beads can be used to bind selectively His-tagged enzymes from crude cell extracts, purified enzymes were used in this study in order to estimate turnover numbers (TONs) with extreme accuracy since the concentration of the enzymes would be exactly known.

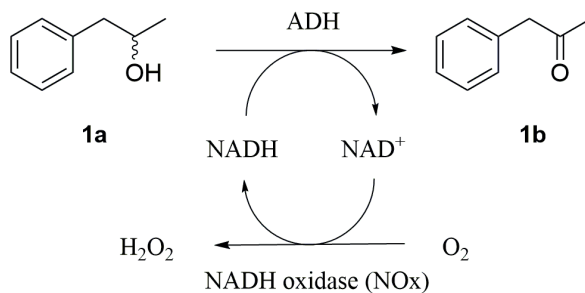
3.2.2 Catalytic activity of purified alcohol dehydrogenases

The catalytic activity of ADHs was determined in two distinct assays. AA-ADH and LBv-ADH

were tested for the oxidation of (*S*)-**1a** or (*R*)-**1a** respectively using an NADH oxidase for recycling of the cofactor (Table 3.1). The catalytic activity of Cm-ADH, Te-ADH-v3, Te-ADH-v3-NAD and Tb-ADH-v2-NAD was determined for the reduction of ketones **2b–6b** to the corresponding alcohol product employing GDH as the cofactor recycling enzyme (Table 3.2). The enzymatic activity of Ch1-AmDH was determined and optimized in previous studies [4c,21].

ADHs employed in this study showed distinct catalytic activity for each of the applied substrates. AA-ADH and LBv-ADH showed conversion to **1b** with 97% and 99% respectively when using disrupted cell extracts expressed at 25 °C (Table 3.1, entries 1 and 4). Cm-ADH displayed only moderate conversion of ketones **2b–6b** with the highest conversion of 46% for ketones **3b** and **5b** (Table 3.2, entries 2 and 4). Te-ADH-v3 and Te-ADH-v3-NAD were tested with ketone **2b** applying either NAD⁺ or NADP⁺ as the cofactor. NADP-dependent Te-ADH-v3 was operating significantly better when NADP⁺ was applied as the cofactor (76%) whereas Te-ADH-v3-NAD showed only a small difference in conversion with either NAD⁺ or NADP⁺ (Table 3.2, entries 6–9). Tb-ADH-v2-NAD was found to be exclusively NAD-dependent as **4b** was only converted in case NAD⁺ was used (Table 3.2, entry 11).

Table 3.1. Activity tests of the expressed ADHs in the oxidation of **1a** to **1b** utilizing NADH oxidase as the cofactor recycling enzyme. Reaction conditions: disrupted cell extract (450 μL, 0.5 g mL⁻¹ wet cells), KPi buffer (total reaction volume: 0.5 mL, 100 mM, pH 8), MgCl₂ (1 mM), NAD⁺ (1 mM), NOx (6 μM), **1a** (20 mM), 21 h, 30 °C, 170 rpm (orbital incubator).



Entry	Enzyme	Expression T [°C]	Substrate	Conv. to 1b [%]
1	AA-ADH	25	(<i>S</i>)- 1a	97
2		30		82
3		37		73
4	LBv-ADH	25	(<i>R</i>)- 1a	> 99
5		30		> 99
6		37		> 99

3.2.3 Co-immobilization of dehydrogenases

For the co-immobilization of dehydrogenases EziG³ Fe-Amber metal-ion affinity beads were chosen which consist of controlled porosity glass material functionalized with a semi-hydrophobic Fe³⁺-embedded polymer surface [13]. This support material was developed for obtaining high recovery of the catalytic activity by facilitating non-covalent interactions between the enzyme surface and the functionalized support material [13]. Facile co-immobilization of both dehydrogenases was performed thereby generating a heterogeneous dual-enzyme biocatalyst (for procedures; Experimental section). Both dehydrogenases were immobilized from the same enzyme solution by mixing AA-ADH and Ch1-AmDH in a molar ratio of 23:35. The progress of the immobilization was monitored over time and the total enzyme loading on the support was determined through detection of the residual concentrations of the enzymes in solution (i.e., Bradford assay, Supporting Information section S5). Complete immobilization of both enzymes was reached within 3 h under the optimized conditions: AA-ADH (23 nmol), Ch1-AmDH (35 nmol), EziG³ Fe-Amber (10 mg, total enzyme loading: 5% w w⁻¹), Tris buffer (1 mL, 50 mM, pH 8.0), 4 °C, 120 rpm (orbital shaker).

3.2.4 Optimizations for the bio-amination with co-immobilized dehydrogenases

Previously, the dual-enzyme hydrogen-borrowing amination was performed with AA-ADH (33 nmol) and Bb-PhAmDH (63 nmol) using the free enzymes in solution [21, 25]. (S)-**1a** (20 mM) was converted into (R)-**1c** with a maximum conversion of approximately 93% in ammonium chloride buffer (2 M, pH 8.7) [4c], which corresponds to TONs of 303 and 159 for AA-ADH and Bb-PhAmDH respectively. In a more recent publication, a maximum obtained conversion of 93–95% was fixed by the thermodynamics of the system under the applied reaction conditions [6b]. Aiming at assessing and optimizing the efficiency of the asymmetric hydrogen-borrowing amination in a co-immobilized ADH-AmDH system, several sets of experiments were performed in which the molar ratio and enzyme loading of the co-immobilized dehydrogenases as well as the concentration of the applied substrate were optimized.

For defining the optimal enzyme molar ratio in the co-immobilized ADH-AmDH system, two sets of experiments were conducted. In the first set, the amount of AA-ADH was kept constant to a non-limiting value (35 nmol), whereas the amount of Ch1-AmDH was varied (2.3–46 nmol). The reactions with co-immobilized enzymes were performed

under standard reaction conditions (total enzyme loading in relation to the support: 5% w w⁻¹, ammonium chloride buffer (0.5 mL, 2 M, pH 8.7), NAD⁺ (1 mM) and 20 mM (S)-**1a**). The highest TON obtained was 788 for Ch1-AmDH by using 11 nmol of enzyme, which correlated to a conversion above 90% (Table 3.3, entry 4; Figure 3.1A). In the second set, the amount of Ch1-AmDH was kept constant to an estimated non-limiting value (23 nmol), whereas the amount of AA-ADH was varied (3.5–70 nmol). The lowest amount of AA-ADH (3.5 nmol) was sufficient to reach the maximum conversion. The estimated TON for AA-ADH was 2688 (Table 3.3, entry 8; Figure 3.1B). The apparent drop in conversion at lower molar loadings of Ch1-AmDH leads to the suggestion that this enzyme catalyzes the rate-limiting step in the hydrogen-borrowing amination process. This observation is supported by previously reported k_{cat}/K_m values for ADH and AmDH (ADH, k_{cat}/K_m : 10⁴–10⁵ s⁻¹ M⁻¹ and AmDH, k_{cat}/K_m : 10²–10³ s⁻¹ M⁻¹) [4c, 7]. Furthermore, control experiments with the use of non-immobilized AA-ADH and Ch1-AmDH provided similar

Table 3.2. Activity tests of expressed ADHs in the reduction ketones **2b–6b** to alcohols **2a–6a** utilizing GDH as the cofactor recycling enzyme. Reaction conditions: purified ADH (15–52 μM), Tris buffer (total reaction volume: 0.5 mL, 50 mM, pH 8), NAD(P)⁺ (1 mM), GDH (0.4 mg mL⁻¹, lyophilized cell powder), substrate (20 mM), 24 h, 30 °C, 750 rpm (Eppendorf thermomixer).

2a: R = *p*-F-Ph-CH₂-

3a: R = PhO-CH₂-

4a: R = *n*-butyl

5a: R = *n*-pentyl

6a: R = Ph

ADH

NAD(P)H NAD(P)⁺

glucose gluconolactone

GDH

Entry	Enzyme	Enzyme conc. [μM]	Cofactor	Substrate	Conv. [%]
1	Cm-ADH	30	NAD	2b	8
2		30	NAD	3b	46
3		30	NAD	4b	10
4		30	NAD	5b	46
5		52	NAD	6b	27
6	Te-ADH-v3	15	NADP	2b	76
7		15	NAD	2b	38±20 ^[a]
8	Te-ADH-v3-NAD	15	NADP	2b	32
9		15	NAD	2b	43
10	Tb-ADH-v2	25	NADP	4b	6
11		25	NAD	4b	99

^[a] Deviation given as absolute difference between two experiments.

results, which demonstrated that immobilization on EziG³ Fe-Amber did not negatively affect the activity of the enzymes (Supporting information section S7 and Table S4).

Conversely, combining the optimum concentrations of co-immobilized ADH-AmDH (AA-ADH: 3.5 nmol, Ch1-AmDH: 11 nmol) only led to moderate conversions (from 34 to 49%) for the amination of (S)-**1a** at 20 mM substrate concentration (Table 3.3, entry 15). A gradual increase in the concentration of (S)-**1a** in the range of 20 to 100 mM produced a further decrease in the TONs for both ADH and AmDH (Supporting information Figure S2 and Table S5).

Finally, the optimal conditions in terms of productivity of the system were found upon using a 23:3.5 nmol ratio of AmDH to ADH for the amination. The calculated TONs were again 2676 and 406 for AA-ADH and Ch1-AmDH, respectively (Table 3.4, entry 1). The productivity of the system with the optimal molar ratio of ADH to AmDH was tested further. The co-immobilized ADH-AmDH cascade was employed with an increased

Table 3.3. Enzyme molar ratio optimization of co-immobilized Ch1-AmDH and AA-ADH on EziG³ Fe-Amber metal ion affinity beads.

Entry	AmDH [nmol]	AA-ADH [nmol]	n	Conv. [%] (R)- 1c ^[a]	1b ^[a]	(S)- 1a ^[a]	TON _{AmDH} ^[a,b]	TON- ADH ^[a,c]
1	2	35	3	6±2	9±1	86±3	246±88	16±6
2	3	35	3	14±5	9±1	77±6	417±158	41±16
3	6	35	3	32±3	8±0	60±4	560±60	92±10
4	11	35	3	90±0	5±0	5±0	788±1	259±0
5	23	35	3	92±0	4±0	4±0	401±1	264±0
6	34	35	3	92±0	4±0	4±0	268±1	264±1
7	46	35	3	91±0	5±0	4±0	199±1	262±1
8	23	3.5	3	94±0	4±0	3±0	408±2	2688±12
9	23	5.2	3	94±0	4±0	3±0	408±1	1791±3
10	23	8.7	3	94±0	4±0	3±0	407±0	1073±1
11	23	17	3	93±0	4±0	3±0	405±1	533±1
12	23	35	3	92±0	4±0	4±0	401±1	264±1
13	23	52	3	92±0	4±0	4±0	399±2	175±1
14	23	70	3	91±0	4±0	4±0	397±1	131±0
15	11	3.5	3	41±8	7±0	52±8	363±67	1194±219

Number of individual experiments (n) is given for each reaction. Immobilization conditions: Tris buffer (1 mL, 50 mM, pH 8.0), EziG³ Fe-Amber (total enzyme loading in relation to the support: 5% w w⁻¹), Ch1-AmDH (as specified), AA-ADH (as specified), 4 °C, 120 rpm (orbital shaker), 3 h. Reaction conditions: ammonium chloride buffer (reaction volume: 0.5 mL, 2 M, pH 8.7), NAD⁺ (1 mM), (S)-**1a** (20 mM, 1.37 µL), 30 °C, 170 rpm (orbital incubator), 48 h. ^[a] Average values reported with standard deviation. ^[b] µmol of converted substrate per µmol of immobilized Ch1-AmDH. ^[c] µmol of converted substrate per µmol of immobilized AA-ADH.

substrate concentration ((S)-**1a**, 20–100 mM). The best performance was revealed between 30 and 50 mM (Figure 3.2, Table 3.4 entries 2 and 4). The highest TONs were 3541 and 538 for AA-ADH and Ch1-AmDH, respectively (Table 3.4, entry 2). To assess and improve the volumetric productivity, the co-immobilization was performed at different total enzyme loadings (1–10% w w⁻¹). Interestingly, performance of the system was not affected even at the highest loading of 10% w w⁻¹ as conversions and TONs remained unaltered (Table 3.5).

Table 3.4. Catalytic activity of co-immobilized Ch1-AmDH and AA-ADH on EziG³ Fe-Amber metal ion affinity beads at increased substrate concentrations.

Entry	(S)- 1a [mM]	n	Conv. [%]			TON _{AmDH} ^[a,b]	TON _{ADH} ^[a,c]
			(R)- 1c ^[a]	1b ^[a]	(S)- 1a ^[a]		
1	20	3	91±3	5±0	4±2	406±11	2676±72
2	30	3	81±7	5±0	15±6	538±43	3541±285
3	40	3	59±3	4±0	36±3	527±30	3471±196
4	50	3	46±4	4±0	50±4	508±41	3346±271
5	70	3	16±3	4±0	80±3	255±53	1681±351
6	100	3	5±1	3±0	91±1	119±21	783±137

Number of individual experiments (n) is given for each reaction. Immobilization conditions: Tris buffer (1 mL, 50 mM, pH 8.0), EziG³ Fe-Amber (total enzyme loading in relation to the support: 5% w w⁻¹), Ch1-AmDH (23 nmol), AA-ADH (3.5 nmol), 4 °C, 120 rpm (orbital shaker), 3 h. Reaction conditions: ammonium chloride buffer (reaction volume: 0.5 mL, 2 M, pH 8.7), NAD⁺ (1 mM), (S)-**1a** (20 mM, 1.37 µL), 30 °C, 170 rpm (orbital shaker), 48 h. ^[a] Average values reported with standard deviation. ^[b] µmol of converted substrate per µmol of immobilized Ch1-AmDH. ^[c] µmol of converted substrate per µmol of immobilized AA-ADH.

Table 3.5. Total enzyme loading optimization of co-immobilized Ch1-AmDH and AA-ADH on EziG³ Fe-Amber metal ion affinity beads.

Entry	Total enzyme loading [% w w ⁻¹]	n	Conv. [%]			TON _{AmDH} ^[a,b]	TON _{ADH} ^[a,b]
			(R)- 1c ^[a]	1b ^[a]	(S)- 1a ^[a]		
1	1	3	89±0	7±0	4±0	387±2	1546±7
2	2	3	92±0	5±0	3±0	402±1	1607±2
3	3	3	93±0	4±0	3±0	404±1	1618±3
4	5	3	93±0	4±0	2±0	406±1	1626±3
5	7	3	93±0	4±0	2±0	407±0	1627±2
6	10	3	94±0	4±0	2±0	407±0	1629±1

Number of individual experiments (n) is given for each reaction. Immobilization conditions: Tris buffer (1 mL, 50 mM, pH 8.0), EziG³ Fe-Amber (total enzyme loading in relation to the support: varied between 1–10% w w⁻¹), Ch1-AmDH (23 nmol), AA-ADH (8.7 nmol), 4 °C, 120 rpm (orbital shaker), 3 h. Reaction conditions: ammonium chloride buffer (reaction volume: 0.5 mL, 2 M, pH 8.7), NAD⁺ (1 mM), (S)-**1a** (20 mM, 1.37 µL), 30 °C, 170 rpm (orbital shaker), 48 h. ^[a] Average values reported with standard deviation. ^[b] µmol of converted substrate per µmol of immobilized enzyme.

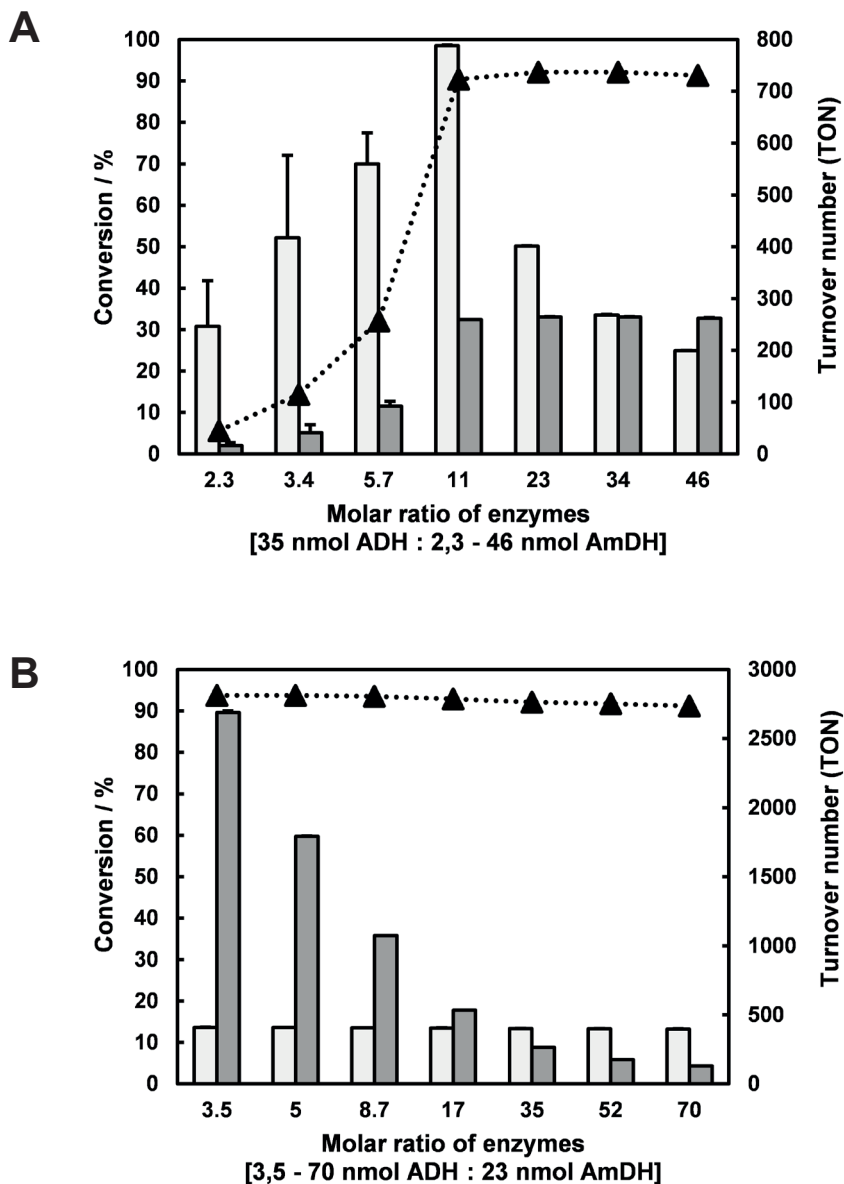


Figure 3.1. Co-immobilization of AA-ADH and Ch1-AmDH on EziG³ Fe-Amber ion-affinity beads altering the molar ratio of enzymes. Conversion of (*S*)-**1a** (20 mM) into (*R*)-**1c** (black triangles), TON_{ADH} (dark gray bars), and TON_{AmDH} (light gray bars) are shown for A) the influence of the amount of immobilized Ch1-AmDH (2.3–46 nmol) at constant amount of immobilized ADH (35 nmol) and B) the influence of the amount of immobilized AA-ADH (3.5–70 nmol) at constant amount of immobilized Ch1-AmDH (23 nmol). Immobilization conditions: Tris buffer (50 mM, pH 8.0, 1 mL), 4 °C, 120 rpm, 3 h. Reaction conditions: ammonium chloride buffer (2 M, pH 8.7, 0.5 mL), NAD⁺ (1 mM), 30 °C, 170 rpm (orbital shaker), 48 h. The data represents the average of three experiments and error bars the standard deviation (n=3).

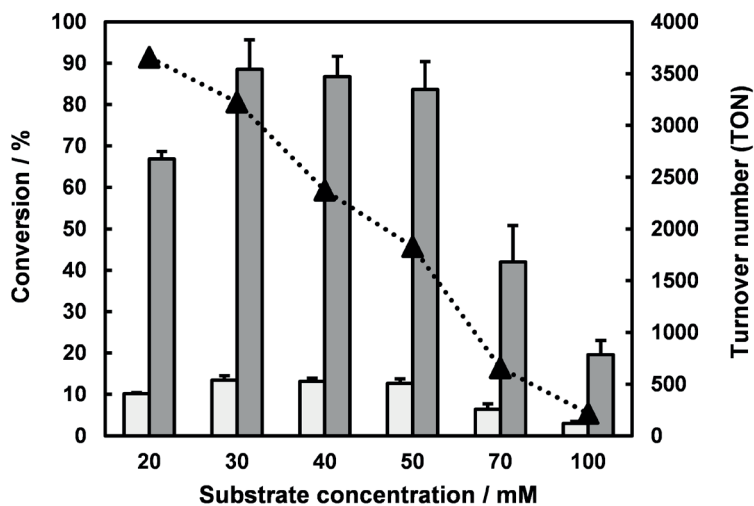


Figure 3.2. Co-immobilized AA-ADH and Ch1-AmDH on EziG³ Fe-Amber ion-affinity beads subjected to higher substrate concentrations. Conversion of (*S*)-**1a** (20–100 mM) into (*R*)-**1c** (black triangles), TON_{ADH} (dark gray bars), and TON_{AmDH} (light gray bars) are shown. The data represents the average of three experiments and error bars the standard deviation (n=3).

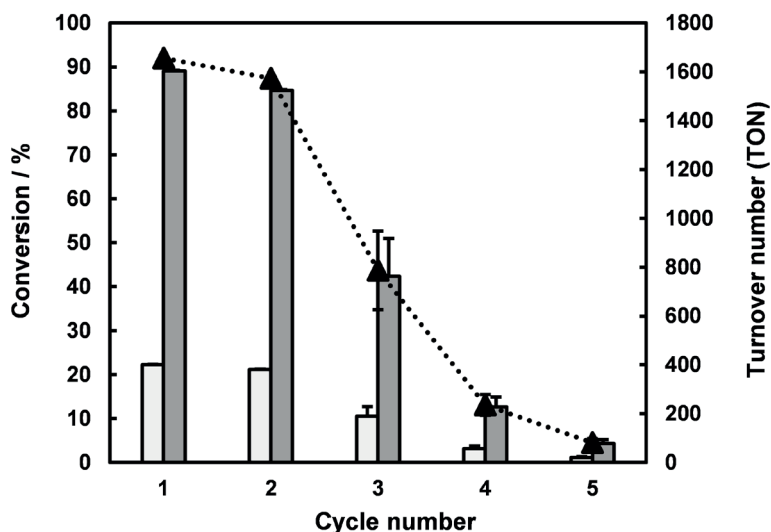


Figure 3.3. Recycling of co-immobilized AA-ADH and Ch1-AmDH on EziG³ Fe-Amber ion-affinity beads. Conversion of (*S*)-**1a** (20 mM) into (*R*)-**1c** (black triangles), TON_{ADH} (dark gray bars), and TON_{AmDH} (light gray bars) are shown. The data represents the average of three experiments and error bars the standard deviation (n=3).

3.2.5 Application of co-immobilized dehydrogenases in the amination of alcohols

The optimized reaction conditions for the amination of (S)-**1a** proved to be suitable for further development of the co-immobilized ADH-AMDH cascade. A small panel of aliphatic- and phenyl-substituted alcohol substrates (S)-**2a–5a** could successfully be converted (up to 95%) with perfect inversion of configuration to the corresponding amine products (>99% *ee* (*R*), Table 3.6, Scheme 3.2). TONs as high as 826 and 1894 were obtained for Ch1-AmDH and AA-ADH respectively. Practical applicability of the co-immobilized ADH-AMDH cascade was demonstrated further by performing the preparative scale amination of (S)-**1a** (20 mM, 50 mg), which resulted in 90% conversion and 80% isolated yield of (*R*)-**1c** (for details; Experimental section).

3.2.6 Elaboration on limitations in recycling of the co-immobilized ADH-AmDH cascade

Biocatalyst recycling is accomplished conveniently through enzyme immobilization and it significantly improves the applicability and scalability of processes. The reusability of the co-immobilized ADH-AmDH cascade system was demonstrated as a proof of principle. Applying consecutive reaction cycles of 24 h, partial activity was retained in the amination of (S)-**1a** in up to five cycles (Figure 3.3). The calculated total turnover number (TTN, i.e. the sum of the TONs from each cycle) were 4195 and 1049 for immobilized AA-ADH and Ch1-AmDH, respectively. The drop in apparent activity over each cycle could partly be attributed to mechanical stress caused by shaking of the immobilized enzymes in the batch reactor (reactor volume: 2 mL). Significant gains in activity recovery were

Table 3.6. Hydrogen-borrowing amination of alcohols (S)-**2a–5a** with co-immobilized AA-ADH and Ch1-AmDH on EziG³ Fe-Amber ion-affinity beads.

Entry	Substrate	n	Conversion ^[a] [%]	<i>ee</i> (<i>R</i>) [%]	TON	
					TON _{ADH} ^[b]	TON _{AmDH} ^[b]
1	(S)- 2a	2	95±0	> 99	2183±4	826±2
2	(S)- 3a	2	28±1	> 99	649±24	241±9
3	(S)- 4a	2	82±11	> 99	1894±254	716±96
4	(S)- 5a	2	95±0	> 99	2173±6	822±2

Number of individual experiments (n) is given for each reaction. Immobilization conditions: Tris buffer (50 mM, pH 8.0, 1 mL), EziG³ Fe-Amber (total enzyme loading in relation to the support: 5% w w⁻¹), Ch1-AmDH (23 nmol), AA-ADH (8.7 nmol) 4 °C, 120 rpm, 3 h. Reaction conditions: ammonium chloride buffer (2 M, pH 8.7, reaction volume: 0.5 mL), NAD⁺ (1 mM), substrate (20 mM), 30 °C, 170 rpm (orbital incubator), 48 h. ^[a] Percentage value of obtained amine product. ^[b] TON is defined as μmol of converted substrate per μmol of enzyme.

observed upon decreasing the orbital shaking speed from 750 rpm to 600 rpm (Eppendorf thermomixer). Particularly, at higher orbital shaking speed, a catalytic activity drop of almost 50% was observed in the second reaction cycle whereas at lower orbital shaking speed more than 85% of activity was recovered (data not shown). However, a dramatic drop in performance was observed in the following third reaction cycle indicating that the immobilized enzymes exhibited low stability under the applied reaction conditions.

Further studies suggested no influence of the applied reaction medium on the stability of the immobilized enzymes during the reaction. Incubation of co-immobilized AA-ADH and Ch1-AmDH in ammonium chloride buffer (2 M, pH 8.7) up to three days showed no changes in the appearance of the biocatalyst. Subsequent addition of substrate (*S*)-**5a** resulted in 95% conversion within 48 hours reaction time. Notably, the purified enzymes were slowly precipitating over time indicating the use of EziG support material to have stabilizing effects. Lowering of the ionic strength in the ammonium chloride buffer from 2 M to 1 M resulted in no apparent change in conversion. However, applying lower ammonium chloride concentrations proved insufficient for acquiring full conversion of (*S*)-**5a** within 48 hours of reaction time (Figure 3.4). Although already applied in catalytic amounts, NAD⁺ cofactor concentrations could be lowered from 1 mM to 0.5 mM without any observable loss in catalytic activity. Further suggested improvements regarding the

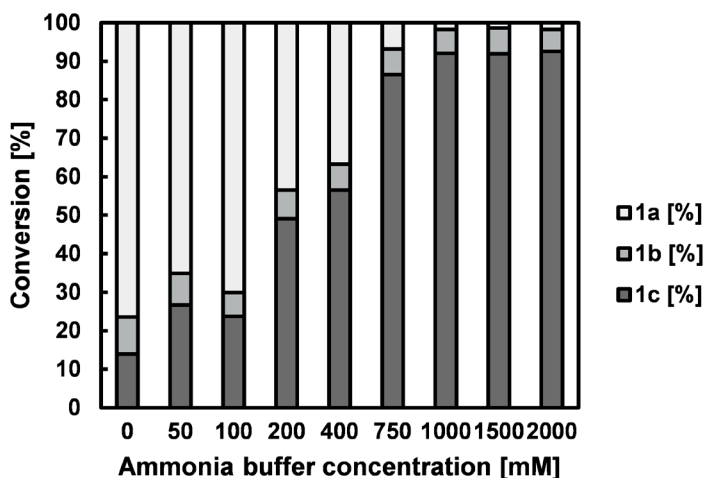


Figure 3.4. Co-immobilized AA-ADH and Ch1-AmDH applied for the hydrogen-borrowing amination of (*S*)-**5a** and varying the concentration of the ammonium species in the reaction buffer. Reaction conditions: co-immobilized AA-ADH and Ch1-AmDH on EziG³ Fe Amber (20 mg, total enzyme loading in relation to the support: 5% w w⁻¹), ammonium chloride buffer (1 mL, concentration varied, pH 8.7), NAD⁺ (1 mM), (*S*)-**5a** (10 mM), DMSO (2.5%, v v⁻¹), 30 °C, 750 rpm (Eppendorf thermomixer), 48 h.

ADH-AmdH cascade system could involve reactor engineering such as application of the immobilized enzymes in a flow reactor. Generally, flow reactors reduce the mechanical stress on enzymes and they possess higher volumetric productivity due to increased mass transfer and diffusion rates. More detailed information on biocatalysis in flow reactors will be provided in Chapter 4. A similar ADH-AmdH cascade was recently applied in a flow reactor employing Ch1-AmdH and an ADH from *Thermoanaerobacter brockii* (TeSADH or Tb-ADH-v2, W110A/G198D) ^[14b]. Ketone **2a** was aminated with a steady-state conversion of ca. 30% producing (*R*)-**2c** with a space-time yield (STY) of 13 g L⁻¹ day⁻¹.

3.2.7 Extending the reactivity of the ADH-AmdH cascade

Application of the ADH-AmdH cascade with co-immobilized enzymes was restricted to the conversion of (*S*)-alcohols to (*R*)-amines. Although development of an (*S*)-selective AmdH to access stereocomplementary amine products has proved challenging by the use of protein engineering, several ADHs are known to accept (*R*)-configured alcohol substrates. Combinations of different ADHs with Ch1-AmdH in the hydrogen-borrowing amination cascade allows for an extended substrate scope by enabling the conversion of (*R*)-alcohols and even racemic alcohols to (*R*)-amines. A selected panel of ADHs was used for the purpose of extending the applicability of the ADH-AmdH cascade: NAD-dependent variant of LBv-ADH from *Lactobacillus brevis* ^[7c, 22], Cm-ADH from *Candida maris* ^[23], NAD-dependent mutant of Te-ADH-v3 from *Thermoanaerobacter ethanolicus* (triple variant, I86A/W110A/C295A ^[24]) and Tb-ADH-v2 from *Thermoanaerobacter brockii* ^[6a]. Since non-selective ADHs for the acceptance of racemic alcohols were not available at the time, a combination of two stereocomplementary ADHs was envisioned in tandem with Ch1-AmdH. This allows for the one-pot synthesis of (*R*)-amines from racemic alcohols.

Previously reported combinations of (*S*)-selective AA-ADH, (*R*)-selective LBv-ADH and Ch1-AmdH were shown to be inactive in the ADH-AmdH cascade under standard reaction conditions (2 M ammonium chloride, pH 8.7, 1 mM NAD⁺, 20 mM (*S*)-**1a**, 30 °C) ^[4c]. Especially, combining LBv-ADH and Ch1-AmdH in one-pot led to precipitation which was attributed to destabilization of his-tagged Ch1-AmdH by free divalent cations originating from LBv-ADH. Co-immobilization of the enzymes on EziG support material was envisioned as to stabilize the system and provide the opportunity for recycling of the biocatalyst. LBv-ADH and Ch1-AmdH were immobilized on EziG³ Fe-Amber in separate batch vials. The immobilized enzymes were later combined in one-pot and tested for the conversion of

(*R*)-**1a** (20 mM). In a parallel experiment both enzymes were combined in one-pot and co-immobilized from the same solution before applying them in the reaction. Interestingly, no conversion was observed in any of the reactions and inactivation could be attributed to observed precipitation of the enzymes from the solution (Table 3.7, entries 1–2).

(*R*)-selective Cm-ADH was chosen as an alternative candidate for LBv-ADH. In combination with AA-ADH and Ch1-AmDH, this enzyme should allow for conversion of racemic alcohols to (*R*)-amines. Co-immobilization on EziG³ Fe-Amber was performed from one solution containing all three enzymes and proceeded within 3 hour of incubation. Subsequently the co-immobilized enzymes were employed in the ADH-AmDH cascade with racemic alcohols (*rac*)-**1a–5a**. Conversions to the corresponding (*R*)-amine products ranged from 29–49% and in all cases with perfect enantiomeric excess (>99% *ee*, Table 3.7, entries 7–11). Interestingly, the remaining substrate after the reaction was found to be predominantly the (*R*)-alcohol. Correlating the conversion to the amine products and the enantiomeric excess of the remaining alcohol substrates provides a strong indication that Cm-ADH did not contribute to the reaction and remained inactive. Instead AA-ADH converted the (*S*)-alcohol to the corresponding ketone which was then further converted by Ch1-AmDH to the (*R*)-amine product. For example, (*rac*)-**5a** was converted to afford 50% of (*R*)-**5c**

Table 3.7. Co-immobilized ADH-AmDH combinations on EziG support material.

Entry	Enzymes	Immobil. method	Molar ratio	Substrate	Conv. ^[a]	ee% ^[b]
			ADH : AmDH		[%]	alcohol
1	LBv-ADH : AMDH	Separate	20 : 20	(<i>R</i>)- 1a	0	n.d.
2	LBv-ADH : AMDH	Combined	20 : 20	(<i>R</i>)- 1a	0	n.d.
3	Te-ADH-v3-NAD : AmDH	Combined	10 : 23	(<i>rac</i>)- 2a	3	n.d.
4	Te-ADH-v3-NAD : AmDH	Combined	10 : 23	(<i>rac</i>)- 3a	3	n.d.
5	Te-ADH-v3-NAD : AmDH	Combined	10 : 23	(<i>rac</i>)- 4a	7	n.d.
6	Te-ADH-v3-NAD : AmDH	Combined	10 : 23	(<i>rac</i>)- 5a	9	n.d.
7	AA-ADH : Cm-ADH : AmDH	Combined	4.4 : 40 : 23	(<i>rac</i>)- 1a	29	50 (<i>R</i>)
8	AA-ADH : Cm-ADH : AmDH	Combined	4.4 : 40 : 23	(<i>rac</i>)- 2a	29	47 (<i>R</i>)
9	AA-ADH : Cm-ADH : AmDH	Combined	4.4 : 40 : 23	(<i>rac</i>)- 3a	23	33 (<i>R</i>)
10	AA-ADH : Cm-ADH : AmDH	Combined	4.4 : 40 : 23	(<i>rac</i>)- 4a	36	> 99 (<i>R</i>)
11	AA-ADH : Cm-ADH : AmDH	Combined	4.4 : 40 : 23	(<i>rac</i>)- 5a	49	> 99 (<i>R</i>)

Immobilization conditions: Tris buffer (50 mM, pH 8.0, 1 mL), EziG³ Fe-Amber (total enzyme loading in relation to the support: 5% w w⁻¹), Ch1-AmDH (23 nmol), AA-ADH (8.7 nmol), 4 °C, 120 rpm, 3 h. Reaction conditions: NH₄Cl (2 M, pH 8.7, reaction volume: 0.5 mL), NAD⁺ (1 mM), substrate (20 mM), 30 °C, 170 rpm (orbital incubator), 48 h. ^[a] Conversion to the amine product. ^[b] Enantiomeric excess of the remaining alcohol substrate.

while alcohol (*R*)-**5b** remained unconverted in solution (>99% *ee*, Table 3.7, entry 11).

Finally, altered cofactor-dependence triple mutated variant of Te-ADH-v3 (I86A/W110A/C295A) ^[24] was engineered in our lab making it applicable for the ADH-AmDH cascade. Unfortunately, this particular variant proved to be dramatically unstable as a purified enzyme. Precipitation of the protein proceeded upon dialysis in KPi and Tris buffers at pH values of 6–8. A small amount of the enzyme could be recovered and was found to be active in the reduction of ketone **2b**. Notably, the enzyme switched cofactor preference from NADP⁺ to NAD⁺, whereas the original triple mutant Te-ADH-v3 showed more consistent conversions in the presence of NADP⁺ (Table 3.2, entries 6–9). Further protein engineering is required to improve the stability and reactivity of the NAD-dependent variant of Te-ADH-v3 since this engineered NAD-dependent ADH variant showed very low conversions in the ADH-AmDH cascade (Table 3.7, entries 3–6). Notably, an active ADH from *Thermoanaerobacter brockii* was reported recently and applied as co-immobilized enzyme on EziG support material in the ADH-AmDH cascade both in batch and continuous flow operation ^[6a].

3.3 Conclusion

The applicability of the asymmetric hydrogen-borrowing alcohol bioamination was improved by co-immobilizing an alcohol dehydrogenase (AA-ADH) with an amine dehydrogenase (Ch1-AmDH) on controlled porosity glass (CPG) Fe^{III} ion-affinity beads (EziGTM). Conversions (up to 95%) and enantiomeric excess values (>99% (*R*)) were comparable to those of reactions performed with isolated enzymes in solution. Notably, recyclability of ADH-AmDH was demonstrated, which led to total turnover numbers that were improved approximately 2 to 15-fold compared with control experiments from this work. Admittedly, the maximum applied substrate concentration (20–50 mM) is currently below the requirements for industrial application. Furthermore, the recyclability is limited to a few reaction cycles despite preliminary reaction medium engineering was performed. One major issue was found to be product inhibition observed in AmDH-catalyzed reactions ^[26]. However, the use of aqueous–organic biphasic media enabled the reductive amination of ketones with AmDHs to proceed up to 96% conversion at a concentration of 400 mM and ^[26a]. Reactivity of the ADH-AmDH cascade towards the conversion of racemic alcohols to (*R*)-amines by applying combinations of stereocomplementary ADHs with Ch1-AmDH was unsuccessful. However, a suitable ADH variant (Tb-ADH-v2, W110A/G198D ^[14b]) was developed recently

and employed in the ADH-AmDH cascade under batch as well as continuous flow operation^[6a]. Hence, future work must focus on evaluating diverse CPG carriers possessing different polymeric films (from hydrophobic to hydrophilic) and on improving the stability of enzymes in aqueous–organic media. This strategy might permit to tune the compatibility between carrier and dehydrogenases depending on the reaction media and conditions. Another option is to extend the hydrogen-borrowing amination to a subsequent biocatalytic step, which would allow for the in-situ removal of the amine product and hence solve the issue of product inhibition along with shifting the thermodynamic equilibrium of the reaction. Thus, apparent kinetics and actual TTNs might increase significantly. Finally, the hydrogen-borrowing amination cascade can be extended to the production of secondary amines combining ADHs with an imine reductase (IREDs) or a reductive aminase (RedAm) as co-immobilized enzymes operating in batch as well as continuous flow.

3.4 Experimental section

3.4.1 General information

(*S*)-alcohols **1a**, **4a–6a** and ketones **1b–6b** were purchased from Sigma-Aldrich (Steinheim, Germany). (*S*)-alcohols **2a**, **3a** were synthesized by previously reported methods [4c]. Amines (*S*)-**1c–5c** and (*R*)-**1c–5c** were synthesized as reference compounds employing commercially available stereocomplementary ω -transaminases ATA-113, ATA-117 (from Codexis, Redwood City, California, US) [27]. Nicotinamide cofactor (NAD⁺) was purchased from Melford Biolaboratories (Chelsworth, Ipswich, UK). Lysozyme from chicken egg white (3.2 mg, Sigma L6876, lyophilized powder, protein 95%, >40000 U/mg protein) was purchased from Sigma-Aldrich (Steinheim, Germany). The Ni²⁺ affinity columns (HisTrap FF, 5 mL) were purchased from GE Healthcare Bio-Sciences (Munich, Germany). Controlled porosity glass EziG³ Fe-Amber metal-ion affinity beads were kindly provided by EnginZyme AB (Stockholm, Sweden).

3.4.2 Expression and purification of dehydrogenases

Dehydrogenase enzymes (AA-ADH and Ch1-AmDH) were expressed as recombinant enzymes in *E. coli* BL21 strains. Details on the expression and purification of the enzymes can be found in Supporting Information section S3.

Other ADHs used in this study were expressed and purified accordingly: LBv-ADH (N-term His₆ enzyme, in *E. coli* BL21 (DE3)), Cm-ADH (C-term His₆, BL21 (C43)), Te-ADH-v3 (N-term His₆, BL21 (DE3)), Te-ADH-v3-NAD (N-term His₆, BL21 (C43)) and Tb-ADH-v2 (N-term His₆, BL21 (DE3)). Detailed information on the enzymes in this study is listed in the section General information on enzymes. Protein yields obtained from purification are listed in Table 3.8. SDS PAGE electrophoresis gels are reported in Figures 3.5 and 3.6.

3.4.3 Activity testing of ADH

Wet cells containing the expressed ADH of interest (0.17 g mL⁻¹, AA-ADH or LBv-ADH) were suspended in KPi buffer (100 mM, pH 8, 1 mM MgCl₂) and disrupted by sonication. The cell extract was obtained after centrifugation (14 krpm, 4 °C, 10 min). To 450 μ L of the cell extract was added 50 μ L stock of

Table 3.8. Protein yields obtained from the purification of dehydrogenases by Ni²⁺ affinity chromatography.

Entry	Enzyme	Protein obtained	Protein yield	Protein yield
		[mg]	[mg _{enzyme} /g _{wet cells}]	[mg _{enzyme} /L _{cell culture}]
1	Ch1-AmDH	244	61	254
2	AA-ADH	500	13	47
3	LBv-ADH	400	50	167
4	Cm-ADH	864	32	183
5	Te-ADH-v3	38	9	48
6	Te-ADH-v3-NAD	n.d. ^[a]	n.d. ^[a]	n.d. ^[a]
7	Tb-ADH-v2	90	30	113

^[a] not determined. Low stability of the protein prevented accurate determination of protein yields.

1 mM NAD⁺ in KPi. NADH oxidase (NOx, 5.5 μM) and (*R*)-**1a** (1.45 μL, 20 mM) for LBv-ADH or (*S*)-**1a** (1.45 μL, 20 mM) for AA-ADH were added. The reactions were shaken (170 rpm, orbital incubator) at 30 °C and quenched after 21 hours with KOH (100 μL, 10 M). The aqueous layer was extracted with EtOAc (2 x 400 μL). The organic layer was dried over MgSO₄ and injected on GC (for details; Analytics, DB1701-30m method A).

Other ADHs were tested as purified enzymes in the reduction of ketones **2b–6b**. Purified ADH of interest (Cm-ADH, 30-52 μM; Te-ADH-v3, 15 μM; Te-ADH-v3, 15 μM; Tb-ADH-v2, 25 μM) was added to a solution of NAD(P)⁺ (1 mM, see also Table 3.2), glucose (60 mM) and GDH (0.4 mg mL⁻¹, lyophilized cell powder) in Tris buffer (reaction volume: 0.5 mL, 100 mM, pH 8.0). Substrate ketone (20 mM) was added and the samples were shaken (750 rpm, Eppendorf thermomixer) for 24 h at 30 °C. Work up was performed by quenching with KOH (100 μL, 10 M) and the aqueous layer was extracted with EtOAc (2 x 400 μL). The organic layer was dried over MgSO₄ and injected on GC (for details; Analytics, DB1701-30m method A).

3.4.4 *General procedure for EziG metal-ion affinity co-immobilization of dehydrogenase*

Purified recombinant proteins Ch1-AmDH (23 nmol) and ADHs of interest (AA-ADH, 8.7 nmol; Te-ADH-v3, 10 nmol; Cm-ADH, 40 nmol) were combined in Tris buffer (1 mL, 50 mM, pH 8.0) at 4 °C. EziG³ Fe-Amber metal ion affinity beads (10 mg, total enzyme loading in relation to the support: 5% w w⁻¹) were suspended in the enzyme solution and the suspension was incubated for 3 hours at 4 °C (orbital shaking, 120 rpm). Bradford assay (980 μL of ready to use Bradford solution plus 20 μL sample, measuring absorbance at λ of 595 nm) was used to monitor the immobilization process over the time as well as to determine the total enzyme loading. The co-immobilized enzymes were collected by sedimentation and the remaining buffer solution was discarded. The immobilized enzymes were used directly in biotransformations.

The same procedure was followed for immobilization at larger scale, typically using 40 mg of purified Ch1-AmDH (920 nmol), 10 mg of AA-ADH (350 nmol) and 500 mg of EziG³ Fe-Amber beads. Full immobilization was obtained after 3 h (total enzyme loading: 10%, w w⁻¹).

3.4.5 *General procedure for analytical scale reactions with co-immobilized dehydrogenases*

EziG³ Fe-Amber beads carrying the immobilized enzymes (20 mg, dry weight, total enzyme loading in relation to the support: 5% w w⁻¹) were suspended in ammonium chloride buffer (0.5 mL, 2 M, pH 8.7) containing NAD⁺ (1 mM). Then, the alcohol substrate **1a–5a** (20 mM, (*S*) or (*R*) or racemic depending on the composition of the immobilized enzymes) was added. The reaction was incubated at 30 °C (170 rpm, orbital incubator or 750 rpm, Eppendorf thermomixer) for 24 h or 48 h. At the end of the reaction, the co-immobilized enzymes were recovered by sedimentation. For the recycling experiments, the co-immobilized enzymes were suspended in fresh reaction buffer and incubated for another reaction cycle of 24 h. The aqueous reaction phase was treated with KOH (100 μL, 10 M) and extracted with EtOAc (2 x 500 μL). The organic layer was dried over MgSO₄ and injected on GC (for details; Analytics, DB1701-30m method A). Derivatization of the samples was performed by adding 4-dimethylaminopyridine into acetic anhydride (40 μL of 50 mg mL⁻¹ stock solution). The samples were shaken in an incubator at RT for 30 minutes. Afterwards, water (300 μL) was added and the samples were shaken for an additional 30 minutes. After centrifugation, the organic layer

was dried over MgSO_4 . Enantiomeric excess was determined by GC with a Variant Chiracel DEXCB column (for details, Analytics, DEX-CB-method A)).

3.4.6 Preparative scale amination reaction with co-immobilized dehydrogenases

The preparative scale reaction was performed in a 50 mL round-bottom flask in ammonium chloride buffer (20 mL, 2 M, pH 8.7) with 1 mM NAD^+ and (*S*)-**1a** (20 mM, 52.4 μL , 0.39 mmol) as a substrate. The reaction was incubated for 24 hours at 30 °C. Work-up of the reaction was performed by separating the beads from the reaction mixture by pipetting. Acidification (pH 2, universal pH indication paper) of the water layer and extraction of the unreacted alcohol and ketone intermediate was performed (EtOAc, 1 x 15 mL). The water layer was basified (pH 12, universal pH indication paper) and the amine product was extracted three times with EtOAc (3 x 15 mL). The organic layer was dried over MgSO_4 and the solvent evaporated to yield a slightly yellow oil (42 mg, 0.31 mmol, 80% yield). ^1H NMR (Figure 3.7, 400 MHz, Chloroform-*d*) δ 7.27 (ddd, $J = 33.6, 14.8, 6.9$ Hz, 5H), 3.20 (dq, $J = 12.4, 6.2$ Hz, 1H), 2.74 (dd, $J = 13.3, 5.4$ Hz, 1H), 2.56 (dd, $J = 13.2, 8.0$ Hz, 1H), 1.69 (s, 3H), 1.15 (d, $J = 6.3$ Hz, 3H).

A small sample of the reaction after 24 hours (0.5 mL) was quenched with KOH (100 μL , 10 M), and extracted with EtOAc (2 x 500 μL). The organic layer was dried over MgSO_4 and injected on GC-FID (for details: Analytics, method: DB1701-60m-A, 93% conversion). The enantiomeric excess of the amine product (*R*)-**1c** was determined after derivatization. Derivatization of the samples was performed by adding 4-dimethylaminopyridine into acetic anhydride (40 μL of 50 mg mL^{-1} stock solution). The samples were shaken in an incubator at RT for 30 minutes. Afterwards, water (300 μL) was added and the samples were shaken for an additional 30 minutes. After centrifugation, the organic layer was dried over MgSO_4 . Enantiomeric excess was determined by GC with a Variant Chiracel DEXCB column (for details: Analytics, DEX-CB-method A, >99% ee).

3.4.7 Analytics

GC analysis was performed according to previously described procedures [4c]. The conversion for the hydrogen-borrowing amination of alcohols was determined by GC using a 7890A GC system (Agilent Technologies), equipped with a FID detector using H_2 as carrier gas with a DB-1701 column from Agilent (30 m or 60 m, 250 μm , 0.25 μm). GC retention times of compounds 1–5 in this study are listed in Supporting Information Table S9.

DB1701-30m method A: constant pressure 13.5 psi, T injector 300 °C, split ratio 40:1, T initial 80 °C, hold 6.5 min; gradient 10 °C/min up to 160 °C, hold 5 min; gradient 20 °C/min up to 200 °C, hold 2 min; gradient 20 °C/min up to 280 °C, hold 1 min.

DB1701-30m method B: constant pressure 13.5 psi, T injector 300 °C, split ratio 40:1, T initial 60 °C, hold 6.5 min; gradient 20 °C/min up to 100 °C, hold 1 min, gradient 20 °C/min up to 280 °C, hold 1 min.

DB1701-60m method A: constant pressure 13.5 psi, T injector 300 °C, split ratio 40:1, T initial 80 °C, hold 6.5 min, gradient 5 °C/min up to 160 °C, hold 2 min; gradient 20 °C/min up to 280 °C, hold 1 min.

DEX-CB method A: constant flow 1.4 mL/min, T injector 250 °C, split ratio 40:1, T initial 100 °C, hold 2 min; gradient 1 °C/min up to 130 °C, hold 5 min; gradient 10 °C/min up to 170 °C, hold 10 min.;

gradient 10 °C/min up to 180 °C, hold 1 min.

3.5 Experimental data

3.5.1 SDS-PAGE

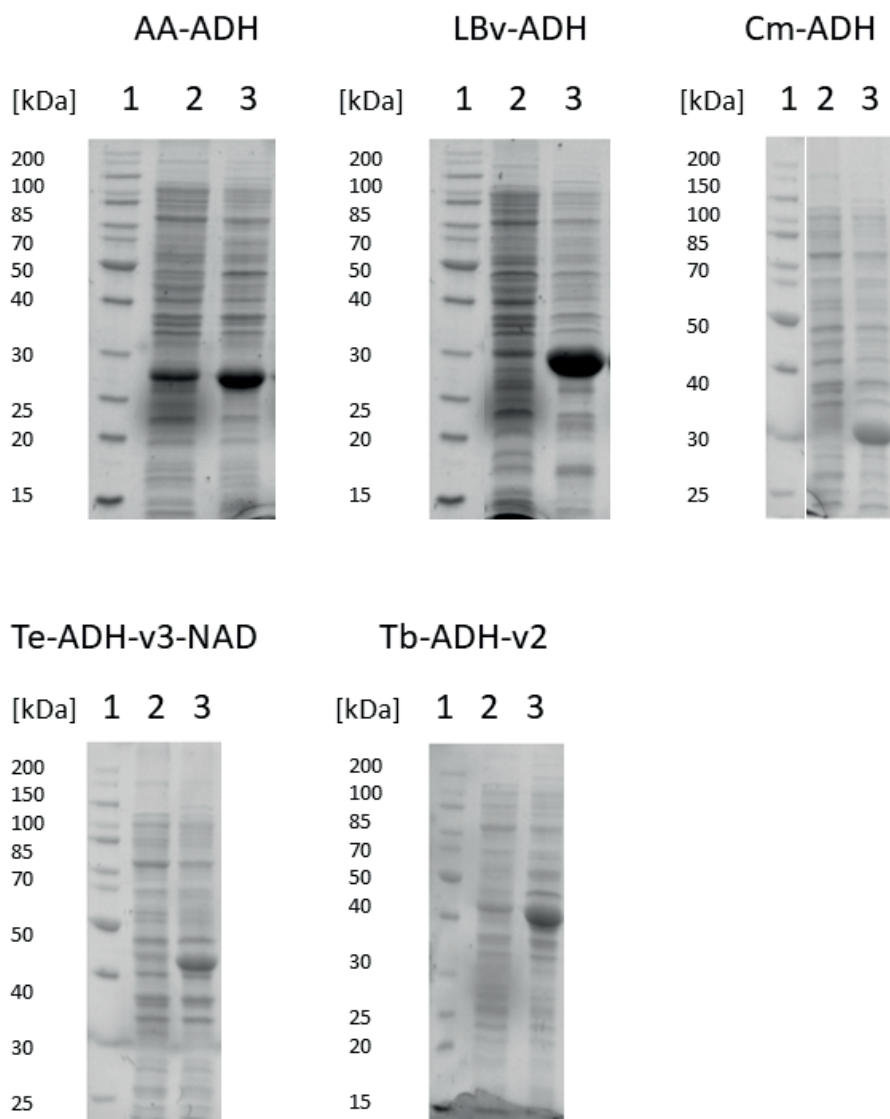


Figure 3.5. SDS PAGE gel electrophoresis of wet cell samples expressing AA-ADH (28.7 kDa), LBv-ADH (28.9 kDa), Cm-ADH (28.3 kDa), Te-ADH-v3-NAD (39.9 kDa) and Tb-ADH-v2 (39.8 kDa) at 25 °C. Entry 1 displays a protein mass reference sample (PageRuler Unstained Protein Ladder, 10 – 200 kDa). Samples in entry 2 and 3 were taken before and after IPTG induction respectively (0.5 mM IPTG). Protein bands were visualized by UV.

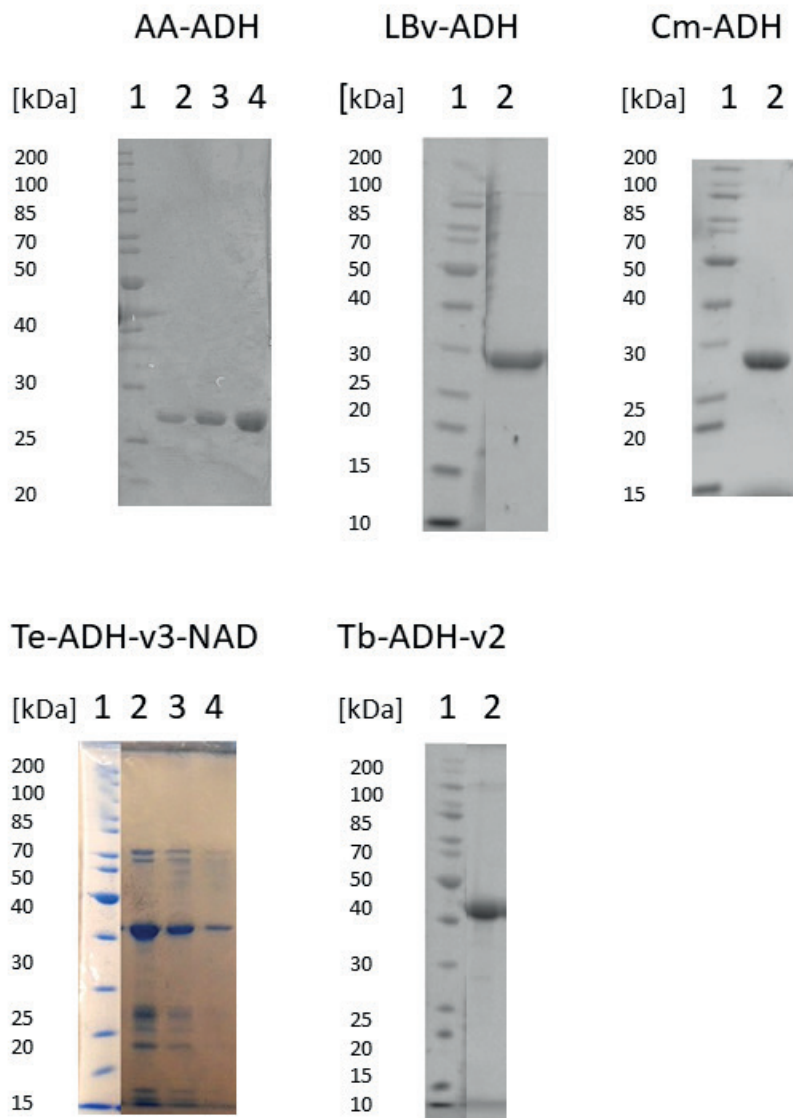


Figure 3.6. SDS PAGE gel electrophoresis of ADHs after purification: AA-ADH (28.7 kDa), LBv-ADH (28.9 kDa), Cm-ADH (28.3 kDa), Te-ADH-v3-NAD (39.9 kDa) and Tb-ADH-v2 (39.8 kDa). Entry 1 displays a protein mass reference sample (PageRuler Unstained Protein Ladder, 10 – 200 kDa). Protein bands were visualized by UV or Coomassie stain.

3.5.2 NMR

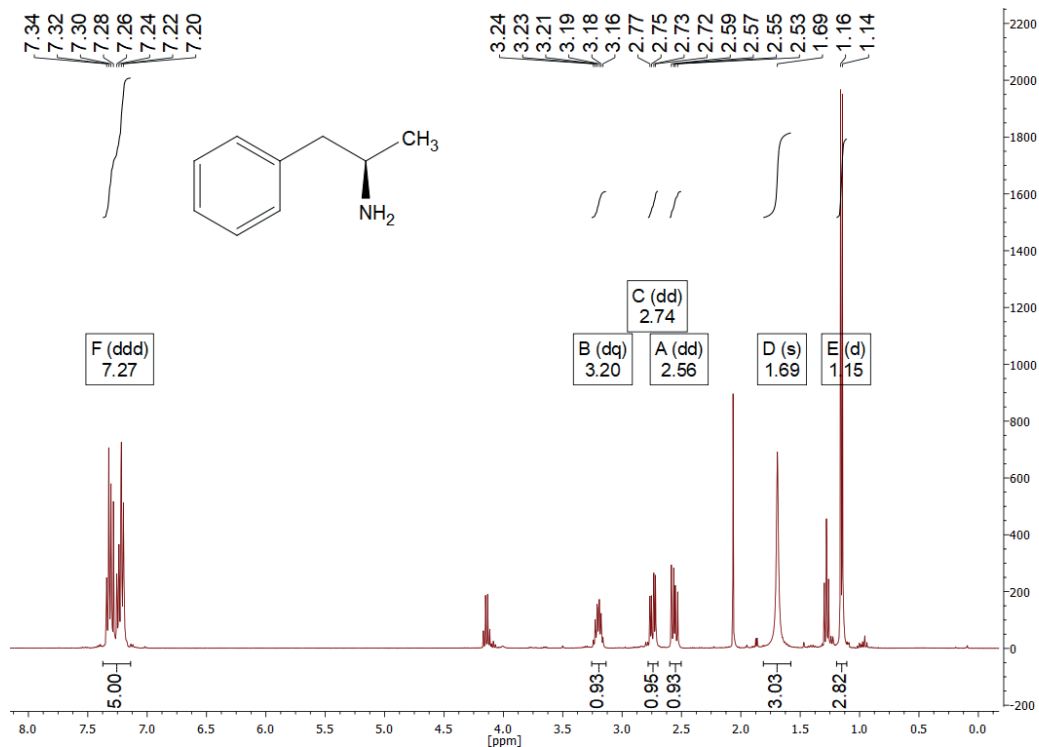


Figure 3.7. ^1H -NMR of (*R*)-**1c** obtained from the preparative scale reaction with co-immobilized dehydrogenases AA-ADH and Ch1-AmDH on EziG³ Fe Amber (400 MHz, Chloroform-*d*).

3.6 References

- [1] Pinggen, D.; Müller, C.; Vogt, D. *Angewandte Chemie International Edition*. **2010**, *49*, 8130–8133.
- [2] Gunanathan, C.; Milstein, D. *Angewandte Chemie International Edition*. **2008**, *47*, 8661–8664.
- [3] a) Bähn, S.; Imm, S.; Neubert, L.; Zhang, M.; Neumann, H.; Beller, M. *ChemCatChem*. **2011**, *3*, 1853–1864; b) Imm, S.; Bahn, S.; Neubert, L.; Neumann, H.; Beller, M. *Angewandte Chemie International Edition*. **2010**, *49*, 8126–8129; c) Grigg, R.; Mitchell, T. R. B.; Sutthivaiyakit, S.; Tongpenyai, N. *Journal of the Chemical Society-Chemical Communications*. **1981**, 611–612; d) Oldenhuis, N. J.; Dong, V. M.; Guan, Z. *Journal of the American Chemical Society*. **2014**, *136*, 12548–12551; e) Pinggen, D.; Diebolt, O.; Vogt, D. *ChemCatChem*. **2013**, *5*, 2905–2912; f) Saidi, O.; Blacker, A. J.; Farah, M. M.; Marsden, S. P.; Williams, J. M. *Angewandte Chemie International Edition*. **2009**, *48*, 7375–7378; g) Zhang, Y.; Lim, C. S.; Sim, D. S.; Pan, H. J.; Zhao, Y. *Angewandte Chemie International Edition*. **2014**, *53*, 1399–1403.
- [4] a) Chen, F. F.; Liu, Y. Y.; Zheng, G. W.; Xu, J. H. *ChemCatChem*. **2015**, *7*, 3838–3841; b) Montgomery, S. L.; Mangas-Sanchez, J.; Thompson, M. P.; Aleku, G. A.; Dominguez, B.; Turner, N. J. *Angewandte Chemie International Edition*. **2017**, *56*, 10491–10494; c) Mutti, F. G.; Knaus, T.; Scrutton, N. S.; Breuer, M.; Turner, N. J. *Science*. **2015**, *349*, 1525–1529.

- [5] Sattler, J. H.; Fuchs, M.; Tauber, K.; Mutti, F. G.; Faber, K.; Pfeffer, J.; Haas, T.; Kroutil, W. *Angewandte Chemie International Edition*. **2012**, *51*, 9156–9159.
- [6] a) Thompson, M. P.; Turner, N. J. *ChemCatChem*. **2017**, *9*, 3833–3836; b) Knaus, T.; Cariati, L.; Masman, M. F.; Mutti, F. G. *Organic & Biomolecular Chemistry*. **2017**, *15*, 8313–8325.
- [7] a) Abrahamson, M. J.; Vazquez-Figueroa, E.; Woodall, N. B.; Moore, J. C.; Bommarius, A. S. *Angewandte Chemie International Edition*. **2012**, *51*, 3969–3972; b) Hoffken, H. W.; Duong, M.; Friedrich, T.; Breuer, M.; Hauer, B.; Reinhardt, R.; Rabus, R.; Heider, J. *Biochemistry*. **2006**, *45*, 82–93; c) Hummel, W.; Riebel, B. *(R)-Specific Alcohol Dehydrogenases from Lactobacillus with Improved Catalytic Activity Using an NAD⁺ Substrate*. May, 1999.
- [8] a) Sheldon, R. A.; Van Pelt, S. *Chemical Society Reviews*. **2013**, *42*, 6223–6235; b) Gutarra, M. L. E.; Miranda, L. S. M.; De Souza, R. O. M. A. *Organic Synthesis Using Biocatalysis*; Goswami, A. Stewart, J. D. (Eds.); Elsevier Inc., 2016, pp. 99–126.
- [9] a) Ren, H.; Zhang, Y.; Su, J.; Lin, P.; Wang, B.; Fang, B.; Wang, S. *Journal of Biotechnology*. **2017**, *241*, 33–41; b) Liu, J.; Pang, B. Q. W.; Adams, J. P.; Snajdrova, R.; Li, Z. *ChemCatChem*. **2017**, *9*, 425–431; c) Sheldon, R. A. *Catalysts*. **2019**, *9*, 261.
- [10] a) Porath, J. *Protein Expression and Purification*. **1992**, *3*, 263–281; b) Porath, J.; Carlsson, J.; Olsson, I.; Belfrage, G. *Nature*. **1975**, *258*, 598–599; c) Ljungquist, C.; Breitholtz, A.; Brinknilsson, H.; Moks, T.; Uhlen, M.; Nilsson, B. *European Journal of Biochemistry*. **1989**, *186*, 563–569.
- [11] Cassimjee, K. E.; Trummer, M.; Branney, C.; Berglund, P. *Biotechnology and Bioengineering*. **2008**, *99*, 712–716.
- [12] a) Cassimjee, K. E.; Kadow, M.; Wikmark, Y.; Svedendahl Humble, M.; Rothstein, M. L.; Rothstein, D. M.; Backvall, J. E. *Chemical Communications*. **2014**, *50*, 9134–9137; b) Planchestainer, M.; Contente, M. L.; Cassidy, J.; Molinari, F.; Tamborini, L.; Paradisi, F. *Green Chemistry*. **2017**, *19*, 372–375; c) Vahidi, A. K.; Yang, Y.; Ngo, T. P. N.; Li, Z. *ACS Catalysis*. **2015**, *5*, 3157–3161; d) Yang, J.; Ni, K.; Wei, D.; Ren, Y. *Biotechnology and Bioprocess Engineering*. **2015**, *20*, 901–907.
- [13] Cassimjee, K. E.; Bäckvall, J. E. *Immobilized Proteins and Use Thereof*. WO2015/115993, August, 2015.
- [14] a) Böhmer, W.; Knaus, T.; Volkov, A.; Slot, T. K.; Shiju, N. R.; Cassimjee, K. E.; Mutti, F. G. *Journal of Biotechnology*. **2019**, *291*, 52–60; b) Thompson, M. P.; Derrington, S. R.; Heath, R. S.; Porter, J. L.; Mangas-Sanchez, J.; Devine, P. N.; Truppo, M. D.; Turner, N. J. *Tetrahedron*. **2019**, *75*, 327–334.
- [15] Assmann, M.; Mugge, C.; Gassmeyer, S. K.; Enoki, J.; Hilterhaus, L.; Kourist, R.; Liese, A.; Kara, S. *Frontiers in Microbiology*. **2017**, *8*, 448.
- [16] Cassimjee, K. E.; Hendil-Forsell, P.; Volkov, A.; Krog, A.; Malmö, J.; Aune, T. E. V.; Knecht, W.; Miskelly, I. R.; Moody, T. S.; Svedendahl Humble, M. *ACS Omega*. **2017**, *2*, 8674–8677.
- [17] Lechner, H.; Soriano, P.; Poschner, R.; Hailes, H. C.; Ward, J. M.; Kroutil, W. *Biotechnology Journal*. **2018**, *13*, 1700542–1170051.

- [18] Cassimjee, K. E.; Federsel, H. J. *Biocatalysis: An Industrial Perspective*; Gonzalo, G. D. María, P. D. D. (Eds.); RSC Publishing; Cambridge, UK, 2018, pp. 345–362.
- [19] Bommarius, B. R.; Schürmann, M.; Bommarius, A. S. *Chemical Communications*. **2014**, *50*, 14953–14955.
- [20] Swamy, K. C.; Kumar, N. N.; Balaraman, E.; Kumar, K. V. *Chemical Reviews*. **2009**, *109*, 2551–2651.
- [21] Knaus, T.; Böhmer, W.; Mutti, F. G. *Green Chemistry*. **2017**, *19*, 453–463.
- [22] Schlieben, N. H.; Niefind, K.; Muller, J.; Riebel, B.; Hummel, W.; Schomburg, D. *Journal of Molecular Biology*. **2005**, *349*, 801–813.
- [23] a) Kawano, S.; Yano, M.; Hasegawa, J.; Yasohara, Y. *Bioscience, Biotechnology, and Biochemistry*. **2011**, *75*, 1055–1060; b) Kawano, S.; Yano, M.; Hasegawa, J.; Yasohara, Y. *Bioscience, Biotechnology, and Biochemistry*. **2011**, *75*, 2155–2161.
- [24] a) Ziegelmann-Fjeld, K. I.; Musa, M. M.; Phillips, R. S.; Zeikus, J. G.; Vieille, C. *Protein Engineering, Design & Selection*. **2007**, *20*, 47–55; b) Musa, M. M.; Lott, N.; Laivenieks, M.; Watanabe, L.; Vieille, C.; Phillips, R. S. *ChemCatChem*. **2009**, *1*, 89–93; c) Patel, J. M.; Musa, M. M.; Rodriguez, L.; Sutton, D. A.; Popik, V. V.; Phillips, R. S. *Organic & Biomolecular Chemistry*. **2014**, *12*, 5905–5910; d) Nealon, C. M.; Welsh, T. P.; Kim, C. S.; Phillips, R. S. *Archives of Biochemistry and Biophysics*. **2016**, *606*, 151–156.
- [25] Abrahamson, M. J.; Wong, J. W.; Bommarius, A. S. *Advanced Synthesis & Catalysis*. **2013**, *355*, 1780–1786.
- [26] a) Pushpanath, A.; Siirola, E.; Bornadel, A.; Woodlock, D.; Schell, U. *ACS Catalysis*. **2017**, *7*, 3204–3209; b) Au, S. K.; Bommarius, B. R.; Bommarius, A. S. *ACS Catalysis*. **2014**, *4*, 4021–4026.
- [27] Koszelewski, D.; Lavandera, I.; Clay, D.; Rozzell, D.; Kroutil, W. *Advanced Synthesis & Catalysis*. **2008**, *350*, 2761–2766.

Chapter 4

Immobilization of ω -transaminases for the kinetic resolution of amines in a continuous flow reactor

This chapter is based on the following publication:

Böhmer, W.; Knaus, T.; Volkov, A.; Slot, T., K.; Shiju, N., R.; Cassimjee, K., E.; Mutti, F., G. *Journal of biotechnology*. **2019**, *291*, 52–60.

Supplementary information is available under: doi: [10.1016/j.jbiotec.2018.12.001](https://doi.org/10.1016/j.jbiotec.2018.12.001).

4.1 Introduction

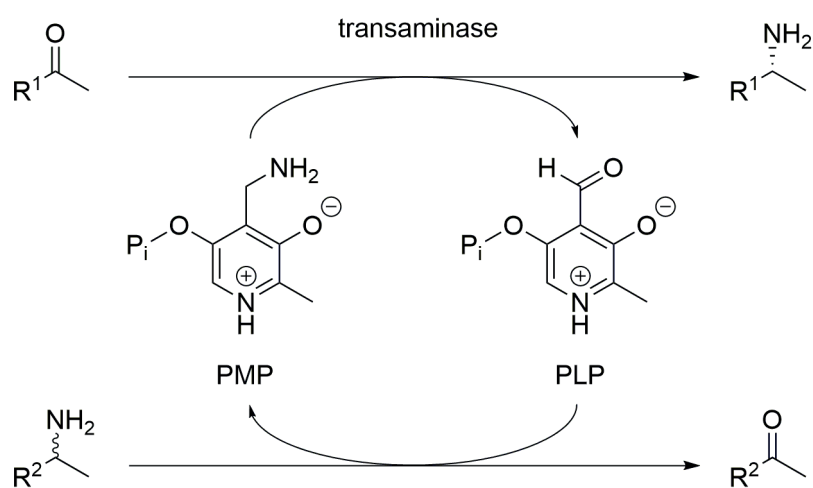
Industrial application of biocatalysts has been expanding, particularly in the pharmaceutical and fine chemical industries ^[1]. Because of their low environmental impact, elevated catalytic efficiency and exquisite selectivity, enzymes are an appealing option for the synthesis of many high value compounds ^[2]. However, the majority of biocatalytic processes are conducted in batch reactors and based on the less costly and time-consuming use of whole cell systems (fermenting, resting or lyophilized cells) or crude cell extracts, which do not require steps for enzyme purification ^[1a, 1b]. An often-common disadvantage of these types of applications is the lack of biocatalyst reusability, which reduces chemical turnover numbers (TONs) and increases the environmental impact. Recyclability of enzymes, along with increased stability, chemical selectivity as well as extended operational window can effectively be enabled by immobilization onto a support material, thereby making the enzyme perform as a heterogeneous catalyst ^[3]. A comprehensive discussion on enzyme immobilization was provided in Chapter 1.

Continuous flow reactors utilizing immobilized enzymes are gaining importance over traditional batch reactors. Applications of flow reactors in biocatalysis, i.e. mesoreactors and microfluidic devices, are numerous and have been reviewed extensively ^[4]. Particularly, enhanced heat and mass transfer in flow devices enables biotransformations with substantially lower reaction times and improved space-time yields (STY). Better process control can result in improved productivities, more efficient reactions and less waste. Additionally, mechanical stress due to mixing is avoided thereby increasing the operational window of biocatalyst stability. The production volume can be increased simply by application of modular flow devices in series or parallel operations. Finally, facile downstream processing enables recovery of products and unreacted starting material by the use of separating devices including membranes, filtration and phase separation units.

ω -Transaminases (ω TAs) are pyridoxal phosphate (PLP) dependent enzymes that produce α -chiral amines by transferring an amino group from a donor molecule to the carbonyl moiety of an acceptor molecule (Scheme 4.1) ^[5]. Application of ω TAs in large scale processes has been demonstrated ^[6]; however, the moderate operational stability upon immobilization hampers the full exploitation of the otherwise tremendous potential of this class of enzymes in organic synthesis. Immobilization of ω -transaminases has been reported in a number of recent studies aimed at improving the overall performance

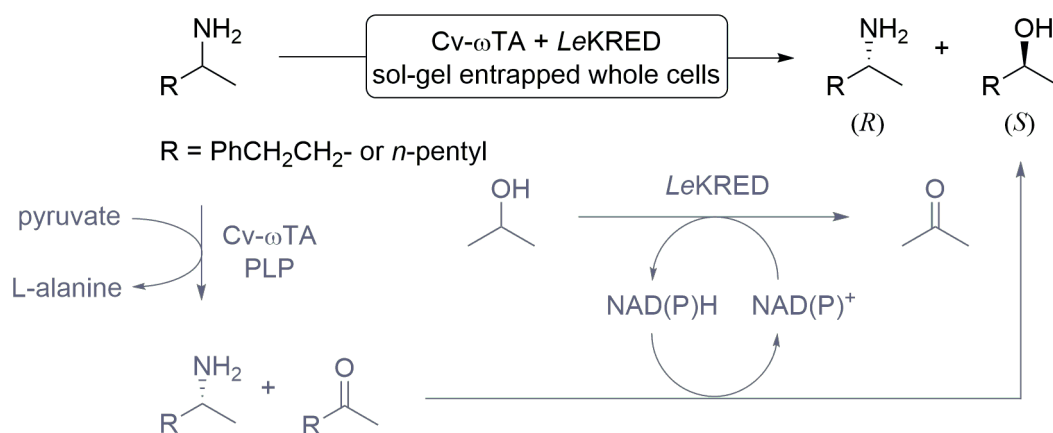
of biocatalysts [7]. Current limitations appear to be the relatively low enzyme loading (per mass unit of support material), as well as the moderate operational stability upon immobilization. The latter can often be improved by operating immobilized ω -TAs in a flow reactor. The application of immobilized transaminases in flow reactors has been performed utilizing mainly immobilized enzyme microreactors (IEMR) or packed-bed reactors (PBR). Immobilization of the enzyme can be performed on the inner walls of the reactor channel or by packing the reactor with the enzyme immobilized on a support material. A select number of ω -TAs employed in flow reactors is also illustrated in this section.

Application of ω -TAs in flow reactors especially for the purpose of multi-enzyme processes benefits largely from the implementation of immobilized whole cell biocatalysts. Low operational stability, substrate or product inhibition effects and their lack of recyclability, makes isolated enzymes in solution be less suitable for cascade reactions. Moreover, entrapment or covalent immobilization improve the applicability of whole cells without requiring additional, and often less economically viable, downstream processing (i.e., cell disruption, enzyme isolation and purification). The disadvantages regarding the use of whole cell systems include lower volumetric activity and very often low reusability, which reduces chemical total turnover numbers (TTNs) and increases the environmental impact. In addition, cell breakage can contaminate the reaction medium and the presence of additional enzymes as impurities may affect the selectivity of the biocatalytic process due to possible side-reactions.



Scheme 4.1. Transaminases require the pyridoxal phosphate (PLP) cofactor to enable the transfer of an amino group from an amine donor, ideally simple and inexpensive, to a prochiral ketone thereby creating valuable chiral α -amines.

Noteworthy contributions have been made in the application of whole cell ω -TAs in flow reactors. Cv- ω TA from *Chromobacterium violaceum* and ketoreductase from *Lodderomyces elongisporus* were entrapped as whole cell biocatalysts in hollow silica microspheres. The sol-gel immobilized biocatalysts were then employed in the kinetic resolution of 4-phenylbutan-2-amine coupled to an enantioselective reduction of the forming ketone which results in a nearly equimolar mixture of enantiomerically pure (*R*)-amine and (*S*)-alcohol (Scheme 4.2) [8]. The miniaturized packed-bed reactor filled with the immobilized whole cell biocatalysts demonstrated nearly full resolution of the racemic amine (7.5 mM substrate concentration, 44% (*R*)-amine and 46% (*S*)-alcohol) within 24 hours reaction time with >99% *ee* for both products. In another study, whole cells containing a (*R*)-selective transaminase from *Arthrobacter* species (AsR- ω TA) and pyridoxal phosphate (PLP) cofactor, were immobilized on methacrylate beads via physical adsorption and the heterogeneous biocatalyst was employed in a continuous flow packed-bed reactor (PBR) in organic solvent [9]. The insolubility of the immobilized whole cell biocatalyst in organic solvent prevented undesired enzyme or cofactor leaching. Under continuous flow operation the amination of several ketones (10 mM) was performed in methyl-tert-butyl ether (MTBE), yielding up to 94% conversion at 50 °C with a residence time (t_r) of 30–60 minutes (Scheme 4.3). The flow reactor could be operated for more than 10 days without showing any significant loss in conversion. Despite lowering the conversion, increased substrate concentrations enabled a higher amine production rate. Finally, facile product recovery was performed by the use of a silica cartridge for trapping amines. Although the application of these whole cell ω -TAs was

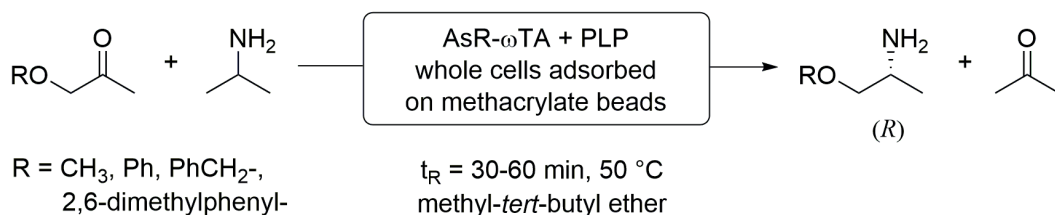


Scheme 4.2. Cv- ω TA from *Chromobacterium violaceum* (Cv- ω TA) and ketoreductase from *Lodderomyces elongisporus* (LeKRED) entrapped as sol-gel co-immobilized whole cells. Synthesis of (*R*)-amines and (*S*)-alcohols through kinetic resolution of racemic amines in a continuous flow reactor [8].

improved, the systems were limited to low flow rates and reaction times up to several days. Low catalyst loading as well as poor cell permeability might contribute to these limitations.

The majority of enzyme flow reactors that have been developed utilize immobilized cell-free ω -TAs. For example, the two-step enzymatic synthesis of (2*S*,3*R*)-2-amino-1,3,4-butanetriol (ABT) was performed utilizing a transketolase (TK) and a ω -TA in coupled PBRs^[10]. The TK catalyzes an asymmetric C-C bond formation whereas the ω -TA catalyzes the amination of the keto-group into an α -chiral amine (Scheme 4.4). Both enzymes were attached to functionalized agarose beads through His-tag affinity immobilization. 83% conversion to ABT was obtained in 20 minutes flow-time at a flow rate of 2 $\mu\text{L min}^{-1}$. With a reactor volume of ca. 10 μL and a substrate concentration of 60 mM, this corresponds to a space-time yield (STY) of 72 $\text{g L}^{-1} \text{h}^{-1}$. Unfortunately, the productivity of the immobilized ω TA decreased within 8 h of reaction time to less than 60% whereas the TK showed 76% productivity after 48 hours. Other noteworthy contributions have been published such as the immobilization of the same dual-enzyme system on the inner channels of AB-NTA derivatized micro-capillaries^[11]. Although full conversion could not be obtained, 0.3 mM of ABT was produced in 40 minutes using 10 mM substrate concentration which corresponds to a STY of 44 $\text{mg L}^{-1} \text{h}^{-1}$. In another study, full conversion to ABT was obtained flowing the dual-enzyme system through a microreactor with polymethacrylate-coated inner channels^[12]. The enzymes and substrates were mixed before entering the reactors and the products were obtained by regular extraction from the aqueous reaction mixture. Although this system does not allow for the recycling of enzymes through the use of immobilization, the microreactor provided higher volumetric productivities (up to 10.8 U mL^{-1}) and the reaction time was reduced 10-fold as compared to batch reactions.

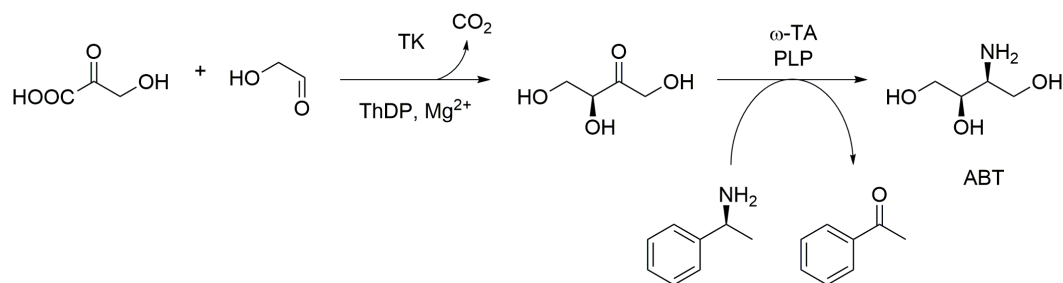
A ω -TA from *Halomonas elongata* (He- ω TA) has been reported to exhibit excellent productivity in the oxidation of amines to aldehydes in a continuous flow reactor^[13]. A



Scheme 4.3. Co-immobilized (*R*)-selective transaminase from *Arthrobacter* species (AsR- ω TA) and pyridoxal phosphate (PLP) cofactor on methacrylate beads employed in a continuous flow packed-bed reactor in organic solvent^[9].

select panel of amines was converted with high conversions (90–99%, 10 mM) within several minutes of reaction time (t_R : 3–10 min.). The enzyme was immobilized on Co^{2+} -functionalized methacrylate beads through metal-ion affinity binding (a detailed description of the concept of metal-ion affinity immobilization follows later). The product was obtained by in-line flow extraction and membrane liquid-liquid separation. Further implementations of the immobilized He- ω TA with a horse liver alcohol dehydrogenase (HLADH) or a ketoreductase from *Pichia glucozyma* (KRED1-Pglu) resulted in an elegant multi-enzymatic closed-loop flow system for the synthesis of primary and secondary chiral alcohols [14]. A small selection of primary and secondary amines (3–5 mM) was converted (t_R : 15–180 min.) utilizing two enzymatic flow reactors connected in series. The alcohol products were obtained by in-line extraction with organic solvent and the remaining aqueous phase was directed back into the reaction thereby creating a closed-loop system (Scheme 4.5).

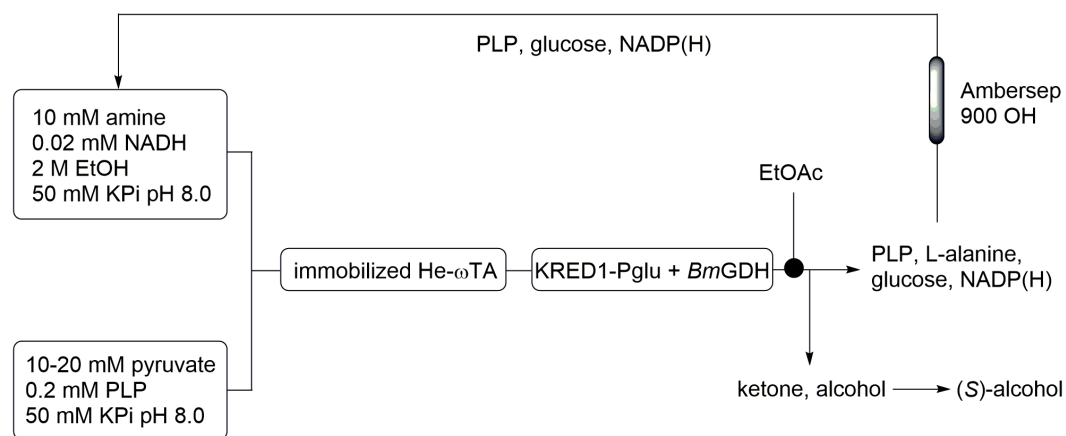
Kinetic resolution is a powerful synthetic tool for obtaining chiral α -amines and ω -transaminases have proved ideal candidates for this purpose when applied in flow reactors. For example, kinetic resolutions of *rac*-MBA, 1-aminotetralin, and 1-aminoinadan were performed using a packed-bed reactor with Ca-alginate entrapped whole cells that contained ω -TA from *Vibrio fluvialis* JS17. A hydrophobic membrane contactor had to be used in order to remove the inhibitory ketone product which was formed in the reaction [15]. Cv- ω TA from *Chromobacterium violaceum* (Trp60Cys) was covalently immobilized on methacrylate beads and employed in the kinetic resolution of *rac*-MBA, 4-phenyl-2-aminobutane or 1-aminotetralin [16]. 10 mM racemic amine was converted in the flow reactor (reactor volume: 0.816 mL, flow rate: 0.5 mL min^{-1}) with a STY of 46 and 54 g $\text{L}^{-1} \text{h}^{-1}$. The use of a flow reactor significantly reduced the time required for immobilization of the enzyme; precipitation of the enzyme, due to higher mechanical stress in batch reactions,



Scheme 4.4. Two-step enzymatic synthesis of (2S,3R)-2-amino-1,3,4-butanetriol (ABT) utilizing a transketolase (TK) and a ω -transaminase (ω -TA). ThDP = thiamine diphosphate.

was prevented. A crude-cell preparation of commercial *N*-SBM-ATA (c-LEcta GmbH, Leipzig, Germany) was immobilized through ionic interactions on the surface of silicon glass microchannels. Surface kinetics were used to describe the kinetic resolution of *rac*-MBA and to predict the performance of two microreactors connected in series [17]. In other studies commercial ATA-117 was employed in the kinetic resolution of *rac*-MBA and derivatives. The ATA was immobilized on macrocellular silica monoliths both by adsorption and by covalent grafting using an amino functionalized surface [18]. Eight functionalized monoliths (estimated reactor volume: 20 mL) were operated in series to obtain full resolution of *rac*-4-bromomethylbenzylamine (STY = 0.35 g L⁻¹ h⁻¹). In another study, ATA-117 was immobilized on the inner surface of 3D printed nylon flow reactors and operated in the kinetic resolution of *rac*-MBA with productivity rates of 20.5 μmol h⁻¹ mg_{enzyme}⁻¹ (STY = 0.73 g L⁻¹ h⁻¹) [19]. Notably, in total 105 catalytic flow cycles were performed with the same batch of enzyme.

Immobilized metal-ion affinity binding is used in many applications, e.g. for protein or peptide purification [20] and immobilization [21]. It involves the use of chelated metal ions (i.e. Ni²⁺, Co^{2+/3+}, Fe^{2+/3+}) connected to the support matrix by spacer molecules onto which the enzyme is adsorbed. The interaction between the enzyme and a chelated metal ion is often specific and can involve enzyme linkers, such as a terminal poly-histidine chain (His-tag) on the enzyme (Figure 4.1). Additionally, non-covalent interactions between the enzyme and the surface of the carrier material are feasible and may contribute to stabilize enzyme regions whose dynamics are important during the catalytic cycle [22]. Moreover, increased apparent catalytic activity is possible upon immobilization because the binding



Scheme 4.5. Closed-loop continuous flow system for the conversion of amines to alcohols utilizing ω -TA from *Halomonas elongata* (He- ω TA) and ketoreductase from *Pichia glucozyma* (KRED1-Pglu) [14].

of protein monomers in close proximity to each other can promote the formation of active oligomeric forms of a given enzyme. This feature can, for instance, be beneficial for ω -transaminases (ω TAs) that generally form homodimeric structures in which the active site consists of shared amino acid residues coming from the two monomeric units [23]. It is known that the association between the two monomeric units of ω -TAs may become labile in solution, particularly in absence of pyridoxal-5'-phosphate (PLP) cofactor [24]. A useful property of metal-ion affinity binding is the possibility to detach the enzyme from the support material once its activity ceased by using chelating reagents, such as imidazole or EDTA. Polymeric materials are generally inexpensive, but high enzyme loading ($>5\%$ w w⁻¹, enzyme/carrier) on this type of carriers is usually unfeasible because of the limited surface area. In this context, controlled-pore glass (CPG) carriers serve as a better alternative because of their porous skeleton that provides a larger surface area for immobilization and efficient mass transfer through interconnecting pores. As was previously described in Chapter 3, a hybrid CPG immobilization material (EziG™) was developed of which the surface of the CPG is coated with a functionalized polymer. The polymeric surface bears chelating groups that are suitable for selective binding of metal ions [22, 25]. For EziG™ immobilization material, Fe³⁺ was selected as preferred metal ion due to its low environmental impact, virtually absent toxicity and increased binding stability [25a]. The CPG-polymeric functionalized hybrid material creates a highly porous network for selective binding of enzymes with loadings up to 30% (w w⁻¹). Moreover, the selectivity of the binding permits immobilization directly from the cell lysate, hence any step for pre-purification of enzyme is unnecessary [22]. Immobilization carriers with high enzyme loadings may cause enzyme crowding which can cause lower enzyme stability [26], but such behavior was not observed for EziG™ support materials. Immobilization on EziG™ support materials

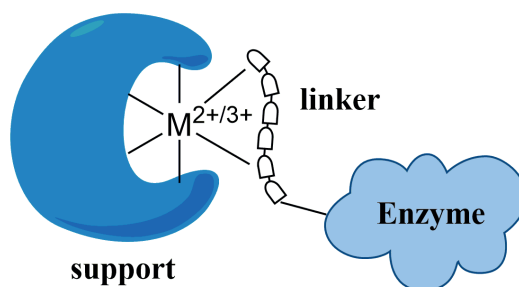


Figure 4.1. Schematic representation: metal-ion affinity immobilization involves the use of chelated metal ions connected to the support material by spacer chelating molecules. Interactions with the enzyme can occur through enzyme linkers, such as His-tag.

has been reported to significantly improve the stability and operational window of an arylmalonate decarboxylase ^[27], *Candida antarctica* lipase ^[28], and a norcochlorine synthase ^[29]. Our group has previously reported the co-immobilization of two dehydrogenases on EziG™ support material and employed the co-immobilized system in hydrogen-borrowing amination of alcohols to obtain α -chiral amines with improved efficiency compared to analogous non-immobilized systems ^[30]. This research was described in Chapter 3.

In this study, the conditions for the optimal immobilization of two stereocomplementary ω -transaminases, AsR- ω TA from *Arthrobacter* species and Cv- ω TA from *Chromobacterium violaceum*, on EziG™ support materials was determined based on the use of different types of immobilization buffers (i.e., composition, concentration, pH) at varied concentrations of PLP cofactor. The performance of the resulting immobilized biocatalysts was then evaluated for the kinetic resolution of *rac*- α -methylbenzylamine (*rac*-MBA) in batch reactions on analytical scale. The applicability of the EziG™-immobilized ω -TAs was significantly improved by implementing them in a continuous flow reactor, which showed high volumetric productivities and industrially relevant space-time yields in the kinetic resolution of *rac*-MBA.

4.2 Result section

4.2.1 Expression and purification of ω -transaminases

Among the pool of available ω -transaminases, two stereocomplementary enzymes were chosen for the immobilization studies: 1) the (*R*)-selective ω -transaminase from *Arthrobacter* species (AsR- ω TA) ^[31]; and 2) the (*S*)-selective ω -transaminase from *Chromobacterium violaceum* (Cv- ω TA) ^[32]. Both enzymes have been extensively studied in the past decade and display perfect stereoselectivities for the amination of a large number of structurally diverse prochiral ketones. The enzymes were obtained as recombinant proteins and purified by Ni²⁺ affinity chromatography (Experimental section). Although not technically required and actually inconvenient for an applied industrial process, purified enzymes were used for this study due to the high accuracy and precision in quantifying the resulting actual amount of immobilized enzyme on the support material. In this manner, an exact evaluation of the catalytic performance (e.g., TON or initial activity) was possible. Nonetheless, the efficiency for the selective immobilization of ω TA from crude lysate on EziG³ was demonstrated. Specifically, the total enzyme loading on the support material was 19% w w⁻¹, which correlates to an estimated yield of immobilization from cell lysate of ca. 90% (without optimization, for

calculations; section Calculations and terminology). In a previous study, enzyme loadings up to 29% (w w⁻¹) were achieved for Cv- ω TA onto EziG™ supports [22]. For the experiments with purified ω -transaminases performed in the current study, an enzyme loading of 10% w w⁻¹ for batch reactions and 15% w w⁻¹ for flow reactions was applied, respectively.

4.2.2 EziG™ support materials

Three types of EziG™ support material possessing distinct surface properties were tested for initial experiments: EziG¹ (Fe-Opal), has a hydrophilic derivatized silica surface; EziG² (Fe-Coral) has a hydrophobic surface polymer; and EziG³ (Fe-Amber) is covered with a semi-hydrophobic polymer surface (Table 4.1). Scanning electron microscope (SEM) images of EziG³ Fe-Amber material show the presence of a highly porous network with a large surface area. Bead sizedistribution and shapes are in accordance with the product specifications (Figure 4.2).

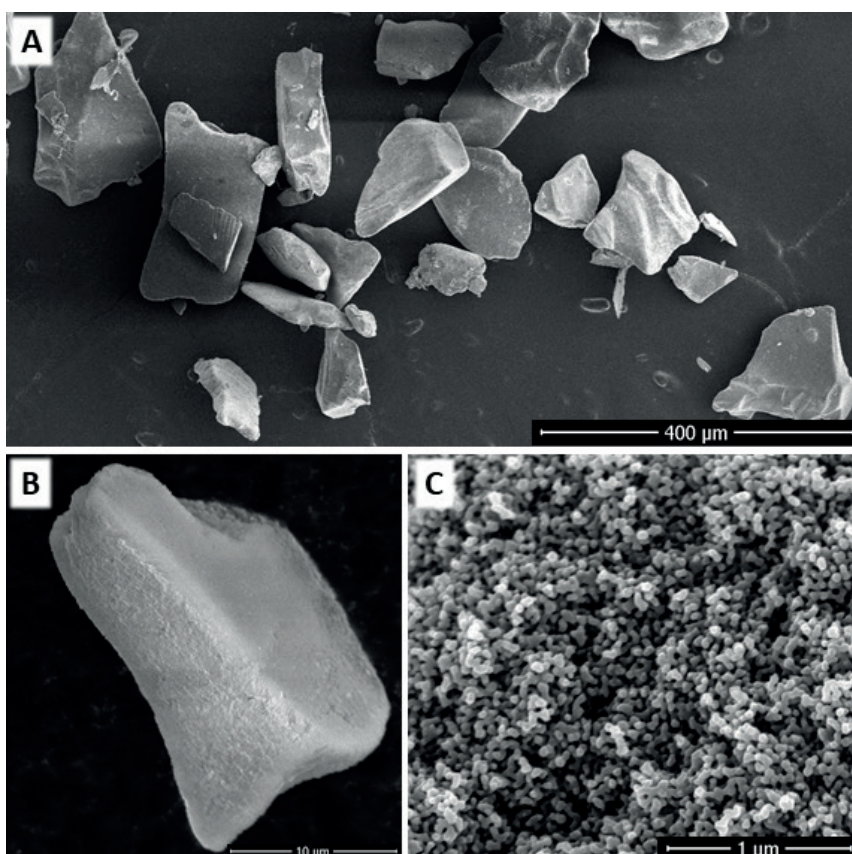


Figure 4.2. SEM analysis of EziG³ (Fe-Amber) with immobilized AsR- ω TA. A) bead distribution at 150 x magnification, B) single bead at 5000 x magnification, C) surface morphology at 35 000 x magnification.

Table 4.1. EziG™ product specifications: particle size 75-125 μm (100-300 mesh), chelated Fe^{3+} >10 $\mu\text{mol/g}$, pore volume 1.8 mL g^{-1} , pH range 5-10.

Entry	Product	Surface	Pore diameter [nm]	Bulk density [g/mL]
1	EziG ¹ Fe Opal	Directly derivatized hydrophilic glass	50±5	0.25-0.32
2	EziG ² Fe Coral	Hydrophobic polymer	30±5	0.21-0.25
3	EziG ³ Fe Amber	Semi-hydrophobic copolymer	30±5	0.21-0.25

4.2.3 Immobilization of ω -transaminases

Immobilization of ω -transaminases AsR- ω TA and Cv- ω TA was performed by incubating the desired amount of enzyme in buffer supplied with EziG™ support material. The progress of immobilization was monitored in time by using a Bradford assay to measure the amount of enzyme remaining in the immobilization buffer (for details: Experimental section). The progress of the immobilization was visible in that the support material turned increasingly yellow during incubation due to the presence of the (yellow) PLP cofactor bound in the active site of the enzyme. AsR- ω TA was immobilized under standard immobilization conditions on EziG™ support materials within 2 h of incubation (Figure 4.3A and Table S3). Affinity binding of AsR- ω TA on the three EziG carrier materials, namely EziG¹-AsR, EziG²-AsR, and EziG³-AsR depending on the support type, proved to be strong, as there was no detectable loss of enzyme from the support material even after incubating the immobilized enzyme in buffer up to 3 days. Longer incubation times were not tested.

4.2.4 Influence of buffer (i.e. ionic strength) and PLP concentration on the immobilization process

The ionic strength of the immobilization buffer greatly influences the immobilization efficiency of many carrier materials. For example, improvements have been reported in covalent coupling of enzymes to epoxy-activated carriers by using high ionic buffer strength. In a first step, a salt-induced association takes place between the macromolecule and the support surface [33], which increases the effective concentration of nucleophilic groups on the protein close to the epoxide reactive sites. However, the salt concentration needed to immobilize an enzyme was reported to be highly protein-dependent [33b]. Hence, the influence of buffer concentration in the case of metal-ion affinity immobilization

with EziG™ supports can vary significantly as well. Immobilization tests of ω TAs on EziG™ supports were performed in KPi buffer (pH 8) with a buffer concentration ranging from 100 mM to 1 M. Figure 4.3B shows that buffer concentrations above 100 mM had a negative influence on the immobilization process; however, the behavior in yield of immobilization of AsR- ω TA versus the buffer concentration proved to be depended on the type of support. The effect on EziG¹ (Fe-Opal) was dramatic, with virtual no immobilization above a concentration of 600 mM KPi. Conversely, EziG² (Fe-Coral) and EziG³ (Fe-Amber) behaved similarly to each other, resulting in a residual 60% immobilization yield at 1 M KPi (Figure 4.3B and Table S4). Thus, the immobilization process is somewhat dependent on the physico-chemical properties of the surface of the support material, albeit the type of immobilization is the same (i.e., Fe-cation affinity to enzyme His6-tag). In addition, phosphate ions might compete with the enzyme for the binding to the Fe-cations that are chelated to the support material. Interestingly, although the stability of free AsR- ω TA in solution at high ionic strength was not tested in a specifically designed experiment, no precipitation of enzyme was observed during the immobilization procedure even at 1 M KPi buffer. PLP plays an important role not only as a cofactor, but also in contributing to the stabilization of the catalytically active dimeric form of the enzyme, whereas the monomeric form is inactive [23, 34]. In order to maintain the dimeric active form of the enzyme, an excess of PLP is commonly supplied during biotransformations with non-immobilized ω TA (5-10 equiv. of PLP to the enzyme) [5]. During preliminary experiments, AsR- ω TA and Cv- ω TA were immobilized in solution, as active biocatalysts in the presence of externally added PLP. However, the concentration of PLP could have a dual impact, such that although adding a surplus of PLP during the immobilization procedure might be beneficial for retaining the activity of ω TAs, high concentrations of PLP might also hamper the immobilization process, as PLP could also interact with the metal cationic centers of the support. Accordingly, EziG™ support materials were separately incubated in 100 mM KPi buffers at varied concentrations of PLP (0.1-5 mM) for 30 min prior to addition of the enzyme. Notably, a dramatic negative effect related to the use of an excess of PLP was observed (Figure 4.3C). Among the three tested support materials, EziG¹ was the most affected by higher buffer concentration (Figure 4.3B) and the least affected by higher PLP concentration (Figure 4.3C). As a general conclusion, for obtaining high immobilization yields, the PLP had to be kept below 0.1 mM (Figure 4.3C and Table S5). Precipitation of enzyme was not observed in any of the experiments. Among the three tested EziG carriers, EziG³ (Fe-Amber)

provided the optimal immobilization yield when using 100mM KPi buffer supplemented with 0.1 mM PLP. Therefore, EziG³ was selected for the subsequent biocatalytic studies.

4.2.5 Influence of type of buffer and pH on the immobilization process

Both the buffer type and its pH value determine the nature of the ionogenic environment around the enzyme. Consequently, the immobilization buffer can significantly influence the stability and activity of the immobilized enzyme. EziG³-AsR was immobilized as previously

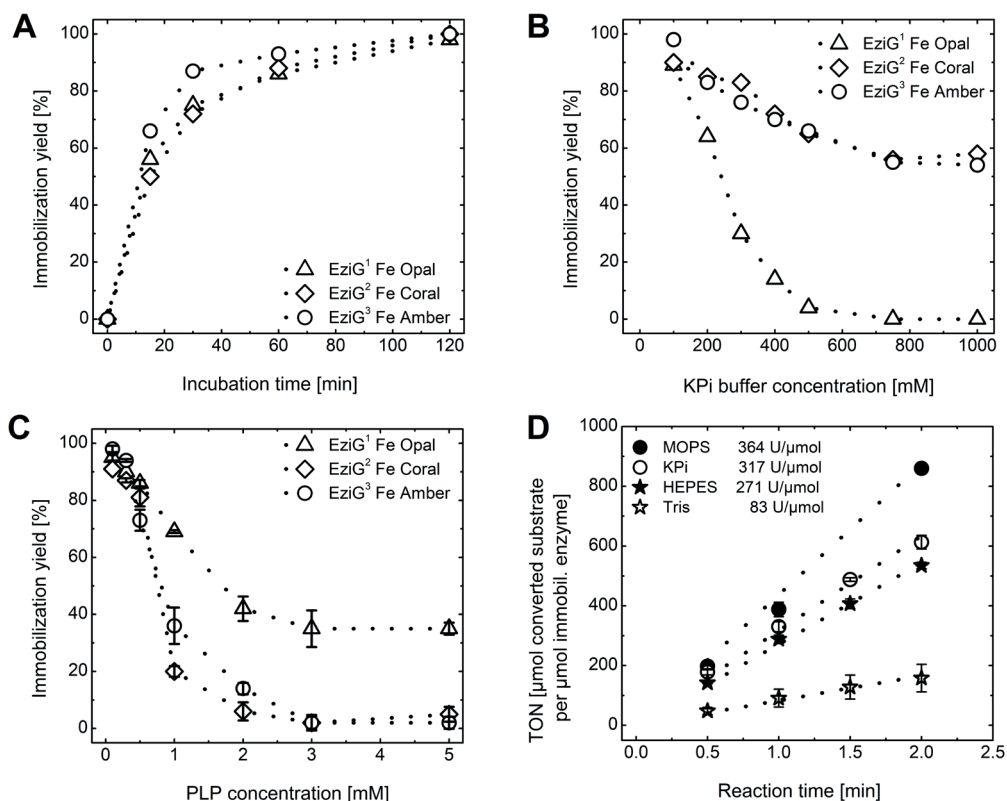
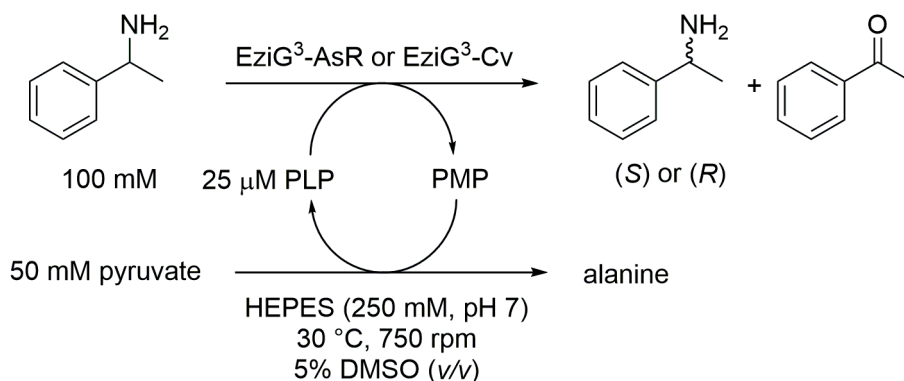


Figure 4.3. Immobilization studies of AsR- ω TA on EziGTM support materials (EziG¹-AsR = triangle, EziG²-AsR = diamond, EziG³-AsR = circle). (A) Immobilization monitored in time. Yield of immobilization (in %) was determined using Bradford assay. (B) Immobilization in KPi buffer with increasing KPi buffer concentration. (C) Immobilization with additional PLP. Error bars display absolute difference between two individual experiments. (D) Immobilization using different immobilization buffers (100 mM MOPS pH 8 = black circle; 100 mM KPi pH 8 = white circle; 100 mM HEPES pH 8 = black star; 100 mM Tris pH 8 = white star). Activity testing in kinetic resolution of *rac*- α -MBA. Error bars display standard deviation over three experiments. Unless stated otherwise; Immobilization conditions: support material (10 mg, total enzyme loading: 10% w w⁻¹), KPi (100 mM, pH 8, 1 mL), PLP (0.1 mM), AsR- ω TA (1 mg, 27 nmol), 4 °C, 120 rpm (orbital shaker), 2 h. Reaction conditions: Immobilized EziG-AsR (10 mg, total enzyme loading: 10% w w⁻¹), *rac*- α -MBA (100 mM), sodium pyruvate (50 mM), DMSO (5%, v v⁻¹), PLP (25 μ M), HEPES buffer (0.5 mL reaction volume, 250 mM, pH 7), 30 °C, 750 rpm (Eppendorf thermomixer).

described in four different types of buffers at 100 mM concentration (MOPS pH 8.0, KPi pH 8.0, HEPES pH 8.0 and Tris pH 8.0), and the resulting biocatalyst activity was determined for the kinetic resolution of *rac*- α -MBA with 0.5 equiv. of pyruvate (Scheme 4.6). Immobilization in MOPS buffer resulted in the highest observed activity of 365 U μmol^{-1} enzyme (Figure 4.3D and Table S6). Conversely, a more than four-fold decrease in activity was observed using EziG³-AsR originated from the immobilization in Tris buffer (83 U μmol^{-1} enzyme). Interestingly, immobilizations in MOPS buffer at pH 6.5, 7 or 7.5 did not significantly affect the initial catalytic activity (379 U μmol^{-1} enzyme, 323 U μmol^{-1} enzyme and 365 U μmol^{-1} enzyme, respectively; for details; Supporting information, Table S7). However, immobilization in MOPS buffer at pH 6 showed a significant drop in activity to 192 U μmol^{-1} enzyme. Lower pH values were not tested due to the reported instability of AsR- ω TA below pH 6 [31].

4.2.6 Studies on single batch kinetic resolution of *rac*- α -MBA catalyzed by ω TAs immobilized on EziG³

A preliminary study using AsR- ω TA as free enzyme in solution displayed slightly lower enzyme activity at 40 °C and significantly decreased enzyme activity at 50 °C (Figure S2 and Table S11). On the other hand, both EziG³-AsR (i.e., immobilized enzyme) and AsR- ω TA (i.e., isolated enzyme) showed no detectable loss of activity upon incubation for 3 days at RT. Accordingly, we decided to perform all of the biotransformations at 30 °C. AsR- ω TA and Cv- ω TA immobilized on EziG³ Fe-Amber, namely EziG³-AsR and EziG³-Cv, respectively, were employed in preliminary experiments for the kinetic resolution of *rac*- α -MBA (100 mM) with 0.5 eq. of pyruvate (Scheme 4.6). EziG³-AsR (10 mg, total enzyme



Scheme 4.6. Immobilized ω -transaminases in kinetic resolution of *rac*- α -MBA (100 mM) with sodium pyruvate (50 mM).

loading: 10% w w⁻¹) showed high activity for the substrate, and perfect kinetic resolution of *rac*- α -MBA was reached within 5 min (>49% conversion and >99% *ee* of unreacted (*S*)- α -MBA; Figure 4.4A and Table S7) with a calculated TON above 900 for this single batch reaction (for details: Calculations and terminology). A similar reaction conducted with the same amount of purified AsR- ω TA in solution required 2 min in order to reach full kinetic resolution (Table S8). EziG³-Cv (10 mg, total enzyme loading: 10% w w⁻¹) catalyzed perfect resolution of *rac*- α -MBA (>49% conversion and >99% *ee* of unreacted (*R*)- α -MBA; Figure 4.4B and Table S9) within 3 h reaction time with a TON above 1300. The lower reaction rate of EziG³-Cv compared with EziG³-AsR was attributed to a lower intrinsic catalytic activity of Cv- ω TA for (*S*)- α -MBA and the lower molar loading of the enzyme (i.e. MW AsR- ω TA: 37.2 kDa; MW Cv- ω TA: 53.6 kDa). In fact, the similar reaction with the same amount of purified Cv- ω TA in solution also required at least 2 h for complete kinetic resolution of *rac*- α -MBA (Table S10). Comparing the preliminary experiments of kinetic resolution using either free enzyme in solution or immobilized enzyme, we noticed that the apparent rate of the reaction is moderately higher when using the former. This phenomenon must not be attributed to a lower intrinsic catalytic activity of the immobilized biocatalysts. In fact, when operating with immobilized enzymes in an aqueous environment, reagents and biocatalyst are in different phases (i.e., heterogeneous catalysis), and therefore mass transfer (i.e., external as well as inside the pores of the carrier) influences the overall kinetics of the process. This is particularly valid for the kinetic resolution of *rac*- α -MBA, which has an elevated reaction rate in homogeneous aqueous systems [35]. Accordingly, the preliminary experiments can be interpreted as a proof of highly retained catalytic activity of the ω -transaminases upon immobilization. These conclusions correlate with the experiments at high substrate loading reported in the next section.

4.2.7 High substrate loading performance of EziG³-AsR

Substrate feed is often a limiting factor for implementation of biocatalysts in large scale processes. As immobilized EziG³-AsR biocatalyst proved to be highly active in preliminary experiments, we performed kinetic resolution at higher concentrations of substrate (Figure 4.5 and Table S13; see SI for experimental details). The resolution of *rac*- α -MBA was observed with increasing productivity up to 600 mM substrate concentration (TON = 2450 for a single batch reaction). Substrate and co-product inhibition are common limitations in ω -transaminase-catalyzed reactions, which explains

the observed drop in conversion at substrate concentration values above 600 mM [36].

4.2.8 Biocatalyst recycling

The main advantage related to enzyme immobilization is the potential for recycling the biocatalysts for subsequent batch reactions. An amount of EziG³-AsR (10 mg, total enzyme loading: 10% w w⁻¹) was repeatedly employed for the kinetic resolution of *rac*- α -MBA (initial concentration per cycle 100 mM) with sodium pyruvate (50 mM). Each cycle of batch reaction was run for 15 min. At the end of each cycle, the reaction buffer was separated from the biocatalyst and worked-up. Then, the same batch of EziG³-AsR biocatalyst was re-suspended in fresh buffer containing the reagents and additional PLP (25 μ M), and another reaction cycle was initiated. This procedure was repeated for 16 reaction cycles, maintaining quantitative conversion in the kinetic resolution using the immobilized enzyme (Figure 4.6 and Table S14). Considering the short reaction time per cycle employed (15 min), this experiment demonstrated the robustness of the reaction system. In total, 388 μ M (*S*)- α -MBA (>99% *ee*) was produced with a notable total TON of 14,400. Interestingly, when no additional PLP (25 μ M) was supplied in each cycle, conversions dropped slightly (approximately 3% per cycle), thus indicating that the specific minimal addition of PLP is beneficial for retaining long-term catalytic activity (data not shown).

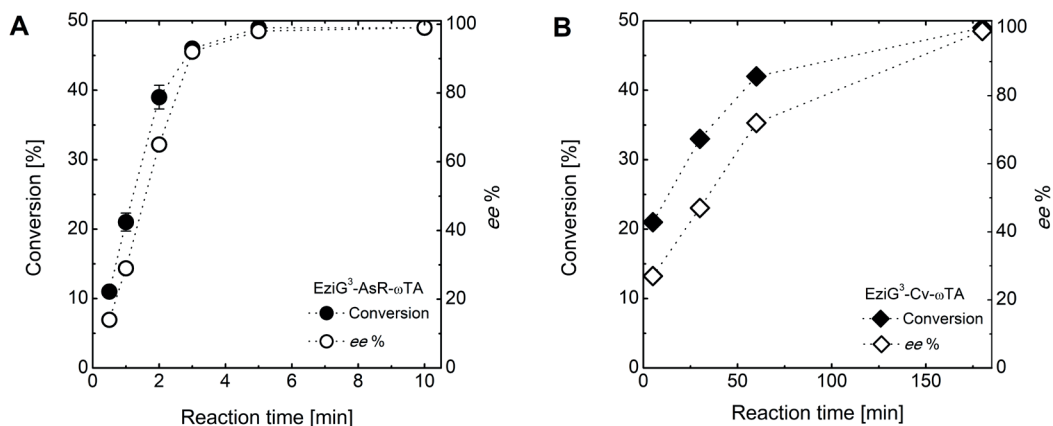


Figure 4.4. (A) Time study of EziG³-AsR (left graph, circles) and B) EziG³-Cv (right graph, diamonds) in kinetic resolution of *rac*- α -MBA. Primary axis displays conversion to acetophenone (black shapes) and secondary axis displays *ee*% of remaining (*S*)- α -MBA (white shapes). Error bars indicate standard deviation over three experiments. Reaction conditions: EziG³-AsR or EziG³-Cv (10 mg, total enzyme loading: 10% w w⁻¹), *rac*- α -MBA (100 mM), sodium pyruvate (50 mM), DMSO (5%, v v⁻¹), PLP (25 μ M), HEPES buffer (0.5 mL reaction volume, 250 mM, pH 7), 30 °C, 750 rpm (Eppendorf thermomixer).

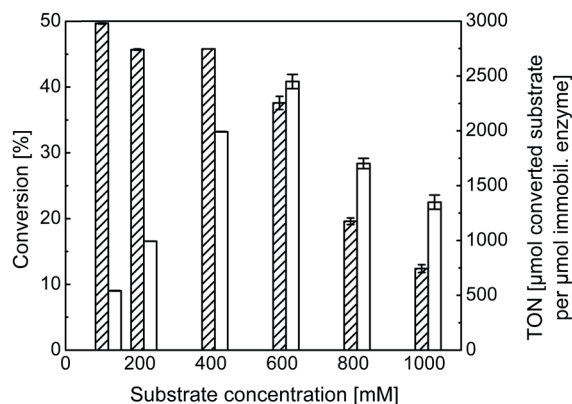


Figure 4.5. Activity of EziG³-AsR in kinetic resolution of *rac*- α -MBA when applying higher substrate loadings. Conversion to acetophenone (striped bars) and TON (white bars) for the reaction catalyzed by the immobilized enzyme. Error bars display standard deviation over three experiments. Reaction conditions: EziG³-AsR (10 mg, total enzyme loading: 17% w w⁻¹), *rac*- α -MBA (concentration varied), sodium pyruvate (0.5 equiv.), DMSO (10%, v v⁻¹), PLP (25 μ M), HEPES buffer (0.5 mL reaction volume, 250 mM, pH 7), 30 °C, 750 rpm (Eppendorf thermomixer), 15 minutes.

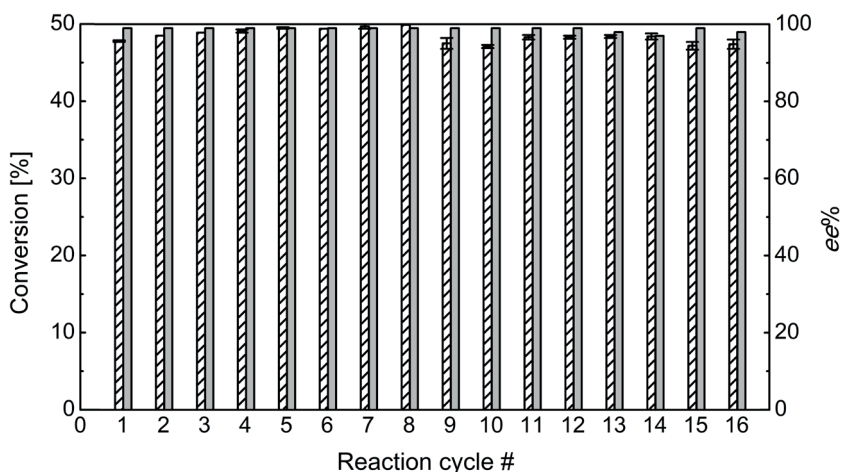


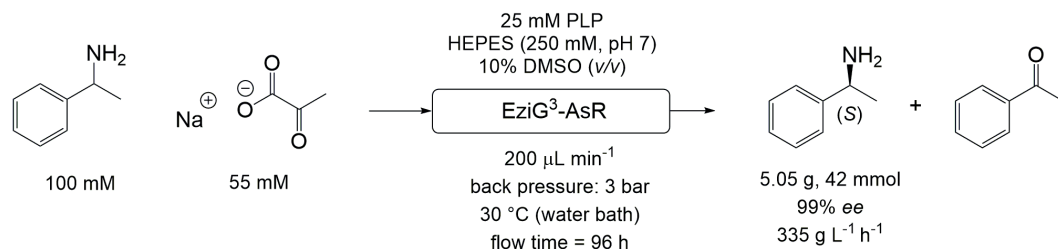
Figure 4.6. Recycling of EziG³-AsR in kinetic resolution of *rac*- α -MBA. Conversion to acetophenone (striped bars) and ee% (grey bars) of the remaining (*S*)- α -MBA. Error bars display standard deviation over three experiments. Reaction conditions: EziG³-AsR (10 mg, total enzyme loading: 10% w w⁻¹), HEPES buffer (0.5 mL reaction volume, 250 mM, pH 7), PLP (25 μ M), sodium pyruvate (50 mM), *rac*- α -MBA (100 mM), DMSO (10%, v v⁻¹), 30 °C, 750 rpm (Eppendorf thermomixer), 15 minutes per reaction cycle.

4.2.9 In-flow immobilization and continuous flow kinetic resolution

Chemical synthesis using immobilized biocatalysts in continuous flow systems is particularly attractive in terms of practicality, reproducibility and improved productivity compared to batch reaction systems. In this context, in-flow immobilization of AsR- ω TA (15 mg) was performed in a stainless-steel column (50 mm length x 2 mm diameter) filled with EziG³ Fe-Amber beads (100 mg, for details: Experimental section). The flow reactor (total volume 157 μ L) was then applied in continuous flow for the kinetic resolution of *rac*- α -MBA (10.9 g, 100 mM) with sodium pyruvate (0.55 equiv.; Scheme 4.7). The reaction buffer mixture was pumped through the column at an average rate of 0.175 mL min⁻¹ (average space time= 54 s) using a Dionex P680 HPLC pump unit. The flow-through was collected in separate 100–200 mL fractions and analytical samples were analyzed by GC. The packed-bed flow reactor was operated for 96 consecutive hours without any detectable loss of catalytic performance, and the kinetic resolution proceeded with perfect enantioselectivity (>49% conversion, >99% *ee* of unreacted (*S*)- α -MBA). The calculated TON was above 110,000 and the space-time yield was 335 g L⁻¹ h⁻¹. After work-up, 5.05 g (42 mmol) of (*S*)- α -MBA were obtained in high chemical and optical purity (93% isolated yield, >99% *ee*).

4.3 Conclusion

In this study, ω -transaminases were implemented as highly active heterogeneous biocatalysts in the production of an α -chiral amine by kinetic resolution. Investigation into the immobilization conditions proved critical for obtaining highly active biocatalysts. The optimal conditions for immobilization on EziGTM supports were found to be the use of 100 mM MOPS buffer supplemented with 0.1 mM PLP. The fundamental design of EziGTM enabled to reach high loading of enzyme per mass unit of support material (20% w w⁻¹). Under the optimized conditions, the immobilized enzyme was recycled for 16 consecutive



Scheme 4.7. Flow reactor set-up in application of EziG³-AsR for kinetic resolution of *rac*- α -MBA.

batch reactions (15 min reaction time per batch), always affording quantitative conversion. Finally, multi-gram scale continuous flow production of (*S*)- α -MBA was performed in a packed-bed flow reactor for 96 consecutive hours without any detectable loss of enzymatic activity. Within the short timeframe of our experiment, the chemical turnover number reached a value higher than 110,000 and a space-time yield of 335 g L⁻¹ h⁻¹. It is noteworthy that erosion of the enantioselectivity of the immobilized ω TA was never observed during operation in either batch- or continuous flow biocatalysis. This research highlights the potential of continuous flow biocatalysis, by selective immobilization of enzymes onto functionalized controlled-pore glass beads through reversible metal-cation affinity binding, for industrial manufacturing of high value chemicals.

4.4 Experimental section

4.4.1 General information

Acetophenone, *rac*- α -methylbenzylamine (*rac*- α -MBA), (*S*)- α -methylbenzylamine ((*S*)- α -MBA), (*R*)- α -methylbenzylamine ((*R*)- α -MBA), and pyridoxal-5'-phosphate (PLP) were purchased from Sigma-Aldrich (Steinheim, Germany). Dimethyl sulfoxide (DMSO) and sodium pyruvate were purchased from TCI Europe (Zwijndrecht, Belgium). Biorad protein assay dye reagent concentrate was purchased from Carl Roth (Karlsruhe, Germany). The following EziG enzyme carrier materials were provided by EnginZyme AB (Stockholm, Sweden): EziG¹ (Fe-Opal); EziG² (Fe-Coral) and EziG³ (Fe-Amber). For the immobilization of enzymes on carrier material, a C-star orbital shaker no. 12846016 (Thermo Fisher Scientific, UK) was used. Biotransformations were performed in an Eppendorf Thermomixer compact 5350 (Germany). Continuous flow experiments were performed with a Dionex P680 HPLC pump unit (Thermo Fischer Scientific, UK). Scanning electron microscopy (SEM) was performed using a FEI Verios 460 scanning electron microscope (Amolf, University of Amsterdam, The Netherlands).

4.4.2 Expression and purification of ω -transaminases

C-terminal His-tagged (*R*)-selective ω -transaminase from *Arthrobacter* sp. (AsR- ω TA, pET21a) [31] and N-terminal His-tagged (*S*)-selective ω -transaminase from *Chromobacterium violaceum* (Cv- ω TA, pET28b) [32] were expressed using *Escherichia coli* BL21 (DE3) as a host organism: 800 mL of LB medium supplemented with ampicillin (100 μ g mL⁻¹ for pET21a) or kanamycin (50 μ g mL⁻¹ for pET28b) were inoculated with 15 mL of an overnight culture. Cells were grown at 37 °C until an OD₆₀₀ of 0.6-0.9 was reached, and the expression of the proteins was induced by the addition of IPTG (0.5 mM final concentration). Protein expression was conducted overnight at 25 °C, and after harvesting of the cells (4 °C, 4500 rpm, 15 min), the remaining cell pellet was re-suspended in lysis buffer (50 mM KH₂PO₄, 300 mM NaCl, 10 mM imidazole, pH 8.0). Cells were disrupted by sonication and PLP (0.5 mM final concentration) was added to the cell lysate. After centrifugation (4 °C, 14,000 rpm, 45 min.), the supernatant was filtered through a 0.45 μ m filter and protein purification was performed by Ni²⁺ affinity chromatography using Ni-NTA HisTrap FF columns (GE Healthcare) according to the manufacturer's instructions. After loading of the filtered lysate, the column was washed with sufficient amounts of washing buffer (50 mM KH₂PO₄, 300 mM NaCl, 25 mM imidazole, pH 8.0), and the target enzyme was recovered with elution buffer (50 mM KH₂PO₄, 300 mM NaCl,

200 mM imidazole, pH 8.0). The process of purification was analyzed by SDS-PAGE (Supporting information, Figure S1). Fractions containing sufficiently pure protein were pooled and dialyzed overnight against potassium phosphate buffer (50 mM, pH 8). Protein solutions were concentrated and their concentrations were determined spectrophotometrically using a Bradford assay (for details: Bradford assay). Protein yields were 285 mg L⁻¹ of cell culture (36 mg g⁻¹ cell pellet) for AsR- ω TA and 100 mg L⁻¹ of cell culture (30 mg g⁻¹ cell pellet) for Cv- ω TA. Enzymes were shock-frozen in liquid nitrogen and stored at -80 °C.

4.4.3 Bradford assay

Biorad protein assay dye reagent concentrate was diluted 5 times with MilliQ water and filtered over a paper filter. The stock solution was freshly prepared before use and kept in the dark at 4 °C. Albumine calibration was performed in the standard range of 200-1000 μ g mL⁻¹ protein. For lower protein concentration (<25 μ g mL⁻¹) the low-concentration assay of 1-20 μ g mL⁻¹ was used. Samples were prepared by mixing 980 μ L stock solution and 20 μ L protein sample (low-concentration assay: 800 μ L stock and 200 μ L protein sample) followed by incubation for 5-10 minutes at RT. Absorption at 595 nm was measured and plotted against the protein concentration. Diluted enzyme samples were then measured in the same fashion in order to determine their concentration.

4.4.4 Optimized conditions for immobilization on EziG carrier materials

A vial containing 10 \pm 0.2 mg of EziGTM support material was cooled down in an ice bath and suspended in the immobilization buffer (MOPS, 1 mL, 100 mM, pH 7.5) supplemented with 0.1 mM PLP. Purified ω -TA (1 or 2 mg, equal to 10-20% w w⁻¹ total enzyme loading to support material) was added to the suspension, and the mixture was shaken with an orbital shaker (120 rpm) for 2 h at 4 °C. Small aliquots from the aqueous phase (20 μ L) were sampled before and after the immobilization procedure, their concentrations were determined using the Bradford assay (for details: Bradford assay), and the yield of immobilization yield was calculated (for details: Calculations and terminology). The immobilized enzyme was obtained by sedimentation, the buffer was removed by pipetting, and the immobilized enzyme was used directly in biotransformations. The same procedure was followed for immobilization at a larger scale, typically using 15 mg of purified ω TA and 100 mg of support material. Full immobilization was obtained after 1.5 h (total enzyme loading per support material: 15% w w⁻¹).

4.4.5 Optimized conditions for kinetic resolution with immobilized ω -transaminases

EziGTM-immobilized ω -transaminases (EziG³-AsR or EziG³-Cv, total enzyme loading: 10 or 20%, w w⁻¹) were employed for the kinetic resolution of *rac*- α -MBA with pyruvate as the amino-group acceptor (Scheme 4.6). Batch reactions were performed on analytical scale (0.5 mL) at 30 °C from 15 min or up to 3 h, depending on the type of experiment. All stock aqueous solutions were prepared in HEPES buffer (250 mM, pH 7.0). EziGTM-immobilized ω -transaminase (10 \pm 0.2 mg, total enzyme loading: 10 or 20%, w w⁻¹) was suspended in HEPES buffer (112.5 μ L, 250 mM, pH 7.0), to which 12.5 μ L of a 1 mM PLP stock solution (final concentration in solution 25 μ M) was added, along with 125 μ L of a 200 mM sodium pyruvate stock solution (final concentration in solution 50 mM) and 250 μ L of a 200 mM *rac*- α -MBA stock solution in DMSO/HEPES buffer (final concentration *rac*- α -MBA 100 mM and DMSO 5% v v⁻¹). The reactions were shaken at 30 °C (Eppendorf thermomixer,

750 rpm). The immobilized enzyme was left to sediment and the reaction mixture was separated from the biocatalyst by pipetting. The reaction mixture was basified with KOH (100 μL , 5 M) and extracted with EtOAc (2 x 500 μL), and the combined organic phase was dried over MgSO_4 . Analysis of the samples for conversion determination was conducted using GC-FID equipped with an achiral column (for details: Analytics). For the determination of the enantiomeric excess, derivatization of the samples was performed with 4-dimethylaminopyridine (DMAP, 50 mg mL^{-1}) in acetic anhydride (100 μL per sample) shaken with an orbital shaker (170 rpm) for 30 min at 25 °C. The samples were quenched by adding water (300 μL) and shaken again (170 rpm) for 30 min at 25 °C. The organic layer was collected, dried over MgSO_4 , and enantiomeric excess was measured on GC equipped with a chiral column (for details: Analytics).

4.4.6 *In-flow immobilization from purified enzyme solution*

AsR- ω TA (15 mg, 403 nmol of purified enzyme) was diluted in MOPS buffer (10 mL, 100 mM, pH 7.5) supplemented with 0.1 mM PLP in an ice bath at 4 °C. A stainless steel column (50 mm length x 2 mm diameter) was filled with EziGTM material (100 mg) and hydrated by flowing MOPS buffer into the column (50 mL, 100 mM, pH 7.5, flow 0.5 mL min^{-1}). Then, the diluted stock solution of AsR- ω TA was loaded onto the column using a peristaltic pump (flow rate: 300 $\mu\text{L min}^{-1}$). MOPS buffer (30 mL, 100 mM, pH 7.5) was flowed through the column to wash out any possibly unbound protein. Buffer samples (20 μL) of the loading enzyme solution and of the flow-through obtained during washing were taken and the enzyme concentration was measured in both samples using the Bradford assay (for details: Bradford assay) in order to calculate the yield of immobilization yield (for details: Calculations and terminology). Immobilization was quantitative; thus, the total enzyme loading per unit of support material was 15% (w w^{-1}). The column containing EziG³-AsR was conditioned by flowing HEPES buffer (30 mL, 250 mM, pH 7, 25 μM PLP, flow 0.5 mL min^{-1}) and subsequently mounted on a Dionex P680 HPLC pump unit equipped with flow controller. This set-up was used for continuous flow kinetic resolution experiments.

4.4.7 *In-flow immobilization from crude cell extract (i.e., cell lysate)*

Immobilization directly from cell lysate of ω TA is of particular interest for large scale application and was performed as follows. While cooling at 4 °C on an ice bath, *E. coli* wet cells containing overexpressed AsR- ω TA (0.62 g wet cells, 36 mg g^{-1} cells) was suspended in MOPS buffer (6 mL, 100 mM, pH 7.5) and disrupted by sonication. The cell debris was removed by centrifugation (4 °C, 14,000 rpm, 45 min), and the soluble fraction containing the enzyme (23% w w^{-1} to support material) was filtered (0.45 μm filter pores). A stainless-steel column (50 mm length x 2 mm diameter) was filled with EziG³ Fe-Amber (100 mg) and hydrated with MOPS buffer (50 mL, 100 mM, pH 7.5, flow 0.5 mL min^{-1}). The soluble protein fraction was loaded onto the column using a peristaltic pump (flow rate: 150 $\mu\text{L min}^{-1}$, residence time (t_R): 63 s). After complete loading (6 mL), the flow was stopped, and the cell lysate was left to incubate in the column for 45 min at 20 °C. This incubation time resulted in the avoidance of even minor enzyme leaching during the subsequent washing steps and reaction. Then, MOPS buffer (50 mL, 100 mM, pH 7.5, flow 0.5 mL min^{-1}) was flowed through the column to wash out any possibly unbound component (e.g. endogenous *E. coli* proteins etc.). The column containing the immobilized AsR- ω TA was conditioned by flowing further with HEPES buffer (30 mL, 250 mM, pH 7, 25 μM PLP) and subsequently mounted on a Dionex P680 HPLC pump unit equipped with flow controller. The amount of immobilized AsR- ω TA per unit of support material was calculated to be 19% (w w^{-1}) based on the difference between protein content in the loading fraction and protein content in the washing fractions (determination with the Bradford assay). The determination

through quantitative analysis of protein fractions on SDS PAGE yielded the same result.

4.4.8 Continuous flow kinetic resolution with EziGTM-immobilized ω -transaminases

ω -Transaminase was immobilized on EziGTM support material (100 mg support plus enzyme, total enzyme loading: 15% w w⁻¹) in a stainless-steel column (50 mm length x 2 mm diameter). A Dionex P680 HPLC pump unit was flushed with HEPES buffer (250 mM, pH 7, 25 μ M PLP). The column containing EziG³- ω TAs was connected to the flow system and heated up to 30 °C in a water bath. The reaction mixture was prepared as follows. Sodium pyruvate (5.4 g, 49.5 mmol, 55 mM final concentration) was dissolved in HEPES buffer (900 mL final volume, 250 mM, pH 7), and *rac*- α -MBA (11.6 mL, 10.9 g, 90 mmol, 100 mM final concentration) was pre-dissolved in DMSO (final cosolvents concentration: 10% v v⁻¹) prior to addition to the HEPES buffer containing the sodium pyruvate. Then, the pH was adjusted to pH 7 and PLP (25 μ M final concentration) was added. The solution was stirred for 1 h at RT in the dark. The reaction mixture was pumped through the column (average flow rate: 0.175 mL min⁻¹), and the product mixture was collected in fractions (ca. 8 mL each hour during the first day of operation, and then 200 mL during nighttime and 100 mL during the daytime). The column was operated for 96 consecutive hours without any detectable decrease of catalytic performance. A small aliquot of each fraction (0.5 mL) was basified with KOH (100 μ L, 5 M) and extracted with EtOAc (2 x 500 μ L). The organic layers were combined, dried over MgSO₄ and analyzed with GC equipped with an achiral column (for details: Analytics). GC-analysis showed that the kinetic resolution proceeded quantitatively (> 49% conversion). The final work-up was performed by initial acidification of the combined collected product fractions to pH 2 with HCl (37%), followed by extraction of the acetophenone byproduct with MTBE (3 x 300 mL). Then, the aqueous phase was basified to pH 14 with KOH (5 M), and the product was extracted with MTBE (3 x 300 mL). The combined organic phase was dried over MgSO₄ and the solvent was removed by reduced pressure to obtain 5.05 g of pure (*S*)- α -MBA (42 mmol, 93% isolated yield) in perfect optical purity (> 99% ee).

4.4.9 Scanning electron microscopy (SEM) analysis

Scanning electron micrographs (SEM) of EziGTM material with immobilized AsR- ω TAs were obtained with a FEI Verios 460 scanning electron microscope in secondary-electron mode. An acceleration voltage of 2-5 kV was used with a beam current of 100 pA at a working distance of 4 mm, and the field immersion mode was applied for an optimized resolution. Samples were placed onto an aluminum stub with carbon film and dried for several hours at 40 °C under vacuum before measurement. Selected samples were also sputter-coated with a layer of Cr (20 nm).

4.4.10 Analytics

Conversions were determined by GC using a 7890A GC system (Agilent Technologies), equipped with a FID detector using H₂ as carrier gas with a DB1701 column from Agilent (30 m, 250 μ m, 0.25 μ m). The enantiomeric excess of derivatized amines was measured using a ChiraSil DEX-CB column from Agilent (25 m, 320 μ m, 0.25 μ m).

DB1701 30 m method: constant pressure 6.9 psi, T injector 250 °C, split ratio 40:1, T initial 60 °C, hold 6.5 min; gradient 20 °C/min up to 100 °C, hold 1 min, gradient 20 °C/min up to 280 °C, hold 1 min.

ChiraSil DEX-CB method: constant flow 1.4 mL/min, T injector 250 °C, split ratio 20:1, T initial 100 °C, hold 2 min; gradient 1 °C/min up to 130 °C, hold 5 min; gradient 10 °C/min up to 170 °C, hold 10 min.; gradient 10 °C/min up to 180 °C, hold 1 min.

Table 4.2. GC retention time of reference compounds.

Entry	Compound	Retention time [min]	GC column
1	<i>rac</i> - α -MBA	10.9	DB1701 30m
2	Acetophenone	11.7	DB1701 30m
3	(<i>S</i>)- α -MBA	31.6	ChiraSil DEX-CB
4	(<i>R</i>)- α -MBA	32.3	ChiraSil DEX-CB

4.5 Calculations and terminology

The data from the immobilization studies were interpreted using the following calculations to define parameters such as yield of immobilization, immobilized enzyme activity, turnover frequency (TOF), and turnover number (TON):

4.5.1 Yield of immobilization

In order to determine how much of the enzyme is immobilized during the process, a Bradford assay (UV absorption at 595 nm, section 4.4.3) was performed before ($A_{595 \text{ initial}}$) and after the immobilization process ($A_{595 \text{ final}}$) for calculating the amount of enzyme bound to the beads, i.e. the yield of immobilization (Equation 1).

Equation 1

$$\text{yield of immobilization [\%]} = \frac{(A_{595 \text{ final}} - A_{595 \text{ initial}})}{A_{595 \text{ initial}}} \times 100\%$$

4.5.2 Turnover number (TON)

After immobilization, the immobilized enzyme was tested for its activity. The conversion of substrate per amount of immobilized enzyme in a given time gives the turnover number (TON) as is defined below in Equation 2.

Equation 2

Turnover of immobil. enz. (TON)

$$= \frac{\left(\frac{\text{Conv. of substrate [\%]}}{100} \right) \times \text{Added substrate [\mu mol]}}{\text{Amount of immobil. enzyme [\mu mol]}}$$

In relation to Equation 2, the amount of immobilized enzyme can be determined by taking into account the amount of enzyme that was added to the beads (before immobilization). Using the immobilization yield, as reported in Equation 1, it is possible to calculate the quantity of enzyme that remained bound to the beads at the end of the immobilization process. Then, it is possible to calculate the exact quantity of enzyme used in each reaction from the amount of beads that was employed (with the enzyme immobilized). Details are given in Equation 3.

Equation 3

Amount of immobil. enzyme [μmol]

$$= \frac{\left(\frac{\text{yield of immobil. [\%]}}{100} \times \text{mass initial added enzyme [\mu g]} \right)}{\text{Enzyme molecular mass} \left[\frac{\mu\text{g}}{\mu\text{mol}} \right]}$$

In which the mass initial added enzyme [μg] is the amount of enzyme added to the beads at the beginning of the immobilization process.

4.5.3 Immobilized enzyme activity or turnover frequency (TOF)

When the turnover number obtained from the activity tests is plotted against time, the slope of this graph (considering the linear range) indicates the immobilized enzyme activity or turnover frequency (TOF). This is shown in Equation 4.

Equation 4

$$\text{Immobilized enzyme activity (or TOF)} = \frac{\text{TON}}{\text{time [min]}}$$

4.5.4 Reaction rate in flow reactors

In flow reactors, several parameters relate to the reaction rate. An important parameter is space velocity (SV, in units of reciprocal time), which is defined by the volumetric flow rate of the reactant stream (V_o , specified at the inlet conditions of temperature and pressure with zero conversion), and the catalyst volume (V_c).^[1] Often catalyst volume (V_c) is equally related to the reactor volume (V_r), which depends on the packing density of the catalyst particles.

Equation 5

$$SV \text{ (space velocity)} = \frac{V_o}{V_r}$$

Space time (τ , in units of time) is the inverse of space velocity and it gives the time required to process one reactor volume:

Equation 6

$$\tau (\text{space time}) = \frac{1}{SV} = \frac{V_r}{V_o}$$

The space time yield (STY) refers to the quantity of product produced per quantity of catalyst per unit time. If the catalyst is well-packed in the full reactor, then the catalyst volume (V_c) can be equated to the reactor volume (V_r).

Equation 7

$$STY (\text{space time yield}) = \frac{\text{product produced [g]}}{(V_r \times \text{time})}$$

Calculation of space-time yield for the flow process with ω -TAs:

$$STY = \frac{5.05 \text{ [g]}}{(157 \text{ [\mu L]} \times 96 \text{ [h]} \times 10^{-6} \text{ [L } \mu\text{L}^{-1}]}) = 335 \text{ g L}^{-1}\text{h}^{-1}$$

4.6 References

- [1] a) Choi, J. M.; Han, S. S.; Kim, H. S. *Biotechnology Advances*. **2015**, *33*, 1443–1454; b) Madhavan, A.; Sindhu, R.; Binod, P.; Sukumaran, R. K.; Pandey, A. *Bioresource Technology*. **2017**, *245*, 1304–1313; c) Prasad, S.; Roy, I. *Recent Patents in Biotechnology*. **2018**, *12*, 33–56; d) Schmid, A.; Dordick, J. S.; Hauer, B.; Kiener, A.; Wubbolts, M.; Witholt, B. *Nature*. **2001**, *409*, 258–268.
- [2] Sheldon, R. A.; Woodley, J. M. *Chemical Reviews*. **2018**, *118*, 801–838.
- [3] a) Sheldon, R. A. *Advanced Synthesis & Catalysis*. **2007**, *349*, 1289–1307; b) Sheldon, R. A.; Van Pelt, S. *Chemical Society Reviews*. **2013**, *42*, 6223–6235.
- [4] a) Tamborini, L.; Fernandes, P.; Paradisi, F.; Molinari, F. *Trends in Biotechnology*. **2018**, *36*, 73–88; b) Britton, J.; Majumdar, S.; Weiss, G. A. *Chemical Society Reviews*. **2018**, *47*, 5891–5918; c) Thompson, M. P.; Peñafiel, I.; Cosgrove, S. C.; Turner, N. J. *Organic Process Research & Development*. **2018**, *23*, 9–18; d) Bolivar, J. M.; Wiesbauer, J.; Nidetzky, B. *Trends in Biotechnology*. **2011**, *29*, 333–342; e) Matosevic, S.; Szita, N.; Baganz, F. *Journal of Chemical Technology and Biotechnology*. **2011**, *86*, 325–334.
- [5] Slabu, I.; Galman, J. L.; Lloyd, R. C.; Turner, N. J. *ACS Catalysis*. **2017**, *7*, 8263–8284.
- [6] Savile, C. K.; Janey, J. M.; Mundorff, E. C.; Moore, J. C.; Tam, S.; Jarvis, W. R.; Colbeck, J. C.; Krebber, A.; Fleitz, F. J.; Brands, J.; Devine, P. N.; Huisman, G. W.; Hughes, G. J. *Science*. **2010**, *329*, 305–309.
- [7] a) Alami, A. T.; Richina, F.; Corroero, M. R.; Dudal, Y.; Shahgaldian, P. *Chimia*. **2018**, *72*, 345–346; b) Basso, A.; Neto, W.; Serban, S.; Summers, B. D. *Chimica Oggi-Chemistry Today*. **2018**, *36*, 40–42; c) Jia, H.; Huang, F.; Gao, Z.; Zhong, C.; Zhou, H.; Jiang, M.; Wei, P. *Biotechnology Reports*. **2016**, *10*, 49–55; d) Mallin, H.; Hohne, M.; Bornscheuer, U. T. *Journal of Biotechnology*. **2014**, *191*, 32–37; e) Neto, W.; Schürmann, M.; Panella, L.; Vogel, A.; Woodley, J. M. *Journal of*

- Molecular Catalysis B.* **2015**, *117*, 54–61; f) Sun, J.; Cui, W. H.; Du, K.; Gao, Q.; Du, M.; Ji, P.; Feng, W. *Journal of Biotechnology.* **2017**, *245*, 14–20; g) Truppo, M. D.; Strotman, H.; Hughes, G. *ChemCatChem.* **2012**, *4*, 1071–1074; h) De Souza, S. P.; Junior, I. I.; Silva, G. M. A.; Miranda, L. S. M.; Santiago, M. F.; Lam, F. L.-Y.; Dawood, A.; Bornscheuer, U. T.; De Souza, R. O. M. A. *RSC Advances.* **2016**, *6*, 6665–6671.
- [8] Nagy-Gyor, L.; Abahazi, E.; Bodai, V.; Satorhelyi, P.; Erdelyi, B.; Balogh-Weiser, D.; Paizs, C.; Hornyanszky, G.; Poppe, L. *ChemBioChem.* **2018**, *19*, 1845–1848.
- [9] Andrade, L. H.; Kroutil, W.; Jamison, T. F. *Organic Letters.* **2014**, *16*, 6092–6095.
- [10] Halim, A. A.; Szita, N.; Baganz, F. *Journal of Biotechnology.* **2013**, *168*, 567–575.
- [11] Matosevic, S.; Lye, G. J.; Baganz, F. *Journal of Biotechnology.* **2011**, *155*, 320–309.
- [12] Gruber, P.; Carvalho, F.; Marques, M. P. C.; O'sullivan, B.; Subrizi, F.; Dobrijevic, D.; Ward, J.; Hailles, H. C.; Fernandes, P.; Wohlgemuth, R.; Baganz, F.; Szita, N. *Biotechnology and Bioengineering.* **2018**, *115*, 586–596.
- [13] a) Planchestainer, M.; Contente, M. L.; Cassidy, J.; Molinari, F.; Tamborini, L.; Paradisi, F. *Green Chemistry.* **2017**, *19*, 372–375; b) Contente, M. L.; Dall'oglio, F.; Tamborini, L.; Molinari, F.; Paradisi, F. *ChemCatChem.* **2017**, *9*, 3843–3848; c) Benítez-Mateos, A. I.; Contente, M. L.; Velasco-Lozano, S.; Paradisi, F.; López-Gallego, F. *ACS Sustainable Chemistry & Engineering.* **2018**, *6*, 13151–13159.
- [14] Contente, M. L.; Paradisi, F. *Nature Catalysis.* **2018**, *1*, 452–459.
- [15] Shin, J.-S.; Kim, B.-G.; Shin, D.-H. *Enzyme and Microbial Technology.* **2001**, *29*, 232–239.
- [16] Abaházi, E.; Sátorhelyi, P.; Erdélyi, B.; Vértessy, B. G.; Land, H.; Paizs, C.; Berglund, P.; Poppe, L. *Biochemical Engineering Journal.* **2018**, *132*, 270–278.
- [17] Milozic, N.; Lubej, M.; Lakner, M.; Znidarsic-Plazl, P.; Plazl, I. *Chemical Engineering Journal.* **2017**, *313*, 374–381.
- [18] Biggelaar, L. V. D.; Soumillion, P.; Debecker, D. *Catalysts.* **2017**, *7*, 54.
- [19] Peris, E.; Okafor, O.; Kulcinskaja, E.; Goodridge, R.; Luis, S. V.; Garcia-Verdugo, E.; O'reilly, E.; Sans, V. *Green Chemistry.* **2017**, *19*, 5345–5349.
- [20] a) Ho, L. F.; Li, S. Y.; Lin, S. C.; Wen-Hwei, H. *Process Biochemistry.* **2004**, *39*, 1573–1581; b) Pessela, B. C. C.; Mateo, C.; Filho, M.; Carrascosa, A.; Fernández-Lafuente, R.; Guisan, J. M. *Enzyme and Microbial Technology.* **2007**, *40*, 242–248; c) Porath, J. *Protein Expression and Purification.* **1992**, *3*, 263–281.
- [21] Cao, G.; Gao, J.; Zhou, L.; Huang, Z.; He, Y.; Zhu, M.; Jiang, Y. *Biochemical Engineering Journal.* **2017**, *128*, 116–125.
- [22] Cassimjee, K. E.; Kadow, M.; Wikmark, Y.; Svedendahl Humble, M.; Rothstein, M. L.; Rothstein, D. M.; Backvall, J. E. *Chemical Communications.* **2014**, *50*, 9134–9137.
- [23] a) Lyskowski, A.; Gruber, C.; Steinkellner, G.; Schurmann, M.; Schwab, H.; Gruber, K.; Steiner, K.

- PLoS One*. **2014**, *9*, e87350; b) Malik, M. S.; Park, E. S.; Shin, J. S. *Applied Microbiology and Biotechnology*. **2012**, *94*, 1163–1171.
- [24] Shin, J. S.; Yun, H.; Jang, J. W.; Park, I.; Kim, B. G. *Applied Microbiology and Biotechnology*. **2003**, *61*, 463–471.
- [25] a) Cassimjee, K. E.; Federsel, H. J. *Biocatalysis: An Industrial Perspective*; Gonzalo, G. D. María, P. D. D. (Eds.); Royal Society of Chemistry, 2018, pp. 345–362; b) Cassimjee, K. E.; Bäckvall, J. E. *Immobilized Proteins and Use Thereof*. WO2015/115993, August, 2015.
- [26] Fernandez-Lopez, L.; Pedrero, S. G.; Lopez-Carrobles, N.; Gorines, B. C.; Virgen-Ortiz, J. J.; Fernandez-Lafuente, R. *Enzyme and Microbial Technology*. **2017**, *98*, 18–25.
- [27] Assmann, M.; Mugge, C.; Gassmeyer, S. K.; Enoki, J.; Hilterhaus, L.; Kourist, R.; Liese, A.; Kara, S. *Frontiers in Microbiology*. **2017**, *8*, 448.
- [28] Cassimjee, K. E.; Hendil-Forsell, P.; Volkov, A.; Krog, A.; Malmo, J.; Aune, T. E. V.; Knecht, W.; Miskelly, I. R.; Moody, T. S.; Svedendahl Humble, M. *ACS Omega*. **2017**, *2*, 8674–8677.
- [29] Lechner, H.; Soriano, P.; Poschner, R.; Hailes, H. C.; Ward, J. M.; Kroutil, W. *Biotechnology Journal*. **2018**, *13*, 1700542.
- [30] a) Böhmer, W.; Knaus, T.; Mutti, F. G. *ChemCatChem*. **2018**, *10*, 731–735; b) Mutti, F. G.; Knaus, T.; Scrutton, N. S.; Breuer, M.; Turner, N. J. *Science*. **2015**, *349*, 1525–1529; c) Thompson, M. P.; Turner, N. J. *ChemCatChem*. **2017**, *9*, 3833–3836; d) Thompson, M. P.; Derrington, S. R.; Heath, R. S.; Porter, J. L.; Mangas-Sanchez, J.; Devine, P. N.; Truppo, M. D.; Turner, N. J. *Tetrahedron*. **2019**, *75*, 327–334.
- [31] Iwasaki, A.; Matsumoto, K.; Hasegawa, J.; Yasohara, Y. *Applied Microbiology and Biotechnology*. **2012**, *93*, 1563–1573.
- [32] a) Kaulmann, U.; Smithies, K.; Smith, M. E. B.; Hailes, H. C.; Ward, J. M. *Enzyme and Microbial Technology*. **2007**, *41*, 628–637; b) Koszelewski, D.; Pressnitz, D.; Clay, D.; Kroutil, W. *Organic Letters*. **2009**, *11*, 4810–4812; c) Koszelewski, D.; Görtzner, M.; Clay, D.; Seisser, B.; Kroutil, W. *ChemCatChem*. **2010**, *2*, 73–77.
- [33] a) Mateo, C.; Abian, O.; Fernandez-Lorente, G.; Pedroche, J.; Fernandez-Lafuente, R.; Guisan, J. M.; Tam, A.; Daminati, M. *Biotechnology Progress*. **2002**, *18*, 629–634; b) Wheatley, J. B.; Schmidt Jr, D. E. *Journal of Chromatography A*. **1999**, *849*, 1–12.
- [34] Chen, S.; Land, H.; Berglund, P.; Humble, M. S. *Journal of Molecular Catalysis B*. **2016**, *124*, 20–28.
- [35] Shin, J.-S.; Kim, B.-G. *Biotechnology and Bioengineering*. **1998**, *60*, 534–540.
- [36] Gomm, A.; O'reilly, E. *Current Opinion in Chemical Biology*. **2018**, *43*, 106–112.

Chapter 5

Application of immobilized ω -transaminases on metal-ion affinity support material in neat organic solvents

This chapter is based on the following publication:

Böhmer, W.; Mutti, F., G. (et al.) *Advanced Synthesis & Catalysis*. 2019, manuscript submitted.

5.1 Introduction

The use of enzymes has been predominantly restricted to their natural, aqueous reaction environment. The majority of biocatalytic reactions on industrial scale are performed in aqueous or bi-phasic aqueous-organic reaction media, with the notable exception of the application of a large number of hydrolases ^[1] as well as some hydroxynitrile lyases ^[2], some oxidoreductases ^[3] and a very few transaminases ^[4]. However, common drawbacks of biotransformations in aqueous medium are the low solubility of hydrophobic substrates and, in certain cases, the occurrence of unwanted side reactions, unfavorable thermodynamic equilibria as well as challenging product recovery ^[5]. Implementation of enzyme catalysis in non-aqueous media can enable reactions that are very challenging or even cannot occur in aqueous environment. Furthermore, it allows for running reactions at increased substrate concentrations, higher reaction temperatures and facilitates down-stream processing.

Current implementation of enzymes in non-aqueous media mostly hampers from the low solvent tolerance of many enzymes in aqueous/co-solvent mixtures (<20% co-solvent). Conversely, prolonged exposure of some enzymes to neat organic solvents, in which no water was present, proved to be non-destructive as enzyme activity in water was fully recovered afterwards ^[6]. In addition, various crystalline enzymes have been shown to retain their native structures in neat organic solvents ^[7]. This phenomenon arises from an inherent conformational rigidity of enzymes in non-aqueous media in the absence of water. However, dynamic and catalytic properties of these enzymes are dependent on the presence of a limited but crucial amount of water. In fact, less than a monolayer of water is required for an enzyme molecule to show activity ^[8]. Computational as well as experimental studies have indicated that higher water content is correlated to increased protein dynamics in non-aqueous media ^[9]. Additionally, initial studies with an alcohol dehydrogenase have shown higher reaction rates when the water content in different reaction solvents was increased ^[10]. However, increasing the water content of the reaction solvent above the water saturation level poses the tendency for the protein to unfold.

Enzyme catalysis in non-conventional media has many advantages over using aqueous media (Table 5.1) ^[11]. These reaction systems are clearly distinct from aqueous media supplied with water-miscible solvents to favor dissolution of insoluble reactants as well as biphasic and reverse-micelles systems where the enzyme is still dissolved in a significant amount of water ^[12]. Optimizations in enzyme microenvironment have led to enhanced stability

and performance in non-aqueous media ^[13]. In addition, distinct selectivity of enzymes has been observed which can be controlled and reversed depending on the solvent of choice ^[14]. Using non-aqueous media for enzyme catalysis enables chemical transformations that are unfavorable in water and it prevents unwanted side-reactions that are often observed in aqueous systems, such as hydrolysis. The use of poorly water-soluble or unstable substrates and reaction intermediates does not represent a drawback anymore, and the recovery of products and insoluble biocatalysts after the reaction becomes feasible. Finally, increased biocatalyst thermostability at lower water levels is often observed and enzyme denaturation is prevented ^[15]. For example, porcine pancreatic lipase ^[16], ribonuclease ^[17], and α -chymotrypsin ^[18] have been shown to possess half-lives of several hours at 100 °C in neat organic solvents whereas in aqueous medium they deactivated within seconds.

Despite several process advantages, enzymes generally possess low catalytic activity in non-aqueous media due to a number of factors (Table 5.1) ^[15, 19]. The bulk protein structure is maintained by non-covalent interactions which are sustained in the presence of water molecules. Solvent molecules with the tendency to strip tightly bound water molecules from the enzyme surface can cause enzyme inactivation. Especially polar solvents can disrupt stabilizing interactions leading to changes in the protein secondary and tertiary structure which ultimately can lead to unfolding of the protein ^[20]. Penetration of solvents into the active site of an enzyme can cease catalytic activity as well as destabilizing transition states. Conversely, non-polar solvents cause severely restricted conformational dynamics of enzymes in non-aqueous media but it can also lead to higher catalytic activity. It has not been clarified whether this phenomenon arises from structural perturbation of the protein by solvent molecules or from the influence of solvent molecules on the thermodynamic ground state of reactants, intermediate transition states or products. Better solvation of substrates into the reaction medium can hamper binding and conversion of the substrate in the active site of the enzyme. Enzymes with hydrophobic active centers operate better in water where desolvation of non-polar substrates is favored. However, in organic solvents the solvation of non-polar substrates is significantly better than in water and diffusion of substrates into the active site of the enzyme can be much slower. For example, higher solubility of substrates in organic solvent has been shown to decrease the catalytic activity of peroxidases by several orders of magnitude ^[21]. Conversely, solvent molecules can lower the transition-state energy of partially-exposed transition states as enzyme-substrate interactions tend to become stronger.

For example, subtilisin Carlsberg has been shown to exhibit more stabilized transition states, and hence higher catalytic activity, in more polar solvents ^[22]. Finally, insolubility of enzymes in non-aqueous media often gives rise to mass transfer limitations and, hence, slower reactions. Especially for highly active enzymes, diffusion is often rate-limiting and it affects enzyme kinetics. Therefore, reaction mixtures have to be vigorously stirred to ensure high volumetric productivity ^[23].

Enzyme activity in non-aqueous media is very distinct from that in water and it is often obtained through pretreatment of the enzyme in the form of lyophilization or immobilization onto a support material. Lyophilization of the enzyme can provoke severe loss in catalytic activity due to the removal of water molecules that are essential for the conformational stability of the enzyme. Therefore, enzyme lyophilization can be performed in the presence of lyoprotectants such as sugars, polyethylene glycol, inorganic salts (notably KCl), substrate-resembling ligands, and crown ethers ^[24]. A more conventional and less destructive method of pretreatment involves enzyme immobilization and subsequent washing of the immobilized enzyme with organic solvent until an active biocatalyst has been obtained. Lipases in particular have been immobilized on various support materials and commercialized for their use in transesterification reactions since unwanted hydrolysis of esters is suppressed in non-aqueous media. For example, Novozym® 435 is a CALB lipase originating from *Candida Antarctica* B immobilized on

Table 5.1. Advantages and limitations of using enzymes in non-aqueous media.

Advantages	Limitations
<ul style="list-style-type: none"> • Increased solubility of non-polar substrates • Suppression of unwanted side-reactions • Often enhanced thermostability • Possible increased mechanical stability • Insolubility of enzymes prevents desorption from immobilization supports • Stabilization of partially-exposed transition states • Alterations in substrate specificity • Ease of enzyme recovery after the reaction • Facile product recovery 	<ul style="list-style-type: none"> • Often lower catalytic activity • Disruption of bulk protein structure • Slower diffusion of substrates into the active site of the enzyme • Mass transfer limitations and rate-limiting diffusion • Penetration of solvent molecules into the active site can cause enzyme inhibition

a hydrophobic acrylic resin and it is currently a widely used lipase in industry [25]. High catalytic activity of lipases in non-aqueous media further resides from the fact that their native protein structure possesses two folding states. In non-aqueous media the protein is in the so-called "open form" in which the active site pocket is accessible to substrate molecules. Conversely, in aqueous environment this substrate pocket is closed due to conformational changes in the protein structure. Reactivity of lipases such as Novozym 435 and their advantages and limitations in organic synthesis have recently been reviewed [1, 26]. Other noteworthy examples of enzymes which were successfully applied in non-aqueous media showing high reactivity and stability include α -chymotrypsin [27], protease from *Aspergillus oryzae* [24a] and subtilisin Carlsberg [28]. In addition, important contributions have been made in enzyme catalysis using ionic liquids [29] and deep eutectic solvents [30].

The residual amount of water in a given solvent (i.e. below water saturation level) is important, but water partitions between all components in the system including solvent, enzyme, support matrix and headspace of the reaction vessel. For analysis and comparison of enzyme performance in different solvents, water activity (α_w) is a more reliable parameter because the hydration state of an enzyme is always determined by α_w regardless of the solvent of choice [15a]. It describes the tendency of water to reside in a certain reaction phase and varies from 1 (being pure water) down to 0 for a completely dry system (see also: section 5.4.8). The effects of α_w on biocatalyst performance in non-aqueous media can only be investigated if the system can operate at controlled α_w (i.e., under equilibrium conditions). Various methods for α_w control have been reported and may consist of a saturated salt solution that is circulated through the reaction via a submerged silicon tubing [31]. Diffusion of water through the tube walls maintains an equilibrium water activity set by the nature of the salt solution used. Another more simple approach involves the use of insoluble hydrate salts. These hydrate salts are used in pairs, such as the monohydrate in combination with the dihydrate or the dihydrate in combination with the heptahydrate, to work as a water buffer and fix α_w of a particular system. The parameter of α_w has been reported for a small selection of hydrate salts [32].

Transaminases (ω -TAs) are pyridoxal phosphate-dependent enzymes that enable the transfer of an amino group from a simple donor molecule to a prochiral carbonyl compound thus generating a wide range of high-value chiral α -amines [33]. They possess significant potential for industrial application due to high turnover rates, excellent enantioselectivity

and economical cofactor regeneration ^[34]. However, application of ω -TAs is often challenging due to the unfavorable reaction equilibrium, enzyme inhibition by substrates and products, or instability of the enzyme under the applied reaction conditions. Although the thermodynamics of the reaction are independent of the enzyme, reaction medium engineering can significantly change the outcome of the reaction. Transamination reactions in aqueous environment often require supra-stoichiometric amounts of an amine donor in order to drive the equilibrium to the product side. The nucleophilicity of amines in water is low, especially in the pH range where ω -TAs are operationally stable (pH 7.0-9.0). In addition, co-products arising from these amine donors are usually better substrates for the enzyme than the supplied prochiral ketone substrate. In non-aqueous media, the solubility of substrates and amine donors for ω -TAs is very different and formation of the desired chiral amine product is much more favored. Interestingly, reports of ω -TAs applied in aqueous media or water-miscible systems are numerous, whereas their use in non-aqueous media with minimal water content is scarcely reported. Perhaps this lack of available studies on ω -TAs in non-aqueous media can be attributed to poorly optimized reaction media, which resulted in low catalytic activities. Nevertheless, there have been several noteworthy contributions that have highlighted the potential of using ω -TAs in organic solvents. For example, crude cell preparation of ω -TA from *Vibrio fluvialis* JS17 has been reported to partially retain enzyme activity in water-saturated ethyl acetate. The enzyme performed the deamination of (*S*)- α -methylbenzylamine using ethyl pyruvate as the amino acceptor with perfect enantioselectivity, although reaction rates were 3-fold lower than in phosphate buffer ^[35]. An immobilized transaminase for the production of Sitagliptin was operated in water-saturated isopropyl acetate (IPAc) with remarkable stability. Interestingly, the enzyme showed deactivation of 0.5%/h over 6 days in completely dry IPAc at 50 °C whereas in water-saturated IPAc no deactivation was observed. The immobilized ω -TA could be used in more than 10 consecutive cycles without any detectable loss of activity (ca. 80% conversion, 50 mM substrate) ^[4a]. In a concomitant independent study, Mutti and Kroutil reported the use of transaminase lyophilized cell extracts to operate with elevated catalytic efficiency in the amination of prochiral ketones. The activity of the lyophilized cell extract was retained in neat organic solvent by addition of a small amount of water and exhibited lack of apparent substrate inhibition. Furthermore, it enabled simple product recovery and easy recycling of the biocatalyst with no observable apparent loss of catalytic activity after 5 cycles, and ca. 50% retained activity after 10

reaction cycles ^[4b]. Using the same strategy, transaminase lyophilized cell extracts from *Bacillus megaterium* and *Arthrobacter* sp. were applied in neat organic solvent for the synthesis of both enantiomers of valinol ^[36]. Furthermore, immobilized whole cells of ω -TA from *Arthrobacter* sp. have been shown to perform the asymmetric amination of prochiral ketones under continuous operation in a flow reactor. The use of an organic solvent for the reaction medium prevented leaching of the PLP cofactor from the enzyme; thus, a number of prochiral ketones could be converted at 50 °C within a residence time of 30-60 minutes. Finally, ATAs have been shown to better tolerate non-aqueous media by employing protein engineering strategies ^[37] or by encapsulation into ionic liquid capsules ^[38].

In Chapter 4 the immobilization of transaminases on controlled porosity glass carrier material (EziG™) for their application in aqueous environment was described ^[39]. Instead, the present chapter reports about the application of both an (*R*)-selective and an (*S*)-selective transaminase as immobilized enzymes in neat organic solvent at controlled α_w . Both enzymes were immobilized on EziG support materials through metal-ion affinity binding. Subsequent optimization of a_w was performed in organic solvent and the immobilized enzymes were applied in the reductive amination of 1-phenoxypropan-2-one (**1a**) using 2-propylamine (**2b**) as the amine donor (Scheme 5.1). Optimization of the reaction system was performed in terms of a_w level, type of support material, reaction solvent, and temperature. These studies revealed that only a specific value of a_w correlates with a high catalytic activity of the immobilized ω TAs. Furthermore, both enzymes showed very distinct conversions at the same a_w value. In analytical scale reactions (1 mL) substrate concentrations as high as 400 mM could be applied and the immobilized ω TA could be recycled up to 4 reaction cycles. Finally, the immobilized (*R*)-selective transaminase was employed in a packed-bed flow reactor in neat organic solvent showing high catalytic performance under the optimal reaction conditions.

5.2 Results and Discussion

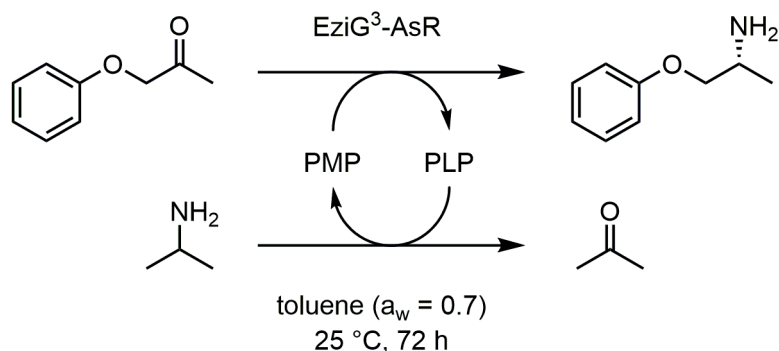
5.2.1 Immobilization and pre-treatment of ω TAs for application in organic solvents

Two stereocomplementary ω -transaminases (ω TA), namely the (*R*)-selective ω TA from *Arthrobacter* species (AsR- ω TA) ^[40] and the (*S*)-selective ω TA from *Chromobacterium*

violaceum (Cv- ω TA)^[41], were chosen for application in neat organic solvents. In this study, we decided to use purified ω TA in order to be able to quantify with high precision and accuracy the amount of immobilized enzyme loaded on the support material. However, the efficiency for the selective immobilization of ω TA from crude lysate on EziG³ (Fe Amber) was previously demonstrated^[39]. Therefore, we applied a typical enzyme loading of 10% w w⁻¹ ω TA.

The immobilization of ω TAs was performed on three types of EziG polymer-coated controlled porosity glass support materials, possessing distinct surface properties. The first type of material, henceforth called EziG¹ (Fe Opal), is covered with a hydrophilic polymeric surface. EziG² (Fe Coral) has a hydrophobic surface polymer and EziG³ (Fe Amber) is covered with a semi-hydrophobic polymer surface (see Table 5.4 for product specifications). Immobilization of ω TAs was performed by incubating the desired amount of enzyme in buffer supplied with EziG carrier material, according to a previously reported protocol^[39]. The progress of immobilization was determined by measuring the amount of enzyme remaining in the immobilization buffer with a Bradford assay (section 5.4.3). AsR- ω TA was immobilized on EziG carrier materials within 3 hours of incubation^[39].

The water content (c_w) of EziG-immobilized ω TA had to be lowered after the immobilization step and controlled during the reaction in organic solvent for obtaining high catalytic activity. Our previously reported methodology based on the lyophilization of ω TAs, as cell extract,^[4b] was not applicable for EziG-immobilized enzymes and resulted in complete loss of catalytic activity. Other attempts aimed at reducing the water content of the immobilized ω TA by gentle flowing of a stream of air or nitrogen gas gave a similar result in aqueous as well as in organic environment. Addition of small amounts of water in an



Scheme 5.1. Reductive amination of phenoxyacetone (**1a**) with isopropylamine (**2b**) as test reaction catalyzed by EziG³-AsR in neat organic solvents at controlled α_w .

attempt to restore catalytic activity of the enzyme did not lead to any improvement.

Optimizing c_w in a heterogeneous organic mixture containing the immobilized ω TA using hydrate salts pair proved to be more successful, especially by introducing an intermediate treatment with a hydrophilic solvent at controlled α_w . By simple washing of the wet immobilized ω TA with hydrophilic organic solvent in the presence of hydrate salts (i.e. $\text{Na}_2\text{HPO}_4 \cdot 2\text{H}_2\text{O}/\text{Na}_2\text{HPO}_4 \cdot 7\text{H}_2\text{O}$ or $\text{Na}_2\text{HPO}_4 \cdot 7\text{H}_2\text{O}/\text{Na}_2\text{HPO}_4 \cdot 12\text{H}_2\text{O}$ were applied as was previously reported [2c]), optimal c_w could be set in the system. Then, the hydrophilic solvent was removed and instead hydrophobic reaction solvents were applied to prevent the stripping of enzyme-bound water and ensure high catalytic activity of the immobilized ω TA during the reaction. Controlled α_w was maintained throughout the reaction only when the active immobilized ω TA was operating in the presence of hydrate salts pair.

The reductive amination of **1a** (50 mM) with **2b** (150 mM) as the amine donor was used as a model reaction (Scheme 5.1). A previous study demonstrated that the application of lyophilized crude cell extract of AsR- ω TA in MTBE operates best at a water activity of $\alpha_w = 0.6$ [4b]. Optimization of c_w for immobilized ω TA with MTBE ($\alpha_w = 0.6$) followed by reductive amination either in toluene ($\alpha_w = 0.6$) or in MTBE ($\alpha_w = 0.6$) resulted in only 4% and 8% conversion, respectively. (Table 5.2, entries 1–2). When EtOAc ($\alpha_w = 0.6$) was used for optimization of c_w and the immobilized ω TA was then applied in toluene ($\alpha_w = 0.6$), a significant increase in conversion was observed (28%, Table 5.2, entry 3). Although sufficiently active immobilized ω TA was obtained using EtOAc at α_w of 0.6, it was postulated that some additional water molecules could be adsorbed by the immobilized ω TA over time, thus reducing its catalytic activity in the reaction. Indeed, when a pair of salts such as disodium hydrogen phosphate di- and hepta-hydrate was added to the reaction mixture (1:1 w w⁻¹, hydrate salts to immobilized ω TA), a remarkable increase in conversion was observed (87%, Table 5.2, entry 4). The addition of the above-mentioned hydrate salts to the reaction mixture also increased significantly the reproducibility of the system and all further experiments were performed with hydrate salts pair in the reaction.

Enzyme ionization effects largely influence the catalytic activity of enzymes in non-aqueous media [11a]. In particular, the effect of pH memory has been studied by tuning the ionization state of functional groups on lyophilized enzymes in aqueous buffer prior to submerging them in non-aqueous media [18, 42]. The pH memory phenomenon is due to the fact that generally the catalytic activity reflects the pH of the last aqueous solution to

which the enzyme has been exposed. Interestingly, the pH of the immobilization buffer did not affect the catalytic activity of EziG³-AsR immobilized from KPi buffers (Table 5.2, entries 6–10). However, a significant drop in conversion was observed when MOPS buffer was used for the immobilization (21%, Table 5.2, entry 5). KPi buffer (100 mM, pH 8.0) enabled a remarkable 96% conversion and further studies were performed using these conditions. EziG³-AsR immobilized from HEPES buffer (100 mM, pH 7.5) or Tris buffer (100 mM, pH 7.5) resulted in 75% and 91% conversion respectively (Table 5.2, entries 11–12).

5.2.2 Influence of support material, reaction solvent and conditions

Most immobilization supports absorb water and the use of different support materials can have a direct effect on the catalytic activity and stability of enzymes in non-aqueous media. For example, Carlsberg subtilisin covalently attached to macroporous acrylic supports was shown to have improved catalytic activity at high c_w as a result of water absorption by the support material [43]. EziG-immobilized ω TAs (EziG¹-AsR, EziG²-AsR, and EziG³-AsR) were applied in toluene (α_w controlled by hydrate salts, Table 5.6) and in the case in which water-saturated solvent was used, no hydrate salts were added. At comparable levels of a_w , the use of EziG¹-AsR and EziG³-AsR resulted in higher conversions than EziG²-AsR (Figure 5.1A and Table 5.7). However, a general trend was observed for all three EziG carrier materials thereby showing higher conversions at increased a_w , with an optimal performance at a value of 0.7 and drastically lowered conversions in water-saturated toluene. Interestingly, more hydrophilic EziG¹-AsR performed better at low α_w supporting the fact that water adsorption by the support material enhances the performance of the immobilized ω TA in low c_w solvents. Conversely, hydrophobic EziG²-AsR showed a dramatic drop in conversion at low a_w . EziG³ (Fe Amber) was chosen as the carrier material for further studies due to its superior performance in the range of $0.4 \leq \alpha_w \leq 0.7$.

Another important parameter controlling the hydration state of immobilized enzymes in non-aqueous media is the solvation of water molecules by the reaction solvent. Hydrophobic solvents or solvents with a high log P value in general serve as better candidates, because they lack the ability to strip the enzyme of essential water molecules [18–19]. Log P is the partitioning coefficient of the solvent for a standard octanol/water two-phase system [44]. EziG³-AsR was tested in different organic solvents at controlled a_w in order to define the optimal solvent for our system (Figure 5.1B). Organic solvents were chosen with log P values ranging from 0.7 to 5.6 (Table 5.8). EtOAc and MTBE with a log P values

Table 5.2. Optimization for EziG3-AsR in organic solvents. Immobilization conditions:

Entry	Immobilization buffer	Equilibration solvent	Reaction solvent	Hydrate salts	Conv. [%] ^[d]
1	KPI (100 mM, pH 8.0)	MTBE ^[a]	MTBE ^[a]	n.a. ^[c]	4±0
2	KPI (100 mM, pH 8.0)	MTBE ^[a]	Toluene ^[a]	n.a. ^[c]	8±1
3	KPI (100 mM, pH 8.0)	EtOAc ^[a]	Toluene ^[a]	n.a. ^[c]	28
4	KPI (100 mM, pH 8.0)	EtOAc ^[a]	Toluene ^[a]	Na ₂ HPO ₄ ·2H ₂ O/Na ₂ HPO ₄ ·7H ₂ O	87
5	MOPS (100 mM, pH 7.5)	EtOAc ^[a]	Toluene ^[a]	Na ₂ HPO ₄ ·2H ₂ O/Na ₂ HPO ₄ ·7H ₂ O	21±2
6	KPI (100 mM, pH 6.0)	EtOAc ^[b]	Toluene ^[b]	Na ₂ HPO ₃ ·5H ₂ O/Na ₂ HPO ₄ ·7H ₂ O	88±6
7	KPI (100 mM, pH 6.5)	EtOAc ^[b]	Toluene ^[b]	Na ₂ HPO ₃ ·5H ₂ O/Na ₂ HPO ₄ ·7H ₂ O	81±14
8	KPI (100 mM, pH 7.0)	EtOAc ^[b]	Toluene ^[b]	Na ₂ HPO ₃ ·5H ₂ O/Na ₂ HPO ₄ ·7H ₂ O	92±4
9	KPI (100 mM, pH 7.5)	EtOAc ^[b]	Toluene ^[b]	Na ₂ HPO ₃ ·5H ₂ O/Na ₂ HPO ₄ ·7H ₂ O	85±7
10	KPI (100 mM, pH 8.0)	EtOAc ^[b]	Toluene ^[b]	Na ₂ HPO ₃ ·5H ₂ O/Na ₂ HPO ₄ ·7H ₂ O	96±1
11	HEPES (100 mM, pH 7.5)	EtOAc ^[b]	Toluene ^[b]	Na ₂ HPO ₃ ·5H ₂ O/Na ₂ HPO ₄ ·7H ₂ O	75±5
12	Tris (100 mM, pH 7.5)	EtOAc ^[b]	Toluene ^[b]	Na ₂ HPO ₃ ·5H ₂ O/Na ₂ HPO ₄ ·7H ₂ O	91±2

EziG³ (Fe Amber, 20 mg), AsR- ω TA (2 mg, 54 nmol, enzyme loading: 10% w w⁻¹), buffer (1 mL, 100 mM, pH as specified), PLP (0.1 mM), 4 °C, 120 rpm, incubation time: 3 h. Reaction conditions: EziG³-AsR (22 mg, enzyme loading: 10% w w⁻¹), reaction solvent (1 mL, α_w as specified), **1a** (50 mM), **2b** (150 mM), 25 °C, 900 rpm, 72 h. [a] $\alpha_w = 0.6$. [b] $\alpha_w = 0.7$. [c] Not applicable. [d] Conversion to amine product in 72 h reaction time. Values are depicted with standard deviation over three experiments.

of 0.7 and 0.9 respectively showed moderate to good conversions whereas, *n*-heptane and *n*-decane (log *P* of 4.0 and 5.6 resp.) performed significantly better. Conversions of 86–96% were obtained with the most non-polar solvents at $0.4 \leq \alpha_w \leq 0.8$ and water-saturated

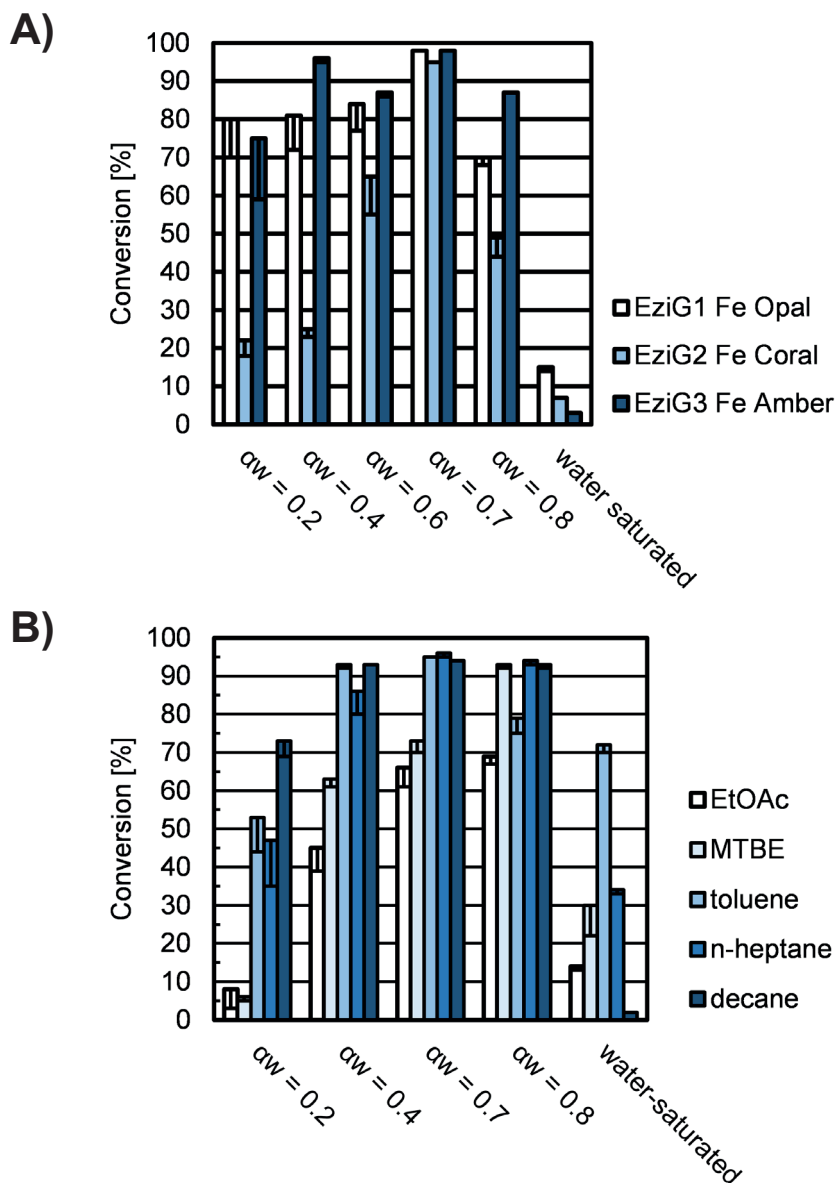


Figure 5.1. Performance of immobilized ω TA in neat organic solvents at controlled α_w . A) AsR-TA on three EziG materials in toluene, and B) EziG³-AsR applied in different reaction solvents. Immobilization conditions: EziGTM (20 mg), AsR- ω TA (2 mg, 54 nmol, enzyme loading: 10% w w⁻¹), KPi buffer (1 mL, 100 mM, pH 8.0), PLP (0.1 mM), 4 °C, 120 rpm, incubation time: 3 h. Reaction conditions: EziG³-AsR (22 mg, enzyme loading: 10% w w⁻¹), hydrate salts (ca. 25 mg), reaction solvent (1 mL, α_w as specified), **1a** (50 mM), **2b** (150 mM), 25 °C, 900 rpm, reaction time: 72 h. Values are depicted with standard deviation over three experiments.

solvents generally showed very poor performance. Toluene at controlled α_w of 0.7 proved to be optimal for the system and full conversion was observed within 48 h reaction time (Figure 5.3A and Table 5.12). Notably, EziG³-Cv (ω TA from *Chromobacterium violaceum*) employed in toluene was found to be most active at $\alpha_w \leq 0.2$ (Figure 5.2 and Table 5.9).

Dependency of α_w on the reaction temperature was tested by applying EziG³-AsR at 25 °C, 40 °C and 50 °C in toluene (controlled α_w). Similar trends in conversion were observed in the range $0.2 \leq \alpha_w \leq 0.7$ with a slight drop at higher reaction temperatures (Table 5.10). The system showed no significant improvement in catalytic activity as was previously observed for the non-immobilized ω TA [39].

5.2.3 Advantages and limitations in performance of the immobilized ω TAs in organic solvents

Literature data and this work support the finding that amine formation might be more favored in organic solvents; therefore, an improvement in productivity of the system was envisioned when applying immobilized ω TA in organic solvents as compared with water. It was previously observed that EziG³-AsR was capable of converting higher substrate concentrations in aqueous environment than the free enzyme in solution [39]. Notably, in organic solvent, the transamination reaction could be performed with just 1 equivalent of **2b** as amine donor (Table 5.11) leading to a remarkable conversion of 76% into **1b** (substrate concentration: 450 mM, 1 equiv. **2b**, product **1b** formation 52 mg; Table 5.14). This means that the unfavorable equilibrium of the transamination reaction in aqueous environment can actually be somehow overcome by applying ω TAs in a proper selection of organic solvents. Additionally, batch recycling of EziG³-AsR at substrate concentrations up to 400 mM was successfully performed. After each reaction cycle (72 h, 1 equiv. of **2b**), the reaction mixture was separated from the biocatalyst and the conversion was measured by GC. Then, the same batch of EziG³-AsR biocatalyst was re-suspended in fresh reaction mixture containing the reagents and another reaction cycle was initiated (Figure 5.3B and Table 5.13). At substrate concentrations of 300 mM and 400 mM a significant drop in conversion was observed after the first reaction cycle, however, resulting in an analytical product yield of 110 mg of **1b** over 4 reaction cycles (TTN = 13600). Although not affecting the catalytic activity of the immobilized ω TA, the biocatalyst had to be transferred to another vial in between reaction cycles due to deterioration of the plastic vial over the time. In subsequent experiments, the reaction has

also been performed in glass vials by adjusting the ratio of hydrate salts and enzyme to 3:1 ($w w^{-1}$). Since current batch recycling is limited to lower substrate concentrations, the use of preparative scale reactions in a batch reactor became undesirable and it was envisioned to obtain better durability of the system by implementing it in a packed-bed flow reactor.

5.2.4 Immobilized ω TAs in organic solvents under continuous flow operation

Performing reactions in continuous flow has become a practical tool for enhancing the lifetime of enzymes [45]. Especially, packed bed flow reactors have received considerable attention in biocatalysis by avoiding additional separation steps and preventing deactivation of the enzyme caused by mechanical stirring in classical bioreactors [46]. The application of EziG³-AsR in a packed-bed reactor for the kinetic resolution of racemic amines has been described in Chapter 4 in which we showed a virtual no loss (i.e., below detection limit under applied reaction conditions) of enzymatic activity [39]. The immobilized ω TA system in organic solvents was envisioned to benefit from application in flow reactors as well by general improvement in volumetric productivity over batch reactors.

EziG³-AsR was applied in a continuous flow set-up for the reductive amination of **1a** with **2b** (Figure 5.5). The reductive amination of **1a** was performed in organic solvent in a

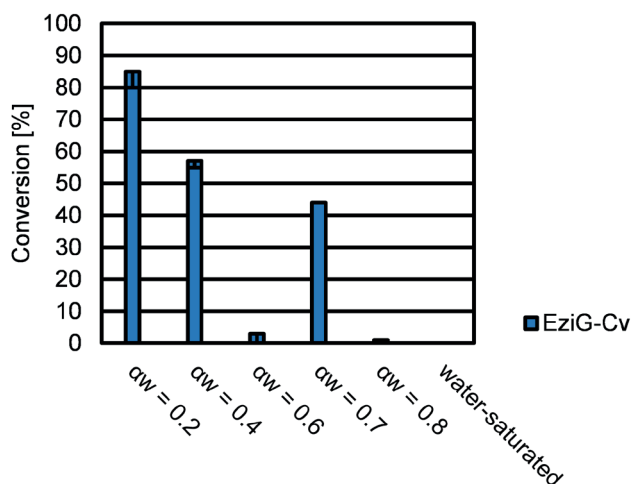


Figure 5.2. Performance of immobilized Cv- ω TA in toluene at controlled α_w . Immobilization conditions: EziGTM (20 mg), AsR- ω TA (2 mg, 54 nmol, enzyme loading: 10% $w w^{-1}$), KPi buffer (1 mL, 100 mM, pH 8.0), PLP (0.1 mM), 4 °C, 120 rpm, incubation time: 3 h. Reaction conditions: EziG³-AsR (22 mg, enzyme loading: 10% $w w^{-1}$), hydrate salts (ca. 25 mg), reaction solvent (1 mL, α_w as specified), **1a** (50 mM), **2b** (150 mM), 25 °C, 900 rpm, reaction time: 72 h. Values are depicted with standard deviation over three experiments.

continuous flow packed-bed reactor (reactor volume: 2 mL, residence time, $t_R = 10$ min, flow rate: 0.2 mL min^{-1}). A solution of **1a** and **2b** in toluene (50 mM **1a**, 150 mM **2b**, 50 mL toluene) was pumped through a stainless steel column containing the immobilized ω TA (EziG³-AsR). The flow system was equipped with a pre-column containing hydrate

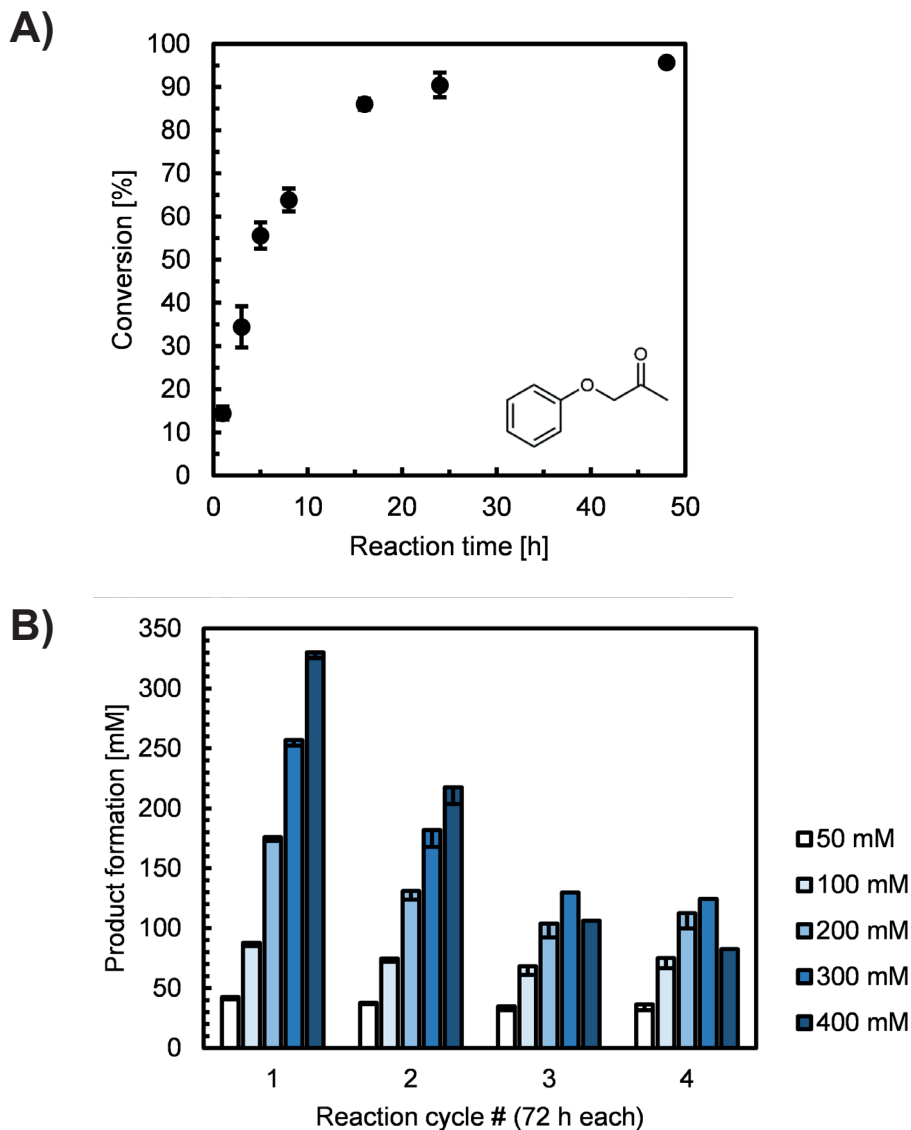


Figure 5.3. Performance of immobilized AsR- ω TA in neat organic solvents at controlled α_w . A) Time study of EziG³-AsR in toluene ($\alpha_w = 0.7$). B) Recycling of EziG³-AsR in toluene ($\alpha_w = 0.7$) at substrate concentrations of 50 mM, 100 mM, 200 mM, 300 mM and 400 mM **1a** and **2b**. Immobilization conditions: EziGTM (20 mg), AsR- ω TA (2 mg, 54 nmol, enzyme loading: 10% w w⁻¹), KPi buffer (1 mL, 100 mM, pH 8.0), PLP (0.1 mM), 4 °C, 120 rpm, incubation time: 3 h. Reaction conditions: EziG³-AsR (22 mg, enzyme loading: 10% w w⁻¹), hydrate salts (ca. 25 mg), reaction solvent (1 mL, α_w as specified), **1a** (50 mM), **2b** (150 mM), 25 °C, 900 rpm, reaction time: 72 h. Values are depicted with standard deviation over three experiments.

salts and the immobilized ω TA inside the flow reactor was mixed with hydrate salts (ratio 2:3) to ensure controlled α_w in the system. In order to reduce flow times, the outlet of the flow reactor was connected to the inlet of the pump creating a loop (Figure 5.5). The flow reactor showed excellent performance in three independent experiments and the ratio between **1a** and **1b** increased gradually to 70% conversion in 72 hours (STY = 1.9 g L⁻¹ h⁻¹) and ca. 90% in 120 hours (Figure 5.4 and Table 5.15). The apparent kinetic of the reaction with the immobilized enzyme appeared to be slightly higher in the first few days, since afterwards the conversion increased more slowly over time. However, it can simply be that the rate of the reverse reaction becomes significant at higher product formation because of proximity to reach a thermodynamic equilibrium. In the three independent experiments from Table 5.15, some discrepancies in the obtained conversions after 120 hours are observable. Especially, in experiment 3, after more than 5 days of operation the activity of the immobilized enzyme dropped (Table 5.15, entries 1–18). This observation has been attributed to inherent technical limitations of the currently non-fully optimized flow set-up, and possibly in relation to the difficulty in buffering the water activity homogeneously on the overall volume of immobilized biocatalyst for a long time. In fact, the immobilized enzyme placed inside the column tends to form one solid and wet unit over time (i.e., thus indicating likely an increase of water content or a non-homogeneous buffering

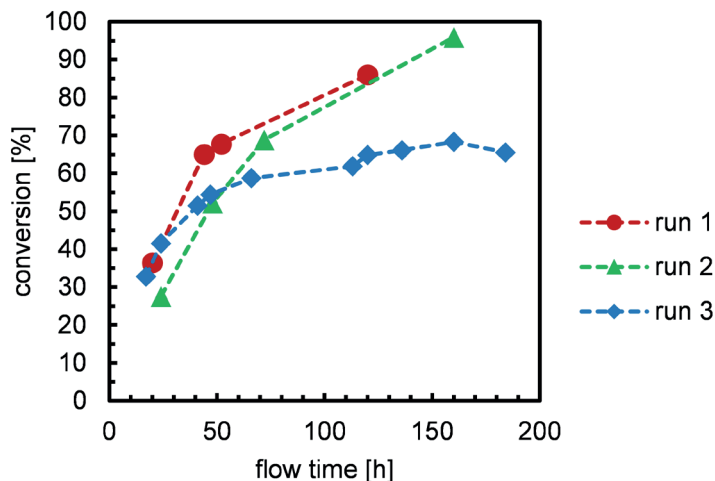


Figure 5.4. Continuous flow production of **1b** by immobilized AsR- ω TA in toluene at controlled α_w . Immobilization conditions: EziGTM (400 mg), AsR- ω TA (40 mg, enzyme loading: 10% w w⁻¹), KPi buffer (100 mM, pH 8.0), PLP (0.1 mM), 4 °C. Reaction conditions: EziG³-AsR (440 mg, enzyme loading: 10% w w⁻¹), Na₂HPO₃•5H₂O/ Na₂HPO₄•7H₂O (ca. 600 mg), toluene (reaction volume: 50 mL, $\alpha_w = 0.7$), **1a** (50 mM), **2b** (150 mM), flow rate: 0.2 mL min⁻¹, RT. Values are depicted with standard deviation over three experiments.

of the water content), which does not allow for a proper flow of the reaction solvent through the immobilized enzyme. It is likely to assume that most of the reaction solvent is passing through the column via the walls and, as a consequence, lower conversions are observed because not all the mass of biocatalyst is effectively participating to the reaction. Further optimization is required in future to solve this technical limitation.

Nonetheless, initial reproducibility of the flow reactor set-up was tested with 20 mM **1a** and 100 mM **2b** in cycles of 24 hours flow time (Table 5.16, entries 1–5). The flow system was operated for 24 h at a constant flow rate (0.2 mL min⁻¹, 20 mL reaction volume, 20 mM **1a**) and the conversion was determined by GC (**1b**: 30 mg day⁻¹). Then, a fresh reaction mixture was loaded and the flow reaction was run for another cycle of 24 h. The same process was repeated for 6 days continuously (24 hours for each reaction cycle) with no observable loss in performance; the pure amine product **1b** was isolated from the collected reaction cycles (150 mg, 82% isolated yield, >99% purity by GC). Notably, the flow reactor was still performing at 50% of its initial activity after 4 weeks of storage at 4 °C (Table 5.16, entries 6–7).

5.3 Conclusion

High catalytic performance of ω TAs immobilized on controlled porosity metal-ion affinity carriers (EziG) in neat organic solvents at controlled α_w was demonstrated in this work. A robust reaction system was developed using hydrate salt pairs for optimizing c_w and hence controlling α_w in non-polar solvents. High catalytic activity was obtained by optimizing the system in terms of immobilization buffer, support material and reaction solvent. Significant improvements in productivity were made when applying higher substrate concentrations and, remarkably, only one equivalent of amine donor was required in the reaction. Recycling experiments proved to be successful, and they enable already to run the reaction at significant levels of substrate concentrations (up to ca. 100 mM), which look promising for a possible industrial application. Finally, the practical applicability of the system was demonstrated in a continuous flow packed-bed reactor producing a chiral amine with good productivity and with only slight loss in activity over several days of operation. Further optimizations in process design are required to overcome the envisioned current limitations such as a homogenous and continuous buffering of the hydration state of the biocatalyst. This work displays the potential of continuous flow biocatalysis in neat organic solvents using selective immobilization of ω TAs on controlled porosity metal-ion affinity support materials.

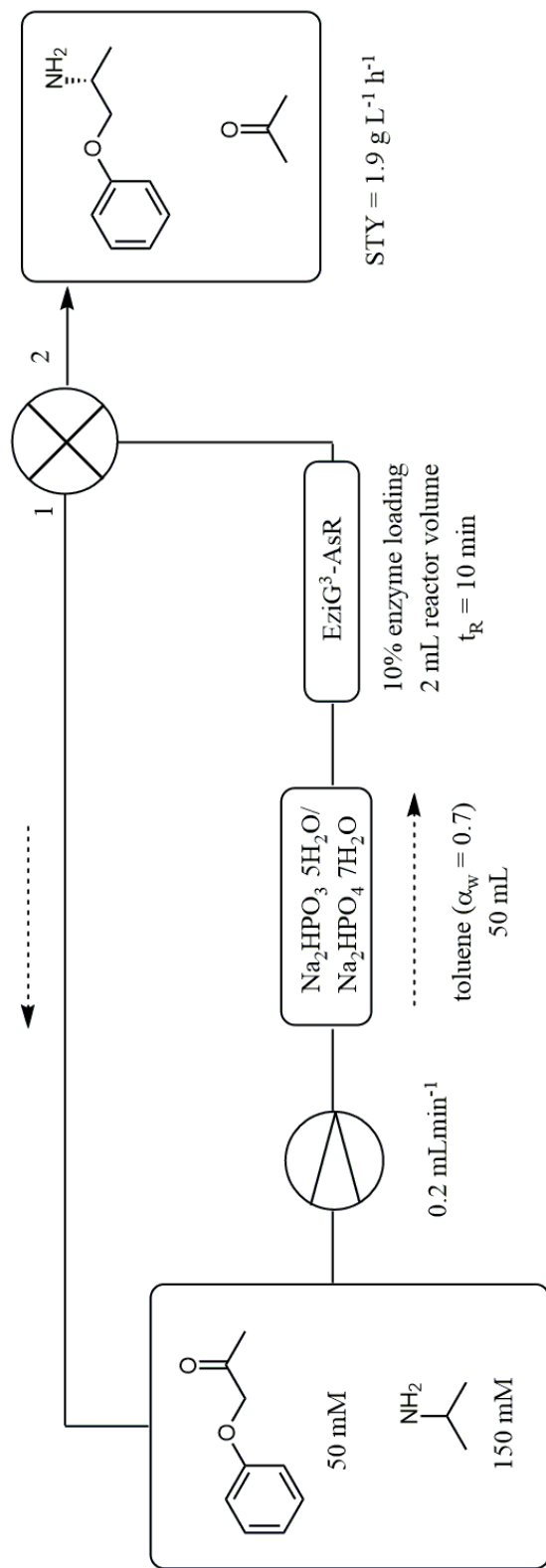


Figure 5.5. General loop set-up for flow reactions in organic solvent with EziG³-AsR. Valve flow direction 1: the reaction mixture is directed back to the inlet of the flow reactor. Valve flow direction 2: product isolation. Reaction conditions: stainless steel column for amination reaction (20 cm x 4 mm) filled with EziG³-AsR (400 mg, enzyme loading: 10% w w⁻¹) and $\text{Na}_2\text{HPO}_3 \cdot 5\text{H}_2\text{O}$ / $\text{Na}_2\text{HPO}_4 \cdot 7\text{H}_2\text{O}$ (600 mg, ratio 1:1 w w⁻¹), stainless steel pre-column for water activity control (5 cm x 10 mm) packed with $\text{Na}_2\text{HPO}_3 \cdot 5\text{H}_2\text{O}$ / $\text{Na}_2\text{HPO}_4 \cdot 7\text{H}_2\text{O}$ (4 g, ratio 1:1 w w⁻¹), reaction solvent (toluene, 20 mL, $\alpha_w = 0.7$), **1a** (55 μL , 20 mM), **2b** (170 μL , 100 mM), flow rate: 0.2 mLmin⁻¹, temperature: RT (21–23 °C).

5.4 Experimental Section

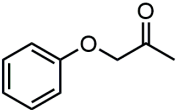
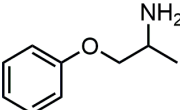
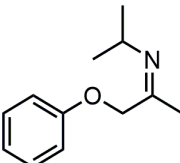
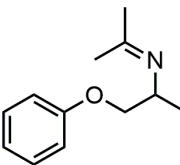
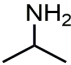
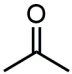
5.4.1 General information

2-propylamine (**2b**), phenoxypropan-2-one (**1a**) and pyridoxal-5'-phosphate (PLP) were purchased from Sigma-Aldrich (Steinheim, Germany). A list of compounds in this study is provided in Table 5.3. The following EziG enzyme carrier material was provided by EnginZyme AB (Stockholm, Sweden): EziG¹ (Fe Opal), EziG² (Fe Coral) and EziG³ (Fe Amber). EziG product specifications are listed in Table 5.4. For the immobilization of enzymes on support material, a C-star orbital shaker no. 12846016 (Thermo Fisher Scientific, UK) was used. Biorad protein assay dye reagent concentrate was purchased from Carl Roth (Karlsruhe, Germany). Biotransformations were performed in an Eppendorf Thermomixer compact 5350 (Germany). Continuous flow experiments were performed with a Dionex P680 HPLC pump unit (Thermo Fischer Scientific, UK). All reaction solvents were filtered (0.45 μ m) and degassed before use.

5.4.2 Expression and purification of ω TAs

C-terminal His-tagged (*R*)-selective ω TA from *Arthrobacter* sp. (AsR- ω TA, pET21a)^[40] and N-terminal His-tagged (*S*)-selective ω TA from *Chromobacterium violaceum* (Cv- ω TA, pET28b)^[41] were expressed

Table 5.3. List of compounds in this study.

Entry	No.	Name	Chemical structure
1	1a	phenoxypropan-2-one	
2	1b	phenoxypropan-2-amine	
3	imine- 1a/2b ^[a]	<i>N</i> -isopropyl-1-phenoxypropan-2-imine	
4	imine- 1b/2a ^[a]	<i>N</i> -(1-phenoxypropan-2-yl)propan-2-imine	
5	2b	2-propylamine	
6	2a	acetone	

^[a] Imine compounds were generated in-situ and detected by GC. These compounds could not be isolated.

in the BL21 (DE3) host organism and purified by Ni²⁺ affinity chromatography using the same procedures as have been described in Chapter 4 [39].

800 mL of LB medium supplemented with ampicillin (100 µg mL⁻¹ for pET21a) or kanamycin (50 µg mL⁻¹ for pET28b) were inoculated with 15 mL of an overnight culture. Cells were grown at 37 °C until an OD₆₀₀ of 0.6-0.9 was reached, and the expression of the proteins was induced by the addition of IPTG (0.5 mM final concentration). Protein expression was conducted overnight at 25 °C, and after harvesting of the cells (4 °C, 4500 rpm, 15 min), the remaining cell pellet was re-suspended in lysis buffer (50 mM KH₂PO₄, 300 mM NaCl, 10 mM imidazole, pH 8.0). Cells were disrupted by sonication and PLP (0.5 mM final concentration) was added to the cell lysate. After centrifugation (4 °C, 14,000 rpm, 45 min.), the supernatant was filtered through a 0.45 µm filter and protein purification was performed by Ni²⁺ affinity chromatography using Ni-NTA HisTrap FF columns (GE Healthcare) according to the manufacturer's instructions. After loading of the filtered lysate, the column was washed with sufficient amounts of washing buffer (50 mM KH₂PO₄, 300 mM NaCl, 25 mM imidazole, pH 8.0), and the target enzyme was recovered with elution buffer (50 mM KH₂PO₄, 300 mM NaCl, 200 mM imidazole, pH 8.0). The process of purification was analyzed by SDS-PAGE (see: Chapter 4). Fractions containing sufficiently pure protein were pooled and dialyzed overnight against potassium phosphate buffer (50 mM, pH 8). Protein solutions were concentrated and their concentrations were determined spectrophotometrically using a Bradford assay (section 5.4.3). Protein yields were 285 mg L⁻¹ of cell culture (36 mg g⁻¹ cell pellet) for AsR-ωTA and 100 mg L⁻¹ of cell culture (30 mg g⁻¹ cell pellet) for Cv-ωTA. Enzymes were shock-frozen in liquid nitrogen and stored at -80 °C.

5.4.3 Bradford assay

Biorad protein assay dye reagent concentrate was diluted 5 times with MilliQ water and filtered over a paper filter. The stock solution was freshly prepared before use and kept in the dark at 4 °C. Albumine calibration was performed in the standard range of 200-1000 µg mL⁻¹ protein. For lower protein concentration (<25 µg mL⁻¹) the low-concentration assay of 1-20 µg mL⁻¹ was used. Samples were prepared by mixing 980 µL stock solution and 20 µL protein sample (low-concentration assay: 800 µL stock and 200 µL protein sample) followed by incubation for 5-10 minutes at RT. Absorption at 595 nm was measured and plotted against the protein concentration. Diluted enzyme samples were then measured in the same fashion in order to determine their concentration.

Table 5.4. EziGTM product specifications: particle size 75-125 µm (100-300 mesh), chelated Fe³⁺ >10 µmol/g. Pore volume: ca. 1.8 mL g⁻¹. pH range: 5-10.

Entry	Product	Surface	Pore	Bulk	Lot#
			diameter [nm]	density [g/mL]	
1	EziG ¹ Fe Opal	Directly derivatized hydrophilic glass	50±5	0.25-0.32	MR010716
2	EziG ² Fe Coral	Hydrophobic polymer	30±5	0.21-0.25	MR011916
3	EziG ³ Fe Amber	Semi-hydrophobic copolymer	30±5	0.21-0.25	EziG-130

5.4.4 Immobilization of ω TAs on EziG support materials

On analytical scale EziG support material (20 ± 0.2 mg) was cooled down in an ice bath and suspended in immobilization buffer (KPi, 1 mL, 100 mM, pH 8.0) supplemented with PLP (0.1 mM). Purified ω -TA (2 mg, equal to 10% w⁻¹, enzyme loading to support material) was added to the suspension. The mixture was shaken on an orbital shaker (120 rpm) for 3 hours at 4 °C. Small aliquots from the aqueous phase (20 μ L) were taken before and after the immobilization procedure, and their concentrations were determined using the Bradford assay (section 5.4.3). Once full immobilization was obtained, the immobilized enzyme was let to sediment and the buffer was removed by pipetting.

The same procedure was followed also for immobilization at higher scale, typically using 40 mg of purified ω TA and 400 mg of EziG support material.

5.4.5 Analytical scale reactions in organic solvents with immobilized ω TAs

EziG-immobilized ω TA (total mass 20 mg, 10% w⁻¹ enzyme loading to support material) and hydrate salts ($\text{Na}_2\text{HPO}_x \cdot y\text{H}_2\text{O} / \text{Na}_2\text{HPO}_z \cdot w\text{H}_2\text{O}$, total mass 20 mg, 1:1, w⁻¹) were suspended in EtOAc (1 mL, at controlled α_w) and shaken for 15 minutes (900 rpm, thermomixer). The immobilized enzyme was let to sediment and solvent was removed by pipetting. The immobilized enzyme with hydrate salts was suspended in EtOAc and the process was repeated two more times. Optimal α_w was obtained and the immobilized enzyme with hydrate salts was washed with reaction solvent (1 mL, at fixed α_w). The immobilized enzyme was let to sediment and solvent was removed by pipetting. Reaction solvent (900 μ L, at fixed α_w) was added. A 10-fold stock of **2b** was prepared in the reaction solvent and added (final concentration: 150 mM, unless otherwise indicated). Finally, **1a** (6.89 μ L, 0.05 mmol, final concentration: 50 mM) was added and the reaction vials were shaken in an upright position (900 rpm, thermomixer) for 72 h at 25 °C. Work-up was performed by drying over MgSO_4 and injection on GC with an achiral column (section 5.4.7). For determination of enantiomeric excess the samples were derivatized using 4-dimethylaminopyridine in acetic anhydride (final concentration: 5 mg mL⁻¹) for 30 minutes (170 rpm, RT). Samples were quenched by addition of water (500 μ L) and shaken for 30 minutes (170 rpm, RT). The organic layer was dried over MgSO_4 and analyzed by GC with a chiral column (section 5.4.7).

5.4.6 Flow reactions in organic solvents with immobilized ω TA

EziG³-AsR (total mass 440 mg, 10% w⁻¹ enzyme loading to support material) and hydrate salts ($\text{Na}_2\text{HPO}_3 \cdot 5\text{H}_2\text{O} / \text{Na}_2\text{HPO}_4 \cdot 7\text{H}_2\text{O}$, total mass 600 mg, 1:1 w⁻¹) were suspended in EtOAc (10 mL, $\alpha_w = 0.7$) and shaken for 15 minutes (120 rpm, orbital shaker). The immobilized enzyme was let to sediment and solvent was removed by pipetting. The immobilized enzyme with hydrate salts was suspended in EtOAc and the process was repeated four more times. Optimal α_w was obtained and the immobilized enzyme with hydrate salts was washed with reaction solvent (10 mL, $\alpha_w = 0.7$). The immobilized enzyme was let to sediment and the solvent was removed by pipetting. The immobilized enzyme with hydrate salts was filled into a stainless steel column (15 cm x 0.4 cm, 2 mL) which was attached to a Dionex HPLC pump. A stainless steel pre-column (5 cm x 1 cm) was filled with hydrate salts (4 g, $\text{Na}_2\text{HPO}_3 \cdot 5\text{H}_2\text{O} / \text{Na}_2\text{HPO}_4 \cdot 7\text{H}_2\text{O}$, 1:1 w⁻¹) and attached in between the pump and the flow reactor. A solution of **1a** (375 μ L, 50 mM final concentration) and **2b** (640 μ L, 150 mM final concentration) in toluene (50 mL, $\alpha_w = 0.7$) was pumped through the flow reactor (equipped with pre-column) at a rate of 0.2 mL min⁻¹. The outlet of the flow reactor was directed back into the reaction mixture as shown in Figure 5.5. Conversions were determined by GC equipped with an achiral column (section 5.4.7). Work-up was performed by evaporation of the reaction solvent and

then the residue was dissolved in 2 M HCl (12 mL). The aqueous layer was extracted with MTBE (3 x 10 mL), then basified to pH 12 with 10 M KOH and extracted again with MTBE (3 x 10 mL). The second organic layer was dried over MgSO₄ and evaporated to dryness yielding the amine product 1b in high purity (>99% purity by GC, >99% ee).

5.4.7 Analytics

Conversions were determined by GC using a 7890A GC system (Agilent Technologies), equipped with a FID detector using H₂ as carrier gas with a HP-5 column from Agilent (30 m, 250 μm, 0.25 μm). The enantiomeric excess of derivatized amines was measured using a ChiraSil DEX-CB column from Agilent (25 m, 320 μm, 0.25 μm). GC retention times of compounds in this study are listed in Table 5.5.

HP-5 method: constant pressure 4 psi, T injector 250 °C, split ratio 30:1, T initial 60 °C, hold 0 min; gradient 5 °C/min up to 150 °C, hold 1 min, gradient 10 °C/min up to 250 °C, hold 1 min.

ChiraSil DEX-CB method: constant flow 1.4 mL/min, T injector 250 °C, split ratio 20:1, T initial 100 °C, hold 2 min; gradient 1 °C/min up to 130 °C, hold 5 min; gradient 10 °C/min up to 170 °C, hold 10 min.; gradient 10 °C/min up to 180 °C, hold 1 min.

Table 5.5. GC retention time of reference compounds.

entry	compound	retention time [min]	GC column and method
1	1a	12.7	HP-5
2	1b	13.9	HP-5
3	imine- 1a/2b	17.6	HP-5
4	imine- 1b/2a	18.5	HP-5
5	(<i>R</i>)- 1b ^[1]	44.7	ChiraSil DEX-CB
6	(<i>S</i>)- 1b ^[1]	43.9	ChiraSil DEX-CB

^[1] Upon derivatization as acetoamido.

5.4.8 Calculations and terminology

Yield of immobilization

In order to determine how much of the enzyme is immobilized during the process, a Bradford assay (UV absorption at 595 nm, section 5.4.3) was performed before ($A_{595 \text{ initial}}$) and after the immobilization process ($A_{595 \text{ final}}$) for calculating the amount of enzyme bound to the support material, i.e. the yield of immobilization (Equation 1).

Equation 1

$$\text{yield of immobilization [\%]} = \frac{(A_{595 \text{ final}} - A_{595 \text{ initial}})}{A_{595 \text{ initial}}} \times 100\%$$

Water activity

Water activity, α_w , is the tendency of water to remain in a certain phase of the reaction system. For immobilized enzymes in neat organic solvents with minimal water content, water is exchanged

between the organic and the solid phase until an equilibrium is established. α_w of a solvent in a particular reaction mixture then equals α_w of the immobilized enzyme. This allows for controlling α_w of a biocatalyst by water-equilibrating the reaction solvent. The value of α_w will increase with increasing water concentration (or mole fraction, x_w). Using the following equation;

Equation 2

$$\alpha_w = x_w \gamma_w$$

where γ_w is the activity coefficient from which α_w can be determined. γ_w depends on the temperature, the pressure and the composition of the liquid phase [10]:

Equation 3

$$RT \ln \left(\frac{\partial G^E}{\partial n_i} \right)_{T,P,n_{j \neq i}}$$

where R is the universal gas constant, T the temperature in K, G^E is the excess function of free Gibbs energy and n_i are the moles of the component i.

Using available vapour-liquid equilibrium (VLE) data, γ_w for EtOAc and MTBE was calculated before using NRTL equations [4b, 47]. The NRTL equation provides a good representation of experimental data for partially miscible as well as completely miscible systems.

For obtaining reaction solvents with defined α_w organic solvents were stirred for 1 hour in presence of sodium dibasic phosphate hydrate salts (1:1, w w⁻¹ ratio of hydrates). Previous studies indicate this time to be sufficient for α_w to reach an equilibrium between the organic and the solid phase [2c]. Equilibrium α_w for organic solvents in presence of Na₂HPO₄/Na₂HPO₄•2H₂O, Na₂HPO₄•2H₂O/Na₂HPO₄•7H₂O, and Na₂HPO₄•7H₂O/Na₂HPO₄•12H₂O was previously determined to be $\alpha_w = 0.16$, $\alpha_w = 0.59$, and $\alpha_w = 0.80$ respectively [2c, 32]. In this chapter Na₂HPO₄•2H₂O/Na₂HPO₃•5H₂O and Na₂HPO₃•5H₂O/Na₂HPO₄•7H₂O were prepared as well with $0.16 < \alpha_w < 0.59$ and $0.59 < \alpha_w < 0.80$ respectively. For simplification α_w of Na₂HPO₄•2H₂O/Na₂HPO₃•5H₂O and Na₂HPO₃•5H₂O/Na₂HPO₄•7H₂O has been depicted as $\alpha_w = 0.4$, and $\alpha_w = 0.7$ respectively (Table 5.6).

Table 5.6. Water activity of organic solvents fixed by using hydrate salt pairs. Combinations of different hydrate salt pairs allow for obtaining different water activity values. Ratio of hydrate salts: 1 : 1 (w w⁻¹).

entry	hydrate salts	α_w	references
1	Na ₂ HPO ₄ /Na ₂ HPO ₄ •2H ₂ O	0.16	[2c]
2	Na ₂ HPO ₄ •2H ₂ O/Na ₂ HPO ₃ •5H ₂ O	$0.16 < \alpha_w < 0.57$ (ca. 0.4)	n.a.
3	Na ₂ HPO ₄ •2H ₂ O/Na ₂ HPO ₄ •7H ₂ O	0.57	[32]
4	Na ₂ HPO ₃ •5H ₂ O/Na ₂ HPO ₄ •7H ₂ O	$0.57 < \alpha_w < 0.80$ (ca. 0.7)	n.a.
5	Na ₂ HPO ₄ •7H ₂ O/Na ₂ HPO ₄ •12H ₂ O	0.80	[32]
6	pure water or water-saturated	1.00	n.a.

Calculation of amine conversion

The reactions with immobilized ω TAs in organic solvents were analyzed by GC (section 4.7). Apart from the substrate **1a** and product **1b**, corresponding imines (imine-**1a/2b** and imine-**1b/2a**, see Table 5.3) were observed due to spontaneous equilibria in organic solvents. The response of the observed imines was determined and compared to those of **1a** and **1b**. GC calibration was performed using 20 mM, 50 mM, or 100 mM **1a** (or **1b**) and measuring the GC peak area. In a second set of samples **1a** (20 mM, 50 mM, or 100 mM) was dissolved in neat **2b** and **1b** (20 mM, 50 mM, or 100 mM) was dissolved in neat **2a** to obtain the imines in nearly quantitative yields (>95%). The GC peak area was plotted against the concentration of analyte (Figure 5.6) and no significant difference in response was observed. Following this observation the conversion to **1b** was calculated in the reaction mixture containing imine-**1a** or imine-**1b** by adding up GC areas of **1a** with those of imine-**1a/2b** and **1b** with those of imine-**1b/2a** in order to obtain the final conversion:

Equation 4

$$\begin{aligned} & \text{final conversion to } \mathbf{1b} [\%] \\ &= \frac{\text{GC area } \mathbf{1b} + \text{GC area imine } \mathbf{1b}}{(\text{GC area } \mathbf{1a} + \text{GC area } \mathbf{1b} + \text{GC area imine } \mathbf{1a/2b} + \text{GC area } \mathbf{1b/2a})} \\ & * 100\% \end{aligned}$$

Reaction rate in flow reactors

In flow reactors, several parameters relate to the reaction rate. An important parameter is space velocity (SV, in units of reciprocal time), which is defined by the volumetric flow rate of the reactant

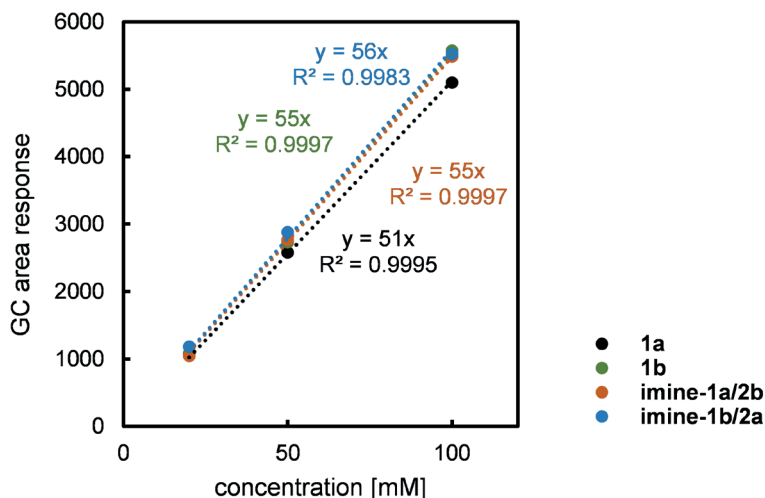


Figure 5.6. GC area response of substrates and products. The GC area response of 20 mM, 50 mM, or 100 mM of **1a** (or **1b**) was measured. Imine formation was generated by dissolving **1a** in neat **2b** (i.e., thus forming imine-**1a**) or **1b** in neat **2a** (i.e., thus forming imine-**1b**).

stream (V_o , specified at the inlet conditions of temperature and pressure with zero conversion), and the catalyst volume (V_c)^[1]. Often catalyst volume (V_c) is equally related to the reactor volume (V_r), which depends on the packing density of the catalyst particles:

Equation 5

$$SV \text{ (space velocity)} = \frac{V_o}{V_r}$$

Space time (τ , in units of time) is the inverse of space velocity and it gives the time required to process one reactor volume:

Equation 6

$$\tau \text{ (space time)} = \frac{1}{SV} = \frac{V_r}{V_o}$$

The space time yield (STY) refers to the quantity of product produced per quantity of catalyst per unit time. If the catalyst is well-packed in the full reactor, then the catalyst volume (V_c) can be equated to the reactor volume (V_r).

Equation 7

$$STY \text{ (space time yield)} = \frac{\text{product produced [g]}}{(V_r \times \text{time})}$$

Calculation of space-time yield for the flow process of EziG³-AsR in organic solvent:

$$\begin{aligned} \text{production of } \mathbf{1b} \text{ [mg]} &= 0.69 \text{ (conv.)} * 0.05 \frac{\text{mol}}{\text{L}} * 0.05 \text{ L} * 151.2 \frac{\text{mg}}{\text{mmol}} \\ &= 0.26 \text{ g} \end{aligned}$$

$$\begin{aligned} STY &= \frac{\mathbf{1b} \text{ [g]}}{(\text{reactor volume [L]} * \text{reaction time [h]})} = \frac{0.26 \text{ [g]}}{(0.002 \text{ [L]} \times 72 \text{ [h]})} \\ &= 1.9 \text{ g L}^{-1}\text{h}^{-1} \end{aligned}$$

5.5 Appendix

This section lists experimental data obtained in the study described in Chapter 5. Values are depicted as actual conversion to amine product with standard deviation over three experiments. Unless otherwise indicated, the following immobilization and reaction conditions were applied:

Immobilization conditions: EziG³ (Fe Amber, 20 mg, lot#EziG-130), AsR- ω TA (2 mg, 54 nmol, enzyme loading: 10% w w⁻¹), KPi buffer (1 mL, 100 mM, pH 8.0), PLP (0.1 mM), 4 °C, 120 rpm, incubation time: 3 h.

Reaction conditions: EziG³-AsR (22 mg, enzyme loading: 10% w w⁻¹), hydrate salts (ca. 25 mg), toluene (reaction volume: 1 mL, $\alpha_w = 0.7$), **1a** (50 mM), **2b** (150 mM), 25 °C, 900 rpm, reaction time: 72 h.

Table 5.7. AsR- ω TA immobilized on EziG support materials tested in organic solvent at controlled α_w (see: Figure 5.1A). The following support materials were applied: EziG¹ (Fe Opal, 20 mg, lot#MR010716) or EziG² (Fe Coral, 20 mg, lot#MR011916) or EziG³ (Fe Amber, 20 mg, lot#EziG-130).

entry	carrier type	α_w	hydrate salts	conv. [%]
1	EziG ¹ Fe Opal	0.2	Na ₂ HPO ₄ /Na ₂ HPO ₄ •2H ₂ O	80±10
2		0.4	Na ₂ HPO ₄ •2H ₂ O/Na ₂ HPO ₃ •5H ₂ O	81±9
3		0.6	Na ₂ HPO ₄ •2H ₂ O/Na ₂ HPO ₄ •7H ₂ O	84±7
4		0.7	Na ₂ HPO ₃ •5H ₂ O/Na ₂ HPO ₄ •7H ₂ O	98±0
5		0.8	Na ₂ HPO ₄ •7H ₂ O/Na ₂ HPO ₄ •12H ₂ O	70±2
6		water-saturated	n.a.	15±1

Table 5.7. (continued).

entry	carrier type	α_w	hydrate salts	conv. [%]
7	EziG ² Fe Coral	0.2	Na ₂ HPO ₄ /Na ₂ HPO ₄ •2H ₂ O	22±4
8		0.4	Na ₂ HPO ₄ •2H ₂ O/Na ₂ HPO ₃ •5H ₂ O	25±2
9		0.6	Na ₂ HPO ₄ •2H ₂ O/Na ₂ HPO ₄ •7H ₂ O	65±10
10		0.7	Na ₂ HPO ₃ •5H ₂ O/Na ₂ HPO ₄ •7H ₂ O	95±0
11		0.8	Na ₂ HPO ₄ •7H ₂ O/Na ₂ HPO ₄ •12H ₂ O	49±5
12		water-saturated	n.a.	7±0
13	EziG ³ Fe Amber	0.2	Na ₂ HPO ₄ /Na ₂ HPO ₄ •2H ₂ O	75±16
14		0.4	Na ₂ HPO ₄ •2H ₂ O/Na ₂ HPO ₃ •5H ₂ O	96±1
15		0.6	Na ₂ HPO ₄ •2H ₂ O/Na ₂ HPO ₄ •7H ₂ O	87±1
16		0.7	Na ₂ HPO ₃ •5H ₂ O/Na ₂ HPO ₄ •7H ₂ O	98±0
17		0.8	Na ₂ HPO ₄ •7H ₂ O/Na ₂ HPO ₄ •12H ₂ O	87±0

Table 5.8. Study of EziG³-AsR applied in different reaction solvents at controlled α_w (see: Figure 5.1B).

entry	reaction solvent	log P	α_w	hydrate salts	conv. [%]
1	EtOAc	0.7	0.2	Na ₂ HPO ₄ /Na ₂ HPO ₄ •2H ₂ O	8±5
2			0.4	Na ₂ HPO ₄ •2H ₂ O/Na ₂ HPO ₃ •5H ₂ O	45±6
3			0.7	Na ₂ HPO ₃ •5H ₂ O/Na ₂ HPO ₄ •7H ₂ O	66±5
4			0.8	Na ₂ HPO ₄ •7H ₂ O/Na ₂ HPO ₄ •12H ₂ O	69±2
5			water-saturated	n.a.	14±1
6	MTBE	0.9	0.2	Na ₂ HPO ₄ /Na ₂ HPO ₄ •2H ₂ O	6±1
7			0.4	Na ₂ HPO ₄ •2H ₂ O/Na ₂ HPO ₃ •5H ₂ O	63±2
8			0.7	Na ₂ HPO ₃ •5H ₂ O/Na ₂ HPO ₄ •7H ₂ O	73±3
9			0.8	Na ₂ HPO ₄ •7H ₂ O/Na ₂ HPO ₄ •12H ₂ O	93±1
10			water-saturated	n.a.	30±8

Table 5.8. (continued).

entry	reaction solvent	log P	α_w	hydrate salts	conv. [%]
11	toluene	2.5	0.2	Na ₂ HPO ₄ /Na ₂ HPO ₄ •2H ₂ O	53±9
12			0.4	Na ₂ HPO ₄ •2H ₂ O/Na ₂ HPO ₃ •5H ₂ O	93±1
13			0.7	Na ₂ HPO ₃ •5H ₂ O/Na ₂ HPO ₄ •7H ₂ O	95±0
14			0.8	Na ₂ HPO ₄ •7H ₂ O/Na ₂ HPO ₄ •12H ₂ O	79±4
15			water-saturated	n.a.	72±2
16	n-heptane	4.0	0.2	Na ₂ HPO ₄ /Na ₂ HPO ₄ •2H ₂ O	47±12
17			0.4	Na ₂ HPO ₄ •2H ₂ O/Na ₂ HPO ₃ •5H ₂ O	86±6
18			0.7	Na ₂ HPO ₃ •5H ₂ O/Na ₂ HPO ₄ •7H ₂ O	96±1
19			0.8	Na ₂ HPO ₄ •7H ₂ O/Na ₂ HPO ₄ •12H ₂ O	94±1
20			water-saturated	n.a.	34±1
21	decane	5.6	0.2	Na ₂ HPO ₄ /Na ₂ HPO ₄ •2H ₂ O	73±4
22			0.4	Na ₂ HPO ₄ •2H ₂ O/Na ₂ HPO ₃ •5H ₂ O	93±0
23			0.7	Na ₂ HPO ₃ •5H ₂ O/Na ₂ HPO ₄ •7H ₂ O	94±0
24			0.8	Na ₂ HPO ₄ •7H ₂ O/Na ₂ HPO ₄ •12H ₂ O	93±1
25			water-saturated	n.a.	2±0

Table 5.9. Study on EziG³-Cv applied in toluene at controlled α_w (see: Figure 5.2). Cv- ω TA (2 mg, 38 nmol, enzyme loading: 10% w w⁻¹) was immobilized using the standard protocol for immobilization and reactions in organic solvents (section 5.4.4-5.4.5).

entry	α_w	EziG ³ -Cv
		conversion [%]
1	0.2	85±5
2	0.4	57±2
3	0.6	3±3
4	0.7	44
5	0.8	1
6	water-saturated	0

Table 5.10. Temperature influence on performance of EziG³-AsR in toluene at controlled α_w . Data at 25 °C is provided in Table 5.8, entries 13-18.

entry	reaction temperature [°C]	α_w	hydrate salts	conv. [%] ^[1]
1	40 °C	0.2	Na ₂ HPO ₄ /Na ₂ HPO ₄ •2H ₂ O	13±8
2		0.4	Na ₂ HPO ₄ •2H ₂ O/Na ₂ HPO ₃ •5H ₂ O	76±4
3		0.6	Na ₂ HPO ₄ •2H ₂ O/Na ₂ HPO ₄ •7H ₂ O	37±9
4		0.7	Na ₂ HPO ₃ •5H ₂ O/Na ₂ HPO ₄ •7H ₂ O	80±2
5	50 °C	0.2	Na ₂ HPO ₄ /Na ₂ HPO ₄ •2H ₂ O	7±2
6		0.4	Na ₂ HPO ₄ •2H ₂ O/Na ₂ HPO ₃ •5H ₂ O	58±32
7		0.6	Na ₂ HPO ₄ •2H ₂ O/Na ₂ HPO ₄ •7H ₂ O	17±2
8		0.7	Na ₂ HPO ₃ •5H ₂ O/Na ₂ HPO ₄ •7H ₂ O	64±6

^[1] Values are depicted as actual conversion to amine product. Error represent the absolute difference between two independent experiments.

Table 5.11. Reductive amination of **1a** by EziG³-AsR in toluene ($\alpha_w = 0.7$) at 25 °C with 1, 2, or 3 equivalents **2b**.

entry	2b [mM]	equiv.	conversion [%]	ee% (<i>R</i>)
1	50	1	84±2	>99
2	100	2	98±0	>99
3	150	3	97±0	>99

Table 5.12. Time study of EziG³-AsR applied in toluene ($\alpha_w = 0.7$) at 25 °C (see: Figure 5.3A).

entry	reaction time [h]	conversion [%] ^[1]	ee% (<i>R</i>)
1	1	15±2	>99
2	3	34±5	>99
3	5	56±3	>99
4	8	64±3	>99
5	16	86±1	>99
6	24	91±3	>99
7	48	96±1	>99

Table 5.13. Recycling of EziG³-AsR in toluene ($\alpha_w = 0.7$) at 25 °C, see: Figure 5.3B).

entry	1a [mM]	2b [mM]	1b formed				1b formed
			[mM]				[mg]
			cycle #1	cycle #2	cycle #3	cycle #4	total
1	50	50	43±2	38±1	35±3	36±5	23
2	100	100	88±3	75±3	68±7	75±8	46
3	200	200	176±3	131±7	104±12	113±13	79
4	300	300	257±5	182±14	130±0	124±0	105
5	400	400	330±5	218±14	106±0	82±0	111

Table 5.14. Reductive amination of **1a** by EziG³-AsR in organic solvent with higher substrate concentrations.

entry	1a [mM]	2b [mM]	conv. [%]	1b formed [mM]	1b formed [mg]
1	50	50	85±4	43	7
2	100	100	88±3	88	13
3	200	200	88±1	176	27
4	300	300	86±2	257	39
5	400	400	83±1	330	50
6	450	450	76±1	344	52
7	500	500	65±6	325	49
8	550	550	55±9	300	45
9	600	600	22±5	133	20
10	650	650	6±2	38	6
11	700	700	2±1	12	2
12	750	750	5±4	35	5
13	800	800	0±0	3	<1

Table 5.15. Continuous flow experiments with EziG³-AsR (see: Figure 5.4). Immobilization conditions: EziG³ (Fe Amber, 400 mg, lot#EziG-130), AsR- ω TA (40 mg, 1.49 mmol, enzyme loading: 10% w w⁻¹), KPi buffer (10 mL, 100 mM, pH 8.0), PLP (0.1 mM), 4 °C, 120 rpm, incubation time: 3 h. Reaction conditions: EziG³-AsR (440 mg, enzyme loading: 10% w w⁻¹), Na₂HPO₃•5H₂O/Na₂HPO₄•7H₂O (ca. 600 mg), toluene ($\alpha_w = 0.7$), **1a** (50 mM), **2b** (150 mM), flow rate: 0.2 mL min⁻¹, RT.

entry	Experiment no.	1a [mM]	2b [mM]	Flow time [h]	1b [%] ^[1]	1a [%] ^[1]
1	1	50	150	20	36	64
2	1			44	65	35
3	1			52	68	32
4	1			120	86	14
5	2	50	150	24	28	72
6	2			48	52	48
7	2			72	69	31
8	2			120	96	4
9	3	50	150	17	33	67
10	3			24	42	58
11	3			41	51	49
12	3			47	54	46
13	3		150	66	59	41
14	3			113	62	38
15	3			120	65	35
16	3			136	66	34
17	3			160	68	32
18	3			184	66	34

^[1] Conversion calculated as described in section 5.4.8.

Table 5.16. Continuous flow experiments with EziG³-AsR testing system durability. Immobilization conditions: EziG³ (Fe Amber, 400 mg, lot#EziG-130), AsR- ω TA (40 mg, 1.49 mmol, enzyme loading: 10% w w⁻¹), KPi buffer (10 mL, 100 mM, pH 8.0), PLP (0.1 mM), 4 °C, 120 rpm, incubation time: 3 h. Reaction conditions: EziG³-AsR (440 mg, enzyme loading: 10% w w⁻¹), Na₂HPO₃·5H₂O/Na₂HPO₄·7H₂O (ca. 600 mg), toluene ($\alpha_w = 0.7$), **1a** (20 mM), **2b** (100 mM), flow rate: 0.2 mL min⁻¹, RT.

entry	Experiment no.	1a [mM]	2b [mM]	Flow time [h] ^[1]	1b [%] ^[2]	1a [%] ^[2]
1	4	20	100	24 (24)	56	44
2	4	20	100	24 (48)	52	48
3	4	20	100	24 (72)	53	47
4	4	20	100	24 (96)	53	47
5	4	20	100	24 (144)	58	42
6	4 (after storage)	20	100	24 (24)	30	70
7	4 (after storage)	20	100	24 (48)	53	47

^[1] Total active time of enzyme batch between brackets. ^[2] Conversion calculated as described in section 5.4.8.

5.6 References

- [1] Salihu, A.; Alam, M. Z. *Process Biochemistry*. **2015**, *50*, 86–96.
- [2] a) Bracco, P.; Busch, H.; Langermann, J. V.; Hanefeld, U. *Organic and Biomolecular Chemistry*. **2016**, *14*, 6375–6389; b) Lanfranchi, E.; Steiner, K.; Glieder, A.; Hajnal, I.; Sheldon, R. A.; Van Pelt, S.; Winkler, M. *Recent Patents in Biotechnology*. **2013**, *7*, 197–206; c) Paravidino, M.; Sorgedraeger, M. J.; Orru, R. V.; Hanefeld, U. *Chemistry*. **2010**, *16*, 7596–7604.
- [3] a) Li, H. M.; Moncecchi, J.; Truppo, M. D. *Organic Process Research & Development*. **2015**, *19*, 695–700; b) Kazandjian, R. Z.; Klibanov, A. M. *Journal of the American Chemical Society*. **1985**, *107*, 5448–5450; c) Müller, G. H.; Lang, A.; Seithel, D. R.; Waldmann, H. *Chemistry – A European Journal*. **1998**, *4*, 2513–2522; d) Randolph, T. W.; Clark, D. S.; Blanch, H. W.; Prausnitz, J. M. *Science*. **1988**, *239*, 387–390; e) Randolph, T. W.; Blanch, H. W.; Prausnitz, J. M. *An Official Publication of the American Institute of Chemical Engineers*. **1988**, *34*, 1354–1360; f) Grunwald, J.; Wirz, B.; Scollar, M. P.; Klibanov, A. M. *Journal of the American Chemical Society*. **1986**, *108*, 6732–6734.
- [4] a) Truppo, M. D.; Strotman, H.; Hughes, G. *ChemCatChem*. **2012**, *4*, 1071–1074; b) Mutti, F. G.; Kroutil, W. *Advanced Synthesis & Catalysis*. **2012**, *354*, 3409–3413.
- [5] Serdakowski, A. L.; Dordick, J. S. *Trends in Biotechnology*. **2008**, *26*, 48–54.
- [6] Klibanov, A. *Trends in Biochemical Sciences*. **1989**, *14*, 141–144.
- [7] a) Fitzpatrick, P. A.; Steinmetz, A. C.; Ringe, D.; Klibanov, A. M. *Proceedings of the National Academy of Sciences of the United States of America*. **1993**, *90*, 8653–8657; b) Gao, X. G.; Maldonado, E.; Perez-Montfort, R.; Garza-Ramos, G.; De Gomez-Puyou, M. T.; Gomez-Puyou, A.; Rodriguez-Romero, A. *Proceedings of the National Academy of Sciences of the*

- United States of America*. **1999**, *96*, 10062–10067; c) Schmitke, J. L.; Stern, L. J.; Klibanov, A. M. *Proceedings of the National Academy of Sciences of the United States of America*. **1997**, *94*, 4250–4255; d) Yennawar, N. H.; Yennawar, H. P.; Farber, G. K. *Biochemistry*. **2002**, *33*, 7326–7336; e) Zhu, G.; Huang, Q.; Wang, Z.; Qian, M.; Jia, Y.; Tang, Y. *Biochimica et Biophysica Acta*. **1998**, *1429*, 142–150.
- [8] a) Zaks, A.; Klibanov, A. M. *Journal of Biological Chemistry*. **1988**, *263*, 8017–8021; b) Rupley, J. A.; Careri, G. *Advanced Protein Chemistry* **1991**, *41*, 37–172.
- [9] a) Soares, C. M.; Teixeira, V. H.; Baptista, A. M. *Biophysical Journal*. **2003**, *84*, 1628–1641; b) Guinn, R. M.; Skerker, P. S.; Kavanaugh, P.; Clark, D. S. *Biotechnology and Bioengineering*. **1991**, *37*, 303–308; c) Affleck, R.; Haynes, C. A.; Clark, D. S. *Proceedings of the National Academy of Sciences of the United States of America*. **1992**, *89*, 5167–5170; d) Eppler, R. K.; Komor, R. S.; Huynh, J.; Dordick, J. S.; Reimer, J. A.; Clark, D. S. *Proceedings of the National Academy of Sciences of the United States of America*. **2006**, *103*, 5706–5710.
- [10] Halling, P. J. *Enzyme and Microbial Technology*. **1994**, *16*, 178–206.
- [11] a) Carrea, G.; Riva, S. *Organic Synthesis with Enzymes in Non-Aqueous Media*; Wiley-VCH Verlag GmbH & Co. KGaA; Weinheim, Germany, 2008; b) Gupta, M. N. *European Journal of Biochemistry*. **1992**, *203*, 25–32.
- [12] Secundo, F.; Carrea, G. *Chemistry*. **2003**, *9*, 3194–3199.
- [13] Bilal, M.; Cui, J.; Iqbal, H. M. N. *International Journal of Biological Macromolecules*. **2019**, *130*, 186–196.
- [14] a) Wescott, C. R.; Noritomi, H.; Klibanov, A. M. *Journal of the American Chemical Society*. **1996**, *118*, 10365–10370; b) Carrea, G.; Ottolina, G.; Riva, S. *Trends in Biotechnology*. **1995**, *13*, 63–70.
- [15] a) Bell, G.; Halling, P. J.; Moore, B. D.; Partridge, J.; Rees, D. G. *Trends in Biotechnology*. **1995**, *13*, 468–473; b) Klibanov, A. M. *Nature*. **2001**, *409*, 241–246.
- [16] Zaks, A.; Klibanov, A. M. *Science*. **1984**, *224*, 1249–1251.
- [17] Volkin, D. B.; Staubli, A.; Langer, R.; Klibanov, A. M. *Biotechnology and Bioengineering*. **1991**, *37*, 843–853.
- [18] Zaks, A.; Klibanov, A. M. *Journal of Biological Chemistry*. **1988**, *263*, 3194–3201.
- [19] Klibanov, A. M. *Trends in Biotechnology*. **1997**, *15*, 97–101.
- [20] Gorman, L. A.; Dordick, J. S. *Biotechnology and Bioengineering*. **1992**, *39*, 392–397.
- [21] Ryu, K.; Dordick, J. S. *Biochemistry*. **1992**, *31*, 2588–2598.
- [22] Kim, J.; Clark, D. S.; Dordick, J. S. *Biotechnology and Bioengineering*. **2000**, *67*, 112–116.
- [23] Dordick, J. S. *Enzyme and Microbial Technology*. **1989**, *11*, 194–211.
- [24] a) Debulis, K.; Klibanov, A. M. *Biotechnology and Bioengineering*. **1993**, *41*, 566–571; b)

- Khmelnitsky, Y. L.; Welch, S. H.; Clark, D. S.; Dordick, J. S. *Journal of the American Chemical Society*. **1994**, *116*, 2647–2648; c) Russell, A. J.; Klibanov, A. M. *Journal of Biological Chemistry*. **1988**, *263*, 11624–11626; d) Broos, J.; Sakodinskaya, I. K.; Engbersen, J. F. J.; Verboom, W.; Reinhoudt, D. N. *Journal of the Chemical Society, Chemical Communications*. **1995**, 255.
- [25] Liese, A.; Seelbach, K.; Wandrey, C. *Industrial Biotransformations*; 2 ed.; Wiley-VCH; Weinheim, Germany, 2006.
- [26] Ortiz, C.; Ferreira, M. L.; Barbosa, O.; Dos Santos, J. C. S.; Rodrigues, R. C.; Berenguer-Murcia, A.; Briand, L. E.; Fernandez-Lafuente, R. *Catalysis Science & Technology*. **2019**, *9*, 2380–2420.
- [27] Roy, I.; Gupta, M. N. *Bioorganic and Medicinal Chemistry Letters*. **2004**, *14*, 2191–2193.
- [28] a) Dorau, R.; Görbe, T.; Humble, M. S. *ChemBioChem*. **2018**, *19*, 338–346; b) Prasad, S.; Roy, I. *Analytical Biochemistry*. **2017**, *534*, 86–90.
- [29] Meyer, L. E.; Langermann, J. V.; Kragl, U. *Biophysics Reviews*. **2018**, *10*, 901–910.
- [30] Gotor-Fernandez, V.; Paul, C. E. *Journal of Biotechnology*. **2019**, *293*, 24–35.
- [31] Wehtje, E.; Svensson, I.; Adlercreutz, P.; Mattiasson, B. *Biotechnology Techniques*. **1993**, *7*, 873–878.
- [32] Zacharis, E.; Omar, I. C.; Partridge, J.; Robb, D. A.; Halling, P. J. *Biotechnology and Bioengineering*. **1997**, *55*, 367–374.
- [33] a) Patil, M. D.; Grogan, G.; Bommarium, A.; Yun, H. *Catalysts*. **2018**, *8*, 254; b) Slabu, I.; Galman, J. L.; Lloyd, R. C.; Turner, N. J. *ACS Catalysis*. **2017**, *7*, 8263–8284.
- [34] Kelly, S. A.; Pohle, S.; Wharry, S.; Mix, S.; Allen, C. C. R.; Moody, T. S.; Gilmore, B. F. *Chemical Reviews*. **2018**, *118*, 349–367.
- [35] Yun, H.; Kim, J.; Kinnera, K.; Kim, B. G. *Biotechnology and Bioengineering*. **2006**, *93*, 391–395.
- [36] Fuchs, C. S.; Simon, R. C.; Riethorst, W.; Zepeck, F.; Kroutil, W. *Bioorganic and Medicinal Chemistry*. **2014**, *22*, 5558–5562.
- [37] Börner, T.; Rämisch, S.; Bartsch, S.; Vogel, A.; Adlercreutz, P.; Grey, C. *ChemBioChem*. **2017**, *18*, 1482–1486.
- [38] Grabner, B.; Nazario, M. A.; Gundersen, M. T.; Lois, S.; Fantini, S.; Bartsch, S.; Woodley, J. M.; Gruber-Woelfler, H. *Molecular Catalysis*. **2018**, *452*, 11–19.
- [39] Böhmer, W.; Knaus, T.; Volkov, A.; Slot, T. K.; Shiju, N. R.; Cassimjee, K. E.; Mutti, F. G. *Journal of Biotechnology*. **2019**, *291*, 52–60.
- [40] Iwasaki, A.; Matsumoto, K.; Hasegawa, J.; Yasohara, Y. *Applied Microbiology and Biotechnology*. **2012**, *93*, 1563–1573.
- [41] a) Kaulmann, U.; Smithies, K.; Smith, M. E. B.; Hailes, H. C.; Ward, J. M. *Enzyme and Microbial Technology*. **2007**, *41*, 628–637; b) Koszelewski, D.; Pressnitz, D.; Clay, D.; Kroutil, W.

Organic Letters. **2009**, *11*, 4810–4812; c) Koszelewski, D.; Göritzer, M.; Clay, D.; Seisser, B.; Kroutil, W. *ChemCatChem*. **2010**, *2*, 73–77.

- [42] Zaks, A.; Klibanov, A. M. *Proceedings of the National Academy of Sciences of the United States of America*. **1985**, *82*, 3192–3196.
- [43] Orsat, B.; Drtina, G. J.; Williams, M. G.; Klibanov, A. M. *Biotechnology and Bioengineering*. **1994**, *44*, 1265–1269.
- [44] Laane, C. *Biocatalysis*. **2009**, *1*, 17–22.
- [45] Britton, J.; Majumdar, S.; Weiss, G. A. *Chemical Society Reviews*. **2018**, *47*, 5891–5918.
- [46] a) Tamborini, L.; Fernandes, P.; Paradisi, F.; Molinari, F. *Trends in Biotechnology*. **2018**, *36*, 73–88;
b) Thompson, M. P.; Peñafiel, I.; Cosgrove, S. C.; Turner, N. J. *Organic Process Research & Development*. **2018**, *23*, 9–18.
- [47] Renon, H.; Prausnitz, J. M. *American Institute of Chemical Engineers Journals*. **1968**, *14*, 135–144.

Samenvatting

Asymmetrische synthese van chirale α -amines met een hoge katalytische efficiëntie is chemisch gezien een grote uitdaging. Amines zijn zeer belangrijke chemische bouwstenen voor de productie van vele farmaceutische stoffen, landbouw-, en fijnchemicaliën. Chemische methoden voor het verkrijgen van deze belangrijke bouwstoffen zijn vaak niet selectief genoeg en gebruiken bovendien fossiele grondstoffen. Alhoewel minder vaak toegepast in de chemische industrie bezitten enzymatische processen zeer hoge chemo-, regio-, en stereoselectiviteit. Daarnaast hebben enzymen een volledige biologische oorsprong. Veel biokatalytische processen zijn echter nog niet geschikt voor de industrie en worden daarom vaak vermeden. Dit proefschrift biedt een ander perspectief en toont de industriële toepasbaarheid van enzymen. Enzymen voor de bio-organische synthese van chirale α -amines, zoals amine dehydrogenases en transaminases, zijn zeer actieve katalysatoren (versnellers) met een hoge chemische efficiëntie. Selectieve immobilisatie van deze enzymen op support materialen creëert heterogene katalysatoren die beter toepasbaar zijn en de productie van chirale α -amines op gram-schaal mogelijk maken in zowel batch als flow. In dit proefschrift is de efficiëntie van geïmmobiliseerde enzymen verder verbeterd door ze toe te passen in organische oplosmiddelen. Problemen die vaak optreden met enzymatische processen in de industrie konden worden voorkomen, zoals lage oplosbaarheid van substraten, ongunstige thermodynamische evenwichten, ongewenste bijproducten en extra zuiveringsstappen. Dit proefschrift toont de potentie van het gebruik van enzymen in bio-organische synthese van waardevolle chemische bouwstoffen en het geeft een kritisch overzicht van de actuele toepassingen in enzyme immobilisatie en biokatalyse in flow.

Acknowledgements

I would like, first of all, to thank my promoters dr. Francesco Mutti and prof. dr. Jan van Maarseveen for their support and dedication to my project and help with the writing of this thesis. I am thankful for the opportunity to work on this project and the confidence you gave me to successfully complete it.

Special thanks to all committee members for their time and dedication to read and evaluate my thesis.

I want to thank Francesco and Tanja both for their support and supervision during the last four years and in particular for providing a well-organised lab environment. This has been of tremendous help during my work and made it possible to obtain high-quality data. Besides that it has been a pleasure to work in the biocatalysis group.

I want to thank Jan and also prof. dr. Henk Hiemstra for their support and encouraging words during some of the more difficult times. The door has always been open for me to ask for your help and I greatly appreciate that.

Within the Biocat group there are three people I can always rely on. Maria, Jan and Vasilis, I think there are not enough words to say thank you for these nice, fun, happy, challenging, but above all enjoyable years we have had together. Many times I'll think back on moments when Maria explained that "farfalle" is not the same as "penne", Vasilis convinced everybody that Rhodes is the most beautiful island in the universe, and Jan attempted to make me ride a motorcycle arguing how many girls you can pick up with that. I wanna say to you, thank you and good luck writing your theses. In life I wish you good health, fortune and prosperity.

Special thanks to Alexey and Karim from EnginZyme for their support and collaboration during the largest part of my PhD. Thank you for your dedication, input, help and supply of immobilization carrier materials.

I wanna thank also my collaboration partners from the Hetcat group, Thierry and Shiju, for their help and work providing solid SEM data which greatly supported the publication in the Journal of Biotechnology.

I want to thank all (former) group members of Biocat and the many people that worked at SOC during my stay for the enjoyable years and nice atmosphere. I wish you all good luck.

I feel most comfortable around my closest friends, members of "het Intellectuele Bierclubje" as we call since a few years. I am very happy we decided to keep up with the tradition to meet on a regular basis after we all left high school. I hope we may do this for some time still and it goes without saying that I thank all of you for the nice times we've been having.

Finally, I want to thank my family for their support and love particularly over the last four years and for their advice, encouragement, patience, understanding, and everything else that is impossible to describe in words. Thank you.

List of publications

- [1] Dzik, W. I.; Böhmer, W.; Bruin, B. de *Multiple Spin-State Scenarios in Organo-metallic Reactivity*, in *Spin States in Biochemistry and Inorganic Chemistry: Influence on Structure and Reactivity*, Swart, M.; Costas, M. (Eds.), Ch. 6, John Wiley & Sons, 2015.
- [2] Knaus, T.; Böhmer, W.; Mutti, F. G. *Green Chem.* **2017**, *19*, 453–463.
- [3] Böhmer, W.; Knaus, T.; Mutti, F. G. *ChemCatChem.* **2018**, *10*, 731–735.
- [4] Böhmer, W.; Knaus, T.; Volkov, A.; Slot, T. K.; Shiju, N. R.; Engelmark Cassimjee, K.; Mutti, F. *G. J Biotechnol.* **2019**, *291*, 52–60.
- [5] Böhmer, W.; Mutti, F. G. *Advanced Synthesis & Catalysis.* **2019**, *submitted*.